Channeling in Purine Biosynthesis: Efforts to Detect Interactions between PurF and PurD and Characterization of the FGAR-AT Complex

by

Aaron A. Hoskins

B.S. Chemistry

Purdue University, 2000

Submitted to the Department of Chemistry

in Partial Fulfillment of the Requirements for the Degree of

Doctor of Philosophy in Biological Chemistry

at the

MASSACHUSETTS INSTITUTE OF TECHNOLOGY

[February 2006]

January 2006

Signature of Author: _____
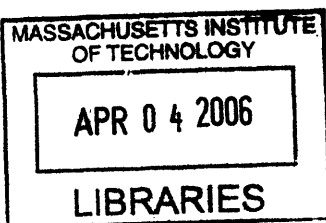
<div align="right">Department of Chemistry

January 19, 2006</div>

Certified by: _____

<div align="right">Professor JoAnne Stubbe

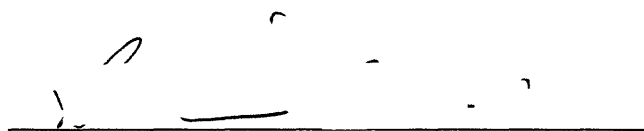Thesis Supervisor</div>

Accepted by: _____

<div align="right">Professor Robert W. Field

Chairman, Departmental Committee on Graduate Students</div>
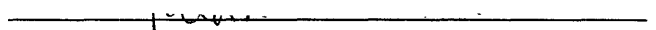
ARCHIVES V.1

This doctoral thesis has been examined by a Committee of the Department of Chemistry as follows:
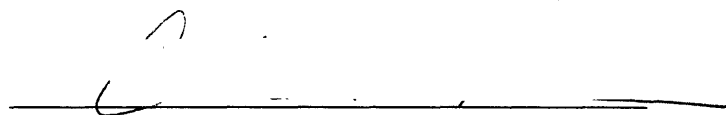
Professor Barbara Imperiali _____

Chairperson

Professor JoAnne Stubbe _____

Thesis Supervisor

Professor Catherine Drennan _____

2

For my parents, grandparents, and aunts.

Acknowledgements

First, I would like to acknowledge my parents (Mom and Dad), grandparents (Boobie and Grampa), Aunt Betty, and Aunt Doris. Without their support, this thesis would not have been possible.

Second, I would like to thank JoAnne for taking me into her lab, teaching me how to assay enzymes, and making me a better scientist.

I gratefully acknowledge all those in the Stubbe lab who have helped and aided me throughout the years. You all mean so much to me.

In particular, I would like to thank Jesse Chen for being the best labmate and friend I can imagine. I'm not sure how I will be able to do science again without having him just 3 feet away. Let's keep the memory of Gertrude Ederle alive.

I would also like to thank Professors Imperiali and Drennan for helpful advice and discussions.

I would like to thank Amy, Niki, Blair, Greg, and Pedja for being the friends that keep me grounded and for making me laugh.

I would like to thank Greg, Graham, Dan, and Diana for getting me out of the lab and for making me realize that I've based my graduate life on lessons learned from a movie staring David Bowie and the Muppets.

I would like to thank Brent Fisher for being such a great friend and a wonderful human being.

I would like to thank Matt and Jeff for reasons too detailed to explain here. Jeff in particular for making a most gracious and unique offer to help me through writing this thesis.

I would like to thank Debby Pheasant for being supportive and enthusiastic and for being there.

I would like to thank members of the Schwalbe lab for giving me a great start in graduate school. Especially Jens, who has turned from a great mentor to a great friend.

I would also like to thank the congregations of the University and Holy Trinity Lutheran Churches for their support. Through God all things are possible.

Channeling in Purine Biosynthesis: Efforts to Detect Interactions between PurF and PurD and Characterization of the FGAR-AT Complex

By

Aaron A. Hoskins

Submitted to the Department of Chemistry in January, 2006 in Partial Fulfillment of the Requirements for the Degree of Doctor of Philosophy in Biological Chemistry

ABSTRACT

Purine biosynthesis has been used as a paradigm for the study of metabolism of unstable molecules. Both phosphoribosylamine (PRA) and N^5-carboxyaminoimidazole ribonucleotide (N^5-CAIR) have estimated half-lives *in vivo* of seconds. In order to avoid metabolite decomposition, one strategy cells could employ is channeling—the direct transfer of a metabolite between enzyme active sites without diffusion into the bulk media. While kinetic evidence for channeling of PRA has been reported between phosphoribosylpyrophosphate amidotransferase (PurF) and glycinamide ribonucleotide synthetase (PurD), no evidence for a PurF:PurD complex has been found. In an effort to detect this complex, stopped-flow fluorescence spectroscopy was used to detect changes in PurF fluorescence that may result from interaction with PurD. Critical to the success of these experiments was incorporation of tryptophan analogs (4-fluorotryptophan and 7-azatryptophan) into the proteins in order to increase signal specificity for PurF. No evidence for a PurF:PurD interaction was found under any of the conditions tested. The implication of this finding is discussed with regard to the PurF:PurD channeling model.

Like all amidotransferase enzymes (ATs), channeling of NH_3 between glutaminase and AT active sites has been implicated in the formylglycinamide ribonucleotide amidotransferase (FGAR-AT). In *B. subtilis*, the FGAR-AT is composed of three proteins: PurS, PurQ, and small PurL. The first characterization of the *B. subtilis* FGAR-AT complex was carried out, and it was determined that a complex between the three proteins can only be isolated in the presence of Mg^{2+}-ADP and glutamine. By analogy to the *Salmonella* FGAR-AT, ADP is believed to be acting as a structural cofactor, while formation of a PurQ-glutamine complex is essential for assembly of the FGAR-AT. Subsequent biophysical studies have indicated that the physiologically relevant form of the FGAR-AT complex contains 2 PurS, 1 PurQ, and 1 small PurL. Further studies on PurQ have identified residues important for catalysis and complex formation, while insight into the small PurL active site has been obtained by studies on the *T. maritima* enzyme. The FGAR-AT complex provides a new system in purine biosynthesis to study metabolite transfer among weakly interacting proteins.

Thesis Supervisor: JoAnne Stubbe
Title: Novartis Professor of Chemistry and Biology

Preface

Portions of the work presented in Chapters 3 and 4 have appeared in the following publications:

1. Hoskins, A.A., Anand, R., Ealick, S.E., and Stubbe, J. "The formylglycinamide ribonucleotide amidotransferase complex from *Bacillus subtilis*: metabolite-mediated complex formation." *Biochemistry*, 43(32), 10314-27.
2. Anand, R., Hoskins, A.A., Stubbe, J., and Ealick, S.E. "Domain organization of *Salmonella typhimurium* formylglycinamide ribonucleotide amidotransferase revealed by X-ray crystallography." *Biochemistry*, 43(32), 10328-42.
3. Anand, R., Hoskins, A.A., Bennett, E.M., Sintchak, M.D., Stubbe, J., and Ealick, S.E. "A model for the *Bacillus subtilis* formylglycinamide ribonucleotide amidotransferase multiprotein complex." *Biochemistry*, 43(32), 10343-52.

Table of Contents

Chapter 3. Characterization of the *B. subtilis* FGAR-AT Complex

Chapter 4. Biophysical Studies on PurS and the FGAR-AT Complex

Chapter 5. Mutagenesis of PurQ and Studies on FGAR-AT Complex Formation

Chapter 6. Identification of Residues Essential for PurL Catalysis and Relationship of

these Residues to Other PurM-Superfamily Members

Appendix

List of Figures

11

13

List of Tables

15

List of Schemes

Chapter 1:

Introduction

It has been estimated that the 1 million polypeptide chains in *E. coli* cytoplasm along with nucleic acids occupy 30% of the cell's total available volume, with macromolecule concentrations of 300-400 mg/mL (*1, 2*). This leaves only 70% available for water, salts, metabolites, and other small molecules. A cell is an amazingly close-packed system with a solvent content similar to that observed in many protein crystals (Figure 1.1). This highly crowded environment is very different from conditions under which enzyme activities are normally determined. A typical enzyme assay consists of monitoring the activity of a single, homogenous enzyme at a concentration of 1-1,000 nM in a buffer containing a few salts and only the small molecules of interest. It is surprising that only recently has the impact of the cellular environment begun to be systematically studied with regard to enzyme function.

In particular, a crowded cellular environment is believed to present a barrier to molecular diffusion which can consequently impact enzymatic activity (*3*). In an excellent analogy, Verkman has compared the 3 barriers to cellular diffusion (fluid-phase viscosity, non-specific binding, and crowding) to driving an automobile (Figure 1.2) (*3*). Cellular diffusion is much like an early-morning commute. The time it takes to reach your destination depends on the speed limit (fluid-phase viscosity), the number of stoplights (non-specific binding), and rush hour traffic (molecular crowding).

Recent advances in fluorescence microscopy have allowed these barriers to be quantified *in vivo*. Using a combination of spot photobleaching and time-resolved fluorescence anisotropy, small molecule diffusion in the cytosol has been studied with 2',7'-bis-(2-carboxyethyl)-5-(and-6)-carboxyfluorescein (BCEF). The diffusion of the fluorophore was found to occur at a rate of $\sim 2 \times 10^{-6}$ cm^2/s *in vivo*, which is ~4 times more slowly than in water (*4*). The
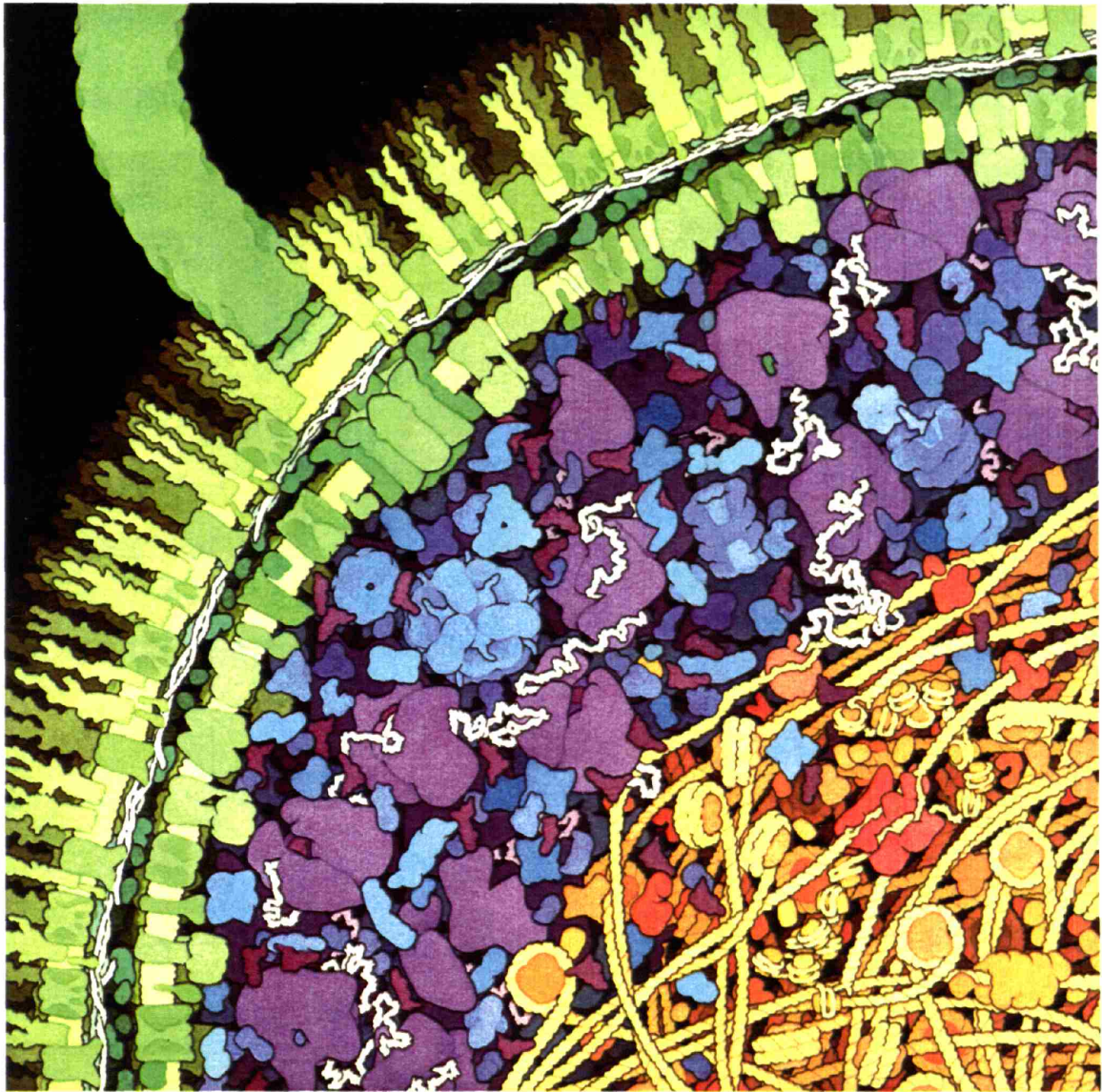
Figure 1.1— An artist's scientific representation of the crowded interior of an *E. coli* cell. Illustration courtesy of David Goodsell, Scripps Research Insitute.

Viscosity | Binding | Crowding

Figure 1.2— Obstacles encountered during diffusion in a crowded cell.

relative contributions of visocity, non-specific binding, and crowding to this diffusion rate were then evaluated. Surprisingly, despite the high concentration of macromolecules, the viscosity of the cytoplasm was determined to be only slightly greater than that of water (~4.5 cPoise), and non-specific binding provided only a minor barrier to diffusion for BCECF (4). The greatest barrier to the probe's cytoplasmic diffusion was determined to be collisions with macromolecules due to crowding.

Diffusion of large molecules has also been studied using either fluorescently-labeled dextrans, green fluorescent protein (GFP), GFP-derivatized metabolic enzymes, or fluorescently-labeled DNA fragments. In all cases, the rates of diffusion were determined to be much lower in cytoplasm than in water ($D_{cyto}/D_{water} < 0.25$) (3). Dextrans larger than 2000 kDa and DNA fragments larger than 250 bp had severely impaired rates of diffusion (3). Most relevant to studies on enzyme activities and metabolism were the diffusion rates of GFP and labeled glycolytic enzymes. When GFP was expressed in CHO cells, it possessed similar diffusion properties compared to BCECF (8.7×10^{-7} cm²/s) (5). However, very different results were obtained for TCA cycle enzymes being expressed in either CHO or COS7 cells as GFP chimeras. In this case, malate dehydrogenase, isocitrate dehydrogenase, citrate synthase, and succinyl-CoA synthetase were all found to diffuse nearly 20-fold slower than GFP alone ($\sim 4 \times 10^{-8}$ cm²/s) (6). These results indicate that the cellular environment can restrict both small molecule and macromolecule mobility.

The effects of crowding on enzyme activity are complicated (7, 8). Based on the results mentioned above, crowding would be expected to lower enzyme activities due to diffusion barriers encountered in forming an enzyme•substrate complex. However, the excluded volume in a crowded environment due to the space occupied by other macromolecules can increase

22

effective concentration, leading to an activating effect. Therefore, the impact of crowding on activity is highly enzyme specific and depends on the contributions of both of these factors. For example, crowding has been shown to increase the activity of rabbit muscle pyruvate kinase (9), inhibit adenosine deaminase (10), and have no net effect on Eco RV endonuclease kinetics due to compensating changes in non-specific binding, V_{max}, and K_m for the DNA substrate (11).

The diffusion rates mentioned above for BCECF give rise to very fast linear velocities compared to the size of an average bacterial cell (0.125 μm/μs versus an average *E. coli* cell size of 2.95 μm x 0.64 μm) (1, 4). Given an intracellular protein concentration of 1 μM, the diffusional transit time for a small molecule between proteins would only be ~1 ms (12). However, if one takes into account the rate of productive encounters in an enzyme active site (which would be dependent on the correct orientation of the active site relative to the small molecule among other factors), the transit time could increase to 0.1-1 s (12). Given this observation and the impact of crowding on both small molecule and macromolecular diffusion, it is a reasonable question to ask if cells have evolved mechanisms to overcome this barrier. Recent advances in prokaryotic biology have indicated that Nature has taken a very sophisticated approach to cytosolic organization in bacteria.

1.1 Organization in the Bacterial Cell

It is now clear that bacterial physiology contains many of the complex features previously associated with eukaryotes. In the early 1990s it was discovered that the membrane chemoreceptors and cytoplasmic chemotaxis proteins in *E. coli* could localize specifically at the cell pole (13). Since then, the picture of a bacterium has changed from a "bag of enzymes" to one of an exquisitely organized set of machines. This is exemplified in studies on asymmetric cell division in *Caulobacter crescentus* and sporulation in *Bacillus subtilis*. In both cases,

protein activities are regulated by transcriptional-timing to produce enzymes only during specific stages of the cell cycle and by localization of enzymes to specific locations within the cell (*14*). Furthermore, it has now been shown in *Caulobacter* that the chromosome position in the cell is tightly controlled and specific genetic loci are found at defined chromosome locations with respect to the cell axis (*15*). This positioning is maintained by careful remodeling and segregation of the chromosome during cell division by transport proteins and linkage to a cytoskeleton formed by the actin homologue MreB (*16*). Evidence for a cytoskeleton has also been found in *E. coli* where the MreB protein filaments are essential for maintaining cell shape (*17, 18*) and the dynamic MinCDE filamentous complex is responsible for localization of the division septum at the cell midpoint (*19*).

The examples mentioned above for organization of the bacterial cell are limited to processes involving either cell division or morphology. Cellular organization of primary metabolic enzymes is less well-understood; however, formation of protein:protein complexes could be used to circumvent many of the diffusion problems encountered in a crowded cellular environment. This may be particularly important in the metabolism of unstable or reactive molecules.

Cellular metabolism proceeds in aqueous solutions at pH ~7 at 37°C despite the chemical instability of many metabolites under these conditions *in vitro*. For example, de novo purine biosynthesis in bacteria (Scheme 1.1) generates two different unstable intermediates. Phosphoribosylamine (PRA) and N^5-carboxyaminoimidazole ribonucleotide (N^5-CAIR) each

Scheme 1.1—de novo Purine Biosynthesis

25

have estimated half-lives *in vivo* on the order of seconds and rapidly decompose either by hydrolysis (PRA) or decarboxylation (N^5-CAIR) (*20*). In addition, phosphoribosylpyrophosphate (PRPP), the precursor to PRA and a common metabolite in many biosynthetic pathways, rapidly decomposes in the presence of Mg^{2+} to a combination of ribose-5'-phosphate, PP_i, and 5'-phosphoribosyl-1',2' cyclic phosphate (*21, 22*). Many other metabolic pathways contain unstable or reactive metabolites including carbamate and carbamoyl phosphate in pyrimidine metabolism (*23, 24*), β-aspartyl phosphate in the aspartate pathway (*25*), and glutamate 1-semialdehyde in 5-aminolevulinic acid synthesis (*26, 27*).

One method that cells could use to avoid metabolite decomposition would be to directly transfer these unstable metabolites between enzyme active sites. This process is called metabolic channeling and is broadly defined as transfer of common metabolites between enzymes without equilibration with the bulk solution (Figure 1.3) (*28*). There are several advantages to channeling including decreasing the metabolite transit time between enzymes, avoiding unfavorable equilibria, segregation of common metabolites from competing pathways, and protection of chemically labile or toxic intermediates (*28*). Channeling sidesteps all of the barriers to cellular diffusion present in the cytosol to provide an elegant solution for metabolism in a crowded environment.

Key to the understanding of the channeling phenomenon is an analysis of the protein:protein complex that is proposed to be involved in metabolite transfer. In the following sections, small-molecule transfer via protein:protein complex formation will be described in two well-studied model systems: carbamoyl phosphate synthetase (CPS) and the bacterial chemotaxis phosphorelay system. CPS is believed to channel NH_3 between two enzymes in a

Free Diffusion
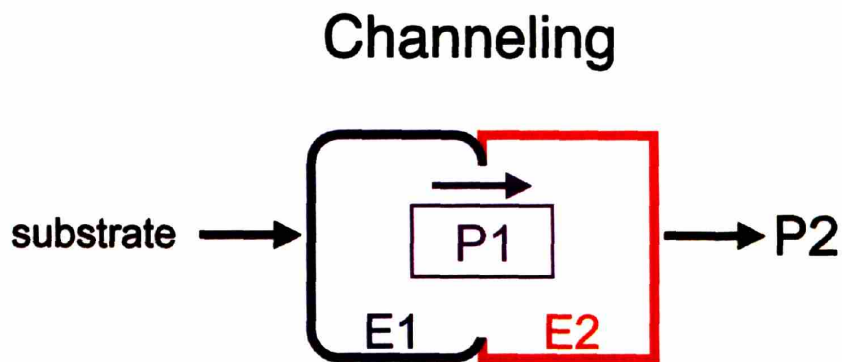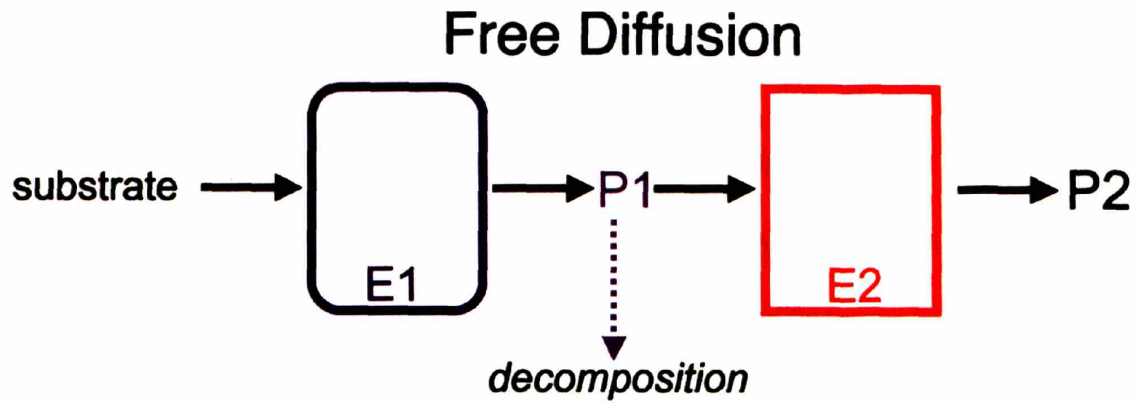
Channeling

Figure 1.3—Free diffusion versus channeling for transfer of common metabolite P1 between enzymes E1 and E2. If metabolite P1 is unstable or reactive, channeling avoids metabolite decomposition that may be encountered during diffusion into the cytosol.

tight protein:protein complex, while bacterial chemotaxis relies on transient protein interactions to catalyze phosphoryl transfer.

1.2 Carbamoyl Phosphate Synthetase: NH_3-transfer in a Tight Enzyme Complex

Amidotransferases (ATs) are enzymes that catalyze hydrolysis of glutamine and incorporation of the liberated NH_3 into another metabolite. These enzymes are ubiquitous in metabolism and can be classified according to their glutaminase active sites (Table 1.1). The largest families are the NTN and triad classes of ATs (29). The NTN class contains a N-terminal cysteine involved in glutamylthioester formation and liberation of NH_3.

Table 1.1: Amidotransferases in Primary Metabolism	
Enzyme	Glutaminase Class
Anthranilate Synthase	Triad
Asparagine Synthetase	NTN
Carbamoyl Phosphate Synthetase (CPS)	Triad
Cobyrinic Acid a,c-Diamide Synthetase	Triad
CTP Synthetase	Triad
Formylglycinamide Ribonucleotide Amidotransferase (FGAR-AT, PurL)	Triad
Glu-tRNA^{Gln} Amidotransferase (GatABC or GatDE)	Amidase or Asparaginase
Glucosamine-6-Phosphate Synthase	NTN
Glutamate Synthase	NTN
GMP Synthetase	Triad
Imidazole Glycerol Phosphate Synthase (HisHF)	Triad
NAD Synthetase (Eukaryotic)	Nitrilase
p-Aminobenzoate Synthase (PabAB)	Triad
Phosphoribosylpyrophosphate Amidotransferase (PRPP-AT, PurF)	NTN

The triad class also contains a catalytic cysteine residue; however, this residue may be located anywhere within the peptide chain and is always followed by a conserved pair of histidine and glutamate residues with a typical consensus sequence of $Cx_{80-100}HPE$ (29). The crystal structures of many AT enzymes have been solved, and every structure contains spatially separated glutaminase and AT active sites (30). This observation has led to a general model in which AT enzymes channel NH_3 between two active sites (30). In the case of the NTN class, intramolecular channeling has been proposed since the glutaminase and AT active sites are always present on the same polypeptide chain. Channel formation and architecture has been well studied in PurF (Scheme 1.1), the prototype for the NTN class, but no general paradigms have emerged for AT enzymes as a whole (31-33).

Triad glutaminases may be located either on the same peptide chain as the AT or on a separate protein. Intramolecular channeling has been proposed in this AT family in the former case and intermolecular channeling in the latter. CPS is the best-studied triad AT and is an example of an enzyme that exhibits intermolecular channeling between two tightly interacting subunits. These subunits can only be separated by denaturation or by the presence of extremely high salt concentrations, and full activity cannot be regained by reconstituting the separated subunits (34-36). CPS catalyzes formation of carbamoyl phosphate from bicarbonate, glutamine, and 2 equivalents of ATP. The enzyme is found as a heterodimer composed of 40 kDa and 120 kDa proteins. The former catalyzes glutamine hydrolysis (1), while the latter catalyzes formation of carbamate (2) and carbamoyl phosphate (3). The overall reaction (4) is thus composed of 3 reactions as shown below.

$$Gln + H_2O \rightarrow Glu + NH_3 \tag{1}$$

$$NH_3 + ATP + HCO_3^- \rightarrow carbamate + ADP + P_i \tag{2}$$

$$\underline{carbamate + ATP \rightarrow carbamoyl\ phosphate + ADP} \tag{3}$$

$$Gln + 2ATP + HCO_3^- + H_2O \rightarrow carbamoyl\ phosphate + 2ADP + P_i + Glu \tag{4}$$
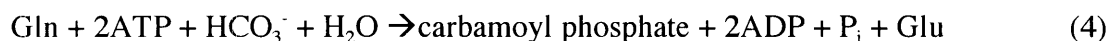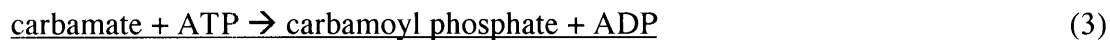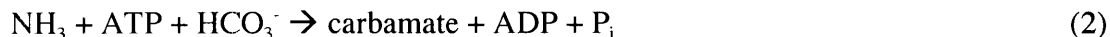
Crystallographic analysis of the CPS complex revealed that the light and heavy subunits have an extensive protein interface (Figure 1.4, ~2150 $\mathring{A}^2$ buried/subunit) (*37*). This interface is formed by 35 inter-protein hydrogen bonds and 36 interactions mediated by water molecules (*38*). The AT and glutaminase activities are coupled across this interface. Detailed kinetic analysis of CPS by the Raushel laboratory has determined that in the presence of ATP and HCO_3^-, glutamine hydrolysis is accelerated from 4 to 1100 min^{-1} in order to synchronize NH_3 and activated-bicarbonate formation for carbamate synthesis (*39*).

The crystal structure of CPS also revealed that three reactions carried out by the enzyme occur in distinct, spatially-separated active sites (Figure 1.4). These active sites are connected by a 96 $\mathring{A}$-long tunnel that winds through the enzyme (*37*). In the tunnel between the glutaminase and carbamate synthetase sites, NH_3 is proposed to channel over a distance of ~45 $\mathring{A}$. This tunnel is largely hydrophilic in character and has an average minimum radius of 3.2 $\mathring{A}$, approximately the same size as NH_3. A larger tunnel (average minimum radius of 3.5 $\mathring{A}$) connects the synthetase and carbamate kinase active sites. This tunnel is hydrophobic and is believed to convey carbamate between active sites within the heavy subunit. Channeling of these metabolites avoids both protonation of NH_3 and carbamate decomposition (half-life at neutral pH of ~70 ms) (*23*).
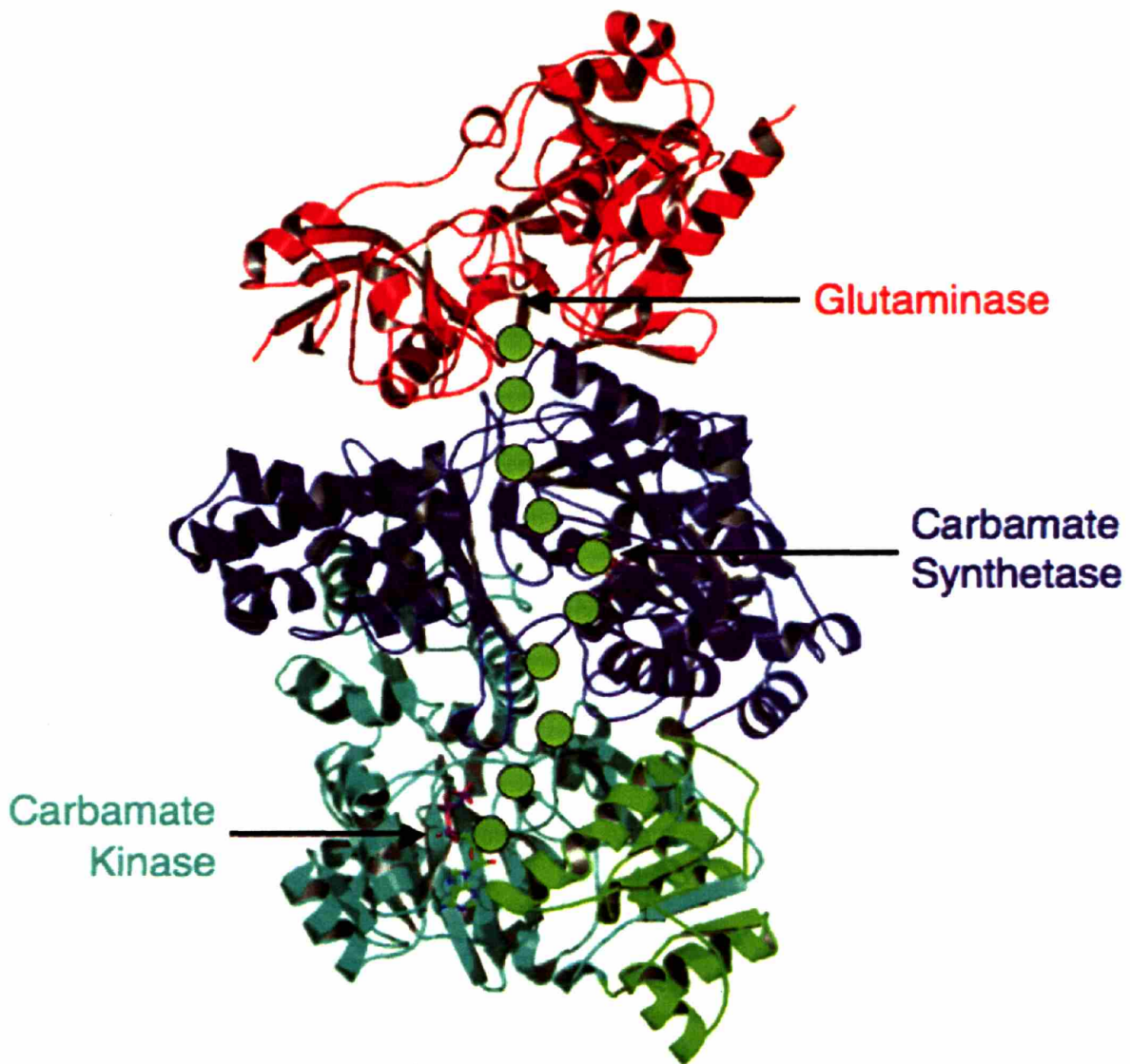
Figure 1.4—Inter- and intramolecular channeling in carbamoylphosphate synthetase (CPS). The overall reaction for CPS is shown above. The crystal structure of the enzyme revealed four domains: a triad glutaminase occupies the light subunit (red) and the carbamate synthetase (blue), carbamate kinase (teal), and regulatory (green) domains occupy the heavy subunit. Inter- and intramolecular tunnels for NH_3 and carbamate (outlined by the green dots) connect the three active sites of the enzyme.

CPS is also the only AT enzyme for which NH_3-channeling has been demonstrated by chemical methods. The evidence for channeling used ^{15}N-NMR to monitor product formation in the presence of 25 mM [^{14}N]-glutamine and 100 mM $^{15}NH_4Cl$ (*40*). If the $^{14}NH_3$ released from glutamylthioester formation does not channel, it should be able to equilibrate with the $^{15}NH_4^+$ present in the buffer. Subsequent diffusion of ammonia (or ammonium) back into the carbamate synthetase active site would result in 80% (100 mM $^{15}NH_4$ ÷ 125 mM total NH_4) of the product being ^{15}N-labeled. In order to avoid carbamoyl phosphate decomposition during acquisition, the reaction was coupled with ornithine carbamoyltransferase and integration of the citrulline product NMR signal showed that < 5% contained ^{15}N, providing evidence that $^{14}NH_3$ is being channeled across the protein:protein interface between the glutaminase and AT active sites of CPS.

1.3 Bacterial Chemotaxis: Phosphoryl Transfer in a Transient Enzyme Complex

Given the crowded cellular environment, one might expect that all protein complexes are pre-organized into very tight interactions as in the case of CPS. However, there are many examples of enzymes that interact weakly, or transiently, with one another. For example, weak interactions are essential for electron transfer proteins involved in photosynthesis and oxidative phosphorylation in order to maintain a continuous flow of electrons (*41*). Interactions between cytochrome *c* and cytochrome *c* peroxidase as well as between photosystem I and cytochrome c_6 or plastocyanin have been kinetically characterized by laser flash absorption spectroscopy. The interactions exhibit very fast on and off rates ($k_{on} \sim 10^7$-10^9 M^{-1} s^{-1} and $k_{off} \geq 10^3$ s^{-1}) but the interaction is sufficiently long-lived to permit electron transfer (*41*). Transient interactions are not limited to electron transfer processes. Thioredoxin interacts weakly with ribonucleotide reductase (RNR), despite a requirement for covalent disulfide reduction of RNR after every

turnover (*42*). One of the best characterized examples of weak protein interactions involved in small molecule transfer is the phospho-relay signaling pathway required for bacterial chemotaxis.

Chemotaxis can be described as the biasing of random movement of the cell towards a higher concentration of a nutrient source (or away from a toxic chemical) (*43*). The movement bias is achieved by altering the frequency at which the flagellar motors spin counterclockwise (which results in bundling of the flagella to produce forward motion) versus clockwise motion (which disrupts the flagellar bundle and induces random tumbling) (*43*). Bacteria are too small to sense a concentration gradient along their body length; so, the chemotactic response is regulated by temporal stimulation of pole-localized transmembrane chemoreceptors. Higher nutrient concentrations result in increased frequency of receptor:metabolite interaction at the cell pole (*43*).

The best-characterized chemotactic signaling pathway is found in the Che system of *E. coli* (Figure 1.5). While the details of the pathway are too complicated to address here, the basis for chemotaxis in *E. coli* begins with interactions between the soluble CheA protein and a trans-membrane methyl-accepting chemotaxis protein (MCP). The MCP acts as a bridge linking the cytosol to nutrient conditions in the periplasm. A decrease in the number of interactions between the MCP and a nutrient binding protein (such as maltose-binding protein) in the periplasm results in a conformational change that is propogated into the cytosol and induces CheA autophosphorylation at His48. This phosphate is transferred via protein:protein complex formation to Asp57 of CheY (Figure 1.5). Phosphorylated CheY can then interact with the flagellar motor and induce clockwise rotation and cell tumbling. CheY can subsequently be dephosphorylated by interaction with CheZ.

33

$$\text{P-CheA} + \text{CheY} \underset{k_{-1}}{\overset{k_1}{\rightleftharpoons}} \text{P-CheA:CheY} \underset{k_{-2}}{\overset{k_2}{\rightleftharpoons}} \text{CheA:CheY-P} \underset{k_{-3}}{\overset{k_3}{\rightleftharpoons}} \text{CheA} + \text{CheY-P}$$

$$\text{-CheA} \Big\Updownarrow \text{+CheA}$$
$$k_{-4} \quad k_4$$

CheA:CheY
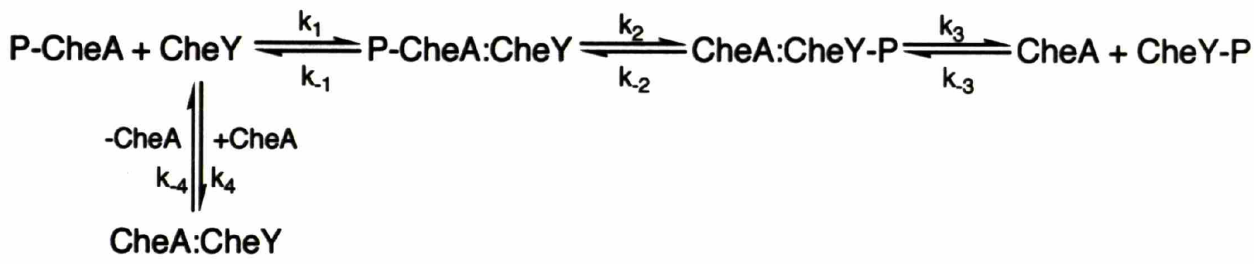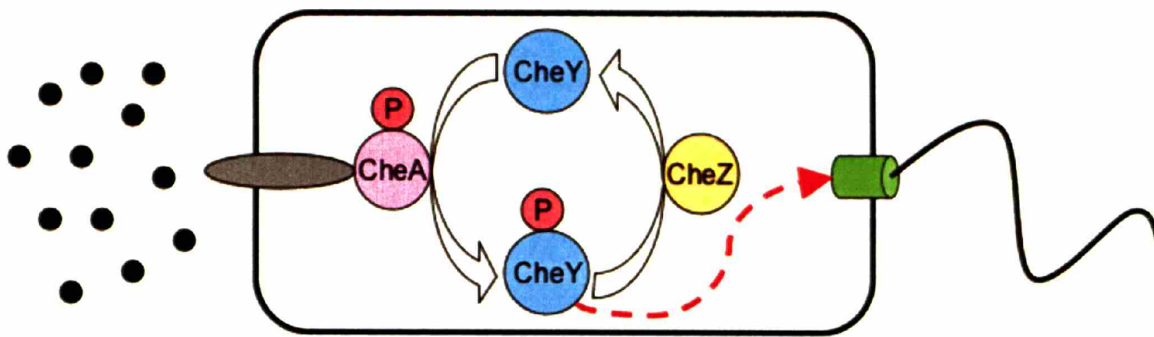
Figure 1.5—(Top) Protein components of the *E. coli* chemotaxis system. A transmembrane protein receptor (grey, also known as a methyl-accepting chemotaxis protein or MCP) senses a chemoattractant. Phosphoryl transfer from His48 of CheA to Asp57 of CheY by protein complex formation triggers accumulation of phospho-CheY, which can then interact with the flagellar motor (green) to initiate clockwise rotation. Phospho-CheY can then be dephosphorylated by CheZ. Other proteins involved in chemotactic signaling (CheB, CheW, and CheR) have been omitted for clarity. (Bottom) The kinetic scheme describing phosphoryl transfer between CheA and CheY.

The chemotactic response is remarkable for both its speed and sensitivity. For example, a chemotactic response is observed in a methylaspartate gradient of 160→163 μM despite only a minimal change in calculated receptor occupancy under these conditions (*44*). These chemotactic responses also occur very rapidly, within ~100 ms of receptor stimulation (*43*). The current model for sensitivity and speed in bacterial chemotaxis relies on signal amplification from the receptor based on kinetic control of phosphoryl transfer between the cytosolic proteins. An essential component of this model is the transient interaction between phospho-CheA (P_i-CheA) and CheY that has been characterized *in vitro* (Figure 1.5).

Rapid-chemical quench methods have been used to analyze phosphoryl transfer kinetics from $^{32}P_i$-CheA to CheY (*45*). Under these conditions, phosphoryl transfer was monitored by SDS-PAGE and phosphorimaging to detecte the phosphorylated proteins after quenching of the reaction with 0.1M EDTA/10% SDS. These experiments were complicated by dephosphorylation of the proteins during analysis; however, data could be accurately modeled after determining half-lives for the phosphoaspartate and phosphohistidine linkages of 115 ± 20 min and 1000 ± 100 min, respectively, under the analysis conditions (*45*). An alternative strategy was used to indirectly detect phosphoryl transfer: changes in CheY tryptophan fluorescence was monitored by stopped-flow spectroscopy and similar results were obtained (*46, 47*). The kinetics are remarkable for several reasons. First, saturation kinetics could be observed for the proteins with a K_m value of 6.5 ± 2 μM between P_i-CheA and CheY at 25°C (*45*). This affinity indicates that the proteins interact relatively weakly in solution, even during phosphoryl transfer. Second, under saturating conditions, the phosphoryl transfer was completed within the dead time of the quench apparatus (2.5 ms) (*45*). Therefore, rate constants for the phosphoryl transfer under saturating conditions had to be extrapolated from concentration- and temperature-

dependence studies. The value for the apparent first-order rate of phosphoryl transfer is remarkably fast, $\sim650 \pm 200$ s^{-1} at 25°C (45). Given cellular CheA and CheY concentrations of 1-5 μM and 10-20 μM, respectively, these values have been used to extrapolate an *in vivo* complex half-life of 2 ms (45).

Using advanced computer simulations, Stewart and coworkers have predicted that these rapid kinetics are essential for the bacterial chemotactic response (47). A loss of one order of magnitude in the rate of phosphoryl transfer (a decrease from ~700s^{-1} to ~70 s^{-1}) was predicted to result in an observable change in chemotaxis based on alteration of the frequency at which the flagella are expected to rotate in a clockwise direction. These predictions have been confirmed with the use of a CheA mutant enzyme that phosphorylates CheY at a 25-fold slower rate *in vitro* (47). When the mutant CheA was expressed in ΔCheA *E. coli*, cell motility was decreased by 75% in a chemotaxis assay compared to the wild-type strain (48). Visual observation of flagellar rotation confirmed that about 66% of the mutant bacteria flagella were being rotated in exclusively a counterclockwise direction (the direction not stimulated by phosphate transfer from CheA to CheY) whereas no counterclockwise movement was observed in the wild-type strain (48).

Given the transient nature of the P_i-CheA:CheY complex, obtaining evidence for the interaction was challenging but successful using a number a methods. These experiments were aided by the fact that CheY can interact with CheA independent of the presence of phosphate (K_d ~1-1.7 μM for CheA, while the K_m for P_i-CheA is ~6.5 μM) (45). Using a fluorescently-derivitized CheY, steady-state and stopped-flow fluorescence spectroscopy have demonstrated CheA and CheY binding interactions (49). Thermodynamic information about interactions between CheA and CheY has been obtained using isothermal titration calorimetry (ITC), and a

hexahistidine affinity tag on CheA was successful in enabling purification of a CheA:CheY complex (*50*). Finally, several crystal structures are available for CheA:CheY protein complexes (*51-53*). In these structures, only the CheY-binding domain of CheA (which has the same affinity for CheY as the full length protein but does not contain the phospho-histidine site) was crystallized with CheY. The hydrophobic interface buried only ~600 Å^2 from each protein. Comparison of the multiple crystal structures suggests that the interface is flexible, consistent with transient complex formation. These results indicate that the bacterial chemotaxis system is a paradigm for studies on transiently interacting proteins involved in small molecule transfer.

1.4 Protein:Protein Complexes and Purine Biosynthesis

The protein interactions illustrated by CPS and CheA:CheY have been used as models for thinking about the role protein complexes play in de novo purine biosynthesis (Scheme 1.1). In particular, the importance of protein complexes in channeling unstable metabolites has been of long-standing interest in the Stubbe Laboratory, and purine biosynthesis has been used as a paradigm for understanding metabolism of unstable intermediates such as phosphoribosylamine (PRA, $t_{1/2}$ *in vivo* ~ 5 s) and N^5-carboxyaminoimidaxole ribonucleotide (N^5-CAIR, $t_{1/2}$ *in vivo* ~ 15 s). The channeling of PRA between *E. coli* phosphoribosylpyrophosphate amidotransferase (PurF) and glycinamide ribonucleotide synthetase (PurD), the first two enzymes in the pathway (Scheme 1.1), has been investigated for a number of years. Like the CheA:CheY phosphotransfer complex, this channeling interaction is expected to be transient in nature. In Chapter 2 of this thesis, efforts are reported to detect complex formation between PurF and PurD by stopped-flow fluorescence spectroscopy.

The presence of two ATs in the pathway (PurF and PurL/PurSQL) affords additional opportunities to study protein complexes involved in channeling. Like all ATs, these enzymes

are proposed to channel NH_3 between glutaminase and AT active sites. The remainder of the thesis will describe efforts to characterize the *B. subtilis* formylglycinamide ribonucleotide amidotransferase (FGAR-AT). This enzyme is a member of the triad family AT enzymes and is composed of a protein complex of PurS, PurQ, and smPurL. Initially, the complex was presumed to be tight as in the cases of CPS and other AT enzymes. However, the data now indicate that tight complex formation is mediated by the presence of metabolites and weak protein interactions may be critical for transient NH_3-channel formation between two active sites.

1.5 Channeling of PRA between PurF and PurD

PurF catalyzes the incorporation of NH_3 released from glutamine hydrolysis into PRPP (Scheme 1.1). While PRA was assumed to be the product of PurF for many decades, the extreme lability of the molecule hampered its characterization. The first experimental evidence for PRA synthesis by PurF came from ^{13}C NMR studies (54). Using 40 μmol of $[1-^{13}C]$- PRPP, an α/β mixture of PRA was formed in the presence of 200 U of PurF and glutamine after 4 min and rapidly decomposed to ribose-5'-phosphate after 10 min. Subsequent saturation- and inversion-transfer NMR experiments allowed determination of the rate constants for PRA anomerization which result in rapid formation of a 60:40 mixture of β:α anomers. The rate of PRA decomposition was studied by using an excess of PurD (glycinamide ribonucleotide synthetase, Scheme 1.1) to convert available PRA to GAR (glycinamide ribonucleotide), a stable compound that can be readily isolated (54). The k_{decomp} was found to be 7.0 x 10^{-4} s^{-1} at pH 8.0 and 18°C. Temperature- and pH-dependence studies on the decomposition rate allowed extrapolation to physiological conditions. These results indicated that PRA half-life *in vivo* (pH 7.5, 37°C) is ~ 5 s.

Given this short half-life, it was postulated that PRA could undergo significant decomposition *in vivo* if it were allowed to freely diffuse between PurF and PurD. A model was proposed in which the PurF•PRA complex interacts transiently with PurD in order to channel PRA and avoid metabolite decomposition. Work by Johannes Rudolph in the Stubbe Laboratory provided steady state kinetic analysis of evidence for channeling of PRA (55). As an initial step in Rudolph's experiments, a free diffusion model (Scheme 1.2) was generated to describe the rate of GAR formation from PRPP by PurF and PurD in a standard coupled assay involving two enzymes and assuming no channeling of PRA.

While the steady state parameters for PRA formation (V_1, PurF activity) and decomposition (k_{decomp}) were easily determined, the parameters for PurD were more difficult to obtain. In order to assay PurD activity, PRA is typically synthesized as an α/β mixture in equilibrium with ribose-5'-phosphate in 1 M NH_4OH. This limits the amount of PRA that can be added to an assay solution without altering pH. Analysis of initial velocity data revealed that PurD exhibits substrate inhibition with PRA ($K_i = 670~\mu M$), which further complicates determination of the K_m for PRA and V_2 (V_{max} for PurD); however, these data could be modeled by fits to standard equations for substrate inhibition. By using parameters obtained for the enzymes and PRA decomposition, a kinetic model for the rate of GAR formation was constructed based upon a standard coupled assay. This model revealed that if a small amount of PurD is added to the assay (which results in a low V_2), the rate of GAR formation will not be coupled to the rate of PRA synthesis by PurF. This would result in an observable lag phase in the rate of GAR synthesis (Figure 1.6).

$$\text{PRPP} \xrightarrow{\text{V}_1} \text{PRA} \xrightarrow{\text{K}_m, \text{V}_2} \text{GAR}$$

$$\text{PRA} \xrightarrow{\text{k}_{\text{decomp}}} \text{R5P}$$
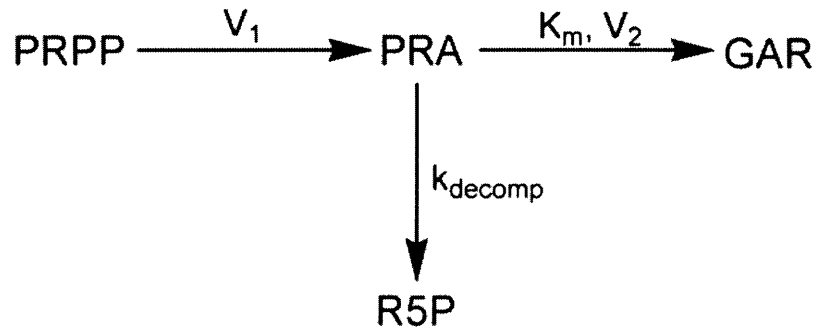
Scheme 1.2—A kinetic scheme for modeling GAR formation from PRPP in a standard coupled assay with PurF and PurD. PRA synthesis is dependent on the PurF reaction velocity (V_1); while GAR formation is dependent on both the PRA concentration (K_m) and PurD reaction velocity (V_2). In addition, a significant portion of PRA will be decomposing to ribose 5'-phosphate (R5P) during the experiment at a constant rate (k_{decomp}).

When experiments were carried out using small amounts of PurD, the rate of GAR

formation observed by Rudolph was inconsistent with the free diffusion model (55). No lag

phase was observed, and the amount of GAR produced significantly exceeded predictions made

from the model (Figure 1.6). Error analysis of the parameters in the free diffusion model (V_1, V_2,

and $K_{m(PRA)}$) indicated that their simultaneous variation by 20% could not account for the

observed kinetics. In addition, this behavior was found to be dependent on both the ratio of PurF

to PurD and the total protein concentration, properties expected for involvement of a

protein:protein interaction (56). Together the data were interpreted to indicate that PRA is being

channeled between PurF and PurD through their transient interactions.

Previous studies to look for interaction between PurF and PurD involved size-exclusion

chromatography (SEC) and co-immunoprecipitation (co-IP), both of which require tight

interactions. No evidence for an interaction could be found with either of these techniques.

However, methods that should report on weaker interactions such as protein-affinity

chromatography, cross-linking in crude extracts and with purified proteins, and steady-state

fluorescence were also unsuccessful. The cross-linking and steady-state fluorescence data were

particularly striking since these experiments were carried out in the presence of PRA. Thus

despite the use of different methods to detect interactions on different time-scales (Table 1.2), no

evidence for a PurF:PurD interaction was found. This provided further evidence that the

enzymes are interacting transiently in solution and that the techniques listed in Table 1.2 did not

have sufficient temporal resolution to detect complex formation.

The requirement for a specific PurF•PRA protein complex as the docking partner for

PurD in the channeling model also requires that PurF undergoes conformational changes during
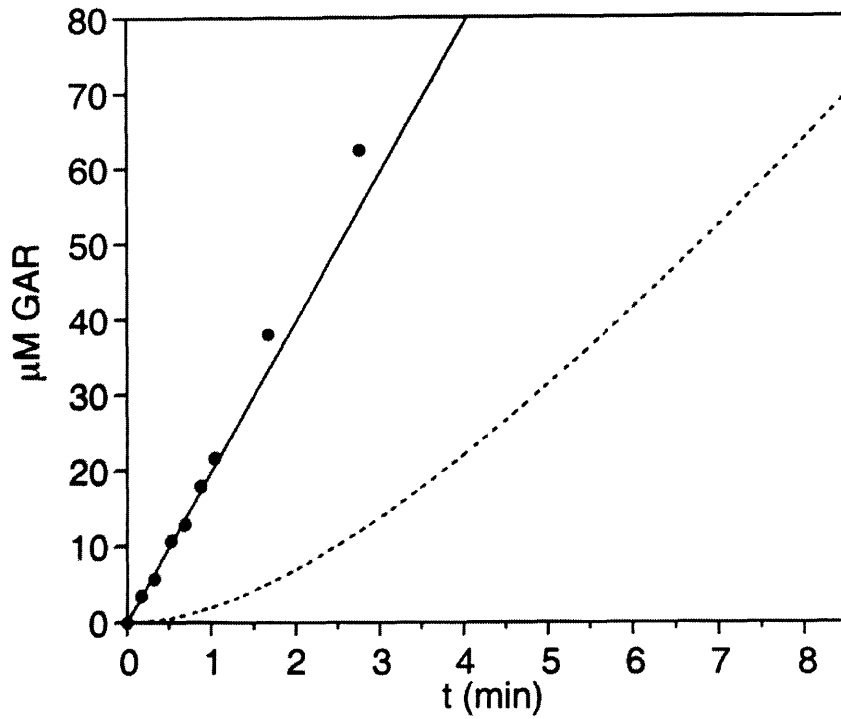
$V_1 = 20\ \mu M/min \quad V_2 = 24\ \mu M/min \quad K_{m,PRA} = 98\ \mu M$

Figure 1.6—Kinetic evidence for PRA channeling obtained by Rudolph and Stubbe. The observed rate of GAR formation (solid line) is linear and exceeds that predicted from diffusion-modeled kinetics for a standard coupled assay (dashed line).

Table 1.2: Techniques Previously Used in Efforts to Detect a PurF:PurD Complex

Technique	Ligands Utilized	Time-Scale	Temperature
Gel Filtration Chromatography	None	Hours	4°C
Co-Immunoprecipitation	1.7 mM PRA, 20 mM Gln, 3 mM ATP	~15 min	0°C
Protein Affinity Chromatography	None	~20 h	4°C
Steady-State Fluorescence	2 mM PRPP, 0.1-2 mM PRA, 10 mM Gln, 1 mM ATP	Minutes	25°C
Cross-linking of Purified Proteins	2 mM PRPP, 0.1-2 mM PRA, 10 mM Gln, 1 mM ATP	0.5-2 h[a]	25°C
Cross-linking in Cell Lysates	2 mM PRPP, 0.1-2 mM PRA, 10 mM Gln, 1 mM ATP	0.5-2 h[a]	25°C

[a]This represents the amount of time that the proteins were exposed to the cross-linking reagents and not the rates of the chemical steps for cross-linking. Since the cross-linking was irreversible, it was expected that a cross-linked product would accumulate in solution over time.

catalysis. Structure determination of the *E. coli* PurF by X-ray crystallography has provided evidence for conformational flexibility (Figure 1.7). Structures of the apo form and "closed" form in the presence of 6-diazo-5-oxonorleucine (DON, a glutamine analog that alkylates the catalytic cysteine present in glutaminase domains) and a carbocyclic analog of PRPP (cPRPP, which also contained Mn^{2+} as a metal ligand) indicated that movements occur in the glutamine-binding loop (blue), PRTase flexible loop (yellow), and the C-terminal helix (green) (Figure 1.7) (*31, 57*). This structural reorganization is believed to be necessary to create an NH_3-channel between the glutaminase and the AT active sites. Additional evidence for conformational flexibility of these loops has been obtained by studying fluorescence changes in PurF upon substrate binding in both the pre-steady and steady state (*32*). These loop movements are discussed in greater detail in Chapter 2. The structure of a PurF•product complex remains unknown.

Open   Closed
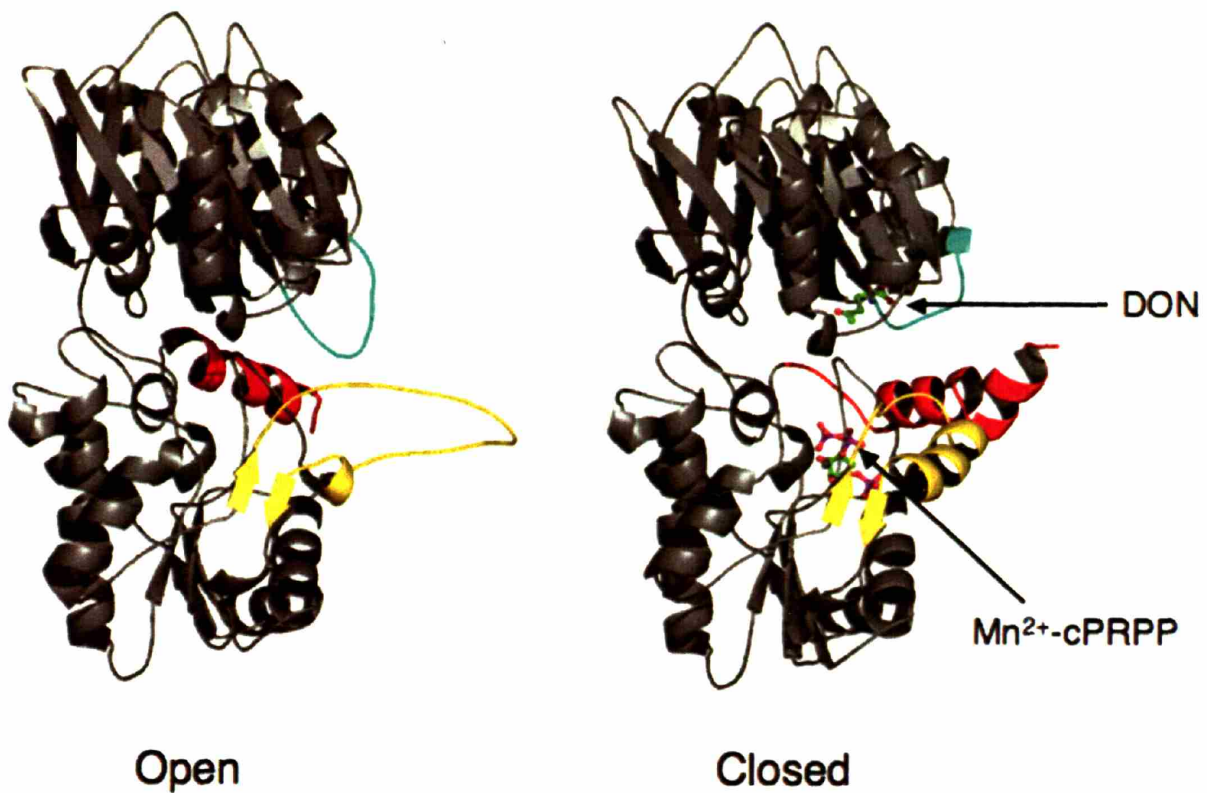
Figure 1.7—X-ray crystallographic studies have shown that upon binding of PRPP and glutamine analogs, PurF goes from an open (1ecb.pdb) to a closed conformation (1ecc.pdb). The PRTase flexible loop (yellow), glutamine-binding loop (teal), and C-terminal helix (red) all undergo large conformational changes. The DON-adduct and cPRPP analog are shown in ball-and-stick representation in the closed structure.

Determination of the crystal structure of apo-*E. coli* PurD by the Ealick laboratory afforded the

opportunity to produce a model for interactions between PurF and PurD (*58*). The structure of

PurD revealed that it is a member of the ATP-Grasp superfamily of enzymes that all utilize acyl-

phosphate intermediates during ATP-dependent amide bond formation (*59*). Analysis of the

crystal structures of the *E. coli* PurF (closed form) and apo-PurD indicated that a docking model

could be constructed that aligns the enzyme active sites (Figure 1.8) (*58*). This model was based

on the observed shape and charge complementarity between the structures. Another central

feature of this model is that the proposed protein interface is comprised of the PurF mobile loops

(Figure 1.9). It was proposed that movement of these loops (specifically the PRTase flexible

loop) during complex formation with PurD leads to PRA channeling.

In Chapter 2, stopped-flow fluorescence spectroscopy has been utilized to provide direct

evidence for transient protein-protein interactions between PurF and PurD. Unlike the methods

listed in Table 1.2, stopped-flow fluorescence spectroscopy can be used to detect transient

interactions during which the complex half-life may be on the order of milliseconds.

Fluorescence reporters site-specifically incorporated into each of the PurF mobile regions have

been examined for changes occurring upon complex formation with PurD. With the use of a 3-

syringe stopped-flow apparatus, interactions between PurF and PurD during PRA synthesis in

the pre-steady state were probed. The success of these experiments hinged upon a dual-labeling

strategy in which tryptophans in PurF and PurD were replaced with unnatural amino acids.

Fluorescence from PurD was reduced by incorporation of 4-fluorotryptophan (4FW) and

additional specificity for PurF fluorescence was gained by incorporation of 7-azatryptophan

(7AW) to monitor fluorescence at $\lambda > 360$ nm. No interactions between PurF and PurD were
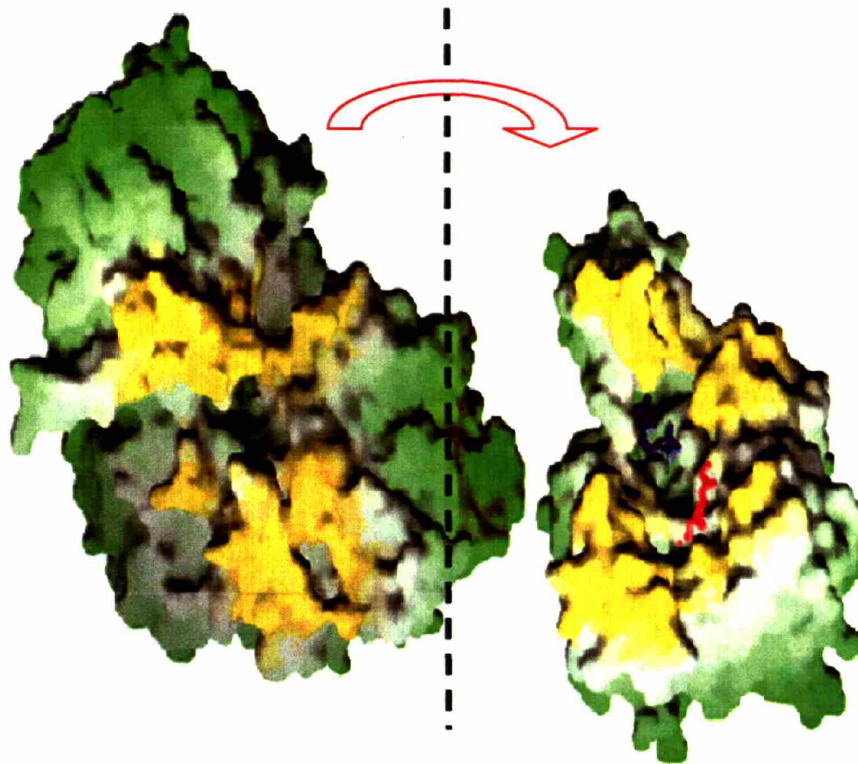
Figure 1.8—The PurF dimer (left) and PurD monomer (right) docking model proposed by the Ealick and Stubbe laboratories. In this view, the docking model has been splayed open along the vertical page axis. Yellow regions on PurF and PurD are proposed to be in contact. Symmetry within the PurF dimer leads to 2 binding sites for PurD, but only one is shown in the figure for clarity. Models for ATP (blue) and GAR (red) are shown in PurD to define the active site.
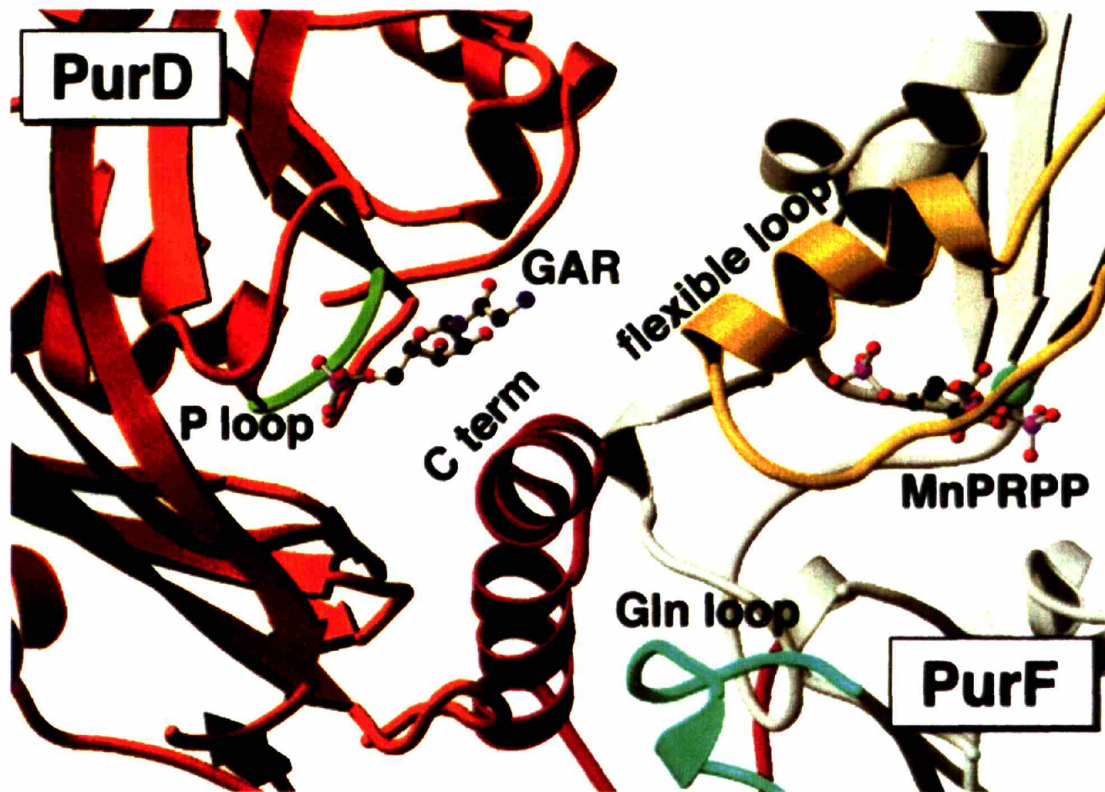
Figure 1.9—In the PurF:PurD docking model, the active sites of PurF (grey) and PurD (red-orange) are proposed to be in contact. The active site of PurF is noted by the substrate analog from the crystal structure (Mn^{2+}-cPRPP). The active site is covered by the PurF mobile loops (the glutamine loop (residues 73-85, teal), the flexible loop (residues 327-350, yellow), and the C-terminal helix (residues 470-499, red)). The location of the PurD active site is shown by a modeled GAR substrate and the partially disordered, ATP-binding P-loop (green).

detected in the pre-steady state using this strategy. The implication of these findings with regard

to the validity of the docking model, transient protein:protein interactions, and PRA channeling

is discussed in detail.

1.6 The B. subtilis FGAR-AT Protein Complex

The fourth step in purine biosynthesis (Scheme 1.1) is carried out by a triad-class AT

enzyme that catalyzes the glutamine- and ATP-dependent conversion of an amide

(formylglycinamide ribonucleotide, FGAR) to an amidine (formyglycinamidine ribonucleotide,

FGAM), ADP, P_i, and glutamate. Searching for *purL* equivalents in diverse genomes has

revealed that this reaction is carried out in different organisms by one of two related enzymes

(Figure 1.10). Gram-negative bacteria and eukaryotes contain a large PurL (lgPurL, ~140 kDa)

that is composed of 4 domains. The N-terminal domain occupies the first ~150 amino acids and

is not homologous to any known protein motif. The middle ~800 amino acids contain two

homologous regions similar to PurM, an enzyme that catalyzes the fifth step of purine

biosynthesis (Scheme 1.1). The C-terminal ~220 amino acids contain a typical triad glutaminase

domain.

Analysis of the purine operon in *B. subtilis* by Zalkin and Nygaard indicated that instead

of one large enzyme, FGAM formation is carried out by a multi-protein complex composed of 3

proteins (Figure 1.10) (*60*). In *B. subtilis*, the smPurL enzyme (~750 amino acids) is

homologous to the central region of lgPurL, and PurQ (~220 amino acids) is a triad glutaminase.

No protein could be found with sequence homology to the N-terminal domain of lgPurL;

however, an *orf* was found in the purine operon near the *smpurL* and *purQ* genes. Genetic

disruption of this *orf* in *B. subtilis* created a purine auxotroph and subsequent analysis indicated

that the protein encoded by this gene (~80 amino acids) was necessary for FGAM

Large PurL (lgPurL)-Gram negative, *Salmonella*
1295 aa

N-terminal Domain

PurM-Like Domain 1 Active Site

PurM-Like Domain 2

Triad Glutaminase
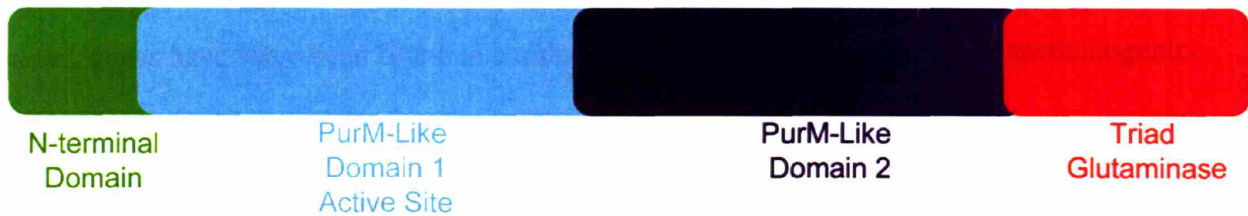
Small PurL (smPurL)-Gram positive, *B. subtilis*
742 aa

PurM-Like Domain 1 Active Site

PurM-Like Domain 2

PurS 84 aa

No Sequence Homology

PurQ 225 aa Triad Glutaminase
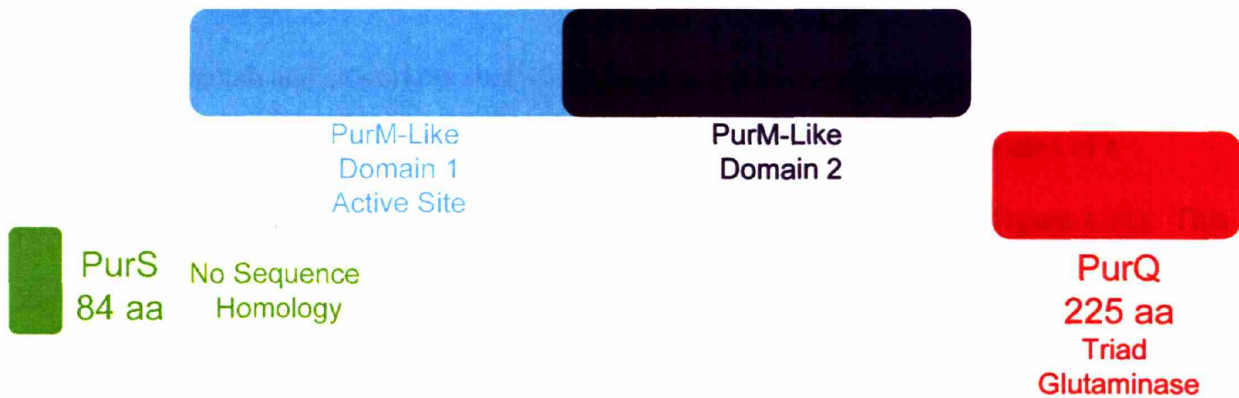
Figure 1.10—Alignments between lgPurL and smPurL, PurQ, and PurS proteins. Sequence analysis suggests that the lgPurLs contain 4 domains. In *B. subtilis*, smPurL is analogous to the central PurM-like domains. PurQ is highly homologous to the C-terminal triad glutaminase domain. PurS has no sequence homology to any domain of lgPurL and is half the size of the N-terminal domain.

formation (*61*). The gene has since been renamed *purS*, and PurS, PurQ, and smPurL were proposed to carry out FGAM formation in an FGAR-AT complex (*61*). The *purS, purQ,* and *smpurL* genes have since been found in a number of Gram-positive, archae, and methanogenic bacteria (*61*).

Prior to the work presented in this thesis, FGAM synthesis has been biochemically characterized exclusively in lgPurLs from *E. coli, Salmonella,* and chicken liver by the Buchanan and Stubbe laboratories. The previous work focused primarily on the mechanism of FGAM formation. Buchanan and coworkers studied in great detail the glutaminase activity and reaction stoichiometry of the enzyme. Much of this work stemmed from one of the first uses of a mechanism-based inhibitor in enzymology, azaserine (O-diazoacetyl-L-serine, Figure 1.11). This glutamine analog stoichiometrically labeled the glutaminase domain of the enzyme on a cysteine (Figure 1.11) (*62*). These studies led Buchahan to the hypothesis that a covalently bound glutamylthioester was directly involved in release of NH_3 and subsequently hydrolyzed to form glutamate. In addition, Buchanan was also able to determine that glutaminase and ATPase activities were coupled in the chicken liver enzyme such that one ADP and one glutamate were produced during each round of FGAM synthesis (*63*).

While Buchanan's work indicated ADP and P_i are produced during every turnover, the identities of any phosphorylated intermediates have remained elusive. In 1980, Westheimer proposed that the enzyme may proceed either by a tetrahedral intermediate generated by NH_3 attack on the amide followed by phosphorylation or by an iminophosphate mechanism, with the latter being the favored and more thermodynamically stable intermediate (Figure 1.12) (*64*). Intriguingly, the same types of mechanisms can be drawn for the PurM-catalyzed reaction (Figure 1.13). The observation of sequence homology between

50
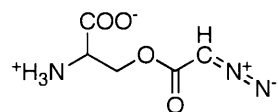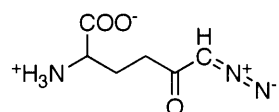
Azaserine

DON
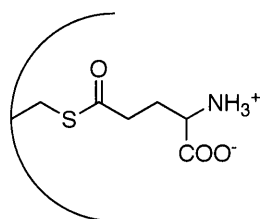
Glutamylthioester (GTE)
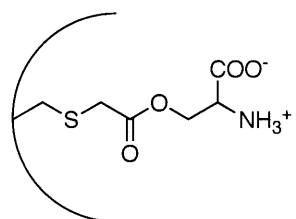
Azaserine Adduct

Figure 1.11—(Top) Structures of the common glutaminase inhibitors azaserine and DON. (Bottom) These inhibitors inactivate the glutaminase by alkylating the catalytic sulfhydryl group to form a stable mimic of a glutamylthioester.
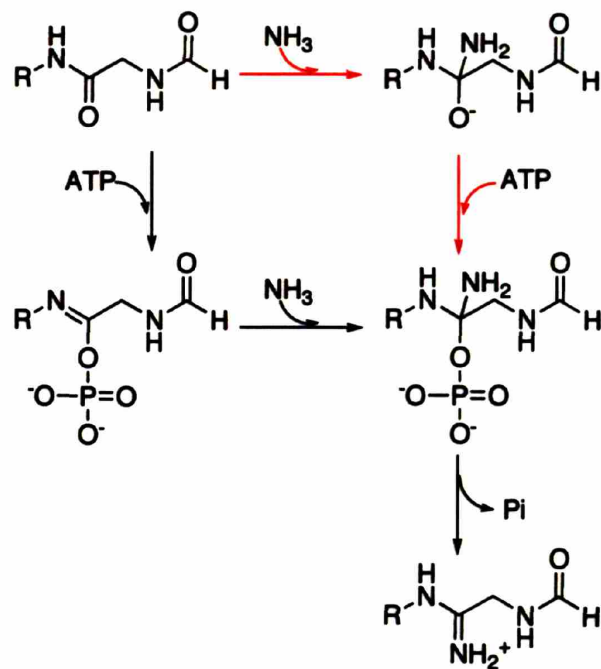
Figure 1.12—Proposed reaction mechanisms for PurL by Westheimer *(64)*. The reaction is believed to proceed either through an iminophosphate intermediate (black arrows) or a tetrahedral intermediate (red arrows). Buchanan has also postulated that the mechanism may involve a phosphorylated-enzyme intermediate (not shown) during phosphate transfer from ATP to FGAR.

PurL and PurM indicated that both enzymes may utilize similar structures to carry out a common set of chemical transformations (20).

Significant efforts to find evidence for a phosphorylated intermediate during PurL or PurM catalysis were carried out by Ernie Mueller in the Stubbe Laboratory (65). Rapid chemical quench measurements, positional isotope exchange (PIX), and ADP/ATP exchange experiments all failed to identify a phosphorylated intermediate in either enzyme. Insight into these reactions was subsequently sought from X-ray crystallography studies, and the structure of E. coli PurM was determined in 1999 by the Ealick and Stubbe Laboratories (66). PurM proved to possess a novel structure and was the founding member of a new superfamily of ATP-binding enzymes that also includes PurL. Unfortunately, due to uncertainties surrounding substrate binding and the inability to co-crystallize either substrates or products with the enzyme, structural clues to the reaction mechanism were difficult to obtain.

Given the limited success in understanding the mechanism or structure of the lgPurLs, a new research direction for this step in purine biosynthesis was sought by focusing on the smPurLs. Chapter 3 describes the first biochemical characterization of an FGAR-AT complex composed of PurS, PurQ, and smPurL. Contrary to expectations, a complex of recombinant B. subtilis PurS, PurQ, and smPurL could not be co-purified even when the proteins were co-expressed in E. coli. The inability to isolate a protein complex indicated that unlike CPS and most other AT enzymes, the FGAR-AT complex may be characterized by weak protein interactions. By reconstituting activity from separately purified proteins, it was determined that PurS was necessary for glutamine, but not NH_3-dependent FGAM synthesis. Protein titrations revealed that the stoichiometry of the FGAR-AT complex consisted of 2 PurS: 1 smPurL: 1 PurQ. Surprisingly, a tight FGAR-AT complex could only be isolated by analytical size
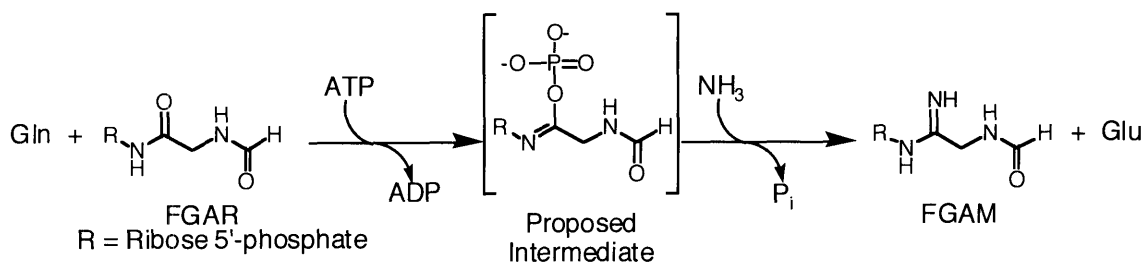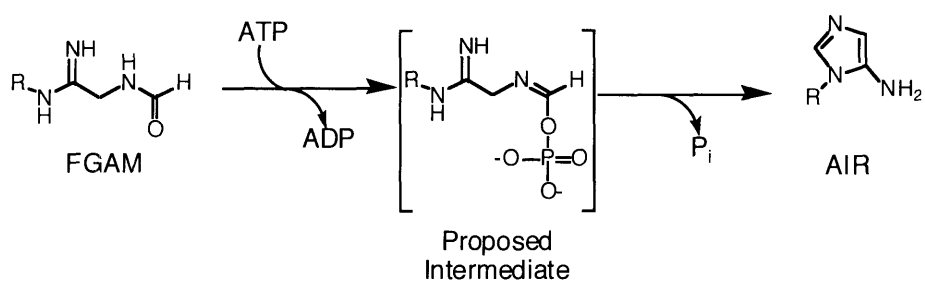
Figure 1.13—Proposed reactions and common iminophosphate intermediates proposed for FGAR-AT (PurL) and AIR synthetase (PurM).

exclusion chromatography in the presence of glutamine and Mg^{2+}-ADP. The role of ADP, a

product of the FGAM synthesis, was not clear until the crystal structure of the *Salmonella* lgPurL

enzyme was solved by the Ealick Laboratory (Figure 1.14) (*67*). This structure indicated that

ADP was not binding in the enzyme active site but appeared to function as a structural cofactor.

The remaining chapters of the thesis explore the structure-function relationship between

the *Salmonella* lgPurL and the *B. subtilis* FGAR-AT. The *Salmonella* lgPurL structure revealed

that it is a multi-domain enzyme composed of an N-terminal domain (residues 1-140), a linker

region (141-214), a central domain containing the active and ADP-binding sites (215-979), and a

triad glutaminase domain (980-1295). One of the most intriguing aspects of the structure was the

N-terminal domain, which appears to link the glutaminase and FGAM-synthetase active sites.

This domain is connected to the body of the enzyme by a long linker region (18 amino acids),

suggesting that it is conformationally flexible. Finally, its location suggested that it may form, in

part, the NH_3-tunnel that connects the two active sites.

The crystal structure of *B. subtilis* PurS presented in Chapter 4 revealed that the PurS

dimer is a structural homolog to the N-terminal domain despite the absence of sequence

homology (*68*). Thus PurS, like the N-terminal domain of lgPurL, may be involved in NH_3-

channel formation. In addition, PurS appeared as a tetramer in two different crystal structures,

and homology modeling revealed that the *B. subtilis* FGAR-AT complex could be composed of

the initially proposed 2 PurS: 1 smPurL: 1 PurQ complex or a 4:2:2 complex. Chapter 4

describes biophysical experiments designed to determine the quaternary structure of PurS and the

FGAR-AT complex in solution.
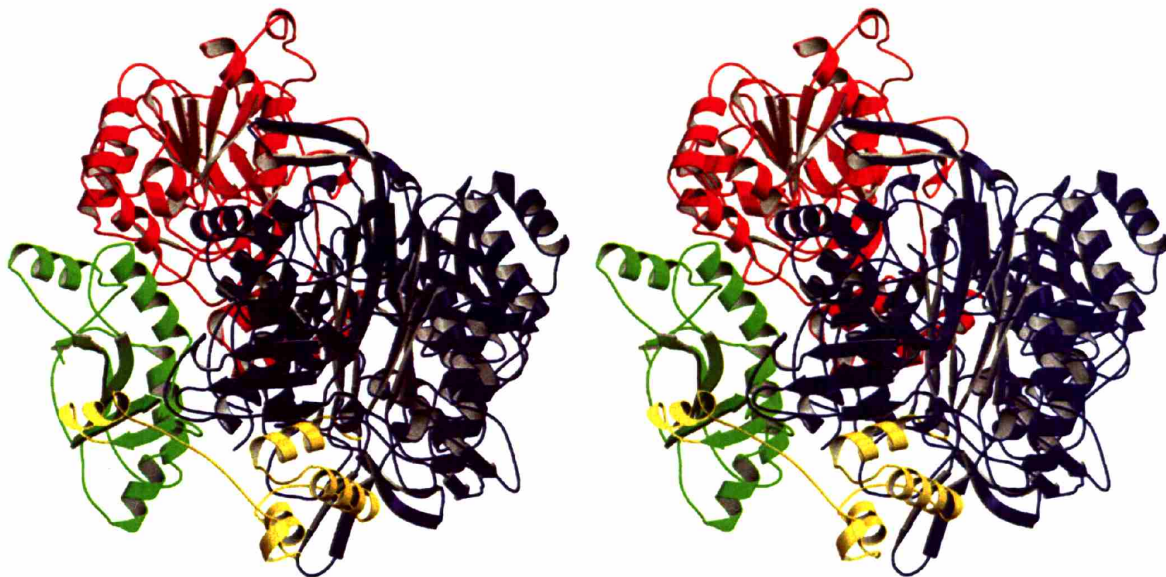
Figure 1.14—Stereoview of the crystal structure of the *Salmonella* lgPurL.The four domains of the enzyme are shown in green (the N-terminal domain), yellow (the linker domain), blue (the central domain containing the active and ADP-binding sites), and red (the triad glutaminase domain).

Chapter 5 focuses on the glutamine-binding properties of PurQ and their impact in FGAR-AT complex formation. PurQ is highly homologous to the glutaminase domain of the *Salmonella* lgPurL (28% identity). Based on the structure of a glutamylthioester observed in the *Salmonella* lgPurL glutaminase active site, site-directed mutagenesis was carried out on conserved residues in PurQ involved in glutamine hydrolysis. FGAR-AT complex formation was then studied by competing the mutant and wild-type PurQs with one another and monitoring glutamine-dependent FGAM synthesis. Together with results obtained during efforts to affinity purify the FGAR-AT complex from *B. subtilis*, these experiments provide additional evidence for the importance of glutamine-binding in complex formation.

The final chapter of this thesis focuses on smPurL and the FGAM synthetase active site. The *T. maritima* smPurL enzyme was cloned, purified, and assayed for NH$_4$Cl-dependent FGAM synthesis. The crystal structure of the apo-enzyme was determined by the Joint Center for Structural Genomics (JCSG) and allowed the determination of several structures in the presence of FGAR, ADP, ATP, and both FGAR and a non-hydrolyzable ATP analog (AMP-PCP) by Maria Morar and Ruchi Anand in the Ealick Laboratory by molecular replacement. These results provided the first insights into the mechanisms of substrate-binding by members of the PurM-superfamily of enzymes. Site-directed mutagenesis of *T. maritima* smPurL and activity assays of the generated mutants confirmed the importance of conserved histidine residues within the active site. These results provided new details concerning the mechanisms of catalysis by PurLs and other members of the PurM-superfamily.

1.7 REFERENCES

(1)   Goodsell, D. S. (1991) Inside a living cell. *TIBS 16*, 203-206.

(2)   Zimmerman, S. B., and Minton, A. P. (1991) Estimation of macromolecule concentrations and excluded volume effects for the cytoplasm of Escherichia coli. *J. Mol. Biol. 222*, 599-620.

(3)   Verkman, A. S. (2002) Solute and macromolecule diffusion in cellular aqueous compartments. *TIBS 27*, 27-33.

(4)   Kao, H. P., Abney, J. R., and Verkman, A. S. (1993) Determinants of the Translational Mobility of a Small Solute in Cell Cytoplasm. *J. Cell Biol. 120*, 175-184.

(5)   Swaminathan, R., Hoang, C. P., and Verkman, A. S. (1997) Photobleaching Recovery and Anisotropy Decay of Green Fluorescent Protein GFP-S65T in Solution and Cells: Cytoplasmic Viscosity Probed by Green Fluorescent Protein Translational and Rotational Diffusion. *Biophysical J. 72*, 1900-1907.

(6)   Haggie, P. M. and Verkman, A. S. (2002) Diffusion of tricarboxylic acid cycle enzymes in the mitochondrial matrix in vivo. Evidence for restricted mobility of a multienzyme complex. *J. Biol. Chem. 277*, 40782-40788.

(7)   Ellis, R. J. (2001) Macromolecular crowding: obvious but underappreciated. *TIBS 26*, 597-604.

(8)   Minton, A. P. (2001) The Influence of Macromolecular Crowding and Macromolecular Confinement on Biochemical Reactions in Physiological Media. *J. Biol. Chem. 276*, 10577-10580.

(9)   Lonhienne, T. G. and Winzor, D. J. (2002) Calorimetric demonstration of the potential of molecular crowding to emulate the effect of an allosteric activator on pyruvate kinase kinetics. *Biochemistry 41*, 6897-6901.

(10)   Lonhienne, T. G. and Winzor, D. J. (2001) Interpretation of the reversible inhibition of adenosine deaminase by small cosolutes in terms of molecular crowding. *Biochemistry 40*, 9618-9622.

(11)   Wenner, J. R. and Bloomfield, V. A. (1999) Crowding effects on EcoRV kinetics and binding. *Biophysical J. 77*, 3234-3241.

(12)   Welch, G. R. and Easterby, J. S. (1994) Metabolic channeling versus free diffusion: transition-time analysis. *TIBS 19*, 193-197.

(13)   Maddock, J. R. and Shapiro, L. (1993) Polar location of the chemoreceptor complex in the *Escherichia coli* cell. *Science 259*, 1717-23.

(14)   Ryan, K. R., and Shapiro, L. (2003) Temporal and spatial regulation in prokaryotic cell cycle progression and development. *Annu Rev Biochem 72*, 367-94.

(15)   Viollier, P. H., Thanbichler, M., McGrath, P. T., West, L., Meewan, M., McAdams, H. H., and Shapiro, L. (2004) Rapid and sequential movement of individual chromosomal loci to specific subcellular locations during bacterial DNA replication. *Proc. Natl. Acad. Sci. U. S. A. 101*, 9257-62.

(16)   Gitai, Z., Dye, N. A., Reisenauer, A., Wachi, M., and Shapiro, L. (2005) MreB actin-mediated segregation of a specific region of a bacterial chromosome. *Cell 120*, 329-41.

(17)   van den Ent, F., Amos, L. A., and Lowe, J. (2001) Prokaryotic origin of the actin cytoskeleton. *Nature 413*, 39-44.

(18)   Wachi, M., Doi, M., Tamaki, S., Park, W., Nakajima-Iijima, S., and Matsuhashi, M. (1987) Mutant isolation and molecular cloning of *mre* genes, which determine cell shape,

sensitivity to mecillinam, and amount of penicillin-binding proteins in *Escherichia coli*. *J. Bacteriol. 169*, 4935-4940.

(19) Shih, Y. L., Le, T., and Rothfield, L. (2003) Division site selection in *Escherichia coli* involves dynamic redistribution of Min proteins within coiled structures that extend between the two cell poles. *Proc. Natl. Acad. Sci. U. S. A. 100*, 7865-7870.

(20) Kappock, T. J., Ealick, S. E., and Stubbe, J. (2000) Modular evolution of the purine biosynthetic pathway. *Curr. Opin. Chem. Biol. 4*, 567-72.

(21) Khorana, H. G., Fernandes, J. F., and Kornberg, A. (1957) Phosphorylation of Ribose 5-Phosphate in the Enzymatic Synthesis of 5-Phosphorylribose 1-Pyrophosphate. *J. Biol. Chem. 230*, 941-948.

(22) Meola, M., Yamen, B., Weaver, K., and Sandwick, R. K. (2003) The catalytic effect of Mg^{2+} and imidazole on the decomposition of 5-phosphoribosyl-α-1-pyrophosphate in aqueous solution. *J. Inorg. Biochem. 93*, 235-242.

(23) Huang, X., Holden, H. M., and Raushel, F. M. (2001) Channeling of substrates and intermediates in enzyme-catalyzed reactions. *Annu. Rev. Biochem. 70*, 149-80.

(24) Allen Jr., C. M. and Jones, M. E. (1964) Decomposition of Carbamylphosphate in Aqueous Solutions. *Biochemistry 3*, 1238-1247.

(25) James, C. L. and Viola, R. E. (2002) Production and Characterization of Bifunctional Enzymes. Substrate Channeling in the Aspartate Pathway. *Biochemistry 41*, 3726-3731.

(26) Nogaj, L. A. and Beale, S. I. (2005) Physical and kinetic interactions between glutamyl-tRNA reductase and glutamate-1-semialdehyde aminotransferase of *Chlamydomonas reinhardtii*. *J. Biol. Chem. 280*, 24301-7.

(27) Luer, C., Schauer, S., Mobius, K., Schulze, J., Schubert, W. D., Heinz, D. W., Jahn, D., and Moser, J. (2005) Complex formation between glutamyl-tRNA reductase and glutamate-1-semialdehyde 2,1-aminomutase in *Escherichia coli* during the initial reactions of porphyrin biosynthesis. *J. Biol. Chem. 280*, 18568-72.

(28) Ovádi, J. (1991) Physiological Significance of Metabolic Channeling. *J. Theor. Biol. 152*, 1-22.

(29) Zalkin, H. and Smith, J. L. (1998) Enzymes utilizing glutamine as an amide donor. *Adv. Enzymol. Relat. Areas. Mol. Biol. 72*, 87-144.

(30) Raushel, F. M., Thoden, J. B., and Holden, H. M. (1999) The amidotransferase family of enzymes: molecular machines for the production and delivery of ammonia. *Biochemistry 38*, 7891-9.

(31) Krahn, J. M., Kim, J. H., Burns, M. R., Parry, R. J., Zalkin, H., and Smith, J. L. (1997) Coupled formation of an amidotransferase interdomain ammonia channel and a phosphoribosyltransferase active site. *Biochemistry 36*, 11061-8.

(32) Chen, S., Burgner, J. W., Krahn, J. M., Smith, J. L., and Zalkin, H. (1999) Tryptophan fluorescence monitors multiple conformational changes required for glutamine phosphoribosylpyrophosphate amidotransferase interdomain signaling and catalysis. *Biochemistry 38*, 11659-69.

(33) Bera, A. K., Smith, J. L., and Zalkin, H. (2000) Dual role for the glutamine phosphoribosylpyrophosphate amidotransferase ammonia channel. Interdomain signaling and intermediate channeling. *J. Biol. Chem. 275*, 7975-9.

(34) Trotta, P. P., Burt, M.E., Haschemeyer, R.H., and Meister, A. (1971) Reversible Dissociation of Carbamyl Phosphate Synthetase into a Regulated Synthesis Subunit and a

Subunit Required for Glutamine Utilization. *Proc. Natl. Acad. Sci. U. S. A. 68*, 2599-2603.

(35)   Matthews, S. L. and Anderson, P. M. (1972) Evidence for the Presence of Two Nonidentical Subunits in Carbamyl Phosphate Synthetase of *Escherichia coli*. *Biochemistry 11*, 1176-1183.

(36)   Trotta, P. P., Pinkus, L. M., Haschemeyer, R. H., and Meister, A. (1974) Reversible Dissociation of the Monomer of Glutamine-dependent Carbamyl Phosphate Synthetase into Catalytically Active Heavy and Light Subunits. *J. Biol. Chem. 249*, 492-499.

(37)   Thoden, J. B., Holden, H. M., Wesenberg, G., Raushel, F. M., and Rayment, I. (1997) Structure of carbamoyl phosphate synthetase: a journey of 96 Å from substrate to product. *Biochemistry 36*, 6305-16.

(38)   Thoden, J. B., Raushel, F. M., Benning, M. M., Rayment, I., and Holden, H. M. (1999) The structure of carbamoyl phosphate synthetase determined to 2.1 Å resolution. *Acta Crystallogr. D Biol. Crystallogr. 55 (Pt 1)*, 8-24.

(39)   Miles, B. W. and Raushel, F. M. (2000) Synchronization of the three reaction centers within carbamoyl phosphate synthetase. *Biochemistry 39*, 5051-6.

(40)   Mullins, L. S. and Raushel, F. M. (1999) Channeling of Ammonia through the Intermolecular Tunnel Contained within Carbamoyl Phosphate Synthetase. *J. Amer. Chem. Soc. 121*, 3803-3804.

(41)   Crowley, P. B. and Ubbink, M. (2003) Close encounters of the transient kind: protein interactions in the photosynthetic redox chain investigated by NMR spectroscopy. *Acc. Chem. Res. 36*, 723-30.

(42)   Kasrayan, A., Birgander, P. L., Pappalardo, L., Regnstrom, K., Westman, M., Slaby, A., Gordon, E., and Sjoberg, B. M. (2004) Enhancement by effectors and substrate nucleotides of R1-R2 interactions in *Escherichia coli* class Ia ribonucleotide reductase. *J. Biol. Chem. 279*, 31050-7.

(43)   Wadhams, G. H. and Armitage, J. P. (2004) Making sense of it all: bacterial chemotaxis. *Nat. Rev. Mol. Cell. Biol. 5*, 1024-37.

(44)   Sourjik, V. and Berg, H. C. (2002) Receptor sensitivity in bacterial chemotaxis. *Proc. Natl. Acad. Sci. U. S. A. 99*, 123-7.

(45)   Stewart, R. C. (1997) Kinetic characterization of phosphotransfer between CheA and CheY in the bacterial chemotaxis signal transduction pathway. *Biochemistry 36*, 2030-40.

(46)   Mayover, T. L., Halkides, C. J., and Stewart, R. C. (1999) Kinetic characterization of CheY phosphorylation reactions: comparison of P-CheA and small-molecule phosphodonors. *Biochemistry 38*, 2259-71.

(47)   Stewart, R. C., Jahreis, K., and Parkinson, J. S. (2000) Rapid phosphotransfer to CheY from a CheA protein lacking the CheY-binding domain. *Biochemistry 39*, 13157-65.

(48)   Jahreis, K., Morrison, T. B., Garzon, A., and Parkinson, J. S. (2004) Chemotactic signaling by an *Escherichia coli* CheA mutant that lacks the binding domain for phosphoacceptor partners. *J. Bacteriol. 186*, 2664-72.

(49)   Stewart, R. C., and VanBruggen, R. (2004) Phosphorylation and binding interactions of CheY studied by use of Badan-labeled protein. *Biochemistry 43*, 8766-77.

(50)   Li, J., Swanson, R. V., Simon, M. I., and Weis, R. M. (1995) The response regulators CheB and CheY exhibit competitive binding to the kinase CheA. *Biochemistry 34*, 14626-36.

(51)   McEvoy, M. M., Hausrath, A. C., Randolph, G. B., Remington, S. J., and Dahlquist, F. W. (1998) Two binding modes reveal flexibility in kinase/response regulator interactions in the bacterial chemotaxis pathway. *Proc. Natl. Acad. Sci. U. S. A. 95*, 7333-8.

(52)   Welch, M., Chinardet, N., Mourey, L., Birck, C., and Samama, J. P. (1998) Structure of the CheY-binding domain of histidine kinase CheA in complex with CheY. *Nat. Struct. Biol. 5*, 25-9.

(53)   Park, S. Y., Beel, B. D., Simon, M. I., Bilwes, A. M., and Crane, B. R. (2004) In different organisms, the mode of interaction between two signaling proteins is not necessarily conserved. *Proc. Natl. Acad. Sci. U. S. A. 101*, 11646-51.

(54)   Schendel, F. J., Cheng, Y. S., Otvos, J. D., Wehrli, S., and Stubbe, J. (1988) Characterization and chemical properties of phosphoribosylamine, an unstable intermediate in the de novo purine biosynthetic pathway. *Biochemistry 27*, 2614-23.

(55)   Rudolph, J. and Stubbe, J. (1995) Investigation of the mechanism of phosphoribosylamine transfer from glutamine phosphoribosylpyrophosphate amidotransferase to glycinamide ribonucleotide synthetase. *Biochemistry 34*, 2241-50.

(56)   Rudolph, J. (1993), PhD Thesis, Department of Chemistry, Massachusetts Institute of Technology, Cambridge, Massachusetts.

(57)   Muchmore, C. R., Krahn, J. M., Kim, J. H., Zalkin, H., and Smith, J. L. (1998) Crystal structure of glutamine phosphoribosylpyrophosphate amidotransferase from *Escherichia coli. Protein Sci. 7*, 39-51.

(58)   Wang, W., Kappock, T. J., Stubbe, J., and Ealick, S. E. (1998) X-ray crystal structure of glycinamide ribonucleotide synthetase from *Escherichia coli. Biochemistry 37*, 15647-62.

(59)   Galperin, M. Y. and Koonin, E. V. (1997) A diverse superfamily of enzymes with ATP-dependent carboxylate-amine/thiol ligase activity. *Protein Sci. 6*, 2639-43.

(60)   Ebbole, D. J. and Zalkin, H. (1987) Cloning and characterization of a 12-gene cluster from *Bacillus subtilis* encoding nine enzymes for de novo purine nucleotide synthesis. *J. Biol. Chem. 262*, 8274-87.

(61)   Saxild, H. H. and Nygaard, P. (2000) The *yexA* gene product is required for phosphoribosylformylglycinamidine synthetase activity in *Bacillus subtilis. Microbiology 146 (Pt 4)*, 807-14.

(62)   French, T. C., Dawid, I. B., Day, R. A., Buchanan, J. M. (1963) Azaserine-reactive Sulfhydryl Group of Formamido-*N*-ribosylacetamide 5'-Phosphate:l-Glutamine Amido-ligase (Adenosine Diphosphate). I. Purification and Properties of the Enzyme from *Salmonella Typhimurium* and the Synthesis of L-Azaserine-C^{14}. *J. Biol. Chem. 238*, 2171-2177.

(63)   Mizobuchi, K. and Buchanan, J. M. (1968) Biosynthesis of the purines. XXIX. Purification and properties of formylglycinamide ribonucleotide amidotransferase from chicken liver. *J. Biol. Chem. 243*, 4842-52.

(64)   Satterthwait, A. C. and Westheimer, F. H. (1980) Monomeric Methyl Metaphosphate: Reactions with Carbonyl Groups. *J. Amer. Chem. Soc. 102*, 4464-4472.

(65)   Mueller, E. J. (1993) PhD Thesis, Department of Chemistry, Massachusetts Institute of Technology, Cambridge.

(66)   Li, C., Kappock, T. J., Stubbe, J., Weaver, T. M., and Ealick, S. E. (1999) X-ray crystal structure of aminoimidazole ribonucleotide synthetase (PurM), from the *Escherichia coli* purine biosynthetic pathway at 2.5 Å resolution. *Structure Fold. Des. 7*, 1155-66.

(67) Anand, R., Hoskins, A. A., Stubbe, J., and Ealick, S. E. (2004) Domain organization of *Salmonella typhimurium* formylglycinamide ribonucleotide amidotransferase revealed by X-ray crystallography. *Biochemistry 43*, 10328-42.

(68) Anand, R., Hoskins, A. A., Bennett, E. M., Sintchak, M. D., Stubbe, J., and Ealick, S. E. (2004) A model for the *Bacillus subtilis* formylglycinamide ribonucleotide amidotransferase multiprotein complex. *Biochemistry 43*, 10343-52.

Chapter 2:

Efforts to Detect a PurF: PurD Complex by Stopped-flow Fluorescence
Spectroscopy

2.1 Introduction

PurF (phosphoribosylpyrophosphate amidotransferase, PRPP-AT) and PurD (glycinamide ribonucleotide synthetase, GAR synthetase) catalyze the first two steps in de novo purine biosynthesis (Scheme 2.1). The amidotransferase catalyzes the formation phosphoribosylamine (PRA), PP_i, and glutamate from phosphoribosylpyrophosphate (PRPP) and glutamine. PurD then converts PRA in the presence of ATP and glycine into GAR, ADP, and P_i. Early experiments on PurF failed to detect PRA and its structure was inferred by trapping with PurD. These studies suggested that PRA was chemically unstable, not surprising given its structure. Subsequent experiments estimated the $t_{1/2}$ of PRA under physiological conditions (pH 7.5, 37°C) to be ~ 5 s (1). The instability of PRA suggested that PurF and PurD have evolved to directly transfer this metabolite between their active sites. Steady state kinetic studies on each protein provided the required kinetic parameters to test the model that PRA was directly transferred from PurF to PurD. The results of these experiments supported the proposal that the first two enzymes in the purine biosynthetic pathway were able to channel this chemically unstable intermediate (2).

To provide further support for this model, efforts were initially undertaken to look for PurF interactions with PurD. Gel filtration chromatography, co-immunoprecipitation (Co-IP) studies using antibodies to both PurF and PurD, protein-affinity chromatography, steady-state fluorescence, and chemical cross-linking were all utilized in attempts to characterize a PurF:PurD complex (2). All of these methods failed to detect any interaction between the enzymes. Gel filtration and protein affinity chromatography experiments are carried out on a time-scale (hours) that would not report on transient interactions. However, the failure to detect a protein complex in the presence of PRA (generated using an equilibrium mixture of ribose-5'-
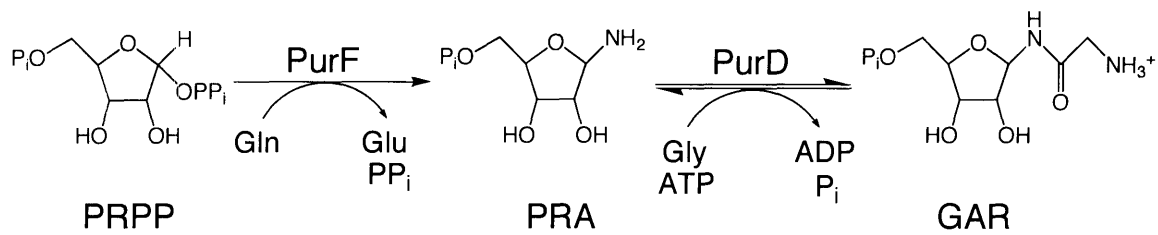
Scheme 2.1—Reactions catalyzed by PurF and PurD.

phosphate and NH_3) using steady-state fluorescence and chemical cross-linking methods is problematic. In particular, the irreversibility of chemical cross-linking should have allowed build-up of a cross-linked protein complex over the course of the experiment (0.5-2 h) even if only a small percentage of the proteins were interacting at any given time. These results led to a model in which PurD reacts transiently with the PurF•PRA product complex (2).

In the years subsequent to these kinetic studies, crystal structures of PurF and PurD provided the basis for thinking about how the two proteins might transiently interact (3-5). Crystallographic analyses of apo PurF and 6-diazo-5-oxonorleucine (DON)-inactivated PurF with a bound Mn^{2+}-carbocylic PRPP (cPRPP) indicated that the enzyme undergoes dramatic structural reorganization upon substrate analog binding (Figure 2.1A) (3). Large movements were observed in the glutamine-binding loop (residues 73-84), the phosphoribosyl transferase (PRTase) flexible loop (326-350), and the C-terminal helix (471-492). In an attempt to characterize these movements, Zalkin and coworkers used steady state and stopped-flow spectroscopic methods to monitor changes in tryptophan fluorescence, taking advantage of the fact that E. coli PurF contains only a single tryptophan (W290) (6). Mutation of this tryptophan to phenylalanine was shown to have no effect on activity. Site-directed mutagenesis was then employed to place tryptophans in each of the three mobile regions to monitor loop or C-terminal helix movement (6). While many mutants were constructed, A82W in the glutamine-binding loop, S345W in the PRTase flexible loop, and F477W in the C-terminal helix (Figure 2.1A) were used as reporters for kinetically-competent conformational changes that accompanied substrate binding to the enzyme (6).

A

Glutamine
Loop
A82W

C-terminal
Helix
F477W

Flexible
Loop
S345W

cPRPP

Open PurF   **Closed PurF**

B

S345W   A82W

F477W

PurF Dimer   **PurD**
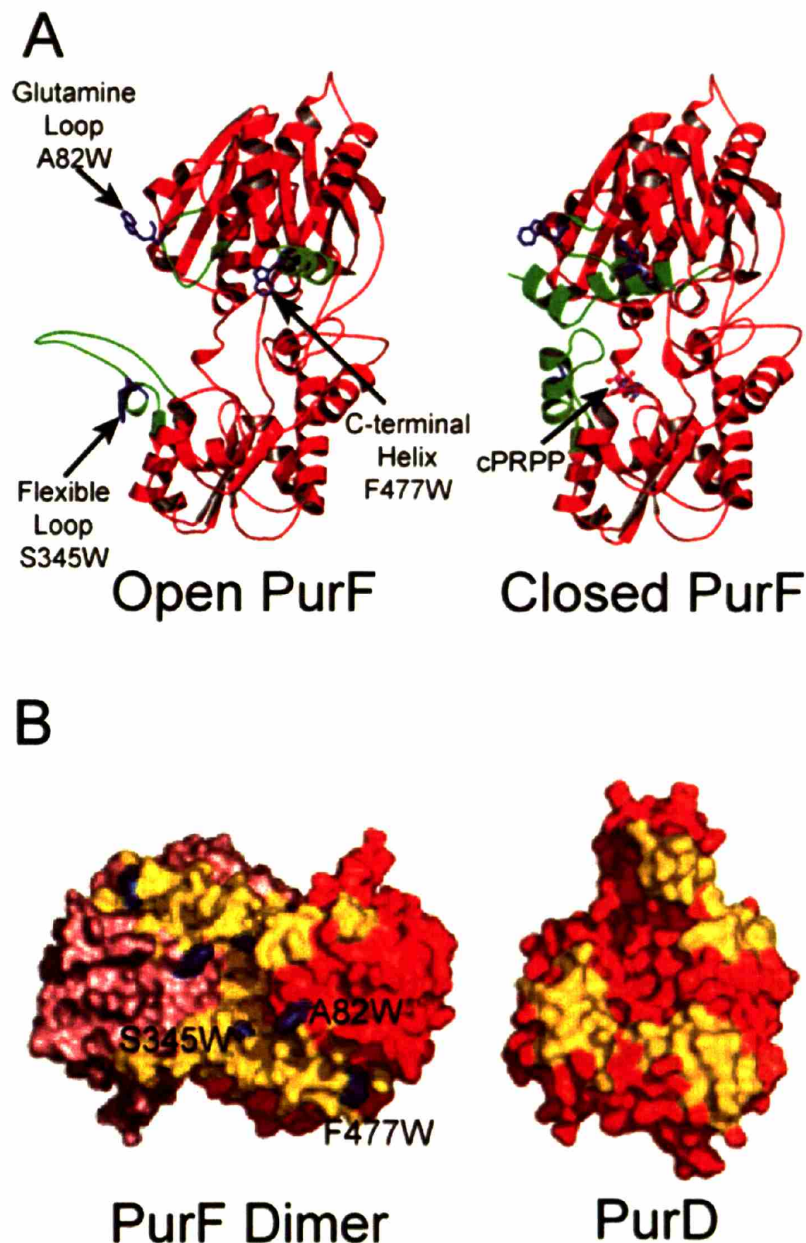
Figure 2.1—(A) Open and closed conformational states of PurF from the PDB files 1ecb.pdb and 1ecc.pdb, respectively. Mobile loops that change conformation upon binding of cPRPP and DON alkylation are shown in green. Tryptophan mutants studied in this chapter are shown in blue and have been mutated *in silico* using SWISS PDB-Viewer from the respective PDB files. In the closed form of PurF, cPRPP and the DON adduct are shown in ball-and-stick representation; however, the DON adduct is obscured by the C-terminal helix. (B) Surface representation of the docking model of PurD onto the PurF dimer as previously described *(5)*. The two halves of the PurF dimer are colored red and pink. Proposed interactions between PurF (1ecc.pdb) and PurD (1gso.pdb) are shown in yellow. Locations of the tryptophan mutants used in these studies are shown in blue and labeled on one of the PurF monomers. (A) and (B) were generated using MacPyMOL (DeLano, W.L., http://www.pymol.org).

The conformational differences in PurF structures between the apo- and substrate-bound forms played a key role in creating the docking model between PurF and PurD proposed by the Ealick and Stubbe Laboratories (*5*). This model was created based on shape and charge complementarity between the PurF dimer and the PurD monomer (Figure 2.1B). While there is some debate concerning PurF quaternary structure in solution and both dimers and tetramers have been observed by X-ray crystallography(*3, 4*), one hypothesis is that the PurF dimer structure closely mimics the PurF•PRA complex, since dimeric structures are observed with DON and cPRPP ligands in the closed PurF active site. Two key features of this docking model were that the active sites of the enzymes were aligned (~28 Å apart) and that the mobile regions of PurF correspond to the interface between PurF and PurD (Figure 2.1). Movement of the PRTase flexible loop after PRA formation was proposed to allow direct transfer of PRA between enzyme active sites (*5*). The experiments described in this chapter were designed to test the proposed docking model and to obtain evidence for transient PurF-PurD interactions. The three mobile regions (A82W, S345W, and F477W) previously studied in detail by Zalkin have been investigated in an effort to detect interactions between PurF and PurD by monitoring changes in PurF fluorescence in the pre-steady state.

Two technical problems must be overcome to test for PurF•PRA transient interactions with PurD. A continuous method to detect interactions is essential as is a method to determine PurF•PRA concentration at different stranges of the pre-steady state. Global incorporation of 7-azatryptophan (7AW, Figure 2.2) into PurF and non-fluorescent 4-fluorotryptophan (4FW, Figure 2.2) into PurD was successful and has provided the required sensitive probes of PurF conformational flexibility in the pre-steady state.
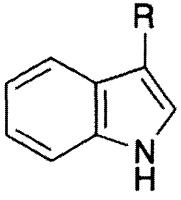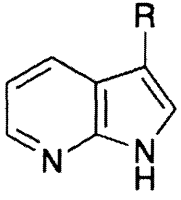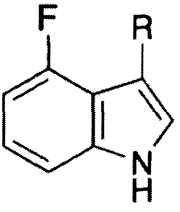
	Tryptophan	7-Azatryptophan	4-Fluorotryptophan
Absorbance	280 and 288 nm	290 nm	265 and 285 nm
ε_{280} (M^{-1} cm^{-1})	5400	6000	3300
Fluorescence	353 nm	403 nm	341 nm
Φ (Quantum Yield)	0.13	0.016	0.001

Figure 2.2—Absorbance and fluorescence properties of tryptophan and the 7AW and 4FW tryptophan analogs used in these studies. Data from Ref. (7)

Determination of the concentration of PurF•PRA, however, has been technically very challenging. First, the instability of PRA precludes direct testing of this interaction. Second, typical pre-steady state experiments using rapid chemical quench have thus far not been successful due to instability of PRPP and PRA and unavailability of a method to rapidly trap PRA. This chapter describes pre-steady state experiments, using 3 syringes, in an attempt to detect interactions between PurF and PurD during PRA synthesis. In addition, a variety of stopped-flow fluorescence experiments have also been carried out to look for PurF:PurD interactions under conditions in which PurF resides in different conformational states. No evidence for interaction between PurF and PurD was found under any of the conditions examined. The implications of these findings and their impact on the docking model and PRA channeling are discussed in detail.

2.2 Experimental

Materials

NADH, ATP, bovine serum albumin (BSA), ribose-5'-phosphate (R5P), phosphoribosylpyrophosphate (PRPP), phosphoenolpyruvate (PEP), and pyruvate kinase/lactate dehydrogenase (pre-mixed glycerol solution 660 U/mL PK, 1350 U/mL LDH, Sigma P-0294) were obtained from Sigma. PRPP solutions were made in 50 mM Tris pH 7.5, frozen in liquid N_2, and stored at -80°C. PRPP concentration was determined enzymatically using the PurF:PurD coupled assay (2). PRA was synthesized chemically, and its concentration determined enzymatically (1). Glycine was obtained from Mallinckrodt and glutamine from Fluka. Scintillation fluid (Emulsifier-Safe) was obtained from Perkin-Elmer. Dowex 50W-X8 resin, 200-400 mesh, was obtained from Bio-Rad. ESI-MS was performed at the MIT Biopolymers Facility. PurF, W290F, A82W/W290F, C1S/A82W/W290F, W290F/S345W,

C1S/W290F/S345W, W290F/F477W, and C1S/W290F/F477W mutant PurFs in pET-plasmids were all the generous gift of Howard Zalkin, Purdue University (*6*).

Sub-cloning of PurD into pET-24a

The wild-type (wt) *purD* gene from pJK33 (*5*) was amplified by PCR with Pfu DNA polymerase (Stratagene) using the PurD-NdeI (5'-GCCATATGAAAGTATTAGTGATTGGTAACG-3') and PurD-BamHI primers (5'-CGGATCCTTAGTTCTGCTCGCGTTCGATAGCG-3'). The product was then digested with NdeI and BamHI and ligated into pET-24a (Novagen) cleaved with the same restriction enzymes. This construct allows IPTG-inducible expression of PurD, and the gene sequence was verified by DNA sequencing (MIT Biopolymers Facility).

Expression of pET-PurD

PurD was expressed as previously described except in *E. coli* BL21(DE3) (*6*).

Growth and Expression of [4FW]-labeled PurD and [7AW]-labeled PurF

Both [4FW]-PurD and [7AW]-PurF were expressed in BL21(DE3) *E. coli* grown in minimal media using methods developed for studies on ribonucleotide reductase (E. Artin, H. Nguyen, and J. Stubbe, unpublished results). The minimal media at pH 7.4 contained 0.5 g/L ala, 0.1 g/L cys, 0.6 g/L gly, 0.25 g/L ile, 0.4 g/L lys, 0.15 g/L phe, 2.1 g/L ser, 0.25 g/L val, 0.5 g/L arg, 0.7 g/L glu, 0.15 g/L his, 0.25 g/L leu, 0.25 g/L met, 0.15 g/L pro, 0.25 g/L thr, 0.15 g/L tyr, 40 g/L glycerol, 2.0 g/L $(NH_4)_2SO_4$, 1.6 g/L KH_2PO_4, 0.5 g/L Na citrate, 10 g/L Na_2HPO_4, 0.5 g/L adenine, 0.3 g/L cytosine, 0.70 g/L guanine, 0.5 g/L uracil, 0.3 g/L thymine, and 4 mM $MgSO_4$. All components except for the amino acids were autoclaved in 865 mL of water/L of media. Amino acids (133 mL) were then added from a 7.5x sterile-filtered solution at pH 9.0. Metals were added to the media from a 1000x stock solution containing 33 g/L $FeCl_3•6H_2O$, 180

mg/L $ZnSO_4 \cdot 7H_2O$, 160 mg/L $CuSO_4 \cdot 6H_2O$, 180 mg/L $CoCl_2 \cdot 6H_2O$, and 38 g/L

$Na_2EDTA \cdot 2H_2O$. Biotin and thiamine were added from sterile filtered solutions to a final

concentration of 25 mg/L and 5 mg/L, respectively. Precipitation from the media was frequently

observed during the growth.

A single colony from a fresh transformation of BL21(DE3) *E. coli* with either pET-PurD

or one of the pET-PurFs was used to inoculate 5 mL of LB with 70 µg/mL kanamycin and

allowed to grow for 10 h at 37°C in a Glas-Col culture rotator at 50 rpm. An aliquot of the

culture (100 µL) was then used to inoculate 100 mL of LB with 70 µg/mL kanamycin and

allowed to grow overnight with shaking at 200 rpm in a 500 mL flask at 37°C. Cells (40 mL)

from the overnight culture were then collected by centrifugation and washed twice with 25 mL

of minimal media. The cell pellet was resuspended in 10 mL of minimal media and used to

inoculate a 1 L culture of minimal media with 70 µg/mL kanamycin. This culture was then

grown at 37°C with shaking at 200 rpm in a 4 L flask.

At $OD_{600} = 0.7$, 200 mg of either DL-4FW or DL-7AW (both from Sigma) were added to

the flask as a solid. After 20 min, IPTG (Promega) was added from a 1 M solution in water to a

final concentration 1 mM. The cells were then allowed to grow for an additional 4 h before the

cell pellet was collected by centrifugation, frozen in liquid N_2, and stored at -80°C.

Purification of wt PurD, [4FW]-PurD, and [7AW]-PurFs

The labeled and unlabeled PurDs and PurFs were purified as previously described for the

wt enzymes with a minor modification (*6, 8*). Cells were lysed using a sonicator to avoid

particulates which interfered with French press cell disruption. Typically, cells from a 1 L

growth were sonicated in a flask cooled in an ice water bath for 16 min at 40% power with

stirring and shaking every 4 min (3/32" microprobe, VirSonic100, VirTis). Enzyme

concentration was determined using the Lowry assay and a BSA standard. The identity of each

PurF mutant was confirmed by ESI-MS. These studies also indicated that all N-terminal

methionines had been removed.

ESI-MS Characterization of the [7AW]-PurF Mutants and [4FW]-PurD

The identity of each PurF mutant was confirmed by ESI-MS with a Sciex Model API 365

triple stage mass spectrometer at the MIT Biopolymers Facility. These studies also indicated

that all N-terminal methionines had been removed. However, the extent of 7AW incorporation

into PurF could not be monitored by ESI-MS because the mass difference between the labeled

and unlabeled enzymes was only 1 Da. On the other hand, extent of 4FW incorporation into

PurD was readily assessed by ESI-MS using wt PurD, [4FW]- PurD, or a mixture of wt/[4FW]-

PurD.

Enzymatic Assays for [7AW]-PurFs and [4FW]-PurD

[7AW]-PurF mutants were assayed at 18°C using a spectrophotometric assay with

PurD/PK/LDH as the coupling enzymes as previously described (2). C1S and DON-inactivated

PurFs, while incapable of glutamine-dependent PRA synthesis, were assayed with the

PurD/PK/LDH coupling enzymes for NH_4Cl-dependent activity. [4FW]-PurD was also assayed

at 18°C as previously described using the spectrophotometric assay with chemically synthesized

PRA (2).

K_m and V_{max} Determinations for the [7AW]-PurF Mutants and [4FW]-PurD

Kinetic constants for the [7AW]-PurFs ($K_{m(Gln)}$, $K_{m(PRPP)}$, and V_{max}) and [4FW]-PurD

($K_{m(PRA)}$, $K_{m(gly)}$, $K_{m(ATP)}$, and V_{max}) were determined as previously described for the wt enzymes

(2). Data for [7AW]-PurFs and for glycine-dependent or ATP-dependent activities in [4FW]-

PurD were fit using non-linear least squares fitting with KaleidaGraph software (Synergy) to

Equation 2.1. As has been previously reported for wt PurD, substrate inhibition was observed

with [4FW]-PurD. These data were fit to Equation 2.2, also with KaleidaGraph software.

$$v = V_{max}[S]/(K_m + [S])$$ (2.1)

$$v = \frac{V_{max}[S]}{(K_m + [S] + \frac{[S]^2}{K_i})}$$ (2.2)

Removal of Diketopiperazine Contamination from Radioactive Glycine Stocks

Diketopiperazine was removed from $[^{14}C(U)]$-glycine stock solutions (New England

Nuclear, now Perkin Elmer) directly before use by passing the solution (10 μCi) through a 1.5

mL column of Dowex 50W-X8 resin (400 mesh) equilibrated in 50 mM ammonium formate pH

3.33. The column was washed with 10 mL of 250 mM formic acid to remove the

diketopiperazine. Glycine was then eluted with 250 mM ammonium formate (pH 7.0).

Fractions containing radioactivity were combined and dried under vacuum. $[^{14}C(U)]$-glycine

was added to 120 mM glycine to a final concentration of 12 mM. The specific activity was

determined by scintillation counting and enzymatic quantitation of glycine using the PurD

spectrophotometric assay.

Channeling Assays

Channeling assays were carried out using the [7AW]-PurF mutants and [4FW]-PurD as

previously described for the wt enzymes (*2*). Each assay was carried out at pH 8.0 and 18°C with

$[^{14}C(U)]$-glycine (specific activity 1,587 cpm/nmol) to monitor GAR formation. Enzyme

activities and the $K_{m(PRA)}$ were determined immediately prior to each experiment. [7AW]-PurF

mutants and [4FW]-PurD were added to achieve product synthesis rates of 10.5 μM PRA/min

and 17 μM GAR/min, respectively, based upon analysis of the activity of each enzyme.

74

Kinetics assuming no interaction between PurF and PurD were modeled based on the parameters measured above and using Equations 2.3 and 2.4 and Microsoft Excel spreadsheet software. The $K_{m(PRA)}$ determined for [4FW]-PurD was 102 μM for a 40:60 equilibrium mixture of α/β-PRA (61 μM for β-PRA alone) (2). The rate of PRA decomposition (k_{decomp}) was 0.005 min^{-1} under these conditions (2).

$$\frac{\delta[PRA]}{\delta t} = V_1 - \frac{V_2[PRA]}{K_{m(PRA)} + [PRA]} - k_{decomp}[PRA] \qquad (2.3)$$

$$\frac{\delta[GAR]}{\delta t} = \frac{V_2[PRA]}{K_{m(PRA)} + [PRA]} \qquad (2.4)$$

Inhibition of [4FW]-PurD by PP$_i$

The inhibitory effects of PP$_i$ on GAR synthesis were determined by assaying [4FW]-PurD in the presence of varying concentrations of PP$_i$ and subsaturating concentrations of the variable substrate (8). A typical assay contained in a final volume of 600 μL: 100 mM Tris HCl pH 8.0, 6 mM Mg(OAc)$_2$, 50 mM KCl, 1.5 mM PEP, 0.2 mM NADH, 4 U PK, and 7 U LDH. The disappearance of NADH (ϵ_{340} = 6,220 M^{-1} cm^{-1}) was used to monitor activity, and the reaction was initiated by the addition of PRA. For PP$_i$ vs. ATP studies, PP$_i$ was varied from 0 to 2.5 mM, ATP was varied from 13-250 μM and PRA was 300 μM and glycine was 3 mM. In the PP$_i$ vs. PRA studies, PP$_i$ varied from 0 to 2.5 mM, PRA from 25-100 μM and ATP was 250 μM and glycine was 3 mM. For the PP$_i$ vs. glycine studies, PP$_i$ was varied from 0 to 2.5 mM, glycine from 50-750 μM with ATP at 250 μM and PRA at 300 μM. Global data analysis was carried out using *Visual*Enzymics (Softzymics, Inc.) and IgorPro (Wavemetrics, Inc.) software. Each data set was fit to Equations 2.4, 2.5, and 2.6, equations for competitive, uncompetitive, and noncompetitive inhibition, respectively. Statistical analysis was carried out using the F test to determine the appropriateness of the chosen inhibition model.

$$v_o = \frac{V_{max}[S]}{K_M(1 + \frac{[I]}{K_{is}}) + [S]} \qquad (2.4)$$

$$v_o = \frac{V_{max}[S]}{K_M + [S](1 + \frac{[I]}{K_{ii}})} \qquad (2.5)$$

$$v_o = \frac{V_{max}[S]}{K_M(1 + \frac{[I]}{K_{is}}) + [S](1 + \frac{[I]}{K_{ii}})} \qquad (2.6)$$

Removal of PP_i Contamination from PRPP for Stopped-Flow Experiments

PP_i contamination in the PRPP stocks was found to contribute to PurD background fluorescence and was removed by pre-incubation with yeast inorganic pyrophosphatase (PPase) at 25°C for 15 min before the addition of PurF. PPase (100 U, Sigma I-1891) was dissolved in 100 mM Tris pH 7.5, 10 mM $MgCl_2$ to a final concentration of 1 U/μL. It was then added at a concentration of 1 U/μmol PRPP to all PRPP-containing buffer solutions used in fluorescence studies.

Inactivation of PurF by DON for Stopped-Flow Experiments

The reaction mixture contained in a final volume of 1 mL: 200 μM PurF, 2 mM PRPP, 10 mM DON, 10 mM $MgCl_2$, and 50 mM Tris HCl pH 7.5. The mixture was incubated at 25°C, and the progress of the inactivation was followed by removal of 5 μL aliquots which were measured for activity using the spectrophotometric assay with PurD. Once the inactivation was complete, the enzyme was dialyzed against 2 x 500 mL 10 mM Tris pH 8.0, 10 mM $MgCl_2$ in a 10 kDa MWCO Slide-A-Lyzer cassette (Pierce) at 4°C overnight. PurF was then assayed for both glutamine-dependent and NH_4Cl-dependent activity.

Steady State Fluorescence of the [7AW]-PurF Mutants and [4FW]-PurD

Steady state fluorescence spectra were obtained using a sensitivity-enhanced PTI QuantaMaster-4 fluorimeter (Photon Technology International) with temperature regulation at 25°C using a Lauda water bath. Spectra were acquired using a constant volume (900 µL) in a 5 mm x 5 mm microcuvette (Starna). All spectra were background corrected using a buffer solution containing all components except for enzyme. Spectra were obtained in 0.5 nm increments at a rate of 0.4 s/nm. All slits were set to 4 nm, and typically 2 scans were averaged during each experiment. The excitation wavelength was set to either 295, 300, or 310 nm depending on the enzyme being studied, and emission was monitored between 320-420 nm. Spectra were collected in 10 mM Tris, 10 mM $MgCl_2$, pH 8.0 at 25°C. Enzyme was added to a final concentration of 2 µM. In the case of C1S PurFs, glutamine and PRPP were also present at 20 mM and 1.5 mM, respectively.

General Stopped-Flow Fluorescence Methods

All stopped-flow experiments were carried out in SF buffer: 10 mM Tris pH 8.0 at 18°C with 10 mM $MgCl_2$. Buffer components associated with each experiment are summarized in Table 2.1. Data was collected on an Applied Photophysics SX.18MV stopped-flow with a measured dead time of ~1.3 ms at 18°C. Samples were excited from a Xenon arc lamp source passed through a monochrometer with slits set to 3 mm. Fluorescence was detected from a PMT mounted directly onto the observation cell with the appropriate cutoff filter as described below. Reaction temperature was controlled at 18°C with the use of a Lauda water bath. Data was collected with oversampling and in-line filtering set to 200 µs. The PMT voltage was set to 80%

Table 2.1: Stopped-Flow Experiments

Number	Experiment	Syringe 1	Syringe 2	Syringe 3
1	PurF•PRPP vs. Gln	10 µM PurF, 3.0 mM PRPP	40 mM Gln	••••
2	PurF•PRPP vs. Gln[a] vs. Buffer	15 µM PurF, 4.5 mM PRPP, 4.5 U/mL PPase	40 mM Gln	20 mM Gln
3	PurF•PRPP vs. Gln vs. PurD	15 µM PurF, 4.5 mM PRPP, 4.5 U/mL PPase	40 mM Gln	15 µM PurD, 20 mM Gln
4	PurF vs. PurD	10 µM PurF	10 µM PurD	••••
5	PurF•PRPP vs. PurD	10 µM PurF, 3.0 mM PRPP, 3 U/mL PPase	10 µM PurD	••••
6	PurF•PRPP•Gln vs. PurD	10 µM C1S PurF, 3.0 mM PRPP, 3 U/mL PPase, 20 mM Gln	10 µM PurD, 20 mM Gln	••••
7	PurF•PRPP•GTE[b] vs. PurD	10 µM DON-PurF, 3.0 mM PRPP, 3 U/mL PPase	10 µM PurD	••••
8	PurF•GTE vs. PurD	10 µM DON-PurF	10 µM PurD	••••

[a]A 10 ms mixing time was used in all 3-syringe experiments. [b]GTE = glutamyl thioester intermediate. The covalent glutaminase inhibitor DON was used to mimic the GTE.

of maximum for each experiment in order to maximize sensitivity. The PMT voltage was reset between experiments; thus, the absolute fluorescence intensities between different experiments are not directly comparable and have all been arbitrarily set to 0 V unless stated otherwise. For each experiment, data (1000 points) were collected between 0-1s for the W290F/S345W and W290F/F477W [7AW]-PurFs and 0-2 s for the A82W/W290F [7AW]-PurF. Data were also collected in a split time base in which 500 data points were collected for the pre-steady state periods described above and 500 data points were collected over the next 50-100 s to monitor changes in the steady state. Data was collected such that the drive pressure was not removed until after the pre-steady state data collection period had been completed. For each experiment, 2-5 kinetic traces were averaged. Data was analyzed using the SX.18MV workstation software, and the quality of the fit judged by the variance as well as the residuals plot.

Stopped-Flow Experiments of [7AW]-PurF•PRPP Mutants vs. Glutamine for Determination of Mixing Time for 3-Syringe Experiments with [4FW]-PurD

Interactions between a pre-formed [7AW]-PurF•PRPP complex and glutamine were studied to examine changes in fluorescence upon glutamine binding and turnover and to determine mixing times to be used in subsequent 3-syringe experiments with PurD. In a typical experiment, 10 µM [7AW]-PurF mutant was pre-mixed with 3.0 mM PRPP and placed into syringe 1. This solution was then rapidly mixed with an equal volume (~60 µL) of 40 mM glutamine in SF buffer from syringe 2 (Experiment 1, Table 2.1). Samples were excited at 300 nm and emission was monitored through a WG 335 nm cutoff filter (Applied Photophysics).

Kinetic traces from the A82W/W290F mutant exhibited fluorescence changes containing 3 distinct phases, and the data were fit to Equation 2.7. Biphasic kinetics were observed with the W290F/S345W and W290F/F477W mutants, and the data were fit to Equation 2.8.

$$\Delta F_{obs}(t) = A_1 e^{-k_1 t} + A_2 e^{-k_2 t} + A_3 e^{-k_3 t} + C \qquad (2.7)$$

$$\Delta F_{obs}(t) = A_1 e^{-k_1 t} + A_2 e^{-k_2 t} + C \qquad (2.8)$$

3-Syringe Stopped Flow Experiments to Detect Interactions between [7AW]-PurF•PRA mutants and [4FW]-PurD

A 3-syringe set-up was used to detect interactions between [7AW]-PurF mutants and [4FW]-PurD during PRA synthesis by monitoring 7AW fluorescence (Experiments 2 and 3, Table 2.1). Syringe 1 contained 15 µM [7AW]-PurF mutant and 4.5 mM PRPP. This solution was then rapidly mixed against an equal volume (100 µL) of 40 mM glutamine from syringe 2. After 10 ms, this reaction mixture was then rapidly mixed with either 15 µM [4FW]-PurD, 20 mM glutamine solution or 20 mM glutamine solution from syringe 3 (100 µL). The final concentrations were 5 µM [7AW]-PurF mutant, 5 µM [4FW]-PurD (if included), 1.5 mM PRPP, and 20 mM glutamine in a volume of 300 µL. Samples were excited at 310 nm and emission

monitored through a 345 nm cutoff filter (Applied Photophysics). The data were fit to Equations 2.7 and 2.8.

2-Syringe Stopped Flow Experiments to Detect Interactions between [7AW]-PurF mutants and [4FW]-PurD during Mimics of Complexes Generated during PurF Catalysis

A summary of the experimental conditions is shown in Table 2.1 (Experiments 4-8). In a typical experiment, active, DON-inactivated, or C1S mutant [7AW]-PurFs (10 μM) in the presence or absence of PRPP (1.5 mM) and glutamine (20 mM) in syringe 1 were rapidly mixed with an equal volume (~60 μL) of a 10 μM [4FW]-PurD solution from syringe 2. Emission was monitored through a 345 nm cutoff filter (Applied Photophysics) using an excitation wavelength of 310 nm.

Analytical Ultracentrifugation Studies on PurF to Determine the Relevance of the Crystallographically-Observed Dimer to the Docking Model

Sedimentation velocity analytical ultracentrifugation (SV-AUC) and sedimentation equilibrium analytical ultracentrifugation (SE-AUC) experiments were performed using an Optima XL-1 analytical ultracentrifuge (Beckman Coulter, Fullerton, CA) at the Biophysical Instrumentation Facility for the Study of Complex Macromolecular Systems (Department of Chemistry, MIT). Sedimentation was monitored by scanning at 280 nm along the length of the cell. Before each experiment, wt PurF was dialyzed against 10 mM Tris, 10 mM $MgCl_2$ pH 8.0 for 24 h in a 10 kDa MWCO Slide-A-Lyzer cassette (Pierce) and subsequently diluted with the dialysis buffer to the desired concentration. SEDNTERP software from Dr. John Philo was used to calculate buffer density (0.99918 g/mL), viscosity (0.01002 Poise), and protein partial-specific volume from the amino acid content (0.7341 mL/g) (*9*).

SE-AUC experiments were performed at speeds of 6,400; 8,000; and 12,000 rpm with PurF concentrations of 7, 14, 21, 29, and 36 μM over the course of 70 h. These experiments were carried out using six-sector Epon centerpieces (110 μL sample volume) with quartz windows in an An60Ti 4-hole rotor at 18°C. Equilibria were analyzed, and data were edited using the program Winreedit (courtesy of Dr. David Yphantis, National Analytical Ultracentrifugation Facility). Global data analysis to determine the number of species in solution and their reduced apparent molecular weight (σ) was carried out using WinNonLin ver. 1.06 software (courtesy of Dr. David Yphantis, National Analytical Ultracentrifugation Facility) in which σ is equivalent to the change in protein concentration (c) versus radius (r) at equilibrium (Equation 2.8). The molecular weight (MW) was determined from σ using SEDNTERP and the protein partial-specific volume ($\bar{v}$), buffer density (ρ), and angular velocity (ω) according to Equation 2.8.

$$\sigma \equiv \frac{d\ln(c(r))}{d(r^2/2)} = \frac{MW(1-\bar{v}\rho)\omega^2}{RT} \qquad (2.8)$$

SV-AUC experiments were carried out at 35,000 rpm over 24 h with wt PurF at 18 μM in 400 μL using double-sector Epon centerpieces with quartz windows in an An60Ti 4-hole rotor at 18°C. In addition, SV-AUC was also carried out on samples of DON-inactivated wt PurF at 18 μM. The inactivation was carried out using procedures described above for the stopped-flow experiments. Data (~100 traces for each experiment) were fit using Sedfit88 software from 1 to 20 S using a continuous distribution of sedimentation coefficients generated by Lamm equation solutions (*10*).

2.3 Results

While many techniques exist to study strong protein-protein interactions, relatively few options exist to study transient interactions. Stopped-flow fluorescence spectroscopy with site-specifically incorporated, environmentally-sensitive fluorophores offers the potential to study these weak interactions in the pre-steady state by monitoring fluorescence changes or fluorescence resonance energy transfer (FRET). The postulate that a PurF•PRA complex is the docking partner for PurD in the channeling model and the chemical lability of PRA made stopped-flow fluorescence the method of choice. Initial experiments focused on site-specific attachment of fluorescent probes to PurF and PurD (at Cys41 and Cys413, respectively) based on the docking model, so that transient interactions could be monitored by FRET. However, this approach was abandoned after difficulties were encountered with labeling procedures and quantitative probe-attachment (data not shown).

Recent experiments by Zalkin and coworkers designed to monitor conformational changes of PurF in the presence of substrates provided an alternative strategy. Zalkin determined that the single tryptophan residue in PurF (W290) could be changed to a phenylalanine with no effect on activity (*6*). His laboratory subsequently generated a variety of single tryptophan mutants in the glutamine-binding loop (A82W/W290F), PRTase flexible loop (W290F/S345W), and the C-terminal helix (W290F/F477W) (Figure 2.1) that were used in stopped-flow fluorescence experiments to monitor conformational changes in PurF in the presence of glutamine and PRPP (*6*). Since these regions constitute the protein:protein interface in the PurF:PurD docking model (Figure 2.1B), changes in the environments of these tryptophan residues by monitoring fluorescence could provide a means to directly test this model.

Detection of PurF Fluorescence Changes in the Presence of PurD Requires Incorporation of

[7AW] into PurF and [4FW] into PurD

The PurF mutants contain a single, site-specifically positioned tryptophan, while PurD

contains 5 tryptophans. Initial studies with PurD and PurF rapidly revealed that PurD was much

more fluorescent than the PurF mutants (Figure 2.3A), which resulted in a high fluorescence

background. The second problem encountered was that PurD fluorescence was very sensitive to

environmental changes (pH, ionic strength, or PP_i concentration). Small changes in PurF

fluorescence were completely masked by large changes in PurD fluorescence making this

approach intractable.

The solution to this problem came from the use of a dual labeling strategy involving the

biosynthetic incorporation of 7AW and 4FW into PurF and PurD, respectively. These analogs

(Figure 2.2) were chosen for their ability to quench PurD fluorescence (4FW has a quantum yield

of 0.001) and to red-shift PurF fluorescence away from normal tryptophan emission (7AW has a

fluorescence λ_{max} of 403 nm). Recent reports have shown successful biosynthetic incorporation

of these tryptophan analogs into a variety of proteins with a high degree of efficiency (>90%

incorporation) (*11-20*). The 5 tryptophans in PurD were globally replaced with non-fluorescent

4FW (see below for details). This incorporation dramatically reduced PurD's fluorescence as

shown in Figure 2.3B. The PurF mutant enzymes were then generated with the single

tryptophan replaced with 7AW, which can be excited specifically in the presence of tryptophan

at 310 nm, and its fluorescence monitored at >360 nm (*21*). Despite the low quantum yield

associated with 7AW (ϕ = 0.016), fluorescence changes were readily detectable because stopped-

flow experiments described subsequently were designed to mimic the high concentrations of
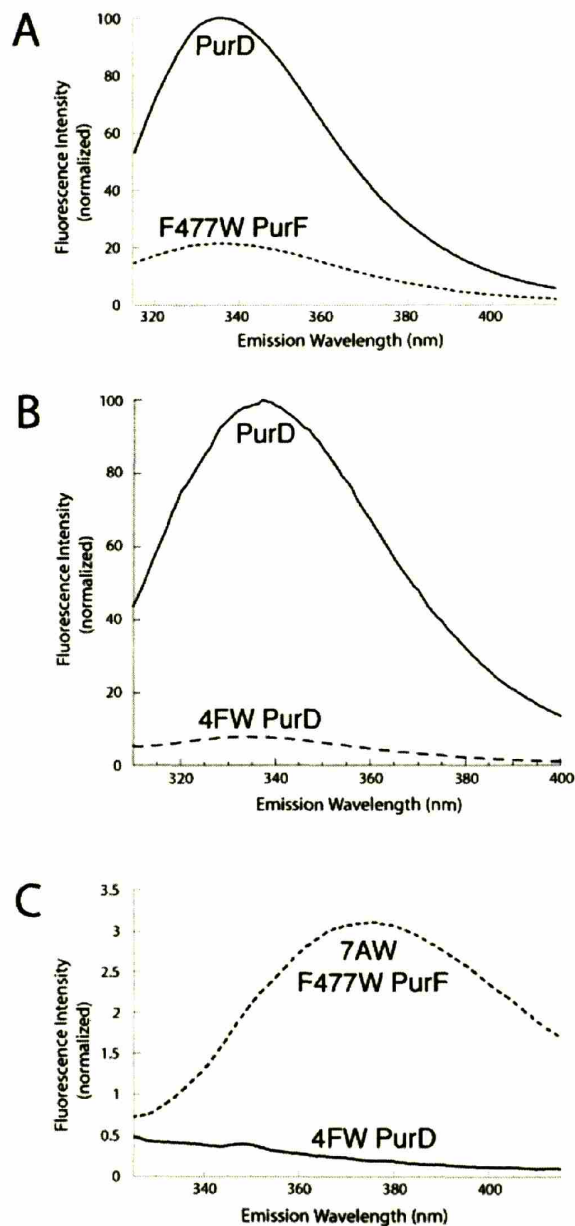
Figure 2.3—(A) Emission spectra of W290F F477W PurF (dashed) and PurD (solid) containing tryptophan. Each sample contains 2 μM protein and was excited at 295 nm. Emission was monitored between 315-420 nm. (B) Emission spectra of PurD (solid) and 4FW-substituted PurD (dashed). Each sample contains 2 μM protein and was excited at 295 nm, and emission was monitored between 310-400 nm. (C) Emission spectra of 7AW substituted W290F F477W PurF (dashed) and 4FW substituted PurD (solid). Each sample contains 2 μM protein and was excited at 310 nm. Emission was monitored between 325-420 nm. The fluorescence intensities present on the y-axis in (A-C) are directly comparable.

PurF and PurD found *in vivo* (2.3-40 μM PurF, 2.6-20 μM PurD) (*22*). By combining [7AW]-PurF and [4FW]-PurD, even the most weakly fluorescent PurF enzyme (W290F F477W) proved to be much more fluorescent than [4FW]-PurD (Figure 2.3C).

Biosynthesis of [7AW]-PurF and [4FW]-PurD

The Stubbe Laboratory has recently incorporated labeled tyrosines into *E. coli* ribonucleotide reductase in high yield and efficiency (E. Artin, H. Nguyen, and J. Stubbe, in preparation). The same strategy was employed to incorporate 4FW into PurD and 7AW into PurF, while maintaining very high levels of protein expression (Figure 2.4A): 80-100 mg PurD/L cell culture and 50-80 mg PurF mutant/L cell culture. Proteins were easily purified to near homogeneity (Figure 2.5). Activities of the purified proteins relative to their wt counterparts and ESI-MS analysis are reported in Tables 2.2-2.5. [7AW]- and [4FW]-analogs appeared to have little effect on enzymatic activity when compared to their tryptophan counterparts. The extent of 4FW incorporation into PurD was determined using ESI-MS (Figure 2.4B). The data show that the predominant protein in solution is [4FW]-PurD containing five 4FWs (MW = 46,030 Da), while only a small contamination of PurD is observed (MW = 45,941 Da).

The 7AW incorporation into PurF cannot be monitored by ESI-MS due to the small increase in molecular weight (1 Da). Analysis of 7AW incorporation by deconvolution of the absorption spectra in an enzyme as large as PurF (which contains 17 tyrosines and 22 phenylalanines) is difficult, and this method is prone to large errors even in small proteins (*7, 23, 24*). As has previously been demonstrated with 7AW incorporation into mannitol permease (*23*), high incorporation levels of 7AW into PurF were expected based on a red-shift in the excitation
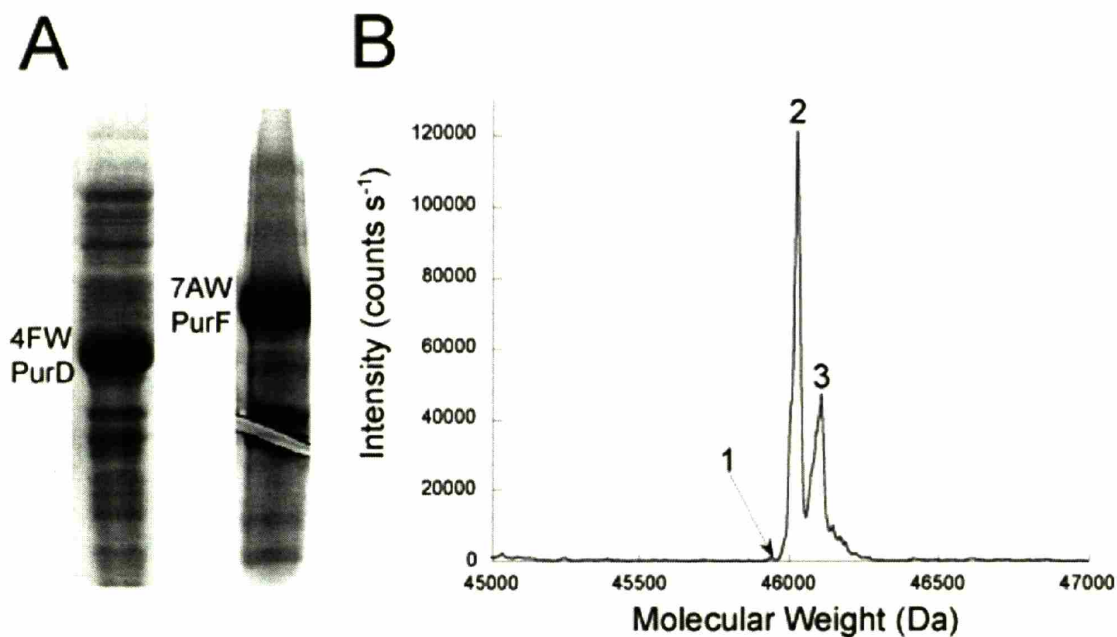
Figure 2.4—(A) 12% SDS-PAGE of BL21(DE3) cells transformed with either pET-PurD or pET-PurF (W290F/F477W) after 4 h of IPTG induction during expression of 4FW-labeled PurD and 7AW-labeled PurF. (B) De-convoluted ESI-MS of [4FW]-PurD. Peak 1, MW = 45,941.0 Da corresponds to contaminating WT PurD, Peak 2, MW = 46030.0 Da corresponds to the fully labeled [4FW]-PurD. Peak 3, MW = 46110.0 Da corresponds to the fully labeled [4FW]-PurD with 2 additional K^+ ions from the enzyme storage buffer.
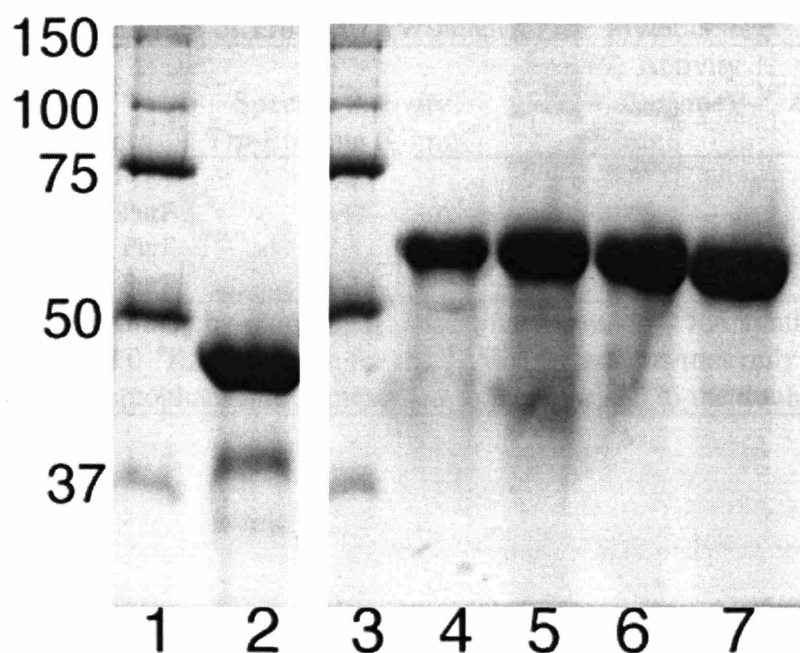
Figure 2.5—12% SDS-PAGE of [4FW]-PurD and [7AW]-PurF mutants show the purity of the enzymes used in these studies. Lanes 1 and 3: Bio-Rad Precision MW markers, Lane 2: [4FW]-PurD, Lane 4: W290F PurF, Lane 5: A82W/W290F [7AW]-PurF, Lane 6: W290F/S345W [7AW]-PurF, Lane 7: W290F/F477W [7AW]-PurF. ~3-5 μg of protein was loaded into each lane.

Table 2.2: Activities of Trp and 7AW-labeled PurF Mutants

PurF Mutant	Specific Activity Trp-Enzyme (U/mg)[a]	Specific Activity 7AW-Enzyme (U/mg)[a]	K_m(PRPP) μM^b	K_m (Gln) μM^b
W290F PurF	5.9[c]	5.9[c]	31	647
A82W/W290F PurF	0.42	0.56	49	616
W290F/S345W PurF	2.3	3.3	52	5901
W290F/F477W PurF	4.2	5.8	41	702

[a]Activity determined by monitoring glutamine-dependent PRA synthesis with PurD at 18°C and pH 8.0 [b]K_m values are for the 7AW-labeled enzymes only [c]This enzyme contains no tryptophans and is presented for comparison to the double mutant enzymes.

Table 2.3: Activities of Glutaminase-Inactivated 7AW PurF Mutants

Inactivated 7AW PurF Mutant[a]	Gln-PRA Specific Activity (U/mg)[b]	NH$_3$-PRA Specific Activity (U/mg)[c]
C1S/A82W/W290F	ND[d]	0.92
A82W/W290F-DON	0.21[e]	1.3
C1S/W290F/S345W	ND	7.0
W290F/S345W-DON	ND	2.2
C1S/W290F/F477W	ND	24.0
W290F/F477W-DON	ND	9.1

[a]The glutaminase site was inactivated by either a C1S mutation or by alkylation with DON. [b]Activity determined by monitoring glutamine-dependent PRA synthesis with PurD at 18°C and pH 8.0 [c]Activity determined by monitoring NH$_4$Cl-dependent PRA synthesis with PurD at 18°C and pH 8.0 [d]No activity could be detected above the background. [e]This enzyme could not be fully-inactivated with DON.

Table 2.4: Kinetic Parameters for WT and 4FW-labeled PurDs

PurD	Specific Activity (U/mg)[a]	K_m(PRA) μM	K_m(ATP) μM	K_m(Gly) μM
WT	42.5[b]	98[b]	170[c]	270[c]
4FW	35.5	102	47	229

[a]Specific activity determined at pH 8.0 and 18°C as previously described (8). [b]Values from (2) [c]Values from (8).

Table 2.5: ESI-MS Results for the Purified Enzymes

Enzyme	Predicted MW (Da)	Observed MW (Da)
4FW PurD	46,030.3	46,030.0
W290F PurF	56,317.8	56,314.0
7AW A82W/W290F PurF	56,433.9	56,433.0
7AW C1S/A82W/W290F PurF	56,417.9	56,424.0
7AW W290F/S345W PurF	56,417.9	56,415.0
7AW C1S/W290F/S345W PurF	56,401.9	56,409.0
7AW W290F/F477W PurF	56,357.8	56,357.0
7AW C1S/W290F/F477W PurF	56,341.8	56,348.0

spectrum and the observation of a shoulder between 290-320 nm (Figure 2.6A). This shoulder

was observed independently of monitoring emission at either 350 or 380 nm, indicating that the

observed fluorescence is due entirely to 7AW (Figure 2.6B).

[7AW]-PurF Mutants and [4FW]-PurD Exhibit Channeling Behavior

In order to use [7AW]-PurF mutants to study channeling interactions with PurD, the

W290F 7AW substitutions as well as the mutations themselves must not interfere with the

channeling process. Thus, as a prelude to the stopped-flow fluorescence experiments, each

protein was characterized individually and each [7AW]-PurF mutant:[4FW]-PurD pair was

shown to exhibit channeling behavior despite the substitutions. [4FW]-PurD was shown to have

$K_{m(PRA)} = 102 \pm 22$ μM and $V_{max} = 35.5 \pm 5.3$ U/mg (2 determinations, Figure 2.7), similar to the

wt PurD values under identical conditions ($K_{m(PRA)} = 98 \pm 12$ μM, $V_{max} = 42.5 \pm 2.5$ U/mg) (*2*).

The specific activities and the K_m values for PRPP and glutamine for all of the 7AW PurF

mutants were determined and are shown in Table 2.2. The A82W mutation, similar to previous

results by Zalkin, has 10-fold lower activity compared to the other mutants,
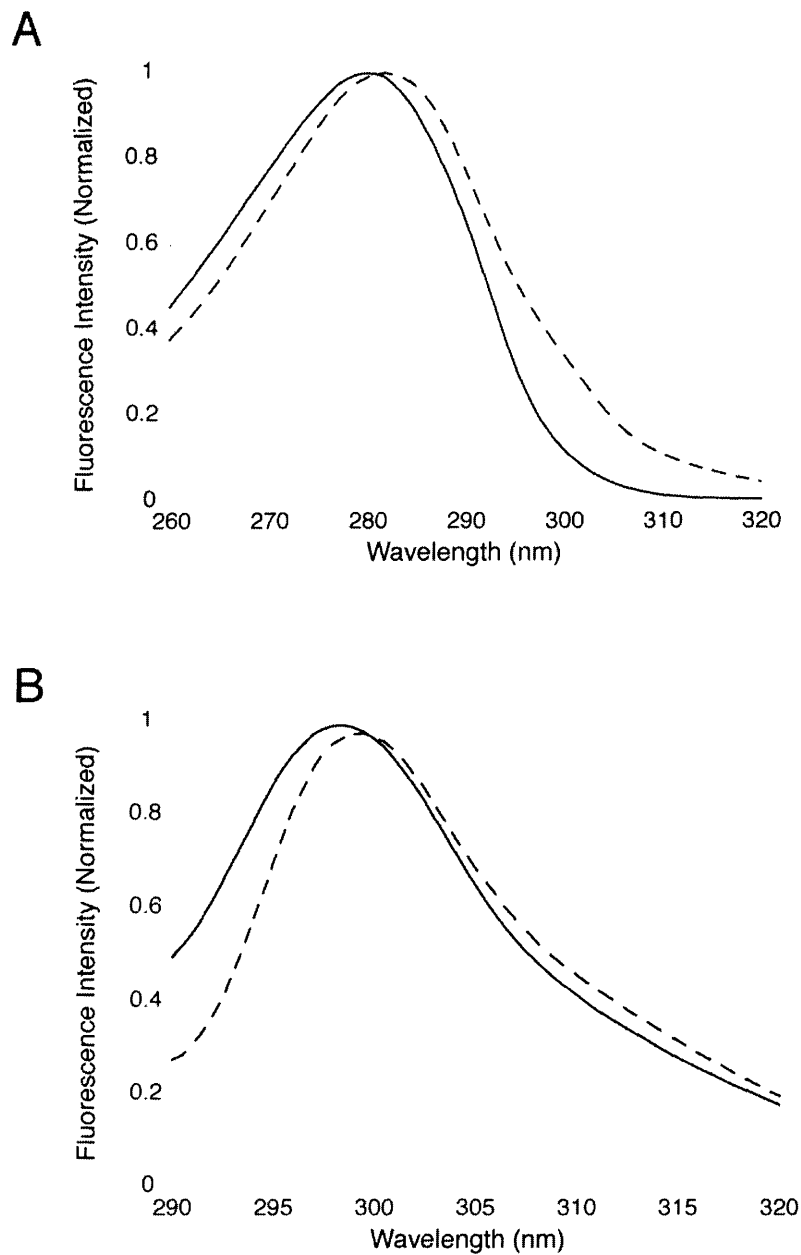
Figure 2.6—Evidence for 7AW incorporation into W290F/F477W PurF. (A) Excitation spectra collected between 260-320 nm while monitoring emission at 380 nm for tryptophan (solid line) and 7AW-labeled (dotted line) PurFs. The red-shift in the excitation spectra and the shoulder between 290-320 nm indicates high levels of 7AW incorporation. (B) The shoulder peak can easily be seen by subtraction of the tryptophan excitation spectrum from the 7AW excitation spectrum. This shoulder is present if the emission is monitored at 350 (solid line) or 380 nm (dotted line), which indicates that the observed fluorescence is due primarily 7AW.

while the S345W mutant has an increased K_m for glutamine. The remaining parameters are similar to those observed for W290F PurF.

Channeling assays were performed as previously described using $V_1 = 10.5$ μM PRA/min and $V_2 = 17$ μM GAR/min (2). As shown in Figure 2.8, by the criteria of no predicted lag phase, all the 7AW PurF mutants appear to channel PRA in the presence of [4FW]- PurD. At extended times, the rates of the S345W and F477W mutants reach the predicted steady-state rates for GAR formation. Thus, these mutations and the tryptophan substitutions do not appear to disrupt the proposed transient PurF:PurD interactions. The A82W/W290F mutant consistently showed a higher rate of GAR formation in channeling assays with [4FW]-PurD than the other mutants. Due to its low activity, ~10x more A82W/W290F PurF was added to the assay solution to maintain a rate of PRA synthesis of 10.5 μM/min compared to wt PurF and other mutants. Previously, channeling between wt PurF and PurD has been shown to possess a dependence on the protein concentration, with increased PRA channeling at higher enzyme concentrations (22). This provides support for the importance of protein:protein interactions in PRA transfer. The enhanced amount of GAR formed with the A82W/W290F mutant could be related to the higher concentration of PurF present in the assays, a possible indicator of PurF:PurD complex formation.

[7AW]-PurF Mutants Fluorescence Changes Can Be Monitored at λ > 360 nm

Given that all of the 7AW PurF mutants appear to channel PRA with [4FW]-PurD, the 7AW fluorescence must next be characterized in the steady state in order to determine excitation wavelengths and emission filters for use in stopped-flow experiments. In these experiments, C1S [7AW]-PurFs were used in which the catalytic cysteine in the glutaminase active site was mutated to a serine in order to prevent glutamine hydrolysis. As previously shown by Zalkin
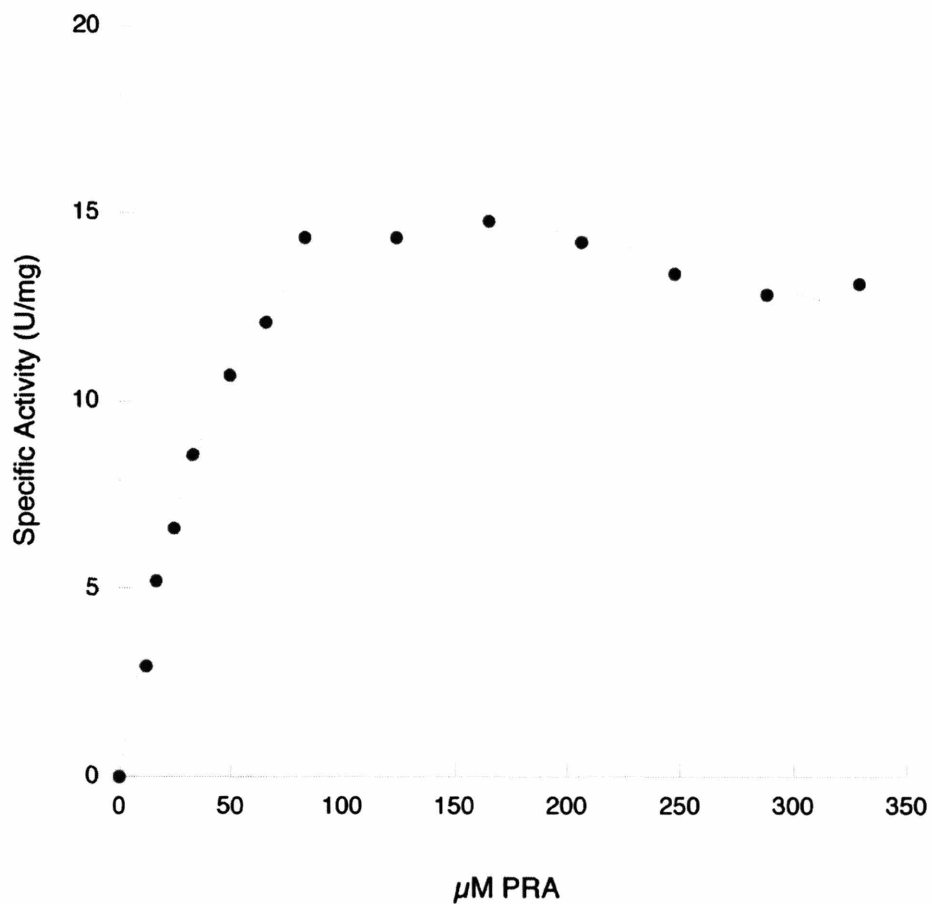
Figure 2.7—Kinetic Parameters for [4FW]-PurD. Data was fit to a model for substrate inhibition (Equation 2.2). For [4FW]-PurD, $K_m = 102 \pm 22\ \mu M$ (α/β), $V_{max} = 35.5\ \mu M \pm 5.3$ U/mg, and $K_i = 210\ \mu M \pm 55\ \mu M$.
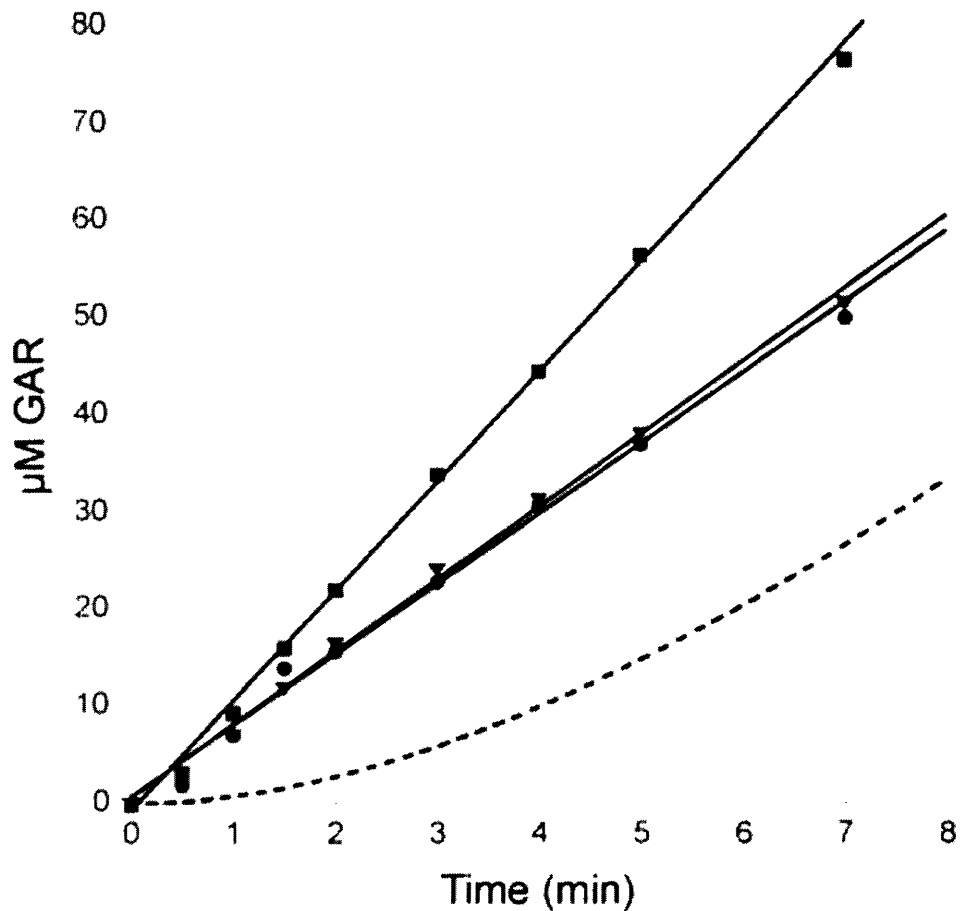
Figure 2.8—Channeling assays of the [7AW]-PurF mutants with [4FW]-PurD using $V_1 = 10.5$ μM PRA/min and $V_2 = 17$ μM GAR/min. (■) = A82W/W290F PurF. (●) = W290F/S345W PurF, (▼) = W290F/F477W PurF. Solid lines represent the best linear fit for each data set. The dashed line represents modeled, diffusion kinetics based on kinetic properties determined for the enzymes (Tables 2.2 and 2.4). W290F/S345W and W290F/F477W PurF display channeling behavior identical to what has previously been observed between wt PurF and wt PurD. A82W/W290F shows an enhanced rate of GAR synthesis.

with the tryptophan-containing PurF mutants, the C1S PurFs can bind PRPP and glutamine

without substrate turnover (6). C1S/A82W/W290F and C1S/W290F/S345W PurFs exhibit

fluorescence changes in response to PRPP- and PRPP- and glutamine-binding similar to those

previously described by Zalkin, albeit with a 20-30 nm red shift in the observed fluorescence due

to 7AW incorporation (Figure 2.9). Interestingly, C1S/W290F/F477W [7AW]-PurF showed a

decrease in fluorescence in the presence of PRPP and PRPP/glutamine. In the corresponding

tryptophan-containing mutant, fluorescence increases were observed (6). These steady state

experiments indicate that [7AW]-PurF fluorescence can be monitored for all the mutants at $\lambda >$

360 nm with excitation at 310 nm, well removed from normal excitation and emission

wavelengths for tryptophan.

[7AW]-PurF Mutants Rapidly Bind Glutamine at 18°C

In order to design stopped-flow experiments to test for interactions between [7AW]-

PurFs and [4FW]-PurD during PRA synthesis, fluorescence changes associated with glutamine

binding to a [7AW]-PurF•PRPP complex followed by enzyme turnover in the absence of PurD

were first characterized in the pre-steady state. These experiments were modeled after those

carried out by Zalkin using inactive C1S PurFs to monitor PRPP and glutamine binding in the

pre-steady state by monitoring tryptophan fluorescence (6).

Steady state fluorescence emission and quenching studies by Zalkin with glutamine,

PRPP, and PRPP followed by addition of glutamine to C1S-PurF mutants support an ordered

addition of substrates to PurF: PRPP followed by glutamine (6). These results are consistent

with steady state experiments carried out using the [7AW]-PurF mutants in which no change in
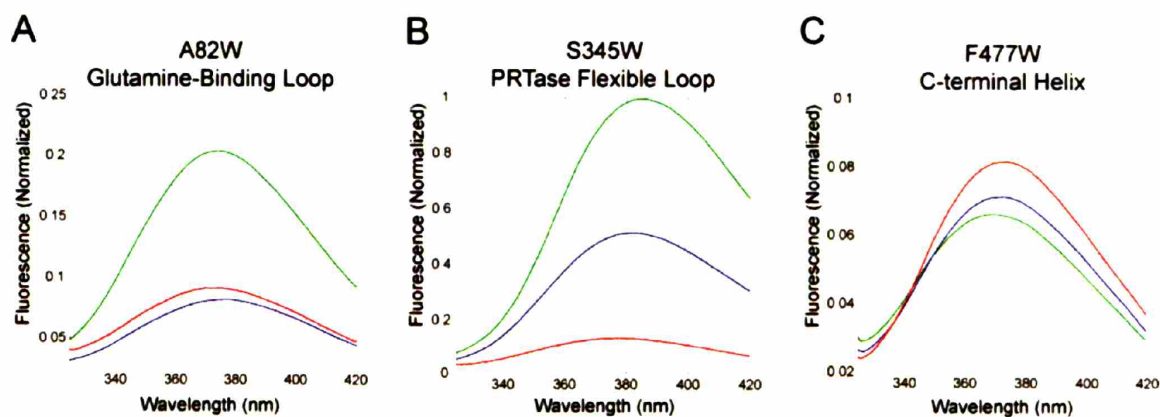
Figure 2.9—Changes in C1S [7AW]-PurF mutant fluorescence upon binding PRPP and Glutamine. Each sample contains 10 mM Tris pH 8.0, 10 mM MgCl$_2$, and 2 μM of the respective C1S W290F PurF mutant. Red = apo enzyme. Blue = enzyme + 1.5 mM PRPP. Green = enzyme + 1.5 mM PRPP + 20 mM L-gln. The fluorescence intensities on the y-axis in A, B, and C are directly comparable.

fluorescence was observed upon addition of glutamine in the absence of PRPP (data not shown).

Kinetic studies further supported an ordered addition as PRPP lowers the K_m for glutamine 100-fold and increased k_{cat} 3-fold (6). By monitoring movement of the PRTase flexible loop with the S345W reporter, Zalkin used stopped-flow tryptophan fluorescence to show that PRPP binds in a rapid, reversible fashion ($K_i = 88$ μM) followed by a slow isomerization (43 s^{-1}) (6). This latter step is proposed to place PurF•PRPP in a conformation to enhance glutamine binding.

Zalkin used a similar approach to study glutamine binding to the PurF•PRPP complex. He demonstrated that glutamine induces conformational changes in all of the PurF mobile regions: the glutamine-binding loop, the PRTase flexible loop, and the C-terminal helix (6). Zalkin further used stopped-flow tryptophan fluorescence and PRTase flexible loop (S345W) and C-terminal helix (F477W) reporter PurFs to measure glutamine binding. Results from the C-terminal helix reporter with changing glutamine concentrations are consistent with a 2-step mechanism of glutamine-binding involving rapid, reversible formation of the PurF•PRPP•Gln ternary complex followed by a slower enzyme isomerization which gives rise to the observed fluorescence changes. While the rate of ternary complex formation could not be determined from this data, the isomerization step was fit to a rate constant of 220 s^{-1} under saturating glutamine conditions (6). These studies, in addition to similar studies with S345W PurF suggest that glutamine-binding is accompanied by rapid conformational changes that convert PurF to an "active" form capable of glutamine-hydrolysis and PRA synthesis (6).

Since the goal of experiments in this chapter is to test for interactions between [7AW]-PurFs and [4FW]-PurD during PRA synthesis, initial experiments were patterned after those described above by Zalkin using active, [7AW]-PurFs. In this case, the observed fluorescence changes are reporting on conformational changes related to both binding and catalysis. In a

typical experiment, a [7AW]-PurF•PRPP complex was pre-mixed and placed into syringe 1. The contents of this syringe were then rapidly mixed with a saturating concentration of glutamine from syringe 2 and changes in fluorescence were monitored for each [7AW]-PurF mutant.

In agreement with Zalkin's findings with tryptophan mutants, multi-phase changes in fluorescence were observed with each PurF mutant upon mixing with glutamine (Figure 2.10A-C). For the glutamine-binding loop reporter (A82W/W290F, Figure 2.10A), data were fit to three distinct exponentials (Equation 2.7, Table 2.6). The rate of the first phase was 235.5 s^{-1} and was found to be dependent on the concentration of glutamine (Figure 2.11). It is assumed that this change is due to initial closure of the glutamine-binding loop accompanying ternary complex formation. The two slower phases occurred with rate constants of 23.9 and 2.9 s^{-1}, both of which are faster than the steady state turnover of 0.53 s^{-1} for this mutant. Neither of these rate constants can be attributed to a specific conformational or catalytic event.

Changes in fluorescence for reporters on the PRTase flexible loop (S345W) and the C-terminal helix (F477W) gave results that were fit to two exponentials (Figure 2.10, Table 2.6). With both the W290F/S345W and W290F/F477W [7AW]-PurFs, a rapid phase (175.9 and 122.0 s^{-1}, respectively) was followed by a slower phase (14.5 and 5.5 s^{-1}). It is possible that the fast phase observed with each mutant represents a similar fluorescence change to that characterized by Zalkin studying glutamine binding to the corresponding inactive C1S PurF•PRPP complexes. The slow change observed with the W290F/S345W [7AW]-PurF during turnover of 14.5 s^{-1} is still faster than the steady state turnover of 3.1 s^{-1}. In contrast, the slow phase with the C-terminal helix reporter (W290F/F477W) was very similar to the observed steady state turnover (both 5.5 s^{-1}). The changes in C-terminal helix fluorescence may thus be reporting on a rate-
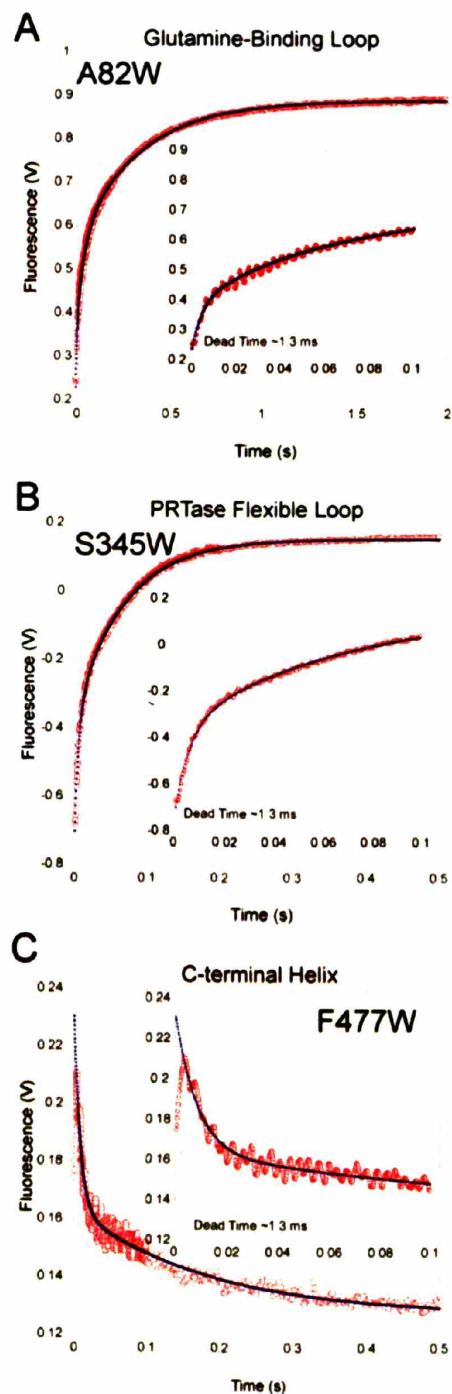
Figure 2.10—Fluorescence changes upon mixing [7AW]-PurF•PRPP with Gln (Experiment 1, Table 2.1). Shown in blue are the fits to the data as described in Table 2.6. In (A) and (B) data was collected with 500 data points between 0 → 0.2 s and 500 data points between 0.2 → 2 s for (A) and 0.2 → 1 s for (B). In (C) data was collected with 500 data points between 0 → 0.1 s and 500 data points between 0.1 → 1 s. The dead time is shown on the expanded regions shown in each trace. The rapid increase in fluorescence observed in (C) was found to occur largely within the instrument dead time, and was therefore not included in the data analysis.
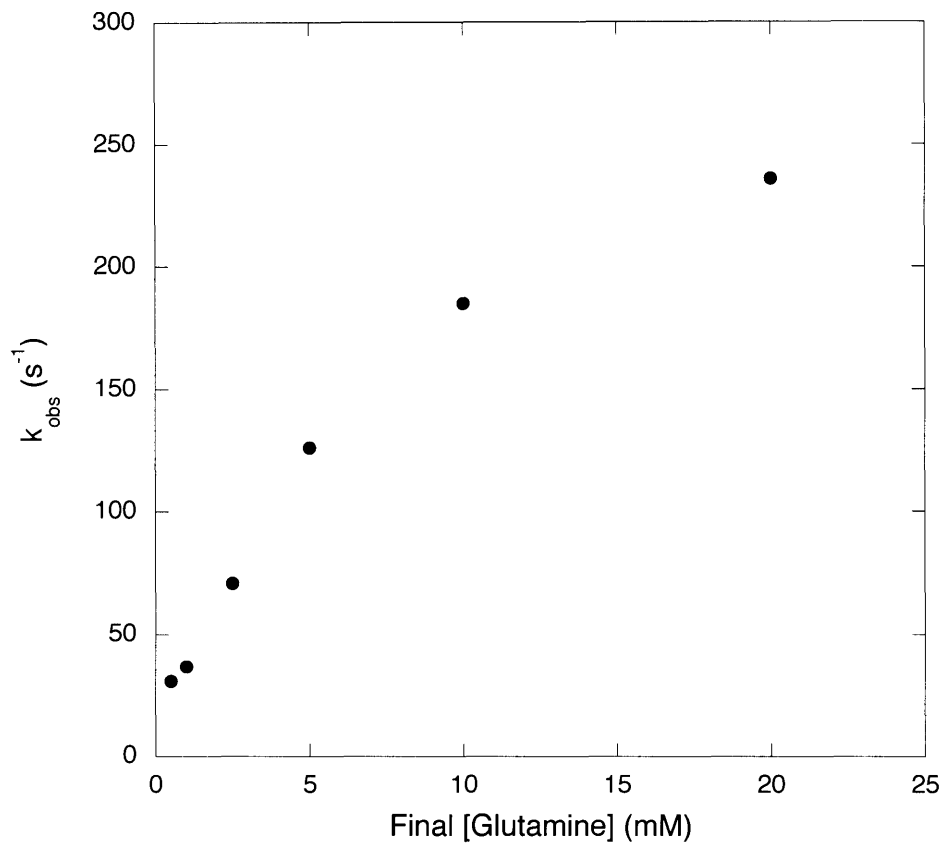
Figure 2.11—The effect of glutamine concentration on the rate of the first phase of the fluorescence changes observed upon mixing A82W/W290F [7AW]-PurF•PRPP in syringe 1 with varying concentrations of glutamine in syringe 2 (Figure 2.10A).

limiting step.   The results from studies on changes with [7AW]-PurF mutant fluorescence

during PRA synthesis are complex and indicate that multiple conformational changes are

occurring in the enzyme after ternary complex formation; however, without knowledge of the

pre-steady state rate of PRA formation and release, one cannot assign these changes to either a

specific chemical or conformational step.

Table 2.6: Calculated Fits for 7AW PurF•PRPP vs. Gln Stopped Flow Experiments

Enzyme	A_1	k_1 (s^{-1})	A_2	k_2 (s^{-1})	A_3	k_3 (s^{-1})	Variance
A82W W290F[a]	-0.176 ± 0.005	235.5 ± 14.1	-0.195 ± 0.003	23.9 ±0.7	-0.325 ± 0.002	2.9±0.1	4.02×10^{-5}
W290F S345W[b]	-0.395 ± 0.003	174.3 ± 3.0	-0.518 ± 0.002	14.5 ± 0.1			3.41×10^{-5}
W290F F477W[b]	0.070 ± 0.002	122.0 ± 4.4	0.036 ± 0.001	5.5 ±0.3			9.14×10^{-6}

[a]Fit to Equation 2.7 from t = 0.002-2 s. [b]Fit to Equation 2.8 from t = 0.002-1 s. [c]Fit to Equation 2.8 from t = 0.002-1 s.

Removal of PP$_i$ Contamination from PRPP Stocks Prior to Stopped-Flow Fluorescence

Experiments due to Interference with PurD

The above experiments set the stage for designing experiments to look for interactions

between the [7AW]-PurF mutants and [4FW]-PurD. During preliminary experiments to look at

this interaction, variable changes in fluorescence were observed upon addition of PurD.

Systematic analysis revealed that rapid mixing of PRPP and PurD resulted in small changes in

PurD background fluorescence (Figure 2.12A). Further investigation revealed that PP$_i$, a product

of PRPP breakdown, was responsible for these observations. These changes could potentially

mask fluorescence changes associated with PurF:PurD interactions in the pre-steady state.

Therefore, a method to remove PP$_i$ from the PRPP stock solutions using yeast inorganic

pyrophosphatase (PPase) was developed. Addition of PPase (~2 µg/mL) completely removed

the background fluorescence, did not interfere with [7AW]-PurF mutant fluorescence, and did
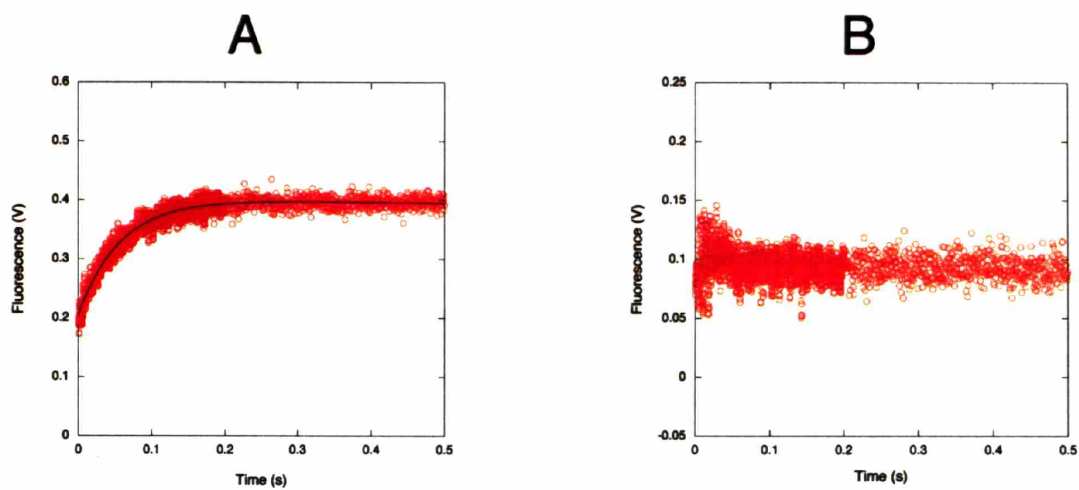
Figure 2.12—PurD background fluorescence due to PP_i contamination of PRPP solutions and removal of PP_i with PPase. (A) [4FW]-PurD (Syringe 1) was rapidly mixed with PRPP (3.0 mM, Syringe 2). (B) The same experiment as in (A) except that the PRPP had been pre-incubated with yeast PPase to destroy contaminating PP_i.
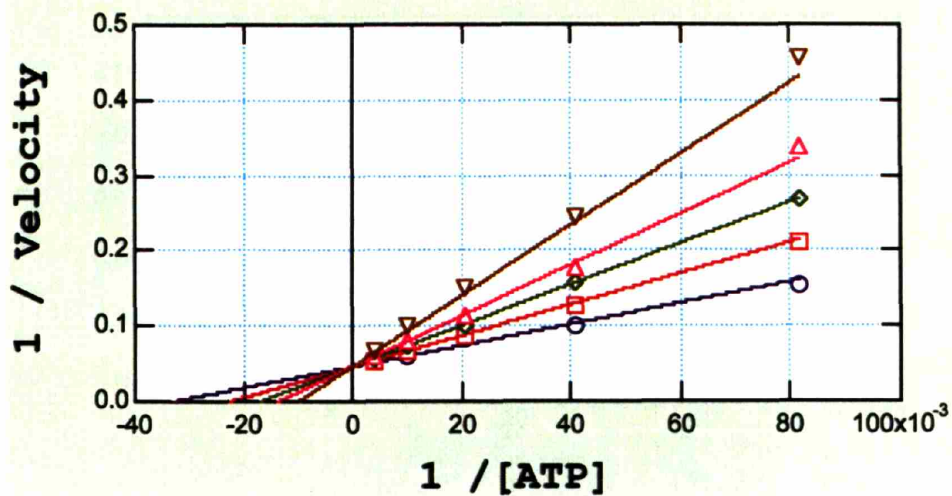
Figure 2.13—Inhibition of [4FW]-PurD by PP_i with respect to [ATP]. PP_i concentrations are 0 (blue), 0.5 (red), 1 (green), 1.5 (pink), and 2.5 mM (brown). The best fit was obtained from a competitive model, $K_{is} = 1.04 \pm 0.06$ mM, $K_m = 30 \pm 1$ μM, $k_{cat} = 21.5 \pm 0.2$ U/mg.
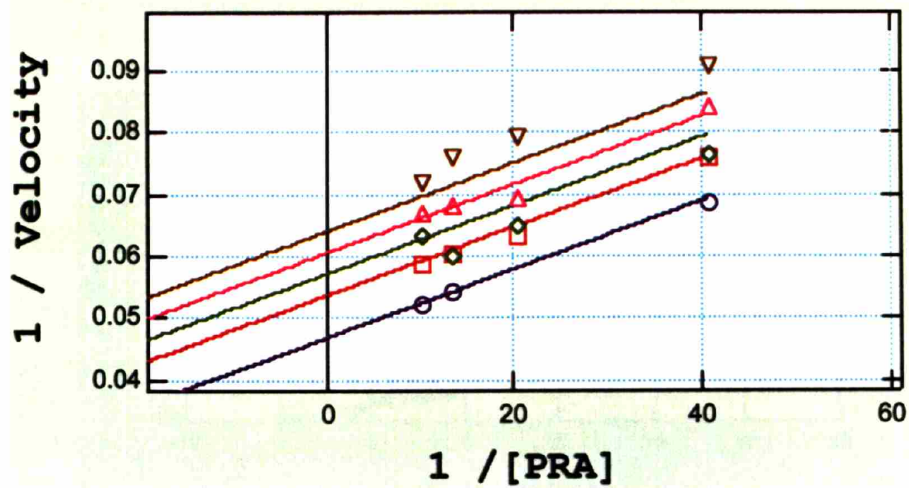
Figure 2.14—Inhibition of [4FW]-PurD by PP_i with respect to [PRA]. PP_i concentrations are 0 (blue), 0.5 (red), 1 (green), 1.5 (pink), and 2.5 mM (brown). The best fit was obtained from a uncompetitive model, $K_{ii} = 6.7 \pm 0.7$ mM, $K_m = 11.8 \pm 1.5$ μM, $k_{cat} = 21.3 \pm 0.6$ U/mg.
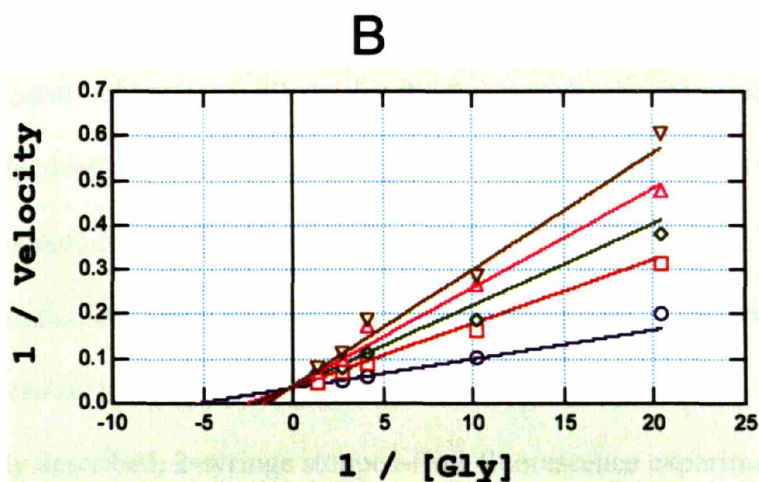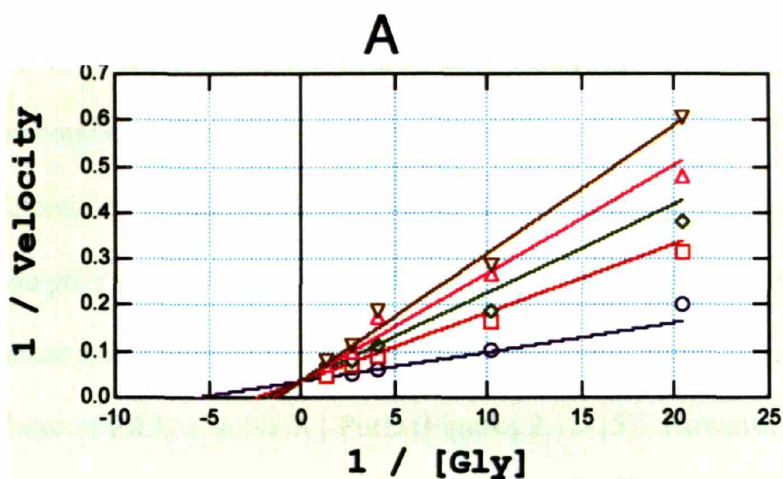
Figure 2.15—Inhibition of [4FW]-PurD by PP_i with respect to [Gly]. PP_i concentrations are 0 (blue), 0.5 (red), 1 (green), 1.5 (pink), and 2.5 mM (brown). The statistically relevant (by the F test) fit was obtained from a competitive model (A), $K_{is} = 0.72 \pm 0.12$ mM, $K_m = 0.18 \pm 0.03$ mM, $k_{cat} = 27.7 \pm 1.8$. The data could also be fit to a noncompetitive model (B), $K_{is} = 0.81 \pm 0.23$ mM, $K_{ii} = 20 \pm 39$ mM, $K_m = 0.18 \pm 0.04$ mM, $k_{cat} = 28.3 \pm 2.3$ U/mg.

not consume PRPP (Figure 2.12B). PRPP solutions used in stopped-flow experiments described

subsequently always contained PPase.

Efforts to determine the basis of the PP_i interaction with PurD were not successful. Not

surprisingly based on prior inhibition studies with PurD, PP_i was found to be a competitive

inhibitor of ATP, either a noncompetitive or competitive inhibitor with glycine, and an

uncompetitive inhibitor of PRA with [4FW]-PurD (Figures 2.13-15). However, the inhibition

constants were all in the mM range (Figures 2.13-15). The amount of PP_i contamination in

PRPP stock solutions (3%) would only give rise to a 50-100 µM contamination in a typical

stopped-flow experiment. Thus, it is unlikely that the fluorescence background associated with

PP_i results from its binding to the PurD active site. Its removal, however, was essential for

stopped-flow experiments described subsequently.

No Detectable Interaction between [7AW]-PurF Mutants and [4FW]-PurD During PRA

Synthesis as Monitored by Stopped-Flow Fluorescence

As previously described, 2-syringe stopped-flow fluorescence experiments of [7AW]-

PurF•PRPP versus glutamine report on conformational changes or chemistry within the enzyme

and are not informative about the pre-steady state rate of PRA formation or dissociation. Due to

the chemical instability of both PRPP and PRA, these values cannot be easily obtained by rapid

chemical quench methods. Chemical instability also complicates determination of the K_d for the

PurF•PRA complex. The inability to form a known concentration of PurF•PRA at defined times

after glutamine mixing with PurF•PRPP unfortunately limits how experiments can be carried out

to test for interactions between [4FW]-PurD and a [7AW]-PurF•PRA complex.

105

Based on 2-syringe experiments of A82W/W290F [7AW]-PurF•PRPP against glutamine, it is assumed that ternary complex formation is fast and leads to a conformational change involving closure of the glutamine-binding loop with a rate constant of 235.5 s^{-1}. A further assumption is that PRA formation occurs sometime after this observable change in fluorescence. Based on these assumptions, a [7AW]-PurF•PRPP•Gln ternary complex with a closed glutamine-binding loop can be exposed to [4FW]-PurD, and fluorescence changes can be monitored. While this experiment probes fluorescence changes accompanying PRA synthesis and [7AW]-PurF conformational changes, it is unclear when and how much [7AW]-PurF•PRA complex is present in the pre-steady state.

The ternary complex was formed using 3-syringe stopped flow methods. [7AW]-PurF and PRPP were first mixed and placed into syringe 1 to form the [7AW]-PurF•PRPP complex necessary for glutamine binding. This solution was then mixed with glutamine from syringe 2 to form the [7AW]-PurF•PRPP•Gln ternary complex. Based on the assumption that the fast change (235.5 s^{-1}) in fluorescence observed with the A82W/W290F [7AW]-PurF mutant is due to glutamine-binding loop closure, a mixing time of 10 ms should allow closure of this loop. This complex was then mixed with [4FW]-PurD from syringe 3 and changes in fluorescence during PRA synthesis were monitored. By comparing results from experiments in which syringe 3 contains either [4FW]-PurD or buffer, changes in fluorescence due to the presence of [4FW]-PurD can be identified and interpreted as evidence for a protein interaction during PRA synthesis.

As shown in Figure 2.16 and Table 2.7, the presence of [4FW]-PurD in syringe 3 made no difference to the observed changes in fluorescence compared to experiments in which syringe 3 contained only buffer. The measured rate constants for the A82W/W290F and W290F/S345W
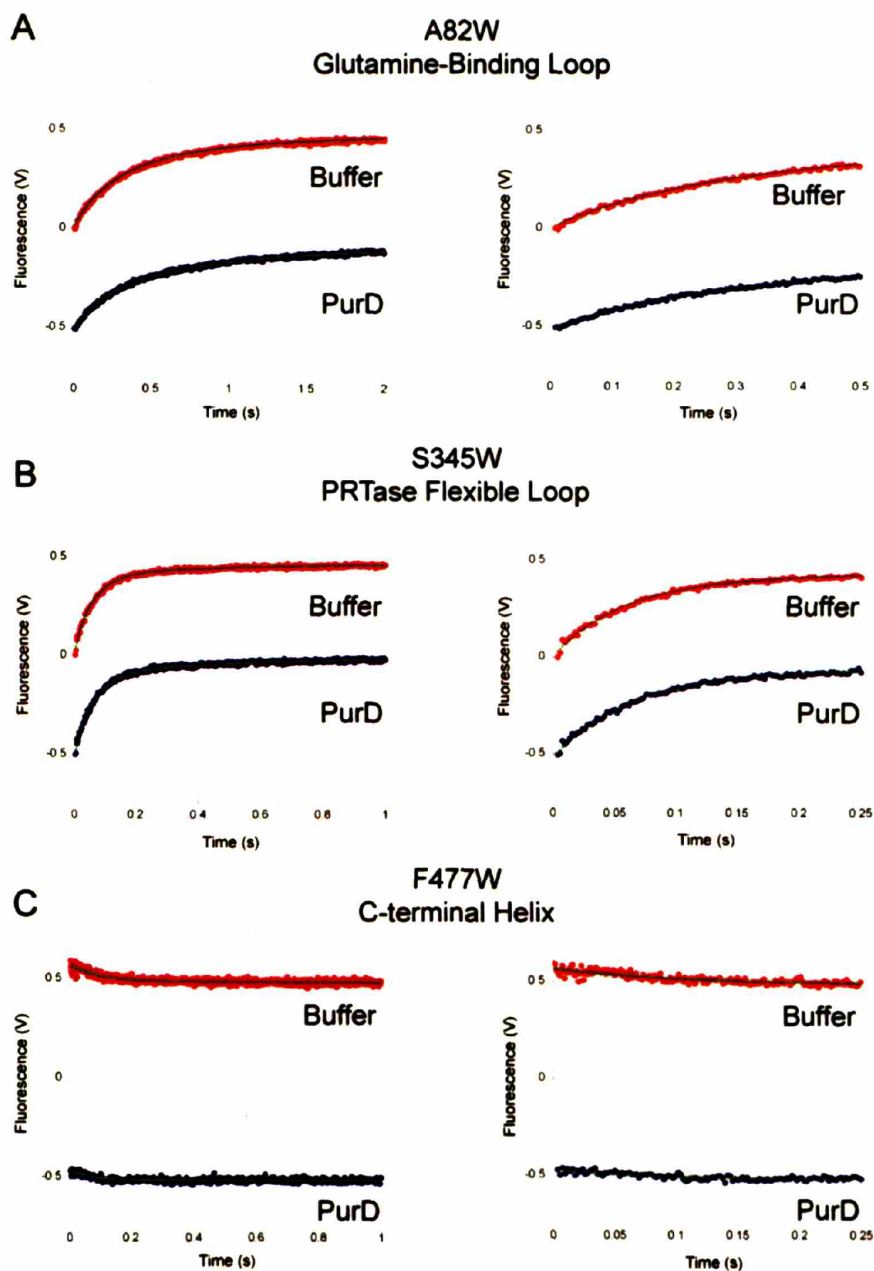
Figure 2.16—3 syringe experiments to detect interactions between [7AW]-PurF Mutants and [4FW]-PurD during PRA synthesis. Syringe contents are described in Table 2.1, Experiments 2 and 3. Solutions from syringe 1 (PurF•PRPP) and 2 (Glutamine) were aged for 10 ms before being mixed with syringe 3 and data collection. Syringe 3 contained either buffer or [4FW]-PurD. Only in the experiment shown in (B) are the changes in fluorescence directly comparable between samples containing buffer and [4FW]-PurD. In all other cases, the addition of fluorescence from [4FW]-PurD necessitated re-zeroing of the PMT detector between samples. Data has been offset for clarity.
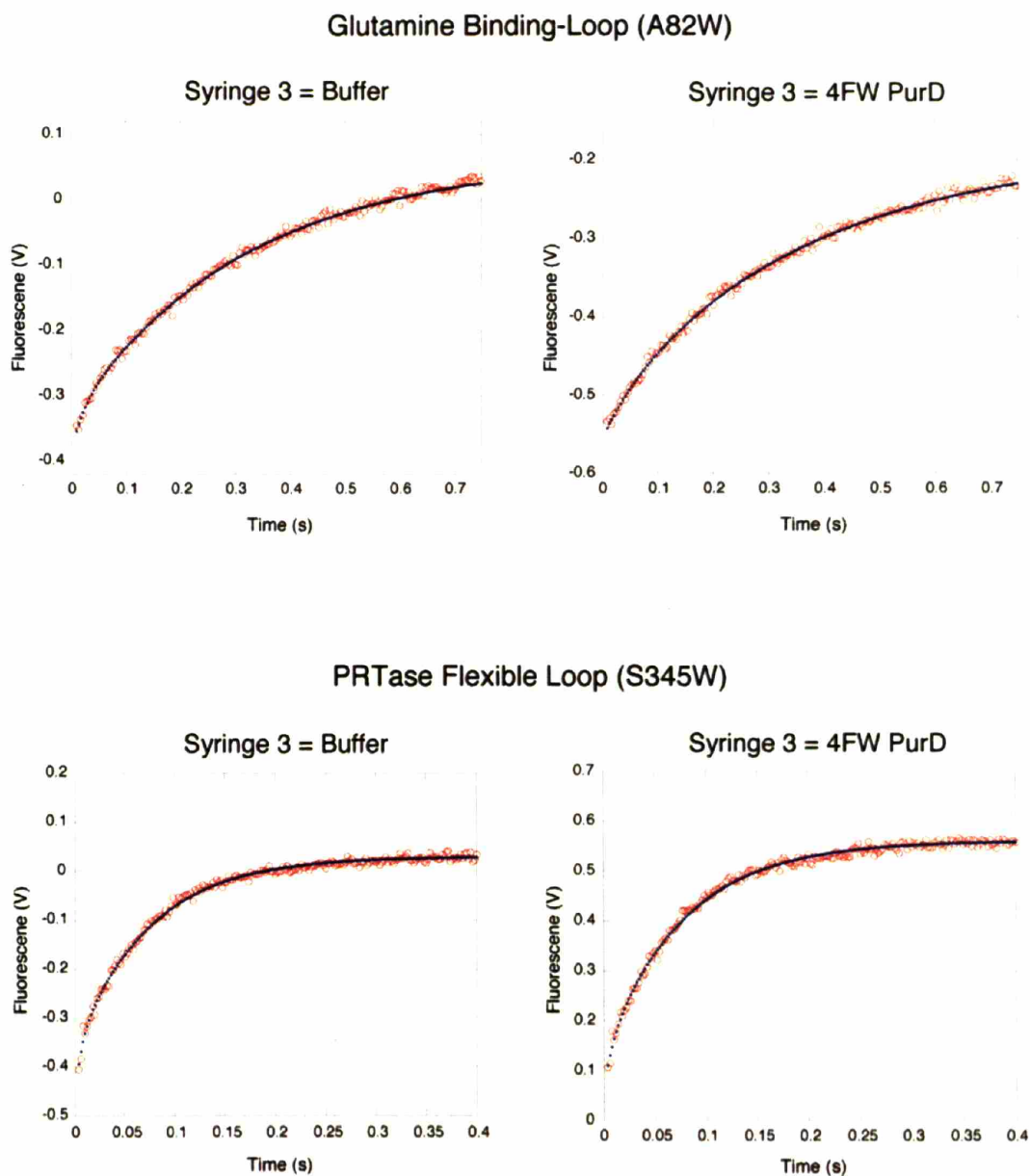
Figure 2.17—Expansion of data from A82W/W290F and W290F/S345W [7AW]-PurFs from Figure 2.16 showing the fits to the data (blue lines). The fitted rate constants (Table 2.7) are similar between the 2-syringe and 3-syringe experiments, independent of the presence of [4FW]-PurD.

[7AW]-PurF changes in fluorescence were similar between the 2-syringe and 3-syringe

experiments (Figure 2.17 and Tables 2.6 and 2.7). These results indicate that the 3-syringe

experiments with a 10 ms mixing time are successfully reproducing data obtained from 2 syringe

experiments of [7AW]-PurF•PRPP versus glutamine. For the W290F/F477W [7AW]-PurF,

increased noise from the 3-syringe experiment led to difficulty in fitting the fast kinetic phase;

however, it is clear that the presence of [4FW]-PurD does not significantly alter the observed

fluorescence changes compared to experiments carried out with buffer (Figure 2.16). Results

from the 3-syringe experiments indicate that [4FW]-PurD is not interacting with any of the

[7AW]-PurFs in a detectable manner during PRA synthesis.

Table 2.7: Calculated Fits 3 Syringe Stopped Flow Experiments of 7AW PurF•PRPP vs. Gln vs. 4FW PurD or Buffer[a]

Enzyme	A_1	k_1 (s^{-1})	A_2	k_2 (s^{-1})	Variance
A82W W290F/Buffer[b]	-0.055 ± 0.006	26.6 ± 5.9	-0.397 ± 0.004	2.7 ± 0.1	3.57×10^{-5}
A82W W290F/PurD[b]	-0.034 ± 0.018	19.1 ± 11.0	-0.329 ± 0.006	2.8 ± 0.5	2.66×10^{-5}
W290F S345W/Buffer[b]	-0.105 ± 0.011	179.7 ± 32	-0.394 ± 0.005	13.6 ± 0.2	4.68×10^{-5}
W290F S345W/PurD[b]	-0.094 ± 0.011	139.7 ± 29	-0.426 ± 0.006	12.6 ± 0.2	6.22×10^{-5}
W290F F477W/Buffer[c]	0.072 ± 0.008	11.0 ± 1.1	0.015 ± 0.007	4.1 ± 1.3	1.10×10^{-4}
W290F F477W/PurD[c]	0.053 ± 0.001	15.2 ± 0.3	-0.001 ± 0.001	2.5 ± 2.8	7.97×10^{-5}

[a] In all cases data was best fit to Equation 2.8 [b]Fit from t = 0.002-0.5 s. [c]Fit from t = 0.002-1 s.

Mimics of Reactive Intermediates of [7AW]-PurF Mutants Reveal No Interactions with [4FW]-PurD by Stopped-Flow Fluorescence

Since the 3-syringe experiments failed to detect any interactions during PRA synthesis,

the possibility was examined that specific [7AW]-PurF•substrate or glutamylthioester complexes

could be recognized by [4FW]-PurD. The stopped-flow experiments were designed based on a

simplified reaction for PurF shown in Scheme 2.2. As noted above, while Zalkin and

coworkers have studied PRPP and glutamine binding to PurF in detail, little is known about the

PurF reaction after ternary complex formation. PurF mechanistic studies have been complicated

$$\text{PurF + PRPP} \underset{}{\overset{}{\rightleftarrows} } \text{PurF}\bullet\text{PRPP} \xrightarrow{k_i} \text{PurF}\bullet\text{PRPP + Gln} \xrightarrow{k_{i\,(2)}}$$

$$\text{PurF}\bullet\text{PRPP}\bullet\text{GLN} \xrightarrow{k_{chem}}$$

PurF•PRA•GTE ⟶ PurF•GTE ⟶ PurF

?

PurF•PRA•GTE ⟶ PurF•PRA ⟶ PurF
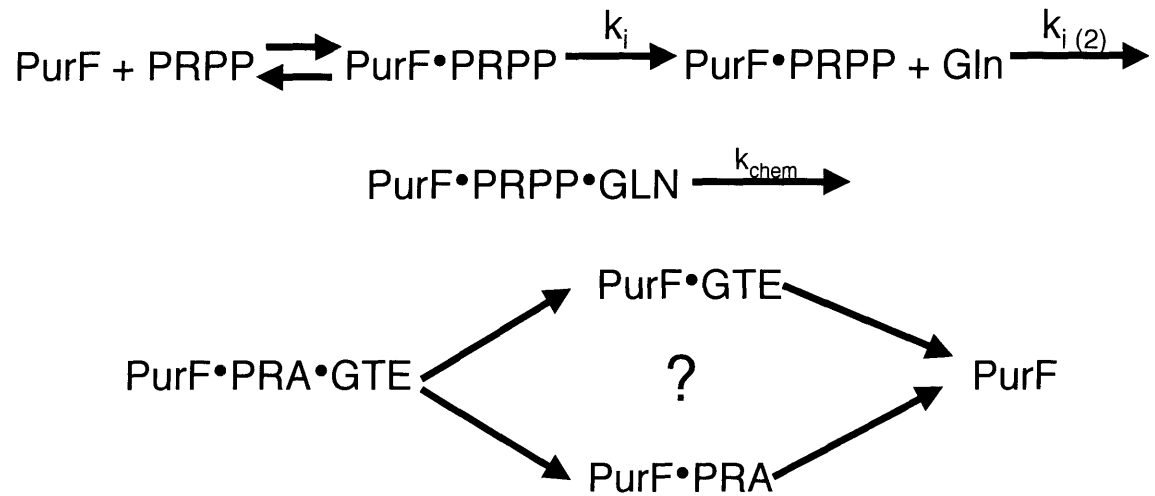
GTE = covalent PurF-glutamylthioester

Scheme 2.2—Hypothetical PurF reaction pathway.

110

by several factors including the irreversibility of the reaction and the instability of both PRPP and PRA. Nevertheless, the hypothetical pathway shown in Scheme 2.2 served as a guide to experimental design. After fast ternary complex formation, a chemical step occurs that leads to formation of PRA and PP_i in one active site (abbreviated as just PRA) and a glutamyl-thioester intermediate (GTE) in the glutaminase domain. Nothing is known about the order of release of products and two possibilities are shown.

Stopped flow methods were used to examine PurD interactions with chemically inert analogs of various PurF complexes shown in Scheme 2.2. The experiments carried out are listed in Table 2.1, numbers 4-8. Initially, [4FW]-PurD interactions with [7AW]-PurF alone were tested (Figure 2.18A). The evidence for an interaction would be a kinetically competent and reproducible change in fluorescence that could be observed above the experimental noise. As expected from previous attempts to measure steady state fluorescence changes, no interaction was observed. In a second set of experiments interactions between PurD and PurF saturated with PRPP were examined. As shown in Figure 2.18B, no interaction was observed in this case either. Interactions between the PurF•PRPP•Gln ternary complex and PurD were tested using inactive C1S PurF mutants which have been previously shown to bind substrates but not turnover (*6*). Again, no change in fluorescence was observed with any mutant (Figure 2.18C).

With the use of the mechanism-based inhibitor DON, several states of PurF containing a stable analog of the GTE can be probed. First, each PurF mutant was inactivated with DON until no detectable glutamine-dependent activity remained. Unreacted DON and PRPP were then removed by dialysis, after which the enzymes were assayed for NH_4Cl-dependent PRA synthesis (Table 2.3). While this inactivation with 10 mM DON and the W290F/S345W and W290F/F477W mutant PurFs was readily accomplished, the A82W/W290F PurF could not be

111
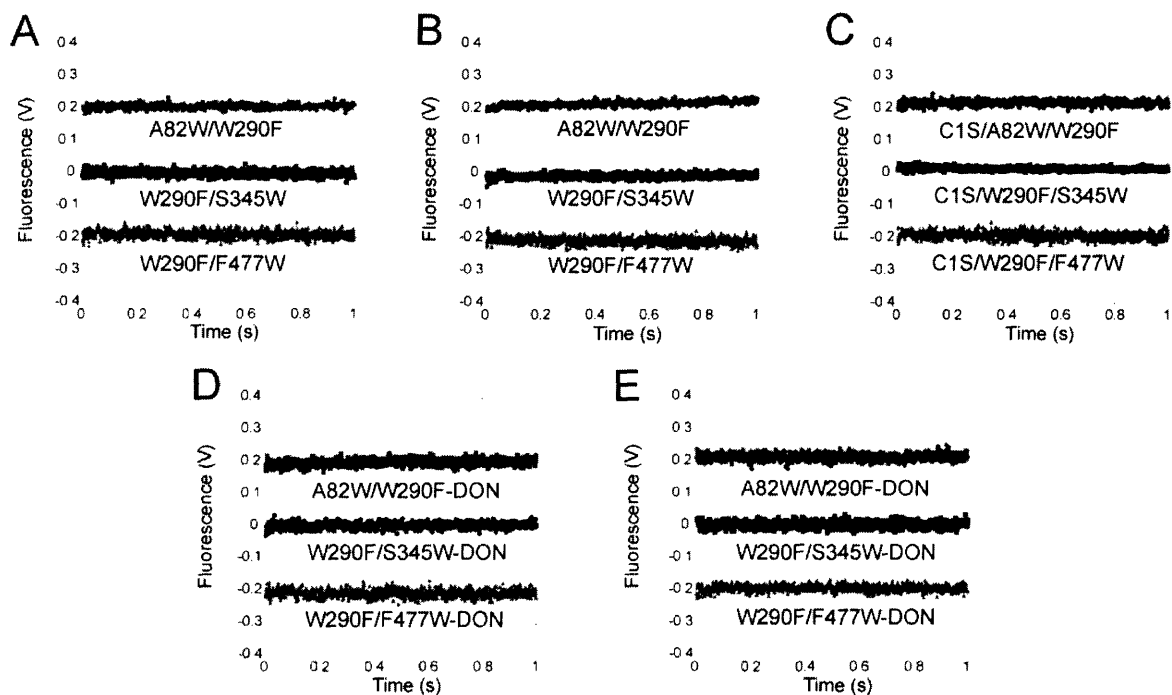
Figure 2.18—2 syringe experiments to test for interactions with [4FW]-PurD at various stages of the PurF reaction pathway. Data has been offset for clarity. (A) PurF vs. PurD (Table 2.1, Experiment 4) (B) PurF•PRPP vs. PurD (Table 2.1, Experiment 5) (C) PurF•PRPP•Gln vs. PurD (Table 2.1, Experiment 6) (D) PurF•PRPP•GTE vs. PurD (Table 2.1, Experiment 7) (E) PurF•GTE vs. PurD (Table 2.1, Experiment 8). No changes in fluorescence were observed for any [7AW]-PurF enzyme under any condition.

completely inactivated. DON appeared to rapidly inactivate ~50-60% of PurF within 15 min, after which no further inactivation was observed. Increasing the inactivation time, raising the temperature to 37°C, adding additional PRPP, or increasing DON concentrations up to 50 mM did not cause any further inactivation. Similar results were observed with the inhibitors azaserine and acivicin, with slightly lower levels of inactivation (data not shown). Thus, experiments with the A82W/W290F contain a mixture of active and DON-inactivated enzyme. Whether or not this observation is related to the enzyme's low specific activity or increased channeling behavior is unknown.

The DON-inactivated [7AW]-PurF mutants were saturated with PRPP, which mimics a hypothetical state in PurF in which NH_3 has been released from glutamine in the glutaminase domain but has not yet been incorporated into PRPP. Importantly, this state also comes closest to mimicking the crystal structure of DON-inactivated PurF bound to cPRPP upon which the docking model was based (*3*). As shown in Figure 2.18D, no interaction between [7AW]-PurF mutants and [4FW]-PurD was observed.

The final experiment was designed to mimic the PurF•GTE. This was performed using DON-inactivated PurF in the absence of PRPP. Again, no change in fluorescence was observed (Figure 2.18E). Together with the 3-syringe experiments, interactions between [7AW] PurFs and [4FW] PurD could not be detected using any of the stopped-flow methods described in this chapter.

Analytical Ultracentrifugation Studies on PurF Provide Evidence for the Use of PurF Trimers or Tetramers in Future Docking Models with PurD

The proposed docking model of PurF and PurD was based on a dimer of PurF interacting with a monomer of PurD in a shape and charge complimentary fashion (*5*). This model depends

113

on the ability to predict interactions between protein surfaces, an essential step of which is the use of a closed, PurF dimer crystal structure. The crystal structure of PurF (Figure 2.1B) was obtained by co-crystallizing DON-inactivated PurF with a carbocyclic PRPP analog (cPRPP) (3). Since this structure contains neither the natural substrate nor an actual glutamylthioester, the structure likely represents a subtle variation of the catalytically active form. In addition, over the years there has been extensive debate about the quaternary structure of PurF. Dimers (MW 112,714 Da), trimers (MW 169,071 Da), and tetramers (MW 225,248 Da) have all been reported using gel filtration chromatography, analytical ultracentrifugation, and chemical cross-linking methods of analysis (2-4, 25). The quaternary structure could have important implications in any docking model and, thus, preliminary SE- and SV-AUC studies were carried out to resolve this issue.

SE-AUC was carried out in Tris buffer at 3 speeds using PurF concentrations ranging from 7-36 μM (Figure 2.19). The choice of buffer and temperature (18°C) was designed to mimic conditions present in channeling assays and stopped-flow experiments. Global data analysis revealed that only a single species was present in solution. This species was determined to have a MW of 194,752 $\pm$ 8,000 Da, which was obtained directly from the reduced MW (0.97259 at 6,400 rpm). This is in good agreement with data obtained by Zalkin for the enzyme in phosphate buffer with 1 mM glutamine at 2.5°C (194,000 Da) (25). Unfortunately, the data do not clearly define a specific PurF species. The MW data obtained by SE-AUC is closest to a PurF trimer, although there is still a 25,000 MW difference. Based on the available crystal structures of PurF, it is unclear what structure a trimeric species would possess.

Intriguingly, slightly different results were obtained by SV-AUC using either the wt or a DON-inactivated enzyme (Figure 2.20). The active PurF enzyme sedimented with an observed

114

A

B
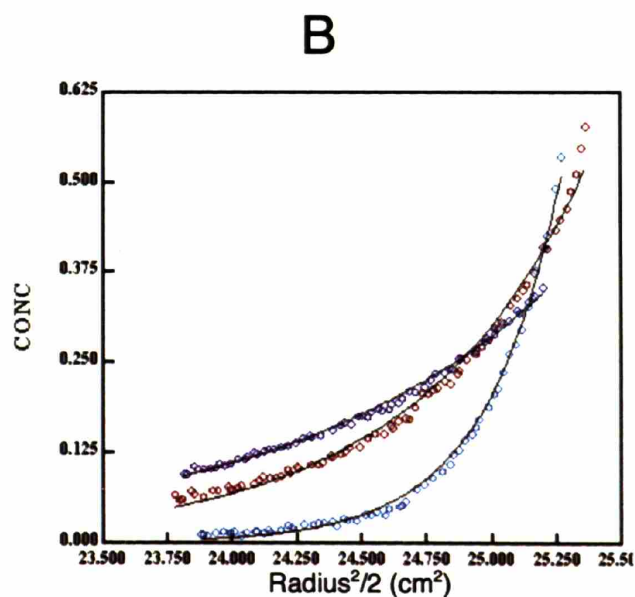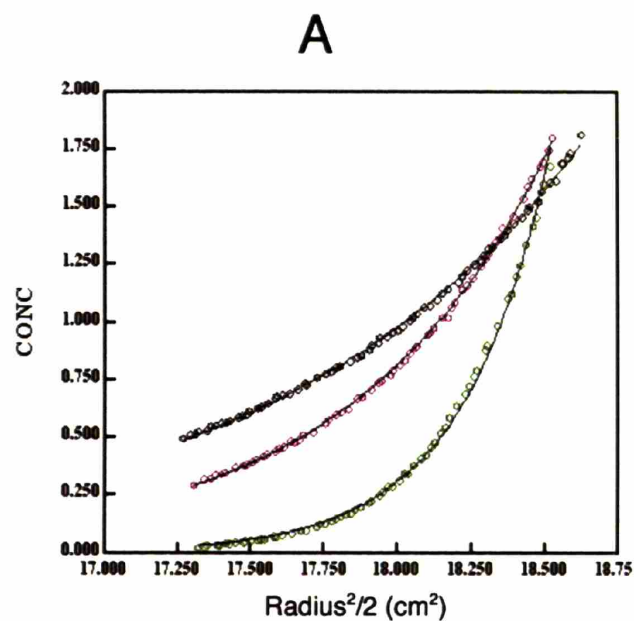
Figure 2.19—Analysis of PurF quaternary structure by SE-AUC. Each data set shows the change in concentration (y-axis) of PurF versus the square of the radial distance (x-axis) at equilibrium. (A) Data from 36 μM PurF at 6,400 (black), 8,000 (red), and 12,000 (green) rpm. (B) Data from 7 μM PurF at 6,400 (dark blue), 8,000 (red), and 12,000 (light blue) rpm. The best-fit lines obtained by global data analysis using WinNonLin software are shown with each data set.
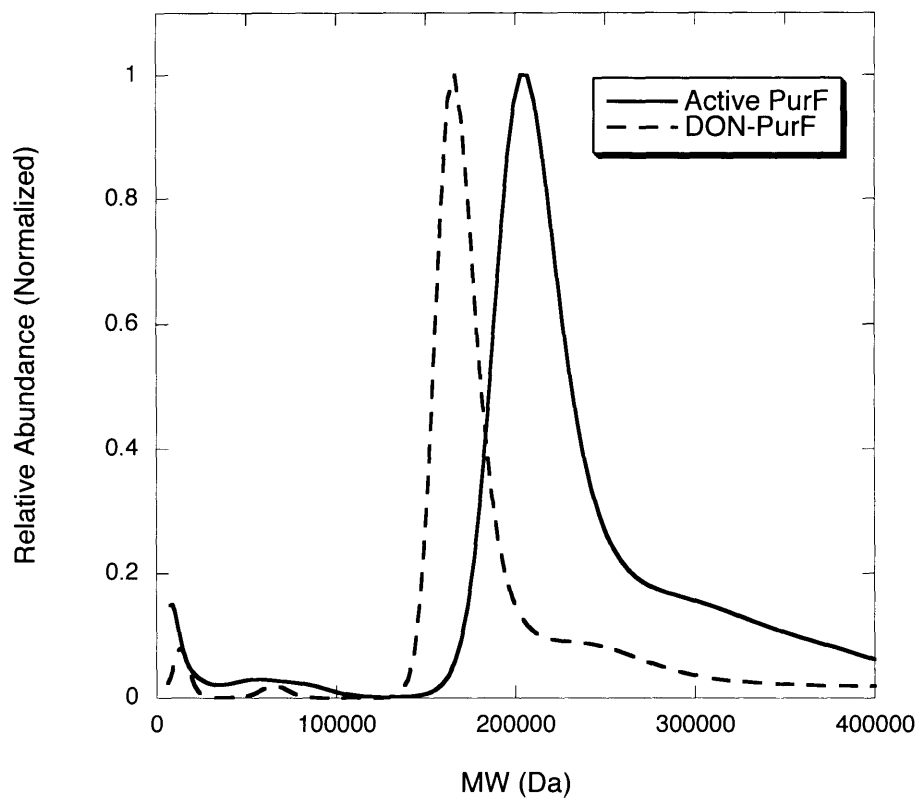
Figure 2.20—Results from SV-AUC experiments to determine PurF quaternary structure. The solid lines indicate data for active PurF (observed MW = 203, 120 Da), while the dashed line shows results for DON-inactivated PurF (observed MW = 166, 450 Da).

MW of 203,120 Da, which is closest to the PurF tetramer MW. However, the DON-inactivated enzyme sedimented as a 166,450 Da species, very close to the PurF trimer MW (Figure 2.20). The possibilities that a structurally-uncharacterized PurF trimer may be the active species in solution and that PurF quaternary structure may change during catalysis complicate any future proposed docking models between PurF and PurD.

2.4 Discussion

Kinetic analysis of GAR formation from PRPP using both PurF and PurD in solution has provided compelling evidence for channeling of PRA between enzyme active sites (2). Kinetic modeling based on the steady state parameters of PurF and PurD can be used to predict the rate of GAR formation with defined amounts of each enzyme with saturating substrates. In typical sets of experiments where a lag phase in GAR formation was predicted to preceed the steady-state rate, no lag phase was detected, that is the GAR produced exceeded predictions made by modeling the free diffusion kinetics (2). The kinetic analysis is robust and even modeling with experimental errors of 20% for PurF and PurD activities, the K_m for PRA, and the rate of PRA decomposition cannot account for the observed rate of GAR formation (2).

Considerable effort was made to show evidence for a PurF:PurD complex to provide further support for a channeling model *in vitro* and *in vivo*—all without success (2). A model was thus formulated that PurD interacts transiently with a PurF•PRA product complex. The presence of PRA is postulated to alter the PurF surface to maximize interactions with PurD and form a transient channeling complex.

Evidence that small molecules can alter weak protein interactions is provided in Chapter 3. The PurS, PurQ, and small PurL proteins from *B. subtilis* catalyze formation of formylglycinamidine ribonucleotide (FGAM) during the fourth step of purine biosynthesis, but

can only form an isolatable complex in the presence of Mg^{2+}-ADP (which acts as a structural cofactor) and glutamine (a substrate). A second example is PabA and PabB proteins involved in *p*-aminobenzoate synthesis. A complex of PabA and PabB has only been isolated in the presence of the glutamine substrate (*26*).

Transient interactions in the channeling model require an alternative method to those previously employed to detect PurF:PurD interactions. Stopped-flow fluorescence using specifically incorporated fluorescent probes has been used to characterize weak, protein-protein interactions. Phosphoryl-transfer between the chemotaxis proteins CheA and CheY, which occurs with a k_{cat} of ~750 s^{-1} and a K_m of ~6.5 μM, has been detected, for example, using this method (*27, 28*). Consequently, the focus of this chapter is on using this method to look for PurF/PurD interactions under physiological concentrations of 5 μM. These efforts required using 7AW and 4FW tryptophan substitutions so that changes in PurF fluorescence could be specifically monitored.

As shown in Figures 2.16, 2.17 and Table 2.7, no interactions between [7AW]-PurF mutants and [4FW]-PurD were detected during PRA synthesis. Definitive interpretation of these results is not possible due to uncertainties surrounding the concentration and timing of PurF•PRA formation during the pre-steady state. While no interactions were observed, it is possible that a sufficiently high enough concentration of [7AW]-PurF•PRA was not generated to allow detection of the desired interaction. Several 2-syringe stopped-flow fluorescence experiments were then employed to investigate the possibility that specific, static [7AW]-PurF complexes might interact with [4FW]-PurD. Complexes were designed to mimic PurF reaction intermediates; however, no change in fluorescence was observed with [4FW]-PurD in any case with any of the [7AW]-PurF mutants (Figure 2.18). Based on these results, it can be concluded

that fluorescent probes on the PRTase flexible loop, the glutamine-binding loop, and C-terminal helix all failed to detect any interaction with PurD during the experiments carried out in this chapter.

There are several possible interpretations of these results. The first is that perhaps the enzymes interact too rapidly to monitor by stopped-flow fluorescence. Given the dead time of the stopped-flow apparatus (~1.3 ms), rates constants of ~500 s^{-1} can be accurately measured (50% completion during the dead time). There is precedence for rapidly interacting proteins in *E. coli*. For the CheA and CheY phospho-transfer interaction, the estimated protein complex half-life *in vivo* is believed to be ~2 ms (*29*). This interaction is too rapid to accurately monitor by stopped-flow spectroscopy under saturating protein concentrations, and a rate of ~800 s^{-1} for the protein association under saturating conditions has been extrapolated from concentration-dependence studies on fluorescence changes that occur during complex formation in the pre-steady state (*27-29*). Similar experiments could be performed on the PurF:PurD system; however, a stronger fluorophore than 7AW should be used to detect possible interactions that may occur in only a small percentage of the PurF in solution.

A second interpretation of these results would be that the docking model is incorrect and that the probes were not placed at the correct positions to monitor protein interactions. As described in the results section, a key component of the docking model is the use of a PurF dimer containing the substrate analogs DON and cPRPP. It is unknown how well this structure mimics the PurF•PRA complex, and it is possible that the enzyme undergoes further conformational changes upon product formation. The use of cPRPP in the crystal structure is particularly problematic since there is kinetic evidence that while this analog is a competitive inhibitor of PRPP, it does not convert the enzyme into an active conformation capable of glutamine

hydrolysis (*30*). Furthermore, the catalytically relevant quaternary structure of PurF remains undetermined. Dimers and tetramers have been observed by crystallography (*3, 4*), while dimers, trimers, and tetramers have all been reported in solution (*2, 25*).

Unfortunately, the AUC experiments presented in this chapter were unable to provide new insight into PurF quaternary structure (Figures 2.19 and 2.20). The AUC experiments indicated that a PurF trimer may be present in solution, although it is unclear what structure this species would have. Future experiments may benefit from the generation of new docking models taking into account alternate PurF structures; however, any reasonable channeling complex should align the enzyme active sites to allow direct transfer of PRA. The most striking result from the stopped-flow experiments is that none of the mobile regions of PurF appeared to interact with PurD in any detectable manner. These results are especially surprising with the W290F/S345W 7AW PurF mutant, since movement of this loop is required for PRA transfer in the docking model. It is currently unclear and seems unlikely that a PurF:PurD channeling complex could be formed that would align the enzyme active sites for PRA transfer and not involve any of the mobile regions that cover the PRPP binding site of PurF.

The final possibility is that the enzymes do not channel PRA, and channeling kinetics are, instead, an artifact of an incomplete kinetic analysis of the enzymes in solution. Due to the reproducibility of the channeling kinetics, this is not the favored interpretation. The largest source of error in the modeling PRA diffusion kinetics between PurF and PurD comes from measurement of the PRA K_m. A large degree of substrate inhibition is observed with PRA, and this could affect the accuracy of this value (Figure 2.7). However, even large errors in the K_m should still result in the observation of a lag phase in the rate of GAR formation during channeling experiments (*2*). In addition, experiments by Zalkin and Smith using heterologous

thermophilic/mesophilic PurF:PurD pairs have provided additional evidence for transfer of PRA between PurF and PurD, although these experiments were not designed to detect a lag phase (*31*). Unfortunately, due to PRPP and PRA instability, a detailed kinetic analysis of PurF and PurD remains challenging. In particular, the amount of kinetic information concerning PRA formation and binding (such as k_{on}, k_{off}, and K_d's) that can be learned from the enzymes and applied to future models of metabolite transfer is limited, and any attempts to measure these values will be extremely difficult. It may be possible in the future to measure the pre-steady state rates of PRA formation and release by PurF using rapid chemical quench methods and a sufficient amount of PurD to trap PRA as a more stable molecule, GAR, for analysis. These experiments would require a detailed kinetic analysis of PurD prior to the experiment to ensure that every step in the conversion of PRA to GAR in the pre-steady state is faster than the PurF kinetics under investigation.

In conclusion, these results provide no evidence for any interaction between PurF and PurD in the pre-steady state, even during PRA synthesis. This indicates that either the interaction is too fast to detect using stopped-flow methods, or that the fluorescent probes were not positioned to detect an interaction. The latter interpretation indicates that the docking model between PurF and PurD may be incorrect. Future stopped-flow experiments may benefit from the use of stable, carbocyclic analogs of PRA (cPRA). cPRA has been synthesized by the Caperelli laboratory and is an efficient substrate for *E. coli* PurD (k_{cat}/K_m 2.1 x 10^3 M^{-1} s^{-1} for ($\pm$) cPRA compared to 2.4 x 10^5 M^{-1} s^{-1} for α/β-PRA) (*32, 33*). Use of cPRA to mimic a PurF•PRA complex may provide additional information concerning PurF structure and PRA binding. However, given previous findings that cPRPP does not bind to PurF in a conformation that activates the enzyme for catalysis (*30*), it is unclear how sensitive the enzyme will be to

substitution of the PRA ribose ring with cyclopentane. A complete kinetic characterization of cPRA binding to PurF followed by pre-steady state kinetic experiments using [7AW]-PurFs and [4FW]-PurD in the presence of cPRA may provide additional data in support of the findings presented in this chapter.

2.5 REFERENCES

(1)   Schendel, F. J., Cheng, Y. S., Otvos, J. D., Wehrli, S., and Stubbe, J. (1988) Characterization and chemical properties of phosphoribosylamine, an unstable intermediate in the de novo purine biosynthetic pathway. *Biochemistry 27*, 2614-23.

(2)   Rudolph, J. and Stubbe, J. (1995) Investigation of the mechanism of phosphoribosylamine transfer from glutamine phosphoribosylpyrophosphate amidotransferase to glycinamide ribonucleotide synthetase. *Biochemistry 34*, 2241-50.

(3)   Krahn, J. M., Kim, J. H., Burns, M. R., Parry, R. J., Zalkin, H., and Smith, J. L. (1997) Coupled formation of an amidotransferase interdomain ammonia channel and a phosphoribosyltransferase active site. *Biochemistry 36*, 11061-8.

(4)   Muchmore, C. R., Krahn, J. M., Kim, J. H., Zalkin, H., and Smith, J. L. (1998) Crystal structure of glutamine phosphoribosylpyrophosphate amidotransferase from *Escherichia coli. Protein Sci. 7*, 39-51.

(5)   Wang, W., Kappock, T. J., Stubbe, J., and Ealick, S. E. (1998) X-ray crystal structure of glycinamide ribonucleotide synthetase from Escherichia coli. *Biochemistry 37*, 15647-62.

(6)   Chen, S., Burgner, J. W., Krahn, J. M., Smith, J. L., and Zalkin, H. (1999) Tryptophan fluorescence monitors multiple conformational changes required for glutamine phosphoribosylpyrophosphate amidotransferase interdomain signaling and catalysis. *Biochemistry 38*, 11659-69.

(7)   Wong, C. Y. and Eftink, M. R. (1998) Incorporation of tryptophan analogues into staphylococcal nuclease: stability toward thermal and guanidine-HCl induced unfolding. *Biochemistry 37*, 8947-53.

(8)   Cheng, Y. S., Shen, Y., Rudolph, J., Stern, M., Stubbe, J., Flannigan, K. A., and Smith, J. M. (1990) Glycinamide ribonucleotide synthetase from *Escherichia coli*: cloning, overproduction, sequencing, isolation, and characterization. *Biochemistry 29*, 218-27.

(9)   Laue, T. M., Shah, B. D., Ridgeway, T. M., and Pelletier, S. L. (1992) in *Analytical Ultracentrifugation in Biochemistry and Polymer Science* (Harding, S. E., Rowe, A. J., and Horton, J. C., Eds.) pp 90-125, Royal Society of Chemistry, Cambridge, U.K.

(10)   Schuck, P. (2000) Size distribution analysis of macromolecules by sedimentation velocity ultracentrifugation and Lamm equation modeling. *Biophysical J. 78*, 1606-1619.

(11)   Perron, M. J., Blouse, G. E., and Shore, J. D. (2003) Distortion of the catalytic domain of tissue-type plasminogen activator by plasminogen activator inhibitor-1 coincides with the formation of stable serpin-proteinase complexes. *J. Biol. Chem. 278*, 48197-203.

(12)   Mohammadi, F., Prentice, G. A., and Merrill, A. R. (2001) Protein-protein interaction using tryptophan analogues: novel spectroscopic probes for toxin-elongation factor-2 interactions. *Biochemistry 40*, 10273-83.

(13)   Zhang, Q. S., Shen, L., Wang, E. D., and Wang, Y. L. (1999) Biosynthesis and characterization of 4-fluorotryptophan-labeled *Escherichia coli* arginyl-tRNA synthetase. *J. Protein Chem. 18*, 187-92.

(14)   Wong, C. Y. and Eftink, M. R. (1998) Incorporation of tryptophan analogues into staphylococcal nuclease, its V66W mutant, and Delta 137-149 fragment: spectroscopic studies. *Biochemistry 37*, 8938-46.

(15)   Bronskill, P. M. and Wong, J. T. (1988) Suppression of fluorescence of tryptophan residues in proteins by replacement with 4-fluorotryptophan. *Biochem. J. 249*, 305-8.

(16)   Browne, D. T. and Otvos, J. D. (1976) 4-Fluorotryptophan alkaline phosphatase from *E. coli*: preparation, properties, and 19F NMR spectrum. *Biochem. Biophys. Res. Commun.* *68*, 907-13.

(17)   Pratt, E. A. and Ho, C. (1975) Incorporation of fluorotryptophans into proteins of *Escherichia coli*. *Biochemistry 14*, 3035-40.

(18)   Soumillion, P., Sexton, D. J., and Benkovic, S. J. (1998) Clamp subunit dissociation dictates bacteriophage T4 DNA polymerase holoenzyme disassembly. *Biochemistry 37*, 1819-27.

(19)   Muralidharan, V., Cho, J., Trester-Zedlitz, M., Kowalik, L., Chait, B. T., Raleigh, D. P., and Muir, T. W. (2004) Domain-specific incorporation of noninvasive optical probes into recombinant proteins. *J. Am. Chem. Soc. 126*, 14004-12.

(20)   Wang, L. and Schultz, P. G. (2004) Expanding the genetic code. *Angew. Chem. Int. Ed. Engl. 44*, 34-66.

(21)   Lotte, K., Plessow, R., and Brockhinke, A. (2004) Static and time-resolved fluorescence investigations of tryptophan analogues--a solvent study. *Photochem. Photobiol. Sci. 3*, 348-59.

(22)   Rudolph, J. (1993) PhD thesis, Department of Chemistry, Massachusetts Institute of Technology, Cambridge, Massachusetts.

(23)   Broos, J., ter Veld, F., and Robillard, G. T. (1999) Membrane protein-ligand interactions in *Escherichia coli* vesicles and living cells monitored via a biosynthetically incorporated tryptophan analogue. *Biochemistry 38*, 9798-803.

(24)   Waxman, E., Rusinova, E., Hasselbacher, C. A., Schwartz, G. P., Laws, W. R., and Ross, J. B. A. (1993) Determination of the Tryptophan:Tyrosine Ratio in Proteins. *Anal. Biochem. 210*, 425-428.

(25)   Messenger, L. J. and Zalkin, H. (1979) Glutamine phosphoribosylpyrophosphate amidotransferase from *Escherichia coli*. Purification and properties. *J. Biol. Chem. 254*, 3382-92.

(26)   Rayl, E. A., Green, J. M., and Nichols, B. P. (1996) *Escherichia coli* aminodeoxychorismate synthase: analysis of pabB mutations affecting catalysis and subunit association. *Biochim Biophys Acta 1295*, 81-8.

(27)   Stewart, R. C., Jahreis, K., and Parkinson, J. S. (2000) Rapid phosphotransfer to CheY from a CheA protein lacking the CheY-binding domain. *Biochemistry 39*, 13157-65.

(28)   Stewart, R. C. and VanBruggen, R. (2004) Phosphorylation and binding interactions of CheY studied by use of Badan-labeled protein. *Biochemistry 43*, 8766-77.

(29)   Stewart, R. C. (1997) Kinetic characterization of phosphotransfer between CheA and CheY in the bacterial chemotaxis signal transduction pathway. *Biochemistry 36*, 2030-40.

(30)   Kim, J. H., Wolle, D., Haridas, K., Parry, R. J., Smith, J. L., and Zalkin, H. (1995) A stable carbocyclic analog of 5-phosphoribosyl-1-pyrophosphate to probe the mechanism of catalysis and regulation of glutamine phosphoribosylpyrophosphate amidotransferase. *J. Biol. Chem. 270*, 17394-9.

(31)   Bera, A. K., Chen, S., Smith, J. L., and Zalkin, H. (2000) Temperature-dependent function of the glutamine phosphoribosylpyrophosphate amidotransferase ammonia channel and coupling with glycinamide ribonucleotide synthetase in a hyperthermophile. *J. Bacteriol. 182*, 3734-9.

(32)   Caperelli, C. A. and Liu, D. (1992) Carbocyclic substrates for de novo purine biosynthesis. Enantiospecific synthesis and enantiospecificity of enzymatic utilization. *J. Biol. Chem. 267*, 9783-7.

(33)   Liu, D. S. and Caperelli, C. A. (1991) Carbocyclic substrates for de novo purine biosynthesis. *J. Biol. Chem. 266*, 16699-702.

Chapter 3:

Characterization of the *B. subtilis* FGAR-AT Complex

3.1 Introduction

The purine biosynthetic pathway requires eleven enzymatic transformations in prokaryotes, each of which has been studied in detail (Scheme 1.1). With the exception of the fourth enzyme in this pathway, formylglycinamide ribonucleotide amidotransferase (FGAR-AT or PurL), all of the enzymes have previously been structurally characterized as well (*1*). FGAR-AT catalyzes the transformation shown in Scheme 3.1 in which glutamine (gln) supplies the ammonia to an ATP-activated, formylglycinamide ribonucleotide (FGAR) to generate ADP, inorganic phosphate (P_i), glutamate (glu), and formylglycinamidine ribonucleotide (FGAM). This reaction can be divided into two half-reactions. In one half-reaction, glutamine is hydrolyzed to glutamate through a covalent thioester intermediate (Equtaion 3.1). In the second half-reaction, ATP is proposed to activate the amide oxygen of FGAR for nucleophilic attack by the ammonia generated in the first half-reaction (Equation 3.2) (*1*).

$$Gln + H_2O \rightarrow Glu + NH_3 \tag{3.1}$$

$$FGAR + ATP + NH_3 \rightarrow FGAM + ADP + P_i \tag{3.2}$$
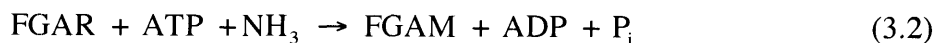
Recently, interest in FGAR-ATs has re-surfaced for several reasons. First, the most extensively studied PurLs, those isolated from *E. coli* and chicken liver, are monomers of MW ~140 kDa (lgPurLs). The large size, more than adequate to convert an amide to an amidine (Scheme 3.1), has lead to the hypothesis that this protein might serve as a scaffold to organize the eleven proteins involved in purine biosynthesis into a biosynthetic metabolon (*1, 2*). No evidence for "tight" interactions have been reported for the proteins in this pathway (*2, 3*). However, the instability of many of the nucleotide intermediates has lead to a model in which
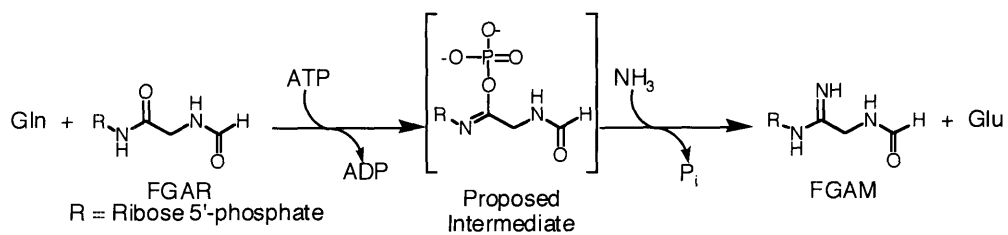
FGAR-AT Catalyzed Reaction
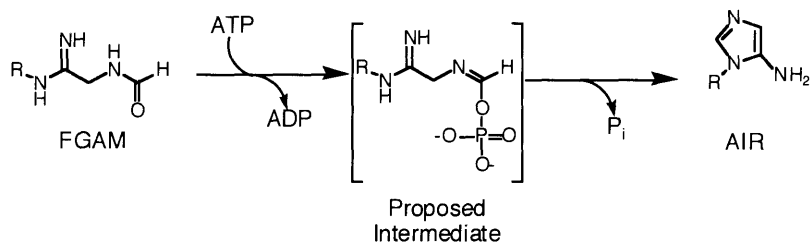
AIR Synthetase Catalyzed Reaction

Scheme 3.1—Proposed mechanisms of the FGAR-AT (PurL) and AIR Synthetase (PurM) catalyzed reactions.

128

transient protein-protein interactions between successive enzymes in this pathway may be important to avoid nucleotide decomposition (*1*).

Second, recent studies on the structure and function of the fifth enzyme in the purine pathway, aminoimidazole ribonucleotide (AIR) synthetase (PurM, Scheme 3.1), in conjunction with genomic sequence information, suggested that PurL might be a member of a new superfamily of ATP requiring enzymes with a unique structural fold (*4, 5*). This superfamily of enzymes, identified only by a DX_4GAXP motif, was proposed to use ATP to phosphorylate an amide oxygen of its substrate to generate an iminophosphate intermediate that is activated for nucleophilic attack (Scheme 3.1). Further information on the structure and function of the FGAR-AT would shine light on this proposal.

As noted above, most of the mechanistic studies on the FGAR-AT have focused on the lgPurLs. In the 1980s, Zalkin and co-workers, studying the contiguous purine biosynthetic operon in *Bacillus subtilis*, sequenced a gene cluster that was composed of *purC*-orf-*purQ*-*purL*-*purF* (*6*). The *purL* gene coded for a protein of only 80 kDa and hence was designated small PurL (smPurL). Furthermore, *purQ* was found to be homologous to triad glutaminase domains including the glutaminase domain of lgPurLs. Recently genetic and biochemical studies by Saxild and Nygaard demonstrated that the orf within this gene cluster is essential for production of FGAM (*7*). This orf has now been designated *purS*. Thus it appears that three proteins (smPurL (80kDa), PurQ (25 kDa), and PurS (10 kDa)) form the *B. subtilis* FGAR-AT. Sequence gazing has further identified PurS homologs in a wide range of Gram-positive bacteria, cyanobacteria, and methanogens. In each case, *purS* is accompanied by a *purL* and a *purQ*. Difficulties encountered during attempts to obtain a structure and elucidate the mechanism of the lgPurLs suggested that the FGAR-AT involving three proteins might be an alternative source of

insight into the amidation process. As an initial step towards this goal, this chapter describes the first expression and characterization of the FGAR-AT complex from *B. subtilis.* This FGAR-AT complex, as with all ATs examined to date, is proposed to supply ammonia from glutamine to FGAR by a channeling mechanism (*8*). This enzyme may therefore provide a paradigm for thinking about the dynamics of protein-protein interactions in channeling of an unstable intermediate in an enzymatic complex as well as between successive enzymes in primary metabolic pathways. The key to the interpretation of many of the findings discussed in this chapter came from the simultaneous structure determination of the *Salmonella* lgPurL by the Ealick Laboratory. The structure of this enzyme will be briefly described and correlated to discoveries made with the *B. subtilis* FGAR-AT complex.

3.2 Experimental

Materials

All reagents were purchased from Sigma or Mallinckrodt and used without further purification unless otherwise indicated. 6-Diazo-5-oxo-L-norleucine (DON) was purchased from BACHEM. Isopropyl β-D-thiogalactoside (IPTG) was purchased from Roche. β–FGAR was prepared from chemically synthesized α/β-GAR using the non-folate dependent glycinamide ribotide transformylase, PurT (*9*). The PurT plasmid was a gift from H. Holden, U. of Wisconsin-Madison (*10*). L-Glutamine was purchased from Fluka and found to contain the lowest percentage of contaminating L-glutamate among commercial sources. DNA primers were obtained from either the MIT Biopolymers Facility or from Invitrogen and were desalted before use. All cloned genes were sequenced at the MIT Biopolymers Facility. ESI-MS and N-terminal protein sequencing were also performed at the MIT Biopolymers Facility. PurM containing a N-terminal histidine tag (MGSSHHHHHHSSGLVPRGSH) was purified as

previously described (his-PurM, specific activity of 1-2 U/mg) (*4*). The *E. coli* and *Salmonella typhimurium* lgPurL enzymes (2 and 3 U/mg, respectively) were purified as described (*11, 12*). Pyruvate kinase (PK) and lactate dehydrogenase (LDH) were used from a premixed glycerol solution (660 U/mL PK, 1350 U/mL LDH Sigma P-0294). Bovine L-glutamate dehydrogenase (GDH) was obtained from Sigma (49 U/mg, Sigma G-2626). All spectrophotometric assays were performed on either a Cary 3 or a Cary 118-OLIS spectrophotometer. In both cases, the temperature was regulated using a Lauda water bath. Protein concentrations were determined using the method of Lowry with a BSA standard unless otherwise indicated (*13*). Calculated extinction coefficients were obtained using the ProtParam program from the EXPASY website (www.expasy.ch). To examine the extent of protein purification, standard SDS-PAGE gels were employed (10% for smPurL and 12.5% for PurQ). Tricine gels (16.5%) were used with PurS (*14*). A Bio-Rad BioLogic LP system was used for protein purifications at 4°C using the procedures mentioned below.

Cloning of the B. subtilis FGAR-AT Components

PurS was cloned from isolated *B. subtilis* genomic DNA (*B. subtilis* strain #1A607, courtesy of A. Grossman, MIT). The gene was cloned using the AmpliTaq DNA Polymerase (Perkin Elmer) and the primers listed in Table 3.1 (primers 1 and 2). The gene was then ligated into the pET-11a vector (Novagen) at the NdeI and BamHI sites. This construct yielded pET-PurS.

PurQ was also cloned from the isolated *B. subtilis* genomic DNA. The gene was first subcloned into pSTBlue-1 (Novagen) (primers 3 and 4, Table 3.1). Amplification with the VENT DNA polymerase (NEB) resulted in an A128T mutant of PurQ. Amplification with the AmpliTaq DNA Polymerase (Perkin Elmer) or the KOD HiFi DNA Polymerase (Novagen)

resulted in the cloning of the wild type (wt) gene. Both genes were then subcloned into pET-24a (Novagen) at the NdeI and EcoRI sites creating pET-PurQ-A128T (A128T mutant) and pET-PurQ-wt.

smPurL was cloned from the pDE51 *B. subtilis* sequencing vector (gift of H. Zalkin, Purdue University) (*6*). The gene was cloned using the Pfu Turbo DNA polymerase (Stratagene) and standard PCR techniques (primers 5 and 6, Table 3.1). The gene was ligated into the pET 24a vector at the NdeI and BamHI sites to create pET-smPurL. The gene isolated by this procedure several times always contained a L513F mutation based on the published sequence (*6*).

In order to co-express all the FGAR-AT components, PurQ A128T and smPurL were placed into pACYC-DUET-1 (Novagen). This vector contains two multiple cloning sites (MCS1 and MCS2) and is compatible with all pET vectors. The gene for smPurL was PCR-amplified from pET-smPurL (primers 6 and 7, Table 3.1) and placed into the NcoI and BamHI sites of MCS1, creating pDUET-L. This method resulted in the insertion of an amino acid at the N-terminus: Met-Ser-Leu was replaced by Met-Gly-Ser-Leu. The gene for PurQ was amplified from pET-PurQ-A128T plasmid (primers 8 and 9, Table 3.1) and placed into MCS2 of pDUET-L at the NdeI and KpnI sites to create pDUET-L-A128T-Q.

Co-expression of the wt PurQ gene with PurS and smPurL was achieved by using Quikchange mutagenesis (Stratagene) with the pDUET-LQ plasmid. The mutagenic primers are listed in Table 3.1 (primers 10 and 11). Plasmids containing the mutation were identified by DNA sequencing. This created plasmid pDUET-L-wt-Q.

Table 3.1: Primers Used in Cloning of the FGAR-AT

ID	Name	Sequence	Restriction Enzyme	Plasmid
1	PurS-F	GCCATATGTATAAAGTAAAAG TTTATGTC	NdeI	pET-PurS
2	PurS-R	CGGGATCCTCACTGTGCGACTA CCTCCTCAAC	BamHI	pET-PurS
3	QDN	TCTTTACTCGAGTCAAGCAGTA GTGACATGAG	XhoI	pET-PurQ-WT and A128T
4	QUP	AGTCGCCATATGAAATTTGCGG TGATTGT	NdeI	pET-PurQ-WT and A128T
5	Bs-L-F	GCCATATGTCACTACTGCTTGA ACCAAGTAAAGAAC	NdeI	pET-smPurL
6	Bs-L-R	CGCATTGGATCCTTAAGCCTTTG ATTTCAGCAAGCATGG	BamHI	pET-smPurL and pDUET-L
7	SL-NcoI	GCCCATGGCACTACTGCTTGAAC CAAGTAAAGAAC	NcoI	pDUET-L
8	Q-NdeI	GCCATATGAAATTTGCGGTGATT GTGTTACCC	NdeI	pDUET-LQ
9	Q-KpnI	GGGGTACCTCAAGCAGTAGTGA CATG	KpnI	pDUET-LQ
10	Q-wt-F	GACGAAACCTTATTCACAGCATG GTACGAAAAGGGAG	N/A	pDUET-LwtQ
11	Q-wt-R	CTCCCTTTTCGTAGGATGCTGTGA ATAAGGTTTCGTC	N/A	pDUET-LwtQ

Co-expression PurS, PurQ, and smPurL

For co-expression of all 3 subunits of the FGAR-AT, BL21-Gold DE3 cells (Stratagene) were transformed with pDUET-L-A128T-Q (or pDUET-L-wt-Q), pET-PurS, and pET-smPurL using the heat-shock method and ~20 ng of each plasmid (15). The cells were selected for growth on LB/agar plates containing 100 μg/mL chloramphenicol, 50 μg/mL ampicillin, and 35 μg/mL kanamycin.

A single colony was used to inoculate 50 mL of LB containing the above antibiotics. The cells were grown overnight at 37°C with shaking at 200 rpm. Cells from this culture were then

collected by centrifugation, washed with fresh LB, and then used to inoculate 2 L of LB containing the above mixture of antibiotics in a 6 L flask. This flask was then shaken at 200 rpm at 37°C. Cells were grown to an OD_{600} of 0.7, at which point they were induced with 1 mM IPTG and grown for an additional 5 h. The cells were then harvested and frozen in liquid nitrogen.

Efforts to Purify the FGAR-AT from Co-expressed Proteins

Glutamine-dependent FGAR-AT activity was monitored at all stages of the purification with the modified Bratton-Marshall assay described subsequently. Cells (4 g) were resuspended in 25 mL of SL buffer (50 mM Tris, 25 mM NaCl, 1 mM EDTA, 1 mM DTT, 5% glycerol, pH 7.8) along with 1 mL of Sigma Protease Inhibitor Cocktail (Sigma P-8465). Cells were then lysed by two passes through a French press at 14,000 psi. Cell debris was removed by centrifugation for 25 min at 17,000 rpm. Streptomycin sulfate (0.2 volumes, 6% w/v in SL buffer) was then added over 15 min, followed by stirring for an additional 15 min. Solids were removed by centrifugation.

The supernatant was next applied to DEAE Sepharose FF (2.5 x 10 cm, Sigma) column equilibrated in SL buffer. The column was washed until the $A_{280} < 0.1$. The protein was eluted with a linear gradient (350 x 350 mL) of 25 to 500 mM NaCl in SL buffer. A flow rate of 2 mL/min was used and 8 mL fractions were collected. The proteins eluted in 3 separate peaks: PurS (~100 mM NaCl), PurQ (~150 mM NaCl), and smPurL (~180 mM NaCl). Glutamine-dependent FGAR-AT activity was observed in fractions at ~170 mM NaCl. These fractions were pooled and concentrated to 40 mg/mL using a YM-3 Centriprep (Millipore). This protein (0.5 mL) was then applied to a Sephacryl S-200 (1.5 x 100 cm, Sigma) column equilibrated in

SL buffer. The column was eluted at 0.3 mL/min and 5 mL fractions were collected and assayed for activity.

Purification of PurS

pET-PurS was transformed into BL21(DE3) *E. coli* cells (Novagen) and grown in LB at 37°C in the presence of 100 μg/mL ampicillin. The cells were typically grown in 2 L with shaking at 200 rpm in a 6 L flask. At an OD_{600} of 0.7-0.9, the cells were induced with 1 mM IPTG and grown for an additional 4 h. The cells were then harvested and frozen in liquid nitrogen.

The cell pellet (6.5 g) was resuspended in 30 mL of S buffer (50 mM Tris, 25 mM NaCl, 1 mM EDTA, 5 mM DTT, pH 7.8) and 1.5 mL of Sigma Protease Inhibitor Cocktail. Cells were then lysed by two passes through a French press at 14,000 psi. Cellular debris was removed by centrifugation at 17,000 rpm for 40 min. Streptomycin sulfate (0.3 volumes, 6% w/v made in S buffer) was then added to the supernatant over 20 min while stirring on ice. The solution was stirred for an additional 20 min and then cleared by centrifugation. DNase I (500 U, Roche) was added to the supernatant, and this solution was allowed to stir at room temperature for 20 min.

The supernatant was next loaded onto a DEAE Sepharose FF (1.5 x 25 cm, Sigma) column equilibrated in S buffer. The column was washed with buffer until $A_{280} < 0.1$. A linear gradient (600 x 600 mL) was applied from 25 to 500 mM NaCl in S buffer. The flow rate was 2 mL/min and 10 mL fractions were collected. PurS eluted at 50 mM NaCl. Protein from this peak was then concentrated with an Amicon device over a YM-30 membrane (Millipore). The concentrated protein was applied to a Sephacryl S-300 (1.5 x 100 cm, Sigma) column equilibrated in S buffer, but the concentration of DTT was lowered to 1 mM. The protein was eluted at a rate of 0.3 mL/min and 5 mL fractions were collected. PurS eluted as a single peak.

The protein was again concentrated with an Amicon device over a YM-30 membrane, followed by a Centriprep YM-30 (Millipore) to 20-40 mg/mL. Glycerol was added to 20% of the final volume, and the protein was rapidly frozen in liquid nitrogen. PurS (13.4 mg/g cells) was obtained in >95% purity. The purified protein had a mass of 9,755 Da by ESI-MS (calculated, 9,755 Da). The final protein was quantified using a calculated $\varepsilon_{280} = 7,680$ M^{-1}cm^{-1}.

Purification of PurQ

pET-PurQ-wt or pET-PurQ-A128T were transformed into BL21(DE3) *E. coli* cells and grown in LB at 30°C in the presence of 70 μg/mL kanamycin. Cells in 2 L of media were grown in 6 L flasks with shaking at 200 rpm. At an OD$_{600}$ of 0.7-0.9, the cells were induced with 1 mM IPTG and grown for an additional 5 h. The cells were then harvested and frozen in liquid nitrogen.

Both the A128T and wt PurQ proteins were purified using the following procedure based on the purification of *E. coli* HisH (*16*). PurQ activity was monitored at all stages of the purification in the absence of PurS and smPurL using the GDH-coupled glutaminase assay described below.

Cells (13 g) were resuspended in 35 mL of Q buffer (50 mM Tris, 1 mM EDTA, pH 7.4) and then lysed by two passes through a French press at 14,000 psi. Solids were removed by centrifugation at 17,000 rpm for 40 min in a Beckman JA-25.50 rotor.

Streptomycin sulfate (10% w/v in Q buffer) was then added to a final concentration of 1% and the solution was stirred on ice for an additional 15 min before centrifugation. The supernatant was applied to a DEAE Sepharose FF column (2.5 x 10 cm) equilibrated in Q buffer. The column was washed until the A$_{280}$ < 0.1. A128T PurQ was eluted with a linear gradient (200 x 200 mL) of 0 to 300 mM KCl in Q buffer. A flow rate of 3 mL/min was employed and 6 mL

fractions were collected. A128T PurQ eluted in the main protein fraction at 100 mM KCl. In contrast, wt-PurQ eluted at 250 mM KCl with a linear gradient (200 x 200 mL) of 0 to 500 mM KCl in Q buffer (data not shown).

The PurQ fractions were then pooled and diluted 1:1 with 40 mM KP_i, pH 7.0. This solution was applied to a Biogel HTP column (2.5 x 5 cm, Bio-Rad) equilibrated in 20 mM KP_i, pH 7.0. The flowthrough and a 40 mL wash were combined and then concentrated with an Amicon device over a YM-30 membrane to 50 mg/mL. This solution (1 mL) was then applied to a Sephacryl S-100 (1.5 x 75 cm, Sigma) column equilibrated in 20 mM KP_i, 100 mM KCl, pH 7.0. The column was eluted at 0.2 mL/min and 5 mL fractions were collected. The protein was then concentrated to 15-30 mg/mL with a Centriprep YM-10 (Millipore). Glycerol was added to a concentration of 20%, and the protein was rapidly frozen in liquid nitrogen and stored at – 80°C. A typical yield of homogeneous A128T PurQ was 9.1 mg/g cells. Purification of wt PurQ resulted in a significantly lower yield (1.5 mg/g cells) of 50-60% homogeneous PurQ. The purified A128T protein had a mass of 24,816 Da by ESI-MS (calculated, 24,814 Da) and was quantified with a calculated $\varepsilon_{280} = 20,580$ M^{-1} cm^{-1}.

Purification of smPurL

pET-smPurL was transformed into BL21(DE3) *E. coli* cells and grown in LB at 27.5°C in the presence of 70 µg/mL kanamycin. The cells were typically grown in 2 L volumes with shaking at 200 rpm in a 6 L flask. At OD_{600} of 0.7-0.9, the cells were induced with 1 mM IPTG and grown for an additional 5 h. The cells were then harvested and frozen in liquid nitrogen.

Cells (8g) were resuspended in 30 mL of SL buffer along with 2 mL of Sigma Protease Inhibitor Cocktail. Cells were then lysed by two passes through a French press at 14,000 psi. Cell debris was removed by centrifugation for 25 min at 17,000 rpm. Streptomycin sulfate (0.2

volumes, 6% w/v in SL buffer) was then added over 15 min while stirring on ice, followed by stirring for an additional 15 min. Solids were removed by centrifugation.

The supernatant was next applied to a DEAE Sepharose FF (2.5 x 14 cm, Sigma) column equilibrated in SL buffer. The column was washed until the $A_{280} < 0.1$. The protein was eluted with a linear gradient (300 x 300 mL) of 0 to 500 mM KCl in buffer SL. A flow rate of 4 mL/min was used and 8 mL fractions were collected. smPurL eluted in the major protein containing peak at 125 mM KCl. The protein was then concentrated to 20 mL with an Amicon device and a YM30 membrane before dialysis overnight in a 12 kD molecular weight cut-off membrane (Sigma D-0405) against 2 x 500 mL of SL buffer. This protein (diluted to 50 mL) was then applied to a Reactive Red 120 Agarose (2.5 x 13.5 cm, Sigma) column equilibrated in SL buffer. The column was washed with 2.5 column volumes of buffer at 1 mL/min. smPurL was then eluted by continuing to wash the column with SL buffer at a flow rate of 3 mL/min until the $A_{280} < 0.1$. The entire elutate was concentrated with an Amicon device over a YM-30 membrane (Millipore) and a Centriprep YM-50 (Millipore) to a concentration of 20-30 mg/mL. Glycerol was then added to 20% and the protein rapidly frozen and stored at -80°C. A typical yield of smPurL was 4.2 mg/g cells. The purified protein had a mass of 80,213 Da by ESI-MS, similar to the 80,194 Da mass predicted by removal of the N-terminal methionine revealed by Edman degradation. The purified protein was quantified with a calculated $\varepsilon_{280} = 51,520$ M^{-1} cm^{-1}.

Enzyme Reconstitution

To reconstitute FGAR-AT activity, 2 equivalents of PurS, 1 equivalent of smPurL, and 1 equivalent of PurQ were combined, in that order, in 100 mM Tris pH 7.5, 5 mM MgCl$_2$ such that the complex concentration was 10-20 μM. The mixture was allowed to equilibrate on ice for 5

min before use and was stable on ice for several hours at these concentrations. Diluted enzyme was prepared from this stock immediately before use.

Enzyme Assays

Enzymatic activity was determined using three different assays: one to monitor FGAM, one for ADP, and one for glutamate. FGAM synthesis was monitored by a coupled assay with his-PurM using the modified Bratton-Marshall assay (*11*). The buffer for the *B. subtilis* enzymes contained in a final volume of 400 μL: 50 mM HEPES pH 7.2, 20 mM $MgCl_2$, 80 mM KCl, 50 mM L-glutamine, 10 mM ATP, 1 mM β-FGAR, and 0.2 U of his-PurM. When the NH_3-dependent activity was determined for smPurL, the glutamine was replaced with 400 mM NH_4Cl. The amount of FGAR was also increased to 2 mM β-FGAR. The reaction was initiated by addition of enzyme and incubated at 37°C before being quenched by the addition of 100 μL of 1.33 M potassium phosphate/20% trichloroacetic acid (TCA) pH 1.4. The AIR product was then derivatized and quantified as previously described (*17*).

ADP formation was monitored using a coupled assay with PK and LDH. The reaction mixture was identical to that described for the modified Bratton-Marshall assay above except that it contained 0.2 mM NADH, 3 mM PEP, and PK (3.0 U) and LDH (6.75 U) in place of his-PurM. In the NH_3-dependent reactions, the glutamine in the buffer was replaced with 400 mM NH_4Cl. The reaction was initiated with the addition of enzyme and was monitored by ΔA_{340} (ε = 6,200 $M^{-1}cm^{-1}$) at 37°C.

Formation of glutamate was monitored using a continuous glutaminase assay (*18*). The assay buffer was identical to the Bratton-Marshall assay buffer except that 2 mM 3-acetylpyridine adenine dinucleotide (APAD, Sigma) was added to the reaction mixture and 20 U of GDH was used as the coupling enzyme instead of his-PurM. Since very high glutamine

concentrations were used in these assays, the reaction buffer was incubated for 10 min at 37°C with GDH to oxidize all the contaminating glutamate. The reaction was then initiated with enzyme and incubated at 37°C. The reaction was monitored by ΔA_{363} ($\varepsilon = 9,100$ $M^{-1}cm^{-1}$).

Determination of Kinetic Parameters

k_{cat} and K_m values were generally determined by varying the concentration of the substrate from 0.2 to 10 times the K_m, while using saturating concentrations of the other substrates. Kinetic parameters were obtained by fitting initial velocity data to Equation 3.3 using non-linear regression analysis with KaleidaGraph (Synergy) computer software.

$$v = V_{max}[S]/(K_m + [S])$$ (3.3)

In cases where substrate inhibition was observed, data were fit to Equation 3.4.

$$v = \frac{V_{max}[S]}{(K_m + [S] + \frac{[S]^2}{K_i})}$$ (3.4)

Parameters for PurQ were determined using the glutaminase assay in the absence of PurS, smPurL, FGAR, and ATP. The K_m value for glutamine was determined by varying its concentration from 0 to 24 mM.

The kinetic parameters for the NH_3-dependent reaction of smPurL were determined using either the modified Bratton-Marshall assay (NH_3, FGAR) or the PK/LDH coupled assay. The $K_{m,app}$ value for β-FGAR was obtained by varying its concentration from 0 to 8 mM in the presence of 400 mM NH_4Cl and 10 mM ATP. The $K_{m,app}$ for NH_3 was obtained by varying the concentration of NH_4Cl from 0 to 700 mM, with 2 mM β-FGAR and 10 mM ATP. Up to 1 U of

his-PurM was added to this reaction to offset the effects of NH_4Cl on his-PurM activity. The concentration of NH_3 was calculated using the Henderson-Hasselbalch equation. The $K_{m,app}$ value for ATP was obtained by varying its concentration from 0 to 2 mM using 2 mM β-FGAR and 400 mM NH_4Cl.

Kinetic parameters for the PurS:smPurL:PurQ complex were determined using either the modified Bratton-Marshall assay or the glutaminase assay. All specific activity and kinetic parameter measurements were made at enzyme concentrations of 0.2-0.4 μM, using the A128T PurQ mutant. The K_m value for β-FGAR was obtained by varying its concentration from 0 to 8 mM using 10 mM ATP and 25 mM glutamine. The $K_{m,app}$ value for ATP was determined by varying its concentration from 0 to 3.25 mM in the presence of 1 mM β-FGAR and 25 mM glutamine. The $K_{m,app}$ glutamine was determined by varying its concentration from 0 to 24 mM in the presence of 1 mM β-FGAR and 10 mM ATP.

Metal Ion Dependence

Metal ion dependence (Mg^{2+} and K^+) was measured by using the glutaminase assay since both the his-PurM and PK coupling enzymes are dependent on these ions. The glutaminase buffer consisted of 100 mM Tris pH 7.2, 2 mM APAD, 10 mM ATP, 1 mM β-FGAR, 25 mM L-glutamine, and 20 U of GDH in a volume of 300 μL. In experiments to examine magnesium dependence, KCl was 80 mM, and the enzyme reconstitution was carried out in Tris buffer without magnesium. The concentration of $MgCl_2$ was varied from 0 to 40 mM. In experiments to test potassium dependence, $MgCl_2$ was at 20 mM, and the concentration of KCl was varied from 0 to 80 mM.

Titrations to Examine the Stoichiometry of the FGAR-AT

Titrations of the FGAR-AT proteins with one another were monitored using the modified Bratton-Marshall assay and could only be successfully performed at enzyme concentrations above 0.1 μM, which required 1 U of his-PurM as a coupling agent.

A. Titrations with PurQ

smPurL (1 nmol) was reconstituted with PurS (2 nmol) and PurQ (0.2 to 4 nmol) in 100 μL of 50 mM HEPES pH 7.2, 20 mM $MgCl_2$, 80 mM KCl, 10 mM ATP, and 25 mM L-glutamine. This mixture was allowed to incubate on ice for 5 min. The enzyme was then diluted 50-fold into the Bratton-Marshall assay buffer at 37°C to initiate the reaction.

B. Titrations with PurS

smPurL (1 nmol) was reconstituted with PurS (0.25 to 4 nmol) and PurQ (1 nmol) in 100 μL of 50 mM HEPES pH 7.2, 20 mM $MgCl_2$, 80 mM KCl, 10 mM ATP, and 25 mM L-glutamine. The incubation and enzymatic reaction were then carried out as described with the titration of PurQ.

pH Rate Profile

The pH rate profile was determined with the Goods series of buffers using the modified Bratton-Marshall assay. The buffers used were MES (pH 5.5-6.25), MOPS (pH 6.5-7.0), HEPES (pH 7.25-8.0), TAPS (pH 8.5), and CHES (pH 9.0-9.5). A typical assay in 400 μL contained 100 mM buffer, 1 mM β-FGAR, 10 mM ATP, and 50 mM L-glutamine. The enzyme concentration for these reactions was 0.2 μM. In determining the pH rate profile for the NH_3-dependent reaction, 2 mM β-FGAR, 10 mM ATP, and 400 mM NH_4Cl were used. The amount of PurM used in the assays varied between 0.2 and 2 U to ensure full coupling of the reaction at all pH values.

Product Stoichiometry of FGAR-AT

Product stoichiometry of the FGAR-AT reaction was determined by measuring endpoint concentrations of ADP, glutamate, and FGAM. Enzymes were reconstituted as described above. The enzyme mixture was then diluted 1:40 into 400 μL of 50 mM HEPES pH 7.2, 20 mM $MgCl_2$, 80 mM KCl, 25 mM L-glutamine, 2 mM β-FGAR, 1.5 mM ATP, 2.5 U/mL his-PurM at 37°C. The reaction was allowed to proceed for several minutes before quenching by immersion in boiling water for 2 min. Precipitated protein was removed by centrifugation. Six time points were taken for the stoichiometry determination and a control reaction containing no FGAR-AT was performed at each time point. The final stoichiometry was determined by averaging the stoichiometries obtained at each time point. In addition, these methods were used to determine the stoichiometry of both the *E. coli* and *S. typhimurium* lgPurLs.

FGAM formation was determined by using the modified Bratton-Marshall assay described earlier to calculate the amount of AIR present in the sample (50 μL).

ADP formation was determined using the PK/LDH assay. The quenched reaction or control (60 μL) was added to 610 μL of 50 mM HEPES pH 7.2, 20 mM $MgCl_2$, 80 mM KCl, 3 mM PEP, 0.2 mM NADH, 3.0 U PK, and 6.75 U LDH, and the ΔA_{340} was measured. The amount of ADP produced by the FGAR-AT was determined by subtracting the control followed by division by 2 to account for ATP consumed by his-PurM.

Glutamate was measured using two methods with GDH. In the first method, 100 μL of the quenched reaction or control was added to 610 μL of 50 mM HEPES pH 7.2, 20 mM $MgCl_2$, 80 mM KCl, 2 mM APAD, and 20 U GDH. The reaction was incubated for 30 min at 37°C and the ΔA_{363}(experimental−control) was measured. In the second method, known concentrations of

glutamate were included in the control reactions to generate a standard curve using the method of Lund (*19*).

DON Inactivation of PurQ

A typical reaction (150 µL) contained 20 µM PurQ, 20 µM smPurL, 40 µM PurS, 0.45 mM FGAR, 0.5 mM ATP, 10 mM DON, 50 mM KP_i pH 7.25, 75 mM NaCl, and 5 mM $MgCl_2$ at 25°C. Inactivation of PurQ alone was carried out in the absence of the other proteins, FGAR, and ATP. The inactivation was monitored as a function of time by removal of 2 µL aliquots, which were diluted into 400 µL of the modified Bratton-Marshall assay buffer. With inactivation of PurQ alone, the assay buffer contained PurS and smPurL as well. The DON-inactivated FGAR-AT mixture was used directly in subsequent SEC experiments without the removal of unreacted DON or substrates.

Analytical SEC to Look for Complex Formation

Analytical SEC was performed at 4°C using a BioCAD Sprint perfusion chromatography system (Applied Biosystems) or at 25°C using a Rainin HPLC with an analytical Bio-Silect SEC250 column (300 x 7.8 mm, Bio-Rad). The column was equilibrated and eluted in filtered and degassed SEC buffer (50 mM KP_i, 75 mM NaCl, pH 7.25). Protein was applied to the column using a 100-µL injection loop and eluted with a flow rate of 1 mL/min. Bio-Rad Gel Filtration standards (a mixture of thyroglobulin (670 kD), gamma globulin (158 kD), ovalbumin (44 kD), myoglobin (17 kD), and vitamin B_{12} (1.4 kD)) were injected prior to each set of experiments. Typically, 0.6 mg of protein in 125 µL of buffer was injected. All solutions were filtered with CENTREX spin filters (Schleicher & Schuell). Experiments were also performed using SEC buffer containing (25 mM L-glutamine and 5 mM $MgCl_2$), (5 mM $MgCl_2$ and 0.5 mM ATP), (5 mM $MgCl_2$, 0.5 mM ADP, and 25 mM L-glutamine), and (5 mM $MgCl_2$, 0.5 mM ATP,

and 0.5 mM β-FGAR). In addition, experiments were performed using enzyme that had either been allowed to synthesize FGAM for 5 min at 37°C before application to the column or had been pre-incubated with a combination of 0.5 mM ADP, 5 mM MgCl$_2$, and/or L-glutamine. Approximate values for molecular weight were determined using the gel filtration standards and by linear-regression analysis using the KaleidaGraph software. Activities of proteins eluting from the analytical SEC column were determined using the modified Bratton-Marshall assay to monitor glutamine-dependent FGAM formation. Peak volumes were determined by integration.

Quantitation of ADP Binding to the Salmonella lgPurL

Salmonella lgPurL (10-20 nmol, specific activity 3 U/mg in 25 mM HEPES pH 7.0, 1 mM glutamine) was diluted into 1 mL of water, and protein was precipitated by immersion into a boiling water bath at 100°C for 10 min. The precipitated protein was then removed by centrifugation, and an absorbance spectrum was taken of the supernatent (220-400 nm) after blanking against a control solution containing no protein. The spectrum revealed only nucleotide in solution by the λ_{max} at 260 nm. The A$_{260}$ value was then used to determine the ADP•protein stoichiometry.

Efforts to Detect ADP Dissociation from the Salmonella lgPurL

Dialysis Experiments: lgPurL was placed into a 30 kDa MWCO Slide-A-Lyzer cassette (Pierce) and dialyzed against 5 x 1 L of 20 mM KP$_i$ pH 7.0 and 10 mM EDTA for 72 h. Aliquots (~250 μL) were periodically removed during the dialysis and the ADP remaining bound to lgPurL was quantified by protein denaturation and measurement of the A$_{260}$ obtained from an absorbance spectrum of the supernatent.

Exchange Reactions with [2,8-^{3}H]-ADP: In a final volume of 500 μL, lgPurL (10 nmol) was mixed with 20 mM KP$_i$ pH 7.0, 5 mM MgCl$_2$, and 1 mM [2,8-^{3}H]-ADP (1,158 cpm/nmol,

Perkin Elmer) at 37°C. Aliquots (100 μL) were removed after 1, 3, 6, and 16 h. The protein was

then separated from the small molecules by passage of the solution through a Sephadex G-50

column (1 x 20 cm, Sigma) equilibrated in 20 mM KP$_i$ pH 7.0 and 5 mM MgCl$_2$. The amount of

[^{3}H]-ADP in the protein-containing fractions was analyzed by scintillation counting.

Quantitation of [8-^{14}C]-ADP Binding to smPurL and the FGAR-AT Complex

Radioactive ADP was used to monitor ADP binding to both smPurL and the FGAR-AT

complex. In a final volume of 250 μL containing 50 mM HEPES pH 7.2, 20 mM KCl, 20 mM

MgCl$_2$, 3 mM [8-^{14}C]-ADP (789 cpm/nmol, Moravek Biochemicals), smPurL (40 nmol) was

added, and the reaction mixture was incubated at 37°C for 5 min.

The sample was then applied directly to a Sephadex G-50 column (1 x 20 cm, Sigma)

equilibrated in the incubation buffer at room temperature. Fractions of 0.5 mL were collected

and 0.2 mL was mixed with 7 mL of Emulsifier-Safe scintillation fluid (Perkin-Elmer) and

analyzed by scintillation counting. The remainder of the fraction was characterized by UV

absorbance at 260 and 280 nm using a Bio-Rad Ultramark plate reader in a 96-well UV-

transparent plate (Corning). Protein content was quantified using both a Lowry assay and by the

A$_{280}$.

[8-^{14}C]-ADP binding to smPurL was also monitored in the presence of PurQ, PurS, or

both proteins by adding 1 molar equivalent of PurQ and/or 2 molar equivalents of PurS to the

smPurL solution. The proteins were allowed to incubate on ice for 5 min before the addition of

ADP. Due to the influence of glutamine on complex assembly, additional experiments were

carried out in the presence of 20 mM L-glutamine.

3.3 Results

Genetic and biochemical studies using crude extracts of *B. subtilis* deletion strains suggested that PurS, smPurL, and PurQ were all required for FGAM synthesis (*7*). Based upon these results, an *in vitro* biochemical characterization of the proteins was initiated. Two approaches were taken to obtain active protein: the first examined co-expression methods and the second involved expression of the individual proteins and reconstitution of the complex. The success of each approach was based upon observation of glutamine-dependent FGAM production (Scheme 3.1) using the modified Bratton-Marshall assay.

Cloning, Co-Expression, and Co-Purification of the FGAR-AT Complex

A variety of different strategies were pursued for co-expression. A128T PurQ and smPurL were cloned into pACYC-DUET-1, yielding pDUET-L-A128T-Q. Subsequent to observations made with purified PurQ containing the A128T mutation versus the wt sequence (see below), the A128T PurQ gene in pDUET-L-A128T-Q was mutagenized to the wt sequence. This plasmid was named pDUET-L-wt-Q.

When these constructs were transformed into BL21(DE3) *E. coli*, expression of A128T PurQ was ~ 20% of soluble protein, while that of smPurL was < 1% of soluble protein (data not shown). pDUET-L-A128T-Q was then co-transformed with pET-PurS. The expression level of PurS was high; however, no expression of A128T PurQ or smPurL was observed (data not shown). Next, pDUET-L-A128T-Q, pET-PurS, and pET-smPurL were all co-transformed, into BL21(DE3) *E. coli*. Under these conditions, PurS, A128T PurQ, and smPurL were all expressed as soluble proteins (Figure 3.1). No smPurL or A128T PurQ were detected in the insoluble protein fraction. The crude cell lysate produced FGAM at 0.4 U/mg (Table 3.2). Given that ~20% of the total protein is associated with the FGAR-AT (estimated from SDS-PAGE, Figure
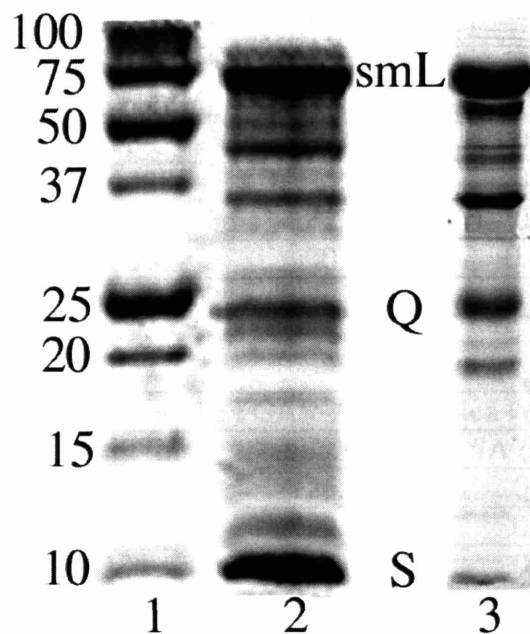
Figure 3.1—15% SDS-PAGE of the co-expressed FGAR-AT. Lane 1, molecular weight markers; lane 2, soluble crude cell lysate; lane 3, the activity-containing fraction from the DEAE column.

Table 3.2: Co-Purification of the FGAR-AT Complex (A128T PurQ)

step	protein (mg)	total units (U)	SA (U/mg)	% yield
cell lysate[a]	399	167.6	0.42	100
streptomycin	328	127.9	0.39	76
DEAE Sepharose	84	22.7	0.27	14
Sephacryl S-200	9.6	0.12	0.013	0.1

[a]From 4 g of cells

Table 3.3: Co-Purification of the FGAR-AT Complex (wt PurQ)

step	protein (mg)	total units (U)	SA (U/mg)	% yield
cell lysate[a]	372	126.5	0.34	100
streptomycin	330	122.1	0.37	76
DEAE Sepharose	105	22.1	0.21	14
Sephacryl S-200	Peak 1 = 42 Peak 2 = 46	Peak 1 = 0.46 Peak 2 = 1.3	Peak 1 = 0.011 Peak 2 = 0.028	1.4

[a]From 3.3 g of cells

3.1), activity for the pure protein was estimated at 2-3 U/mg. Similar results were observed for co-expression of wt PurQ from the pDUET-L-wt-Q plasmid (Table 3.3).

Purification of the FGAR-AT complex was attempted using DEAE Sepharose anion-exchange chromatography. During chromatography, the three proteins separated (Figure 3.2) based on SDS-PAGE analysis. One peak of FGAR-AT activity was observed using the Bratton-Marshall assay. The specific activity of this complex (Figure 3.1, lane 3) had fallen to 0.27 U/mg due to dissociation of the complex during chromatography (Table 3.2). The fractions containing activity were pooled and applied to a Sephacryl S-200 SEC column. During elution, smPurL completely separated from PurS and A128T PurQ, which co-migrated under these conditions (Figure 3.3). In addition, only very low levels of activity were recovered (0.013 U/mg, Table 3.2). Thus, the proteins of the FGAR-AT are weakly associated. Purification results obtained with wt PurQ or A128T PurQ were very similar under co-expression conditions (Tables 3.2 and 3.3). These results indicate that any study of the subunit stoichiometry, assembly, and kinetic
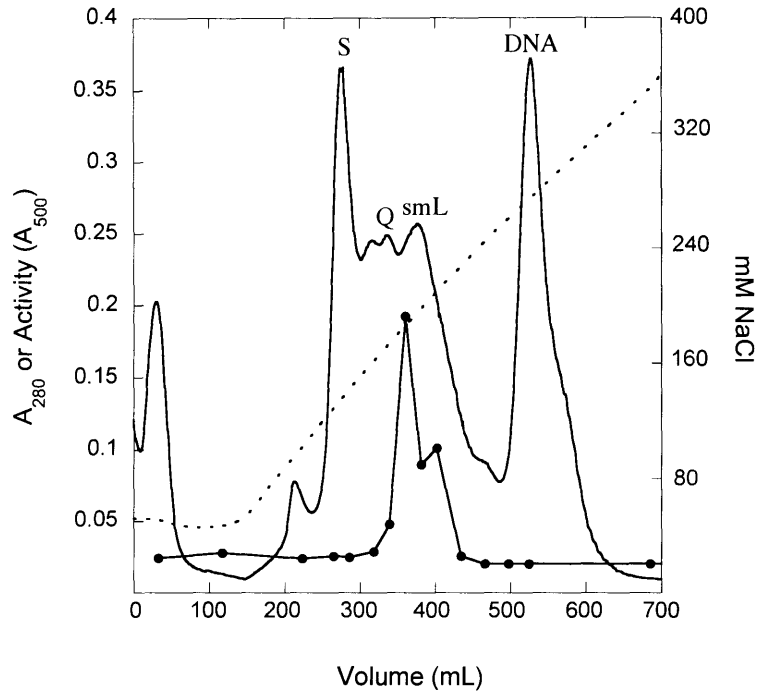
Figure 3.2—DEAE elution chromatogram of the co-expressed FGAR-AT complex using A128T PurQ. The solid line represents the A_{280} values and the dashed line represents the [NaCl]. Activity (●) was measured as A_{500} using the glutamine-dependent Bratton-Marshall assay. The elution of PurS (S), PurQ (Q), smPurL (smL), and cellular DNA are noted.

150
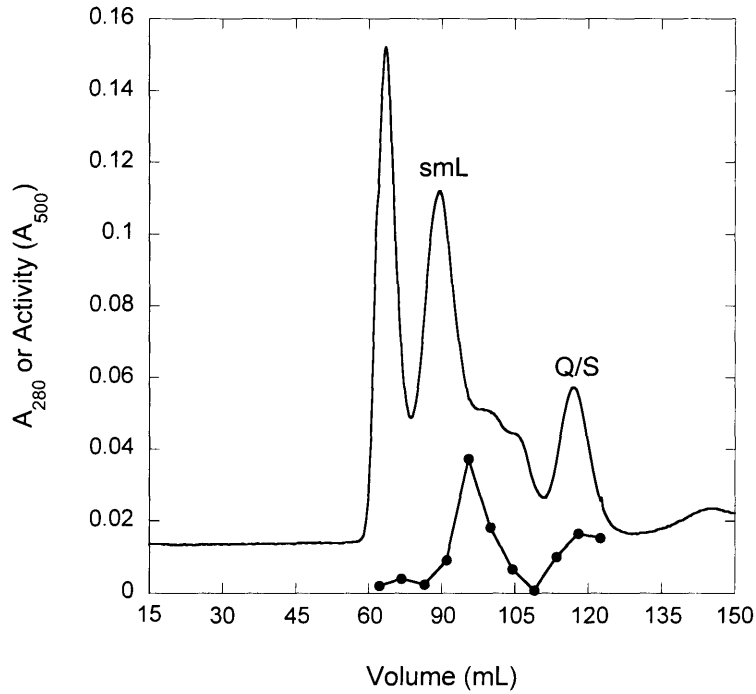
Figure 3.3—Sephacryl S-200 SEC elution chromatogram of the activity-containing fractions from the DEAE column. Activity (●) was measured as A_{500} using the glutamine-dependent Bratton-Marshall assay. Elution of PurS (S), A128T PurQ (Q), smPurL (smL) are noted.

parameters of the FGAR-AT complex must be carried out by reconstituting the separately purified enzymes or by identification of other components that allow for co-purification of the intact complex.

Cloning, Expression, and Purification of the Individual FGAR-AT Components

PurS: The *purS* gene was cloned from *B. subtilis* genomic DNA and ligated into pET-11a. The protein was over-produced in *E. coli* and was purified to homogeneity (Figure 3.4, lane 4) by DEAE anion-exchange chromatography followed by size exclusion chromatography (SEC) (Figures 3.5 and 3.6). Typical yields were ~ 13 mg/g cells. The molecular weight of the protein was confirmed by ESI-MS.

PurQ: The *purQ* gene was also cloned from *B. subtilis* genomic DNA and placed into pSTBLUE-1. The gene was then subcloned into pET-24a for protein expression. *E. coli* containing this plasmid were grown at 30°C to obtain soluble protein. PurQ was purified on a DEAE Sepharose anion-exchange column (Figure 3.7). The fractions eluting at 100 mM KCl were pooled, diluted with phosphate buffer, and loaded onto a Biogel HTP column. The flow-through of the column contained PurQ. The eluate was concentrated and loaded onto a SEC column (Figure 3.8). The resulting PurQ was homogenous by SDS-PAGE (Figure 3.4, lane 2) with typical recoveries of 9 mg/g cells. The activity of PurQ was monitored using the continuous glutaminase assay (Table 3.4). The variability in total activity is due to removal of an endogenous glutaminase activity from *E. coli* during the purification (Figure 3.8). The molecular weight of PurQ determined by ESI-MS was 24,816 Da (calculated 24,784), suggesting that the clone contained a mutation.
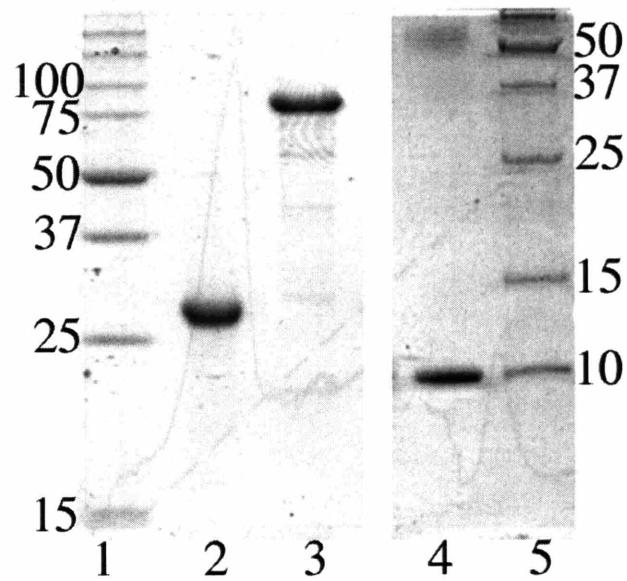
Figure 3.4—12% SDS-PAGE (lanes 1-3) and 16.5% tricine (lanes 4-5) gels of the purified FGAR-AT components. Lanes 1 and 5, molecular weight markers; lane 2, A128T PurQ; lane 3, smPurL; lane 4, PurS. 2 μg of each protein was loaded.
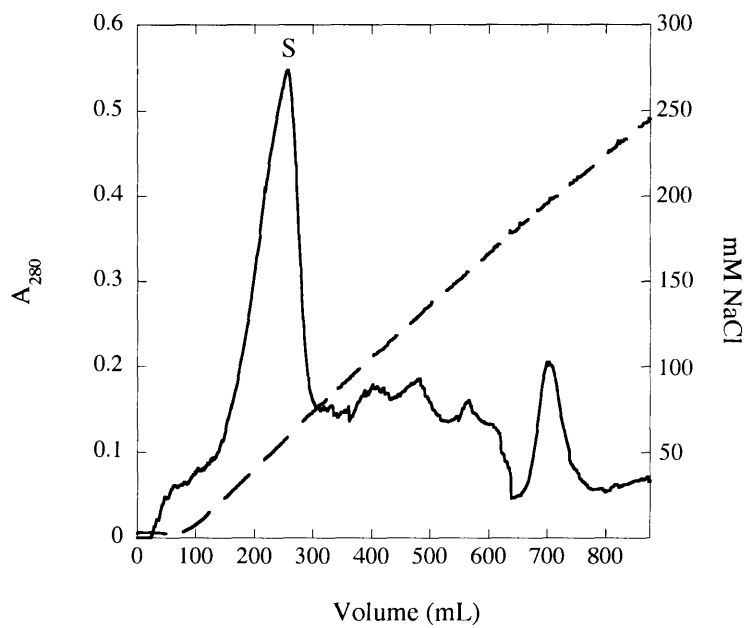
Figure 3.5—DEAE Elution profile of PurS. Elution of PurS (S) is noted.
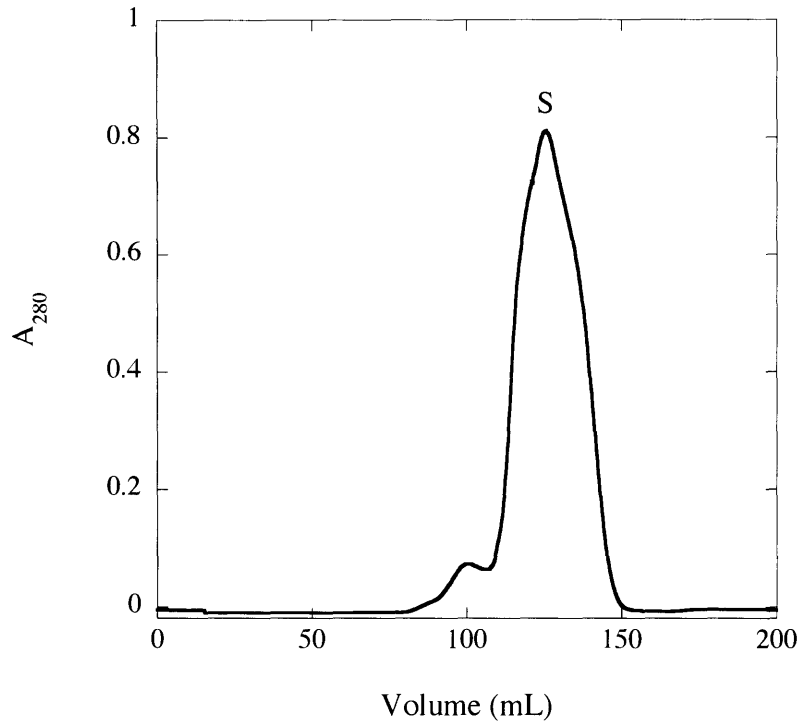
Figure 3.6—Sephacryl S-300 elution profile of PurS. The elution of PurS (S) is noted.

Subsequent to purification, the gene was sequenced which revealed an A128T mutation consistent with the ESI-MS data. This residue is not conserved among PurQ enzymes. To establish the actual identity of this residue, *purQ* was recloned from genomic DNA in five separate reactions, using the high fidelity KODHiFi DNA polymerase. Sequencing of all of the PCR products revealed an alanine at position 128. The wt-gene was also placed into pET-24a. The purification of the wt PurQ protein was carried out as described for the A128T mutant. However, the protein behaved differently from the mutant on DEAE Sepharose, eluting at 250 mM KCl. The purity of wt PurQ (50-60% homogeneous by SDS-PAGE, data not shown) and recovery were both low. A variety of additional chromatographic methods were examined in an effort to obtain homogeneous protein, all without success. The specific activity of the purified wt PurQ using the glutaminase assay was 20 nmol min^{-1} mg^{-1}, higher than that of the mutant (5 nmol min^{-1} mg^{-1}). However, the specific activity of the wt PurQ in the FGAM synthesis assay described later was ten fold lower (0.12 U/mg vs. 1.2 U/mg) than the mutant PurQ. It is possible that the high glutaminase activity of the wt PurQ could be due to an endogenous *E. coli* glutaminase, as was seen in the SEC purification of the A128T mutant. In the reconstitution experiments described subsequently, the A128T PurQ has been employed.

step	protein (mg)	total units (U)	SA (U/mg)	% yield
cell lysate[a]	1159	3.93	0.003	100
streptomycin	1214	1.52	0.001	39
DEAE Sepharose	303	2.14	0.007	54
HTP Biogel	204	3.39	0.02	86
Sephacryl S-100	118	0.590	0.005	15

Table 3.4: Purification of A128T-PurQ

[a]From 13 g of cells
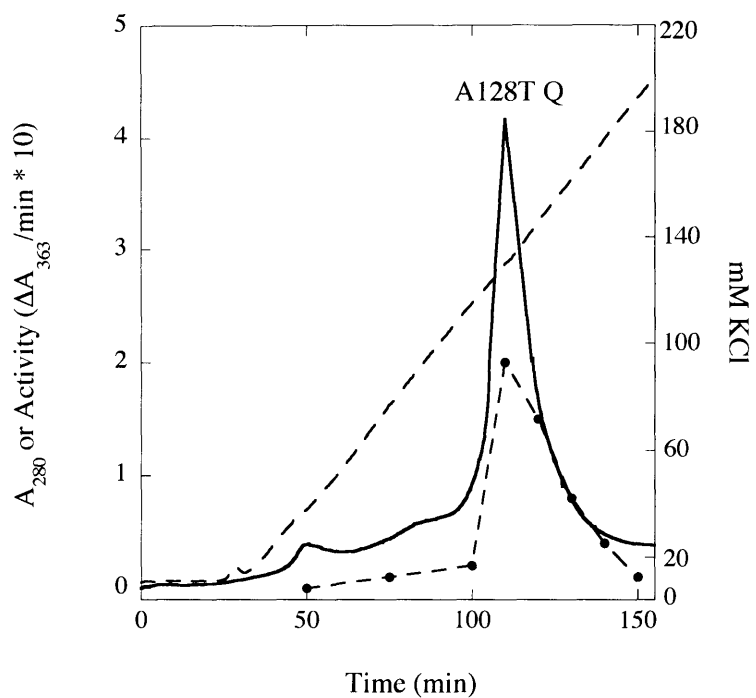
Figure 3.7—DEAE elution profile of A128T PurQ. Activity (●) was measured using the coupled GDH assay and is expressed in terms of the change in A_{363} per min × 10 in order to plot the A_{280} and relative activity on the same axis.
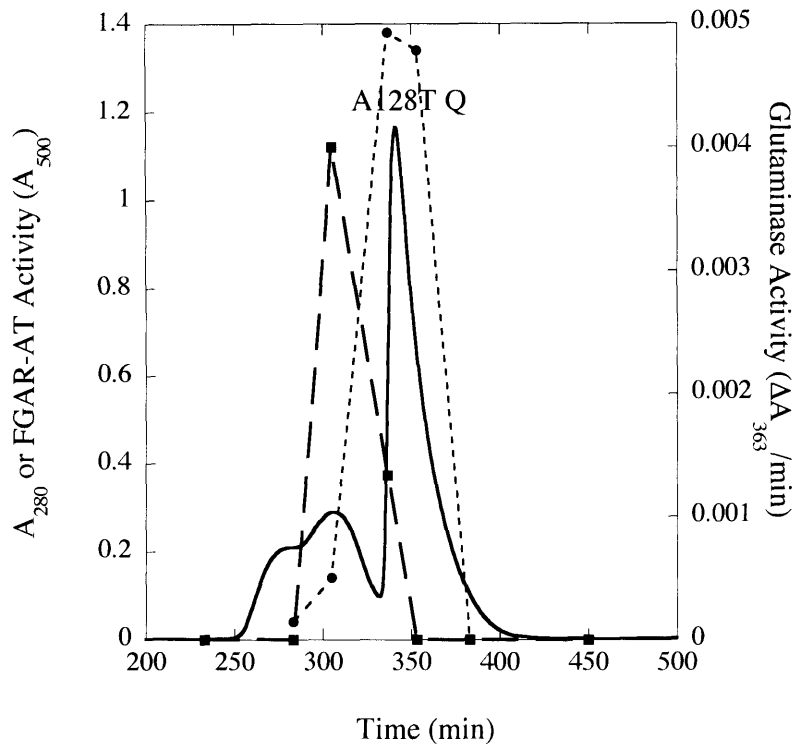
Figure 3.8—Sephacryl S-200 SEC elution profile of A128T PurQ. FGAR-AT activity (●, dotted line) is represented as A_{500} from the gln-dependent Bratton-Marshall assay. Glutaminase activity (■, dashed line) is represented as the change in A_{363} per min from the GDH-coupled assay. Notice that an endogenous *E. coli* glutaminase co-purified with PurQ. The glutaminase was removed during SEC and eluted at 300 min. PurQ eluted at 350 min.

It is interesting to note that both wt and A128T PurQ behaved similarly during the co-expression experiments (Tables 3.2 and 3.3). This indicates that the low activity and inability to purify wt PurQ may originate from expression of the enzyme in the absence of smPurL and PurS.

smPurL: The *purL* gene was amplified by PCR from the pDE51 sequencing vector and then ligated into pET-24a (6). Sequencing of the cloned gene revealed a L513F mutation, which resulted from a single nucleotide mutation (CTC to TTC) in the codon. In contrast with the observations with the *purQ* gene, a similar set of experiments revealed that the wt smPurL contains a phenylalanine at position 513, not a leucine as previously reported (6). All work has thus been carried out with smPurL containing F513.

In contrast to the co-expression experiments described above, expression of smPurL alone resulted in aggregation and inclusion bodies. To maximize expression of soluble smPurL, *E. coli* containing the *smpurL* expression plasmid were grown at 27.5°C. The enzyme was purified using DEAE Sepharose anion exchange chromatography (Figure 3.9) followed by chromatography on Reactive Red Agarose 120. The red agarose column removed inactive aggregates of smPurL that eluted in the flowthrough of the column. These aggregates, unable to re-equilibrate with active smPurL, accounted for 40% of the soluble smPurL. The active smPurL also flowed through the dye affinity column, but only subsequent to the elution of the aggregate. A small amount of smPurL remained bound to the column and eluted at 250 mM NaCl. While recoveries from this column were low (18% of units, Table 3.5), recovery was sacrificed for purity to enhance crystallographic efforts. The smPurL was typically recovered at 4 mg/g of cells and judged to be 90% homogeneous based on SDS-PAGE (Figure 3.4, lane 3). N-terminal protein sequencing of smPurL indicated loss of methionine, consistent with the ESI-MS
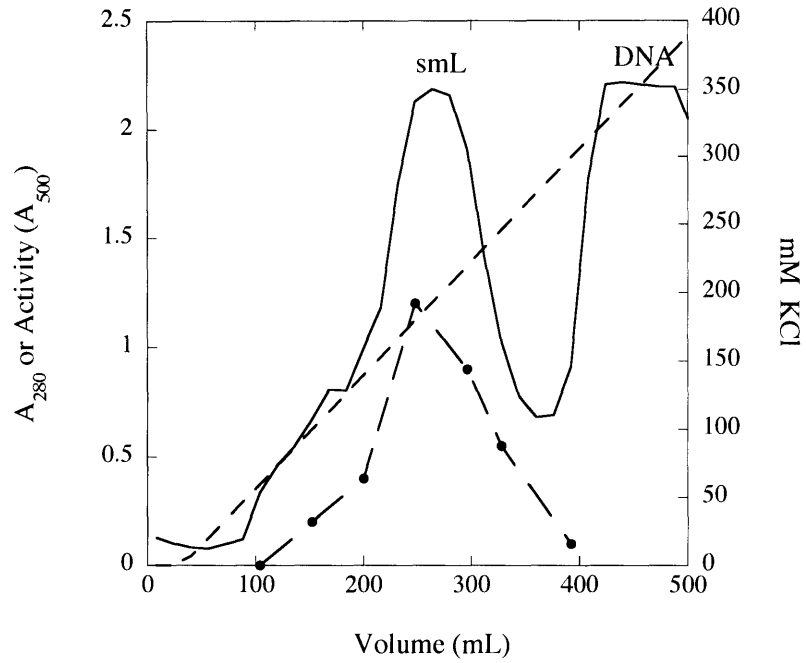
Figure 3.9—DEAE elution profile of smPurL. The activity ($\bullet$, dashed line) is expressed as A_{500} from the NH_3-dependent Bratton-Marshall assay. Elution of smPurL and cellular DNA is noted.

molecular weight. Activity of smPurL (33 nmol min^{-1} mg^{-1}) was monitored using the Bratton-Marshall assay with NH$_4$Cl as the ammonia source. Under these conditions, PurS and PurQ were not needed for FGAM synthesis.

Table 3.5: Purification of smPurL				
step	protein (mg)	total units (U)	SA (U/mg)	% yield
cell lysate[a]	800	6.07	0.008	100
streptomycin	778	4.25	0.006	70
DEAE Sepharose	236	5.43	0.02	89
Reactive Red Agarose 120	34	1.11	0.03	18
[a]From 8 g of cells				

Reconstitution of Enzymatic Activity

Based on the stability and solubility problems encountered with both PurQ and smPurL, it is perhaps not surprising that reconstitution of FGAR-AT proved to be challenging. Attention to the concentration and ratios of the proteins in the reconstitution mixture as well as the order of addition of the proteins was essential. Reconstitutions were carried out on ice to avoid aggregation of both A128T PurQ and smPurL that was observed at higher temperatures ($\geq$ 25°C). The concentration of enzymes in the assay mixture was also critical to the success of the reconstitution.

Determination of Subunit Stoichiometry: Initial efforts focused on determination of the stoichiometry of PurS, smPurL, and A128T PurQ required to achieve maximal FGAR-AT activity. After extensive experimentation, successful titrations were shown to require premixing of all three component proteins at ~10 µM at 4°C in the presence of glutamine and 10 mM MgATP. It was later determined that the ADP necessary for reconstitution of activity (see below) could be completely supplied by ADP contamination present in the 10 mM ATP (data not

shown). This mixture was then diluted 100-fold into the assay buffer at 37°C and monitored for

FGAM production. The results of a typical titration of A128T PurQ with PurS and smPurL (2:1)

are shown in Figure 3.10 (●). The titration reveals that maximal activity is achieved at a ratio of

A128T PurQ to smPurL of 1:1. PurS was titrated with A128T PurQ and smPurL (1:1) using a

similar procedure. Under these conditions, 2 equivalents of PurS are needed for maximal

activity (Figure 3.10, ■). These results suggest the stoichiometry of PurS: smPurL: PurQ is

2:1:1.

Steady-State Kinetics

As noted in the introduction, FGAM synthesis can be divided into 2 half-reactions (Eq.

3.1 and 3.2): the hydrolysis of glutamine to glutamate and NH_3 and ATP-dependent amidine

formation. Kinetic characterizations of the individual components (PurQ and smPurL) as well as

the complex (PurS, smPurL, and PurQ) have been investigated. The results are summarized in

Table 3.6 and are shown in comparison to previously studied lgPurLs.

Glutaminase Activity of PurQ: PurQ is a member of the triad class of glutaminases that

includes PabA (the glutaminase of the PabA/PabB aminodeoxychorismate synthase), HisH (the

glutaminase of the HisH/HisF imidazole glycerol phosphate synthase), and the lgPurLs (*11, 16,*

18, 20). In all cases, these enzymes possess very low (or in some cases undetectable)

glutaminase activity in the absence of the amidotransferase and/or other substrates. The kinetic

parameters of the A128T-PurQ are summarized in Table 3.6. As in the case of PabA and the
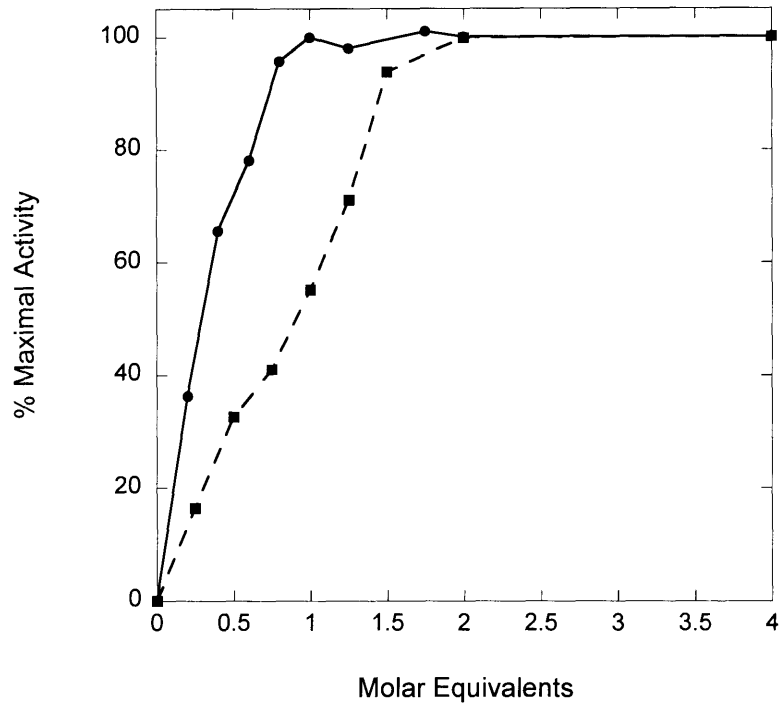
Figure 3.10—Determination of the ratio of PurS: smPurL: PurQ required for maximal activity. (●) 2 PurS: 1 smPurL (10 μM) and variable amounts of PurQ (0 to 40 μM) were pre-incubated at 4°C for 5 min. The reaction mixture was then diluted 100-fold and assayed for FGAM production. (■) 1 PurQ: 1 smPurL (10 μM) and variable amounts of PurS (0 to 40 μM) were pre-incubated at 4°C for 5 min. The reaction mixture was then diluted 100-fold and assayed for FGAM production.

chicken liver lgPurL, a lag phase was present in the kinetics prior to the reduction of APAD (*18, 21*). The activity of A128T PurQ alone (0.002 s^{-1}) is 0.08% that in the complex. The presence of smPurL, PurS, and MgATP did not increase the activity. However, incubation with smPurL and PurS (2 PurS: 1 smPurL: 1 PurQ) and β-FGAR increased the turnover 30-fold (0.066s^{-1}). No additional increase in glutaminase activity was observed upon addition of the non-hydrolyzable ATP analog β,γ-methyleneadenosine 5'-triphosphate (AMP-PCP).

Table 3.6: Selected Kinetic Parameters of FGAR-AT Enzymes

Property	smPurL[a]	PurQ	FGAR-AT Complex[a]	E. coli[b]	Chicken Liver[c]
K_m FGAR	2.5 mM		507 μM	30 μM	100 μM
K_m ATP	398 μM		181 μM	51 μM	1.5 mM
K_m Gln		2.5 mM	1.3 mM	64 μM	40 μM
K_m NH$_3$	~3.5 mM			54 mM	10 mM
Magnesium[d]			20 mM	20 mM	20 mM
Potassium[d]			20 mM	10 mM	60 mM
k_{cat} FGAM synthesis (s^{-1})[e]	0.044		2.49	5.00	0.47
k_{cat} Glutaminase (s^{-1})[f]		0.002	0.066	0.001	0.002

[a]For smPurL and the FGAR-AT complex these values are $K_{m,app}$ due to substrate inhibition. [b]Values from (*11*). [c]Values from (*22*) and (*21*). [d]Defined as the concentration of Mg^{2+} or K$^+$ required for maximal activity. [e]Measured by the rate of FGAM synthesis using either NH$_3$ or gln as the nitrogen source. [f]Measured by the rate of gln hydrolysis using the continuous glutaminase assay in the absence of FGAM synthesis. For the FGAR-AT complex, this was measured in the presence of FGAR but not ATP.

Amidotransferase Activity of smPurL: smPurL alone can catalyze formation of FGAM in the presence of NH$_4$Cl with a turnover number of 0.044 s^{-1}, 1.8% the rate of FGAM synthesis using glutamine. This number is similar to those previously reported for the *E. coli* (2%) and chicken liver lgPurLs (5%) (*11, 23*).

The steady state kinetic parameters of smPurL with ammonia have been investigated at pH 7.25 (see pH rate profile, Figure 3.12) and are shown in Table 3.6. FGAM formation was measured using the Bratton-Marshall assay, and ADP production was measured using the

PK/LDH assay. Substrate inhibition was observed at concentrations of $NH_4Cl > 400$ mM and β-FGAR > 2 mM. While the inhibition seen with β-FGAR could be fit to Equation 3.4, inhibition kinetics observed with NH_4Cl could not be fit to standard inhibition equations. The K_ms reported in Table 3.6 are therefore apparent K_ms ($K_{m,app}$).

Activity of the FGAR-AT Complex: The three assays described above have been used to measure FGAM, ADP, and glutamate formation by the FGAR-AT complex. These assays were performed using the ratio of 2 PurS: 1 smPurL: 1 A128T PurQ and at protein concentrations > 0.1 μM. At lower enzyme concentrations, the specific activity of the complex dropped sharply (Figure 3.11). This result may be related to the high FGAR-AT enzyme concentration *in vivo* (see Chapter 4) and the K_d for the protein interactions. Similar to observations made in the smPurL assays, β-FGAR exhibited substrate inhibition at > 2 mM. Consequently, Equation 3.4 was used to fit the data, giving a K_m of 507 μM. Kinetic analyses to determine $K_{m,app}$s for glutamine and ATP were carried out at 1 mM β-FGAR (Table 3.6). The FGAR-AT complex gave a turnover number of 2.5 s^{-1}, which is comparable to that of lgPurLs (Table 3.6). While the assays to measure FGAM and glutamine formation gave complementary results, the coupled PK/LDH assay monitoring ADP formation was problematic. Long lag phases were observed. Similar assays on the *E. coli* and *S. typhimurium* lgPurLs exhibited no lag phases. The source of the lag phase was determined to be associated with the ATP regenerating system because addition of PK and PEP (or, alternatively, creatine kinase and phosphocreatine) resulted in the observation of lag phases in the glutaminase and Bratton-Marshall assays. These results suggested that a small amount of ADP is required for FGAR-AT complex assembly and turnover. The source of the ADP in these assays appears to be from background ATPase
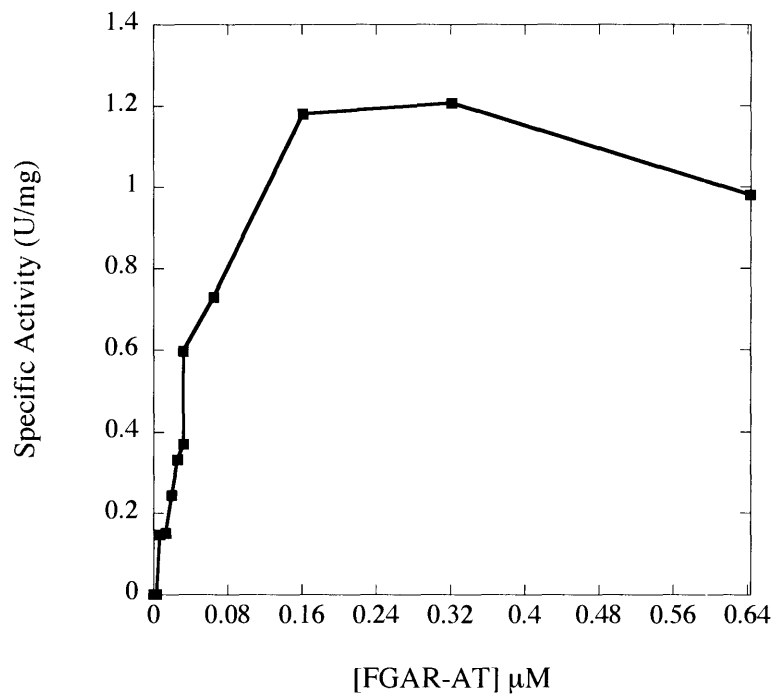
Figure 3.11—Concentration dependence of the specific activity of the FGAR-AT complex. The FGAR-AT complex was reconstituted as described and diluted into assay buffer at varying concentrations.

activity of the his-PurM coupling enzyme and from ADP contamination of the ATP stocks (data not shown).

Metal Ion Dependence: As with both the *E. coli* and chicken liver lgPurLs, the FGAR-AT reaction for the smPurL was found to be metal ion dependent (*11, 22*). Magnesium is required for the reaction, while saturating potassium levels stimulated FGAM synthesis 5-fold. The optimal magnesium and potassium concentrations were 20 mM. These values are similar to those previously reported for the lgPurLs (Table 3.6).

pH Dependence of the FGAR-AT Reaction: During these efforts to examine the NH_3-dependent smPurL activity, the assays were initially carried out at elevated pH ($\geq$ 8.0). Previous studies of the ammonia dependence of many glutamine-requiring enzymes have shown that elevated pH is essential to increase the concentration of available NH_3 (*11, 16*). At pH 8.0, however, no activity was detected for smPurL. This prompted studies of the pH-dependence of the FGAR-AT reaction. As shown in Figure 3.12, the complex has a sharp pH profile with an optimum of ~7.0. The pH rate profile for the NH_3-dependent reaction is very similar to the glutamine reaction, with a shift of the pH optimum to pH ~7.25. These results indicate that the pH-dependence of this enzyme resides on smPurL.

Stoichiometry of the Reaction: Given the complexity associated with optimization of the active FGAR-AT, the product stoichiometry of the reaction was carefully examined. It was determined to be 1 FGAM: 1.1 $\pm$ 0.2 ADP: 1.7 $\pm$ 0.2 glutamate, in contrast to the expected results of 1:1:1. The glutamate was quantitated by two independent methods (experimental section). As a control for this assay, the ratio of FGAM to glutamate formation was determined for the *E. coli* and *S. typhimurium* lgPurLs. It was found to be 1: 1.5 $\pm$ 0.1 and 1: 1.6 $\pm$ 0.1, respectively. These results contrast with the earlier report of 1 ADP: 1 glutamate for the chicken
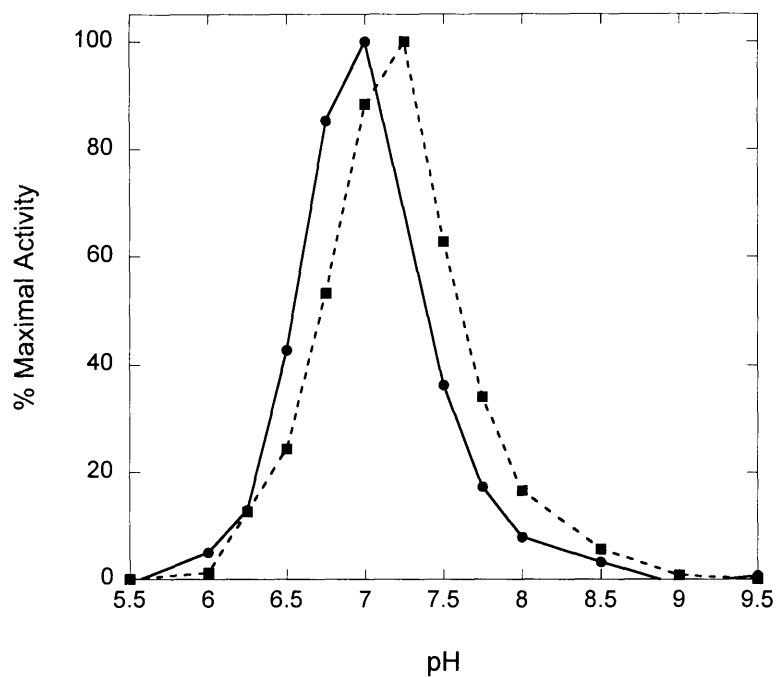
Figure 3.12—pH dependence of the FGAR-AT reaction using either glutamine (●) or NH_3 (■) as the nitrogen source.

liver lgPurL (*21, 22*). These results with 3 bacterial FGAR-ATs indicate that under these assay conditions glutamine hydrolysis is uncoupled from FGAM production.

DON Inactivation of PurQ

Support for catalytic coupling of the glutaminase activity to substrate interactions within the smPurL enzyme was sought using the mechanism-based inhibitor 6-diazo-5-oxo-L-norleucine (DON). This compound inactivates many glutaminases by alkylating the cysteine required for covalent catalysis (*20*). A128T PurQ was also inactivated by DON but required the presence of smPurL, PurS, MgATP, and β-FGAR. The half-life for inactivation was < 1 s when saturating in all substrates. A128T PurQ mixed with DON alone lost only 70% of its activity after more than 20 h at 25°C. Therefore, formation of the FGAR-AT complex and binding of MgATP and FGAR accelerates the rate of DON labeling by a factor of 10^4. This rate acceleration is comparable to the 1250-fold increase in glutaminase activity seen upon complex formation and FGAM synthesis (Table 3.6). This feature is common to all ATs, but it is still not well-understood.

Evidence for FGAR-AT Complex Formation

Analytical SEC on a Bio-Rad Bio-Silect SEC250 column was used to study the quaternary structure of PurS, PurQ, smPurL individually and in the FGAR-AT complex. While this column has limited resolution, the small excluded volume was essential for equilibrating the column with substrates (FGAR, glutamine, ATP) to determine if their presence alters complex formation.

As shown in Figure 3.13, PurS, A128T PurQ, and smPurL all migrated as discrete species when separately injected. PurS (Figure 3.13, A) and A128T PurQ (Figure 3.13, B) eluted with identical retention volumes of 6.8 mL. smPurL eluted at 5.4 mL (Figure 3.13, C). Thus,
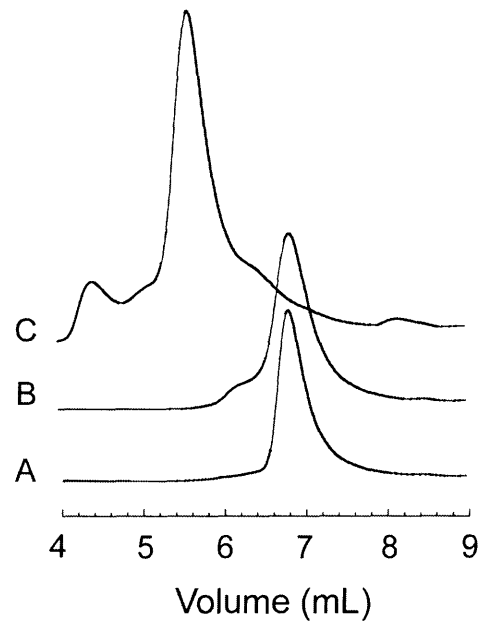
Figure 3.13—Analytical SEC results of the FGAR-AT component proteins injected individually. PurS (A), PurQ (B), and smPurL (C) elute at 6.8, 6.8, and 5.4 mL, respectively. The shoulders on the left hand side of the PurQ and smPurL peaks represent aggregated protein.

complex formation could be monitored by disappearance of the PurS and A128T PurQ peaks and by either an increase in the smPurL peak or the appearance of a new peak in the chromatogram.

In an effort to obtain direct evidence for a FGAR-AT complex, analytical SEC was carried out on PurS, smPurL, and A128T PurQ mixed at different ratios and concentrations in the presence and absence of substrates (ATP, FGAR, glutamine, and Mg^{2+}) and at different temperatures. A typical set of results are shown in Figure 3.14, A. With the proteins alone or in the presence of Mg^{2+}-ATP, glutamine, or β-FGAR, no evidence of complex formation was seen at either 4 or 25°C.

The kinetics studies suggested that Mg^{2+}-ADP facilitated formation of an active form of the FGAR-AT, an observation further supported by the presence of a tight binding $(Mg^{2+})_3$-ADP in the structure of the lgPurL (*12*). Thus, 2 PurS: 1 smPurL: 1 A128T PurQ was pre-incubated with Mg^{2+}-ADP. Analytical SEC again revealed no complex formation. However, if the complex had been pre-incubated with Mg^{2+}-ADP and glutamine and injected onto a column equilibrated with glutamine, a decrease in the PurS/PurQ peak was observed concomitant with an increase in the smPurL peak (Figure 3.15). The eluted complex had a specific activity of 0.8 U/mg, and the presence of all three proteins was confirmed by SDS-PAGE. Surprisingly, substoichiometric percentages (49%) of PurS and A128T PurQ were present in the complex. Finally, if both the FGAR-AT complex and the column were pre-incubated with Mg^{2+}-ADP and glutamine, the FGAR-AT was observed to fully form for the first time (84% of PurS and A128T PurQ complexed) and had a specific activity of 2.1 U/mg (Figure 3.14, B). These results indicate that complex formation is dependent on the presence of both Mg^{2+}-ADP and the glutamine substrate.
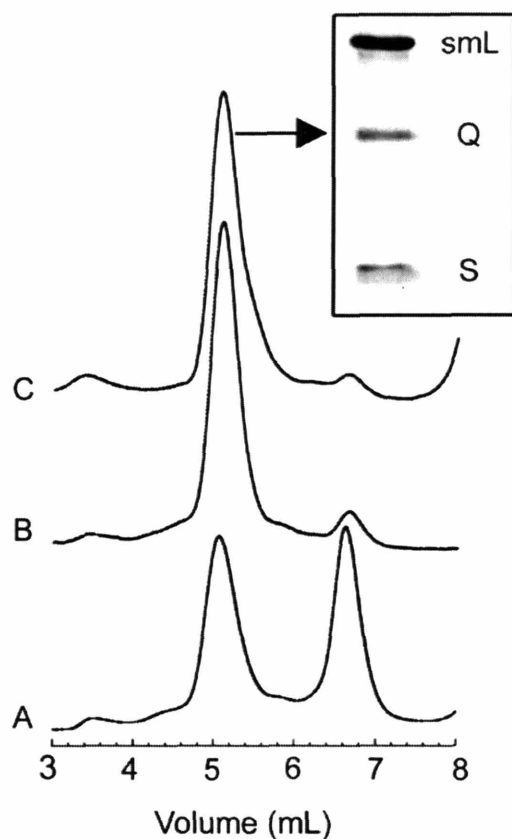
Figure 3.14—SEC evidence for the importance of the small molecules glutamine and ADP in complex formation. (A) Injection of 2 PurS: 1 smPurL: 1 PurQ gave complete separation of the components. PurS and PurQ elute at 6.8 mL , while smPurL elutes at 5.2 mL. Inclusion of glutamine, Mg^{2+}-ATP, Mg^{2+}-ADP, or β-FGAR gave similar results. (B) Injection of 2 PurS: 1 smPurL: 1 PurQ pre-incubated with (glutamine, Mg^{2+}-ADP) and inclusion of (glutamine, Mg^{2+}-ADP) in the elution buffer gave complex formation (confirmed by SDS-PAGE, inset). (C) Injection of 2 PurS: 1 smPurL: 1 PurQ inactivated with DON and chromatographed with Mg^{2+}-ADP in the elution buffer also showed complex formation. *Inset:* 15% SDS-PAGE showing the presence of PurS, PurQ, and smPurL in the 5.2 mL peak from (B).

172
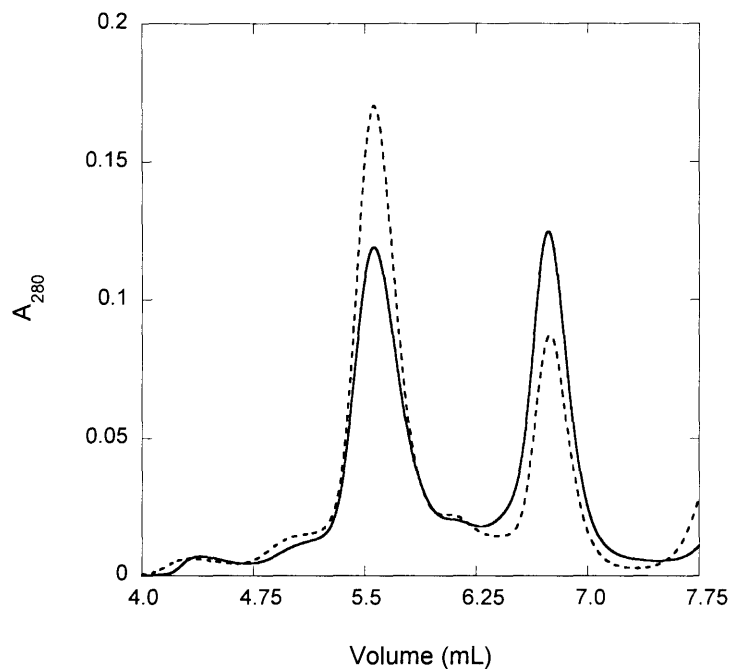
Figure 3.15—Partial complex formation observed with pre-incubation of 2 PurS: 1 smPurL: 1 PurQ with Mg^{2+}-ADP and glutamine and elution with only glutamine included in the SEC buffer. The solid line shows the FGAR-AT proteins eluted in only SEC buffer. The dotted line shows formation of the FGAR-AT complex initiated by including glutamine in the SEC buffer.
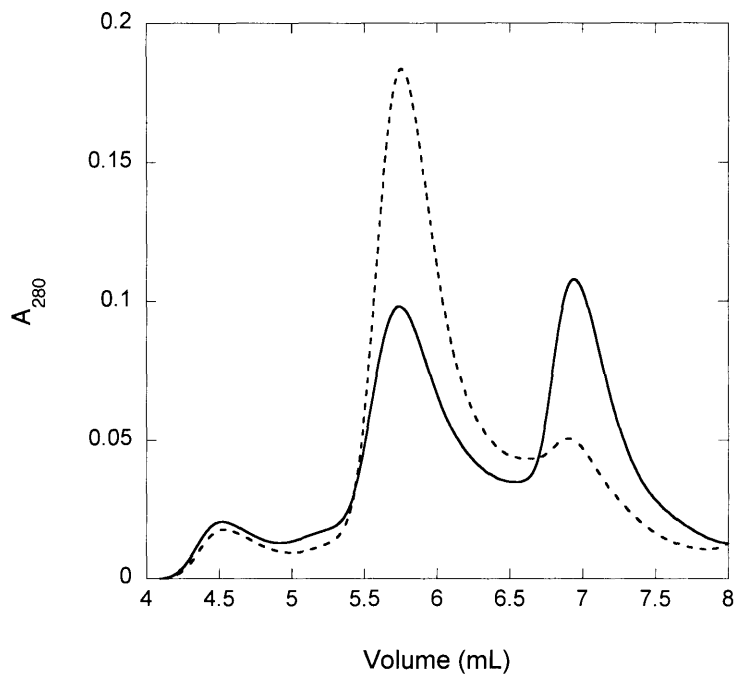
Figure 3.16—Partial 2 PurS: 1 smPurL: 1 PurQ complex formation observed with DON-inactivated PurQ. The solid line shows the 2 PurS; 1 smPurL: 1 PurQ proteins eluted in SEC buffer. The dotted line shows the 2 PurS; 1 smPurL: 1 PurQ proteins eluted in SEC buffer after DON-inactivation of PurQ.

Previous studies on assembly of channeling complexes in other glutamine-requiring ATs suggested that the presence of a glutamine analog such as DON facilitated complex formation (*24*). The 2 PurS: 1 smPurL: 1 A128T PurQ complex was therefore inactivated with DON and examined by analytical SEC in the absence of glutamine. While a complex was seen, it contained only 46% of the included PurS and A128T PurQ (Figure 3.16). The addition of Mg^{2+}-ADP to the column elution buffer resulted in 92% of the PurS and A128T PurQ complexed with smPurL (Figure 3.14, C). These results indicate that the DON-inactivated A128T PurQ can also trigger complex formation and suggest that the role of glutamine in complex formation may result from glutamine bound as a thioester. Together this work shows that Mg^{2+}-ADP and either a covalently or non-covalently bound glutamine are absolutely essential to form the active FGAR-AT complex. A tight, transient complex may form to specifically channel the ammonia released from PurQ.

ADP Binding to the Salmonella lgPurL

The crystal structure of the *Salmonella* lgPurL reveals a tightly-coordinated $(Mg^{2+})_3$-ADP bound to the enzyme (*12*). ADP was not added during the purification or during the crystallization, indicating that the nucleotide was inserted during heterologous expression in *E. coli* and remained bound during lgPurL's purification. This observation immediately provided a link between the lgPurL crystal structure and observations made while examining activity of the *B. subtilis* FGAR-AT in which Mg^{2+}-ADP was shown to be necessary for activity and tight complex formation. As a result of these observations, ADP binding to the *Salmonella* lgPurL was investigated. The ADP•lgPurL stoichiometry could easily be determined by precipitating the enzyme and measuring the amount of ADP released into solution. These results indicated that ADP was bound quantitatively to lgPurL with a ratio of 1.02 ADP: 1 protein. Similar

experiments carried out with the *B. subtilis* smPurL detected no aborbance at 260 nm, indicating that ADP that had not co-purified with the enzyme.

Co-purification of stoichiometric ADP with the *Salmonella* lgPurL requires that it is tightly bound. Efforts to detect ADP dissociation from lgPurL without enzyme denaturation were unsuccessful. Neither extensive dialysis, nor exchange with [^{3}H]-ADP into lgPurL could detect ADP dissociation. These results indicate that ADP is bound to *Salmonella* lgPurL with very high affinity.

Isolation of smPurL•ADP Complexes

Since ADP did not co-purify with the *B. subtilis* smPurL, experiments were carried out to see if a smPurL•ADP complex could be isolated after mixing the protein with ADP. Incubation of smPurL with [^{14}C]-ADP resulted in 0.073 equivalents of nucleotide co-purifying with the protein using Sephadex G-50 chromatography (Table 3.7). However, ADP binding to smPurL was stimulated by the presence of A128T PurQ, PurS, and glutamine. Under these conditions 0.43 equivalents of ADP co-chromatographed with the protein (Figure 3.17, Table 3.7). No evidence for dissociation during chromatography was apparent. When PurS and A128T PurQ were mixed individually with smPurL, A128T PurQ appeared to have the greatest effect on ADP binding since 0.27 equivalents of ADP could be isolated with the protein (Table 3.7). The impact of PurS and A128T PurQ on ADP binding provides further evidence for the connection between ADP and FGAR-AT complex formation.

Table 3.7: Quantitation of [^{14}C]-ADP Binding to smPurL		
Proteins	Glutamine	Ratio ADP:smPurL
smPurL	----	$0.073 \pm 0.005 : 1$
smPurL/PurS	20 mM	$0.14 \pm 0.02 : 1$
smPurL/PurQ	20 mM	$0.27 \pm 0.04 : 1$
smPurL/PurQ/PurS	----	$0.31 \pm 0.06 : 1$
smPurL/PurQ/PurS	20 mM	$0.43 \pm 0.03 : 1$
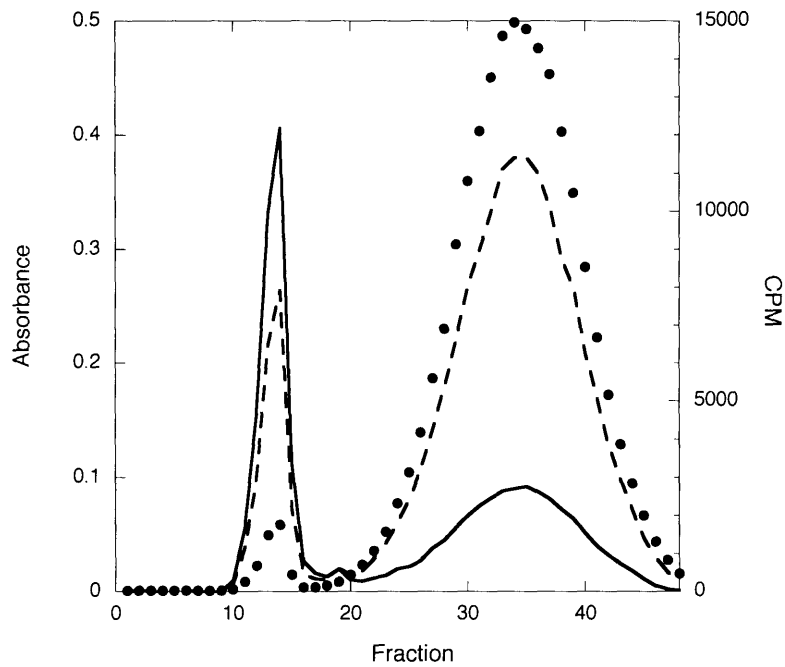
Figure 3.17—Isolation of a smPurL:nucleotide complex by G-25 Sephadex gel filtration chromatography. 150 μM of the FGAR-AT complex (2 PurS: 1 smPurL: 1 PurQ) was incubated with 3 mM ^{14}C-ADP and 20 mM L-glutamine. Excess ADP was then removed by the G-25 Sephadex column. The solid and dashed lines represent the absorbance at 280 and 260 nm, respectively. The dotted line represents the amount of radioactivity in each fraction (CPM).

One result from these experiments that warrants further investigation is the low ADP•smPurL stoichiometry (Table 3.7). Radioactive ADP that co-eluted with the protein from the G-50 column always appeared as a sharp peak, with little discernable tailing (Figure 3.17). This indicates that the smPurL•ADP complex was likely not equilibrating on the column. The low stoichiometry could be indicative of protein misfolding and aggregation during the experiment, which has been a common problem in studies of the *B. subtilis* FGAR-AT. Future experiments designed to monitor both smPurL aggregation and nucleotide binding may be able correlate these two phenomena.

3.4 Discussion

Amidotransferases (ATs) are enzymes that catalyze the reaction of ammonia (derived from the amide moiety of glutamine) with a wide range of substrates found in many metabolic pathways to generate an aminated product. Seminal structural experiments on two ATs, phosphoribosylpyrophosphate AT (PRPP-AT or PurF, the first step in the purine biosynthetic pathway) and carbamoyl phosphate synthetase (CPS, in the pyrimidine biosynthetic pathway) suggested a general model for all ATs in which the glutaminase activity is located on a domain that is spatially separated from the AT domain (*24, 25*). The separation between the active sites in the two domains of PurF and CPS is, for example, 20 Å and 45 Å, respectively (*24, 25*). The long distance and the biochemical evidence that the "NH$_2$" moiety of the glutamine amide is found in the final product requires that ammonia is channeled between these two domains (*26*). The structural composition and the mechanism of formation of the channels within proteins have recently received much attention but as yet no general principles have emerged (*8*).

The *B. subtilis* FGAR-AT provides a new system to study communication between several active sites and ammonia channeling in an AT complex. All ATs contain one of two

178

highly conserved glutaminase domains either fused to the AT domain directly or on a separate polypeptide (20). The triad glutaminase domain was identified based on conservation of a putative catalytic triad of cysteine, histidine, and glutamic acid; however, in many cases, the acidic residue has been shown not to be essential for activity, and, thus, the triad nomenclature is a misnomer (27, 28) (see Chapter 5). The B. subtilis FGAR-AT is unique among all triad class ATs in that the enzyme is composed of three proteins (PurS, PurQ, and smPurL) instead of two.

The affinities between the glutaminase and AT proteins in a number of systems have been reported. In the cases of CPS, anthranilate synthase (TrpEG), and imidazole glycerol phosphate synthase (HisHF), the glutaminase domain is tightly bound to the AT, and the subunits remain complexed during purification (16, 29, 30). In the case of p-aminobenzoate synthase (PabAB), the two proteins separate during SEC at 4°C (18). However, if PabA and PabB are pre-incubated with glutamine at 37°C and SEC is performed at 25°C, complex formation is now observed (31). The diversity of the strength of subunit interactions and the coordination of activities and NH_3 channeling between proteins raises many questions concerning general mechanisms of AT catalysis. In particular, the mechanism of NH_3 channeling between weakly interacting subunits remains largely unknown. As noted in Chapter 2, the phenomenon of channeling of chemically unstable intermediates via transient protein interactions has been of long standing interest in the Stubbe Laboratory. The B. subtilis FGAR-AT complex offers another system within purine biosynthesis to explore this phenomenon.

The weak interactions between PurS, PurQ and smPurL became apparent when despite their heterologous co-expression in E. coli, the proteins separated during all chromatographic efforts for purification. Under the co-expression conditions, the solubility and stability of smPurL were greatly enhanced relative to smPurL expressed alone or in the presence of PurS.

These observations and the high levels of activity in crude extracts prior to purification suggested that the FGAR-AT components are interacting in the cell.

An additional observation during the co-expression experiments concerned the activities of the wt and A128T PurQs. When co-expressed, the activites of wt and A128T PurQ were comparable; however, when PurQ was isolated individually, the enzymes behaved very differently. The wt PurQ possesses much lower activity than the A128T PurQ mutant and could not be purified to homogeneity. The reason for these differences in behavior is unclear given that A128 is a non-conserved amino acid and is believed to be located on a solvent-exposed loop based on threading models using the structure of lgPurL. This loop appears to reside in a location not involved in complex formation or catalysis.

Given the inability to isolate an assembled FGAR-AT complex, efforts turned towards reconstituting the protein complex. The reconstitution was monitored by the glutamine-dependent FGAM synthetase activity, and titrations suggest the active AT contains PurS, smPurL, and PurQ in a ratio of 2:1:1 (Figure 3.10). The stoichiometry of products produced by the reconsituted FGAR-AT was 1.7 glutamates per ADP and FGAM. This uncoupling propensity is shared by both the *E. coli* and *S. typhimurium* enzymes but not the chicken liver enzyme (*22*). It is interesting to note that measurements made by Buchanan and coworkers on the chicken liver lgPurL indicated that the glutaminase activity could be drastically uncoupled from ADP formation using several glutamine analogs (*21*). For example, the enzyme hydrolyzed ~5 equivalents of γ-glutamylhydroxamate for each ADP consumed at 58% the rate of the normal reaction.

Various degrees of reaction coupling have been reported in the literature for other ATs. Both CPS and HisHF have been kinetically well-characterized and show stoichiometric product

180

formation (*32, 33*). On the other hand, asparagine synthetase B possesses a glutaminase activity 1.5-fold faster than asparagine formation, similar to results obtained for FGAR-AT (*34*). A detailed kinetic analysis of asparagine synthetase B suggests that uncoupling results from glutamine hydrolysis in the absence of the adenylated-aspartate intermediate formed during asparagine synthesis from aspartate and ATP and a 1:1 product ratio is only observed under sub-saturating glutamine concentrations (*34*). In one extreme example, cobyrinic acid *a,c*-diamide synthetase has been shown to hydrolyze 8 equivalents of glutamine for every product formed (*35*). The source of the reaction uncoupling in FGAR-AT is not understood; however, it may related to difficulties in enzyme reconstitution, ADP co-factor binding, or aggregation. Due to a lack of pre-steady state kinetic information, it is difficult to determine if the reaction uncoupling is due to NH_3 leaking from a putative channel between the glutaminase and FGAM synthetase sites or if it is due to glutamine hydrolysis in the absence of the proper FGAR and ATP intermediate in the AT site.

The most startling finding during these efforts to assemble an active FGAR-AT complex was the dependence on Mg^{2+}-ADP. Mg^{2+}-ADP was necessary for both activity and isolation of a protein complex by analytical SEC. An explanation for the role of ADP-binding became clear when Ruchi Anand (Ealick Laboratory, Cornell University) solved the crystal structure of the *Salmonella* lgPurL enzyme at a resolution of 1.9 Å (*12*). The N-terminal histidine-tagged enzyme (specific activity 4.4 U/mg) was crystallized by addition of 2.0 M $(NH_4)_2SO_4$ to a 15 mg/mL enzyme solution in 25 mM HEPES pH 7.1 and 1 mM glutamine. Of the 1295 amino acids in the native enzyme, all could be fit to the electron density except for residues 448-466 which form a mobile loop that closes over the amidotransferase active site. The structure of the

enzyme has been described in extensive detail elsewhere (*12*); so, only the results pertinent to this chapter are discussed.

The structure of lgPurL revealed that the enzyme contains 4, largely independent domains (Figures 3.18 and 3.19). The N-terminal domain adopts an unusual half-barrel fold that contacts both the glutaminase and AT-domains. The N-terminal domain is connected to the body of the enzyme by a linker domain (18 residues) culminating in a 3-helix bundle (Figure 3.19). The length of the linker domain and its weak side chain electron density suggested that the N-terminal domain may be highly mobile and interact only transiently with the glutaminase and AT domains.

The active sites of the glutaminase and AT domains are spaced ~30 Å apart; however, a well-defined NH_3 tunnel similar to that observed in CPS was not observed in the crystal structure. The lack of a channel may be due to crystallization of the enzyme in a catalytically incompetent conformation resulting from the presence of a glutamylthioester in the glutaminase domain (described in greater detail in Chapter 5). Previous studies on *E. coli* lgPurL indicated that while a glutamylthioester adduct readily forms upon incubation of the enzyme in the presence of glutamine, the resulting complex is neither kinetically nor chemically competent for catalysis (*11, 36*). Like PurF, the NH_3 tunnel in the FGAR-AT may be formed transiently during the reaction, and elucidation of the NH_3 tunnel is the focus of current crystallographic efforts on lgPurL by the Ealick Laboratory. At this stage, two possible routes for NH_3 have been identified (Figure 3.20). The favored route (Figure 3.20A) includes many conserved residues and is predicted to involve interactions with the N-terminal domain; however, this awaits experimental verification.
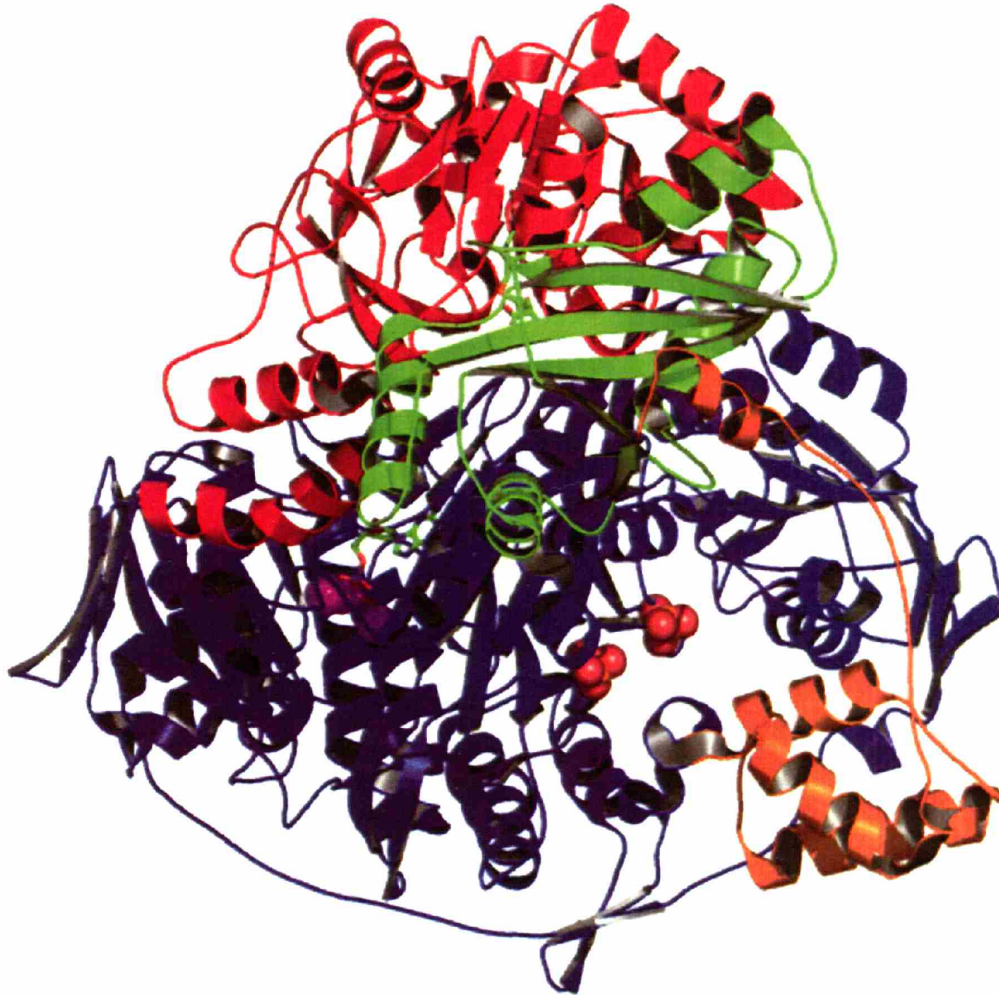
Figure 3.18—Structure of the *Salmonella* lgPurL enzyme. The N-terminal (green), linker (yellow-orange), FGAM synthetase (blue), and glutaminase (red) domains are shown. Sulfates present in the active site are shown in spacefilling representation. The $(Mg^{2+})_3$-ADP cofactor is shown in both spacefilling and stick representation (partially obscured by the FGAM synthetase domain).
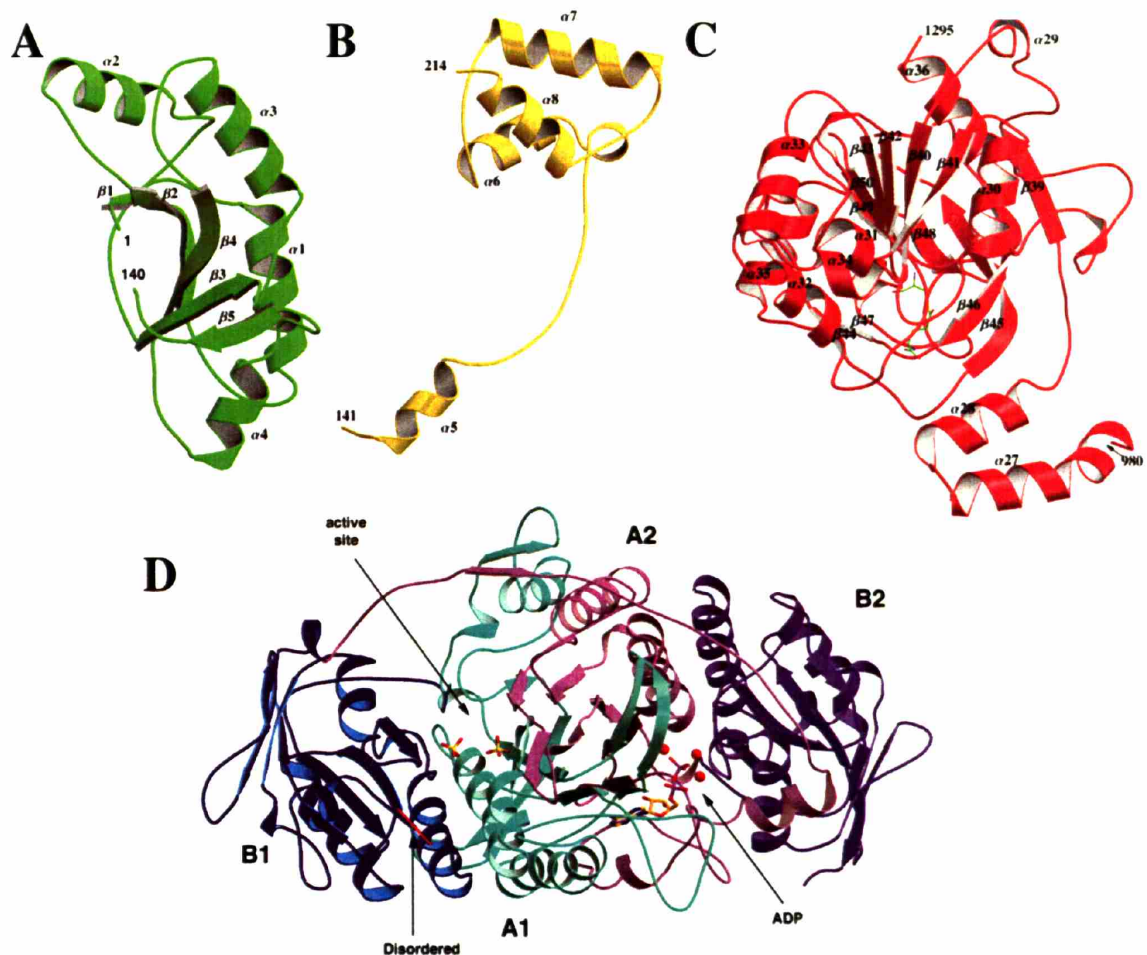
Figure 3.19—Domains of the FGAR-AT. (A) the N-terminal domain (notice the half-barrel shape), (B) the linker domain, (C) the glutaminase domain, and (D) the FGAM synthetase domain. The FGAM synthetase domain is colored to highlight the symmetry between the A1/B1 (N-terminal) and A2/B2 (C-terminal halves). The active site lies in a cleft between the A1 and B1 domains. The $(Mg^{2+})_3$-ADP site is related to the active site by the symmetry of the pseudo-dimeric fold. Figure courtesy of Ruchi Anand, Cornell University.
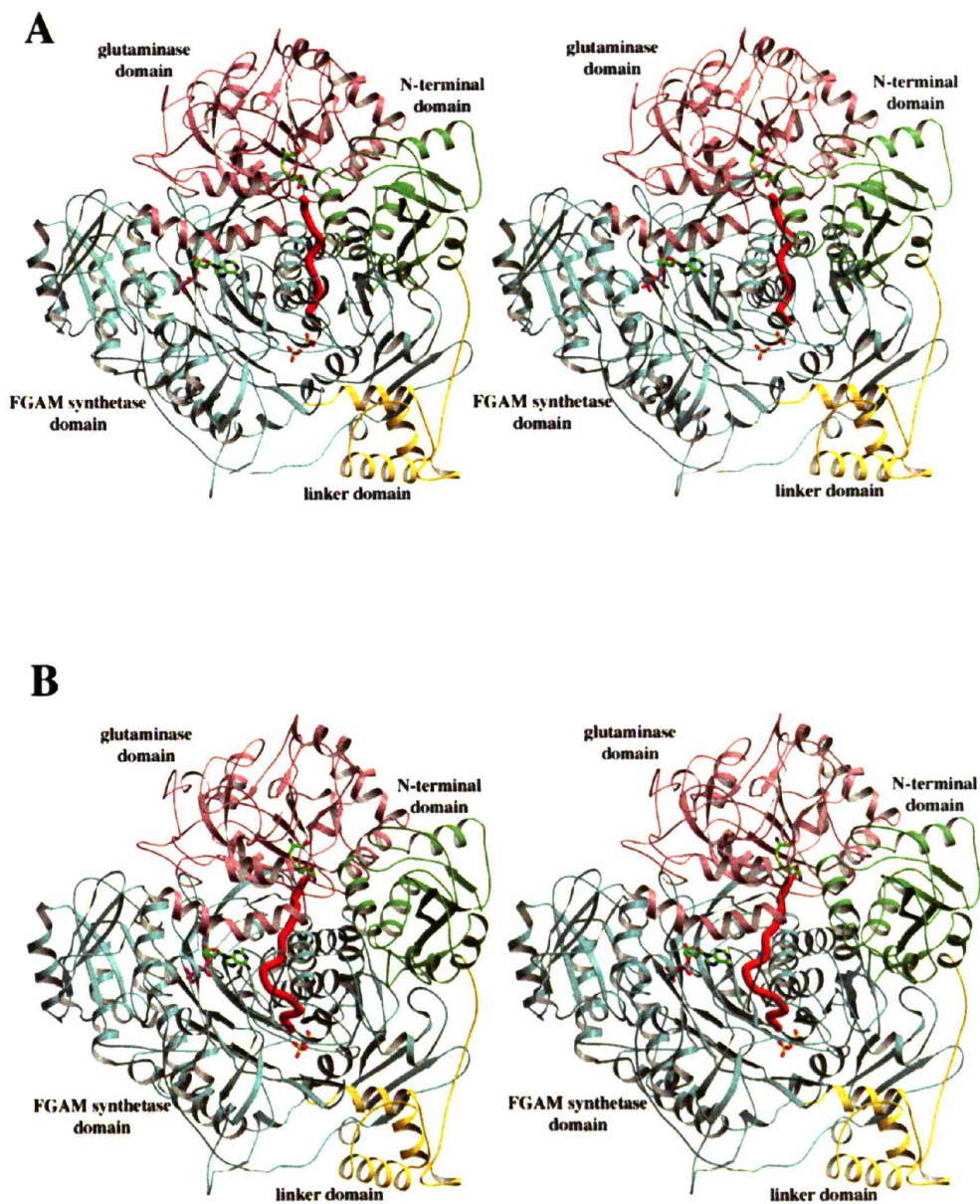
Figure 3.20—Stereoviews of 2 possible NH$_3$ tunnels present in the *Salmonella* lgPurL structure. (A) shows the favored channel which contains the most conserved residues, involves active participation of the N-terminal domain, and is the most direct path between the active sites. (B) shows an alternate path which contains more hydrophobic residues than (A) and passes near the ADP binding site. Figure courtesy of Ruchi Anand, Cornell University.

185

The AT domain shows a high degree of 2-fold pseudosymmetry between the N-terminal and C-terminal halves (Figure 3.19). These halves are also connected by a 27-residue linker region. Sequence alignments of many lgPurLs and mapping of conserved residues to the structure indicated that AT active site resides in the N-terminal half of this domain. Surprisingly, a tightly bound $(Mg^{2+})_3$-ADP was found in the symmetry related-active site in the C-terminal half (Figure 3.21). The ADP was not added during either the purification or crystallization and thus co-purified with enzyme isolated from $E.\ coli$. Analysis presented in this chapter of ADP-binding to the $Salmonella$ lgPurL indicated that ADP is bound stoichiometrically with the enzyme and can only be removed by protein denaturation. Sequence and structural information has indicated that the $(Mg^{2+})_3$-ADP binding site (referred to from now on as the auxiliary nucleotide site) has degenerated from an active site over the course of lgPurL evolution and is not a second active site. The current working model is that ADP is acting as a structural cofactor that allows correct orientation of the glutaminase domain (which docks on top of the auxiliary nucleotide site) above the FGAM synthetase active site. This orientation may be essential for NH_3 channeling.

Unlike lgPurL, no ADP could be detected bound to purified $B.\ subtilis$ smPurL. If ADP is playing a similar role in smPurL to that proposed for lgPurL, then the weaker affinity could explain why the addition of exogenous ADP was necessary for formation and activity of the $B.\ subtilis$ FGAR-AT complex. It is proposed that the requirement for Mg^{2+}-ADP is due to the $B.\ subtilis$ smPurL requiring this metabolite to bind in its own auxiliary nucleotide binding site to act as a structural cofactor for complex formation. In support of this proposal, sequence alignments and homology modeling (Figure 3.22) show that Mg^{2+}-ADP-binding residues are remarkably well-conserved between the $Salmonella$ lgPurL and $B.\ subtilis$ smPurL. Only ~0.1
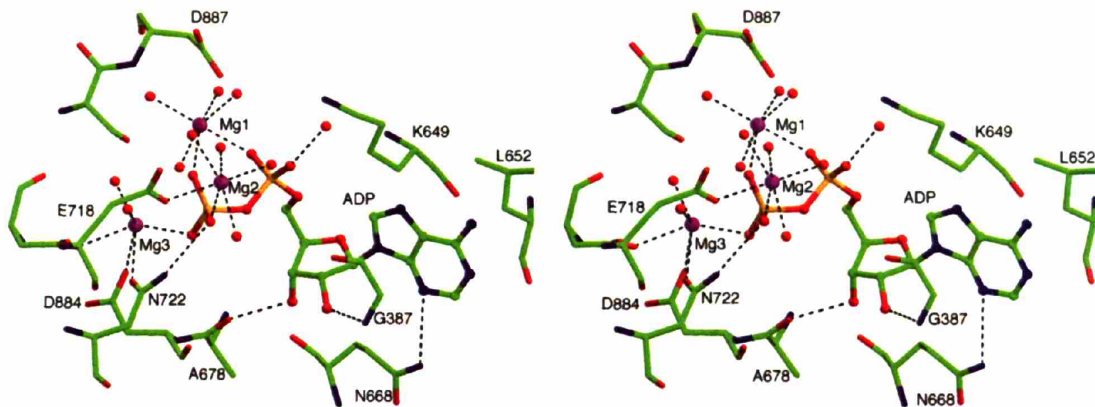
Figure 3.21 — Stereoview of the $(Mg^{2+})_3$-ADP site. Notice that the ADP is tightly coordinated. Figure courtesy of Ruchi Anand, Cornell University.
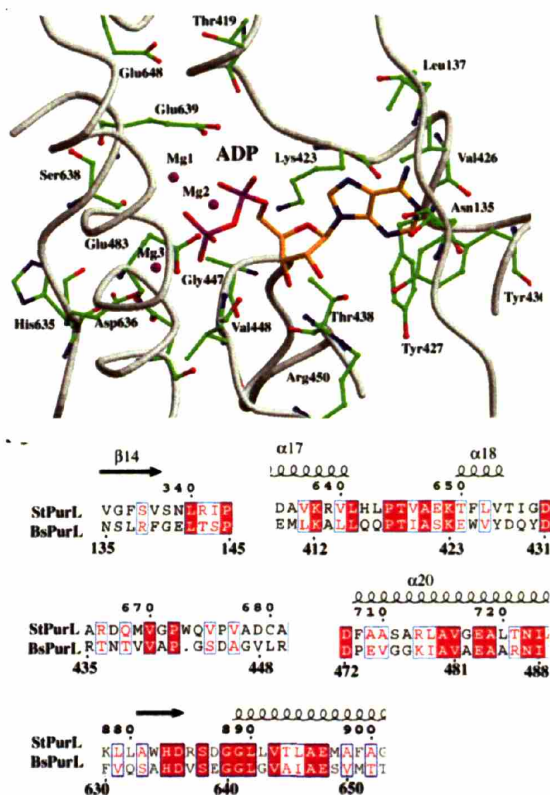
Figure 3.22—(Top) A structural model for the *B. subtilis* smPurL ADP-binding site. (Bottom) Structure-based sequence alignment of *B. subtilis* smPurL and *Salmonella* lgPurL showing conservation of residues in the auxiliary nucleotide site.

equivalents of ADP were observed in attempts to isolate an ADP•smPurL complex by gel

filtration chromatography (0.073 ADP: 1 smPurL), and this indicates that ADP may be bound

more weakly to smPurL than in lgPurL and dissociate during protein purification. ADP binding

was stimulated by the presence of PurQ, PurS, and glutamine (0.43 ADP: 1 smPurL, Table 3.7),

which further highlights the relationship between ADP and formation of the FGAR-AT complex.

The results presented in this chapter describe the first biochemical characterization of an

FGAR-AT composed of three proteins. Chapter 4 describes the structure of several PurSs and the

formation of a structural model for the B. subtilis FGAR-AT that is consistent with the

biochemistry reported in this chapter. The data suggest that the FGAR-AT complex and lgPurL

enzymes will be structurally very similar. The weak protein interactions observed within the

FGAR-AT complex and their ability to change as a function of Mg^{2+}-ADP and glutamine

binding are particularly intriguing. These results clearly demonstrate the role small molecule

metabolites can play in altering protein-protein interactions and highlights the importance of

studying protein complexes under a variety of physiological conditions. The influence of

glutamine on the complex formation is investigated further in Chapter 5. This work provides an

alternate system to PurF and PurD (Chapter 2) in the purine pathway for future investigations on

the importance of channeling of chemically reactive intermediates between weakly interacting

proteins.

3.4 References

(1)   Kappock, T. J., Ealick, S. E., and Stubbe, J. (2000) Modular evolution of the purine biosynthetic pathway. *Curr. Opin. Chem. Biol. 4*, 567-72.

(2)   Gooljarsingh, L. T., Ramcharan, J., Gilroy, S., and Benkovic, S. J. (2001) Localization of GAR transformylase in *Escherichia coli* and mammalian cells. *Proc. Natl. Acad. Sci. U. S. A. 98*, 6565-70.

(3)   Rudolph, J. and Stubbe, J. (1995) Investigation of the mechanism of phosphoribosylamine transfer from glutamine phosphoribosylpyrophosphate amidotransferase to glycinamide ribonucleotide synthetase. *Biochemistry 34*, 2241-50.

(4)   Li, C., Kappock, T. J., Stubbe, J., Weaver, T. M., and Ealick, S. E. (1999) X-ray crystal structure of aminoimidazole ribonucleotide synthetase (PurM), from the *Escherichia coli* purine biosynthetic pathway at 2.5 Å resolution. *Structure Fold Des 7*, 1155-66.

(5)   Mueller, E. J., Oh, S., Kavalerchik, E., Kappock, T. J., Meyer, E., Li, C., Ealick, S. E., and Stubbe, J. (1999) Investigation of the ATP binding site of *Escherichia coli* aminoimidazole ribonucleotide synthetase using affinity labeling and site-directed mutagenesis. *Biochemistry 38*, 9831-9.

(6)   Ebbole, D. J. and Zalkin, H. (1987) Cloning and characterization of a 12-gene cluster from *Bacillus subtilis* encoding nine enzymes for de novo purine nucleotide synthesis. *J. Biol. Chem. 262*, 8274-87.

(7)   Saxild, H. H. and Nygaard, P. (2000) The *yexA* gene product is required for phosphoribosylformylglycinamidine synthetase activity in *Bacillus subtilis. Microbiology 146 (Pt 4)*, 807-14.

(8)   Raushel, F. M., Thoden, J. B., and Holden, H. M. (2003) Enzymes with molecular tunnels. *Acc. Chem. Res. 36*, 539-48.

(9)   Marolewski, A., Smith, J. M., and Benkovic, S. J. (1994) Cloning and characterization of a new purine biosynthetic enzyme: a non-folate glycinamide ribonucleotide transformylase from *E. coli. Biochemistry 33*, 2531-7.

(10)   Thoden, J. B., Firestine, S. M., Benkovic, S. J., and Holden, H. M. (2002) PurT-encoded glycinamide ribonucleotide transformylase. Accommodation of adenosine nucleotide analogs within the active site. *J. Biol. Chem. 277*, 23898-908.

(11)   Schendel, F. J., Mueller, E., Stubbe, J., Shiau, A., and Smith, J. M. (1989) Formylglycinamide ribonucleotide synthetase from *Escherichia coli*: cloning, sequencing, overproduction, isolation, and characterization. *Biochemistry 28*, 2459-71.

(12)   Anand, R., Hoskins, A. A., Stubbe, J., and Ealick, S. E. (2004) Domain organization of *Salmonella typhimurium* formylglycinamide ribonucleotide amidotransferase revealed by X-ray crystallography. *Biochemistry 43*, 10328-42.

(13)   Lowry, O. H. R., Nira, J., Farr, A. L., Randall, R. J. (1951) Protein measurement with the Folin phenol reagent. *J. Biol. Chem. 193*, 265-75.

(14)   Schaegger, H. and Von Jagow, G. (1987) Tricine-sodium dodecyl sulfate-polyacrylamide gel electrophoresis for the separation of proteins in the range from 1 to 100 kDa. *Anal. Biochem. 166*, 368-79.

(15)   Sambrook, J., Fritsch, E.F., and Maniatis, T. (1989) *Molecular Cloning A Laboratory Manual*, Second Edition, Cold Spring Harbor Laboratory Press, Cold Spring Harbor.

(16)   Klem, T. J. and Davisson, V. J. (1993) Imidazole glycerol phosphate synthase: the glutamine amidotransferase in histidine biosynthesis. *Biochemistry 32*, 5177-86.

(17) Schendel, F. J. and Stubbe, J. (1986) Substrate specificity of formylglycinamidine synthetase. *Biochemistry 25*, 2256-64.

(18) Roux, B. and Walsh, C. T. (1992) p-aminobenzoate synthesis in *Escherichia coli*: kinetic and mechanistic characterization of the amidotransferase PabA. *Biochemistry 31*, 6904-10.

(19) Lund, P. and Magasanik, B. (1965) *N*-Formimino-L-glutamate Formiminohydrolase of *Aerobacter aerogenes. J. Biol. Chem. 240*, 4316-4319.

(20) Zalkin, H. and Smith, J. L. (1998) Enzymes utilizing glutamine as an amide donor. *Adv. Enzymol. Relat. Areas. Mol. Biol. 72*, 87-144.

(21) Li, H. C. and Buchanan, J. M. (1971) Biosynthesis of the purines. 33. Catalytic properties of the glutamine site of formylglycinamide ribonucleotide amidotransferase from chicken liver. *J. Biol. Chem. 246*, 4713-9.

(22) Mizobuchi, K. and Buchanan, J. M. (1968) Biosynthesis of the purines. XXIX. Purification and properties of formylglycinamide ribonucleotide amidotransferase from chicken liver. *J. Biol. Chem. 243*, 4842-52.

(23) Mizobuchi, K. and Buchanan, J. M. (1968) Biosynthesis of the purines. XXX. Isolation and characterization of formylglycinamide ribonucleotide amidotransferase-glutamyl complex. *J. Biol. Chem. 243*, 4853-62.

(24) Krahn, J. M., Kim, J. H., Burns, M. R., Parry, R. J., Zalkin, H., and Smith, J. L. (1997) Coupled formation of an amidotransferase interdomain ammonia channel and a phosphoribosyltransferase active site. *Biochemistry 36*, 11061-8.

(25) Thoden, J. B., Holden, H. M., Wesenberg, G., Raushel, F. M., and Rayment, I. (1997) Structure of carbamoyl phosphate synthetase: a journey of 96 Å from substrate to product. *Biochemistry 36*, 6305-16.

(26) Mullins, L. S. and Raushel, F. M. (1999) Channeling of Ammonia through the Intermolecular Tunnel Contained within Carbamoyl Phosphate Synthetase. *J. Amer. Chem. Soc. 121*, 3803-3804.

(27) Roux, B. and Walsh, C. T. (1993) p-Aminobenzoate synthesis in *Escherichia coli*: mutational analysis of three conserved amino acid residues of the amidotransferase PabA. *Biochemistry 32*, 3763-8.

(28) Huang, X., and Raushel, F. M. (1999) Deconstruction of the catalytic array within the amidotransferase subunit of carbamoyl phosphate synthetase. *Biochemistry 38*, 15909-14.

(29) Trotta, P. P., Burt, M.E., Haschemeyer, R.H., Meister, A. (1971) Reversible Dissociation of Carbamyl Phosphate Synthetase into a Regulated Synthesis Subunit and a Subunit Required for Glutamine Utilization. *Proc. Natl. Acad. Sci. U. S. A. 68*, 2599-2603.

(30) Zalkin, H. and. Hwang, L. (1971) Anthranilate Synthetase from *Serratia marcescens. J. Biol. Chem. 216*, 6899-6907.

(31) Rayl, E. A., Green, J. M., and Nichols, B. P. (1996) *Escherichia coli* aminodeoxychorismate synthase: analysis of pabB mutations affecting catalysis and subunit association. *Biochim. Biophys. Acta 1295*, 81-8.

(32) Miles, B. W. and Raushel, F. M. (2000) Synchronization of the three reaction centers within carbamoyl phosphate synthetase. *Biochemistry 39*, 5051-6.

(33) Myers, R. S., Jensen, J. R., Deras, I. L., Smith, J. L., and Davisson, V. J. (2003) Substrate-induced changes in the ammonia channel for imidazole glycerol phosphate synthase. *Biochemistry 42*, 7013-22.

(34)   Tesson, A. R., Soper, T. S., Ciustea, M., and Richards, N. G. (2003) Revisiting the steady state kinetic mechanism of glutamine-dependent asparagine synthetase from *Escherichia coli*. *Arch. Biochem. Biophys. 413*, 23-31.

(35)   Fresquet, V., Williams, L., and Raushel, F. M. (2004) Mechanism of cobyrinic acid a,c-diamide synthetase from *Salmonella typhimurium* LT2. *Biochemistry 43*, 10619-27.

(36)   Mueller, E. M. (1993), PhD thesis, Department of Chemistry, Massachusetts Institute of Technology, Cambridge.

Chapter 4:

Biophysical Studies on PurS and the FGAR-AT Complex

4.1 Introduction

In *B. subtilis*, FGAM synthesis is carried out by a complex of three proteins: PurS (84 amino acids), PurQ (227 aa), and smPurL (742 aa). The first biochemical characterization of this complex was described in Chapter 3. In those studies, PurS was determined to have no enzymatic activity or sequence homology to any known protein; however, it was necessary for glutamine-dependent FGAM synthesis. Maximal activity was achieved when the protein complex was reconstituted with a ratio of 2 PurS: 1 smPurL: 1 PurQ. The requirement for a protein in addition to the glutaminase (PurQ) and AT (smPurL) subunits makes the FGAR-AT complex unique among ATs with a triad glutaminase domain. Experiments designed to co-purify the FGAR-AT complex resulted in dissociation of the components during chromatography. Thus, PurS interacts weakly with smPurL and PurQ. An isolatable protein complex could only be obtained when Mg^{2+}-ADP and glutamine were included in the elution buffer during chromatographic analysis.

In order to facilitate elucidation of the role of PurS in FGAM synthesis, the crystal structure of the *B. subtilis* PurS was determined (*1*). The structure revealed that PurS is dimeric with 2800 $Å^2$ buried surface area and is structurally homologous to the N-terminal domain of lgPurLs (Figure 4.1). The conservation of structure between the PurS dimer and the N-terminal domain of lgPurL was surprising given that even after a structure-based sequence alignment (Figure 4.1), the proteins share little sequence homology. The structure of PurS clarifies two findings described in Chapter 3. First, the need for PurS in glutamine-dependent FGAM synthesis becomes clear. The role of PurS

194

PurS **N-terminal Domain**
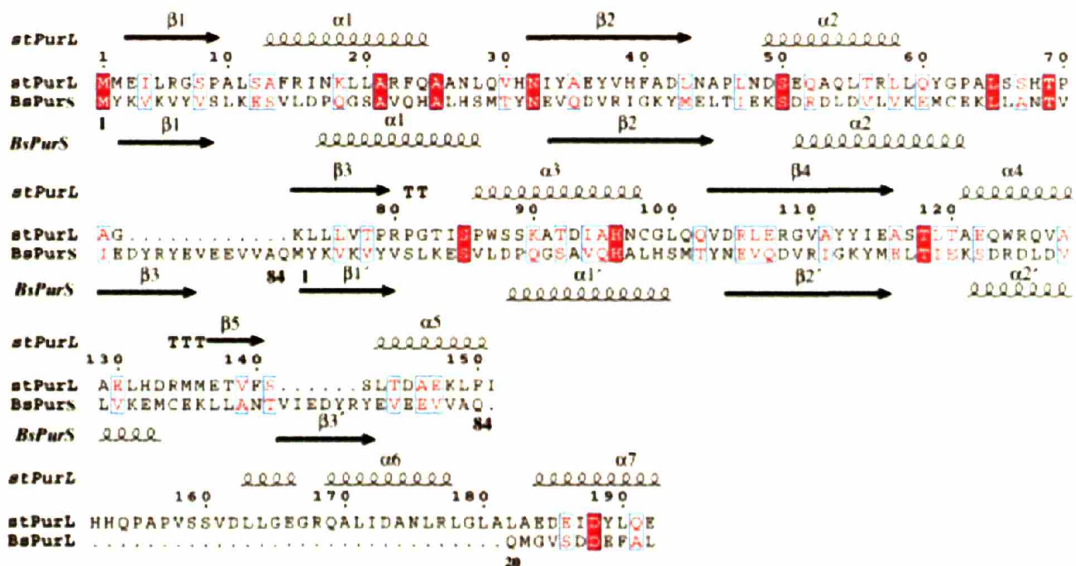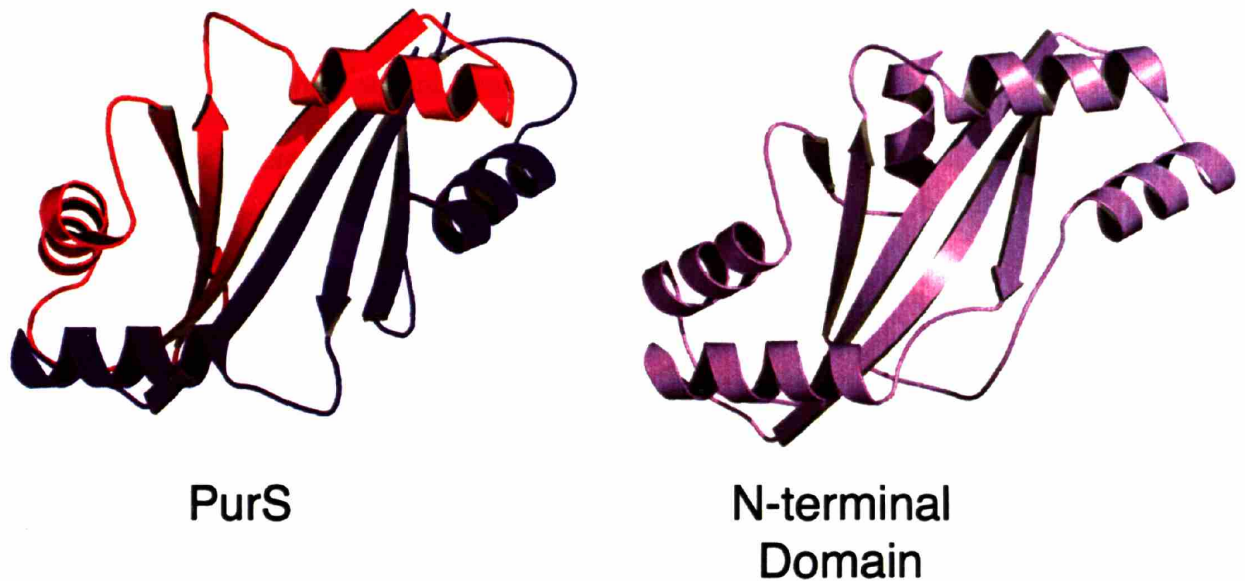
Figure 4.1—(Top) A comparison of the *B. subtilis* PurS dimer (left) and the N-terminal domain of the *Salmonella* lgPurL (right). The strong structural homology indicates that the N-terminal domain evolved from PurS after gene duplication and fusion events. (Bottom) A structure based sequence alignment of PurS and the N-terminal domain indicates very little sequence homology despite the similar structures.

195

may be similar to the proposed role of the N-terminal domain of lgPurL: linking the glutaminase and AT domains. Second, maximal FGAR-AT activity was achieved when 2 equivalents of PurS were incubated with 1 equivalent of PurQ and smPurL. The PurS dimer recapitulates the structure of the N-terminal domain of lgPurLs.

Crystal structures of PurS were determined from 2 different crystal forms: $P2_1$ and C2 at pH 7.3 and 5.6, respectively. In both crystal forms, a tetramer of PurS was observed (Figure 4.2) (1). The PurS tetramer forms by hydrogen-bonding interactions between β-strands of adjacent dimers and results in a 12-stranded β-barrel structure. While the barrels in the $P2_1$ and C2 crystal forms appear similar, the hydrogen bonding interactions at the dimer:dimer interface shift register in the different crystal forms (Figure 4.3).

Recently, the crystal structures of several PurSs from different organisms have also been determined. The structure of the *T. maritima* PurS also forms a tetramer (Figure 4.2); however, in this case the β-barrel formed by the tetramer is more asymmetric than that observed with the *B. subtilis* protein. A different tetramer structure was observed for the *M. thermoautotrophicum* PurS (Figure 4.2) (2). In this case, a histag used to purify the protein has been proposed to disrupt possible interactions between β-strands that comprise the β-barrel, resulting in its crystallization in an alternate tetrameric structure (1). Additional evidence for a *M. thermoautotrophicum* PurS tetramer has been reported by size-exclusion chromatography (2).

Based on the structures of PurS dimers and tetramers and the *Salmonella* lgPurL structure, a homology model for the *B. subtilis* FGAR-AT complex was created (Figure 4.4) (1). In the homology model, PurS plays an analogous role to the N-terminal domain

B. subtilis
P2₁

B. subtilis
C2

T. maritima

M. thermoautotrophicum
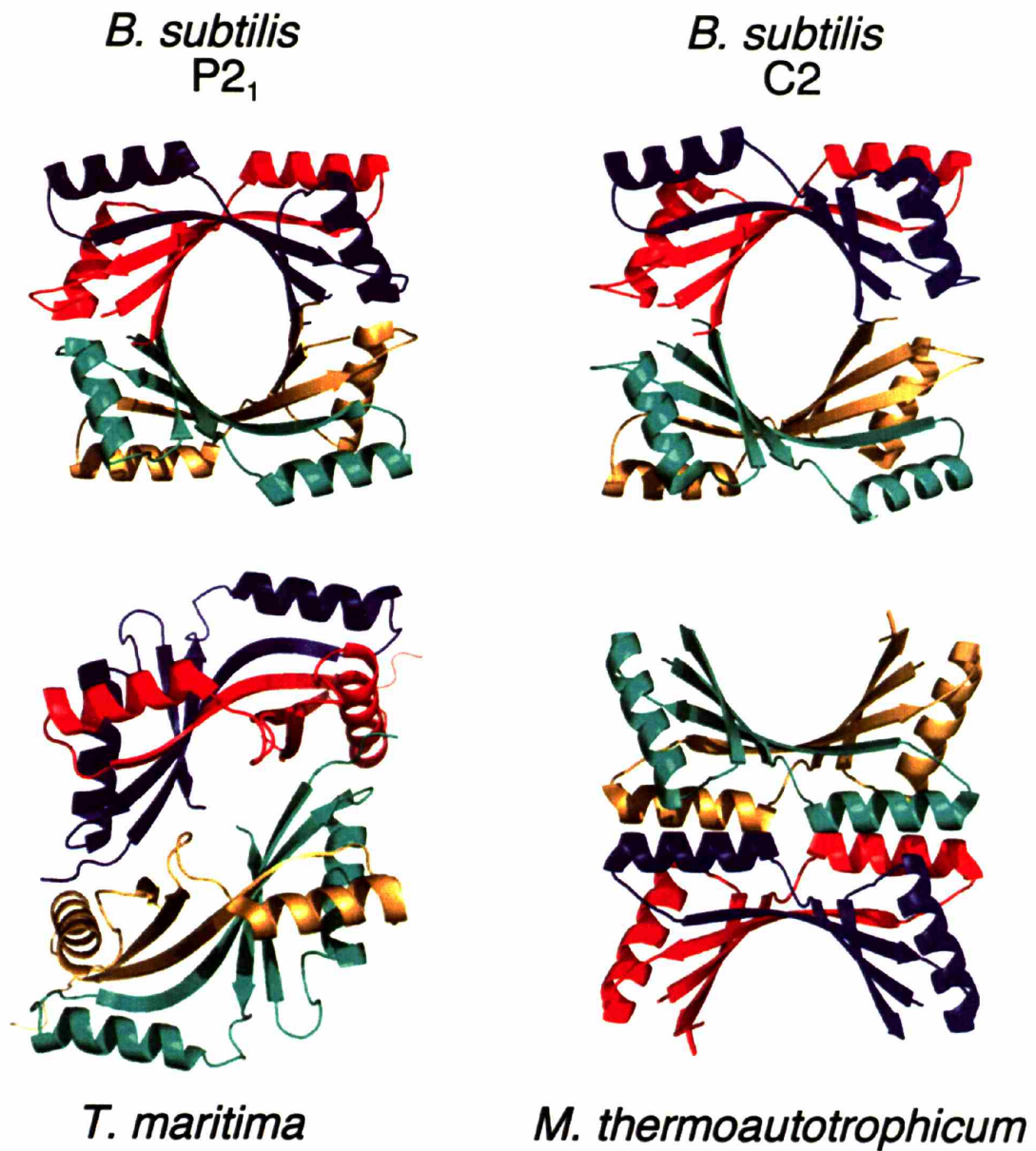
Figure 4.2—Structures of PurS tetramers observed in various organisms. Clockwise from Top Left: *B. subtilis* P2₁ crystal form (1TWJ.pdb), *B. subtilis* C2 crystal form (1T4A.pdb), *M. thermoautotrophicum* (1GTD.pdb), *T. maritima* (1VQ3.pdb).

197
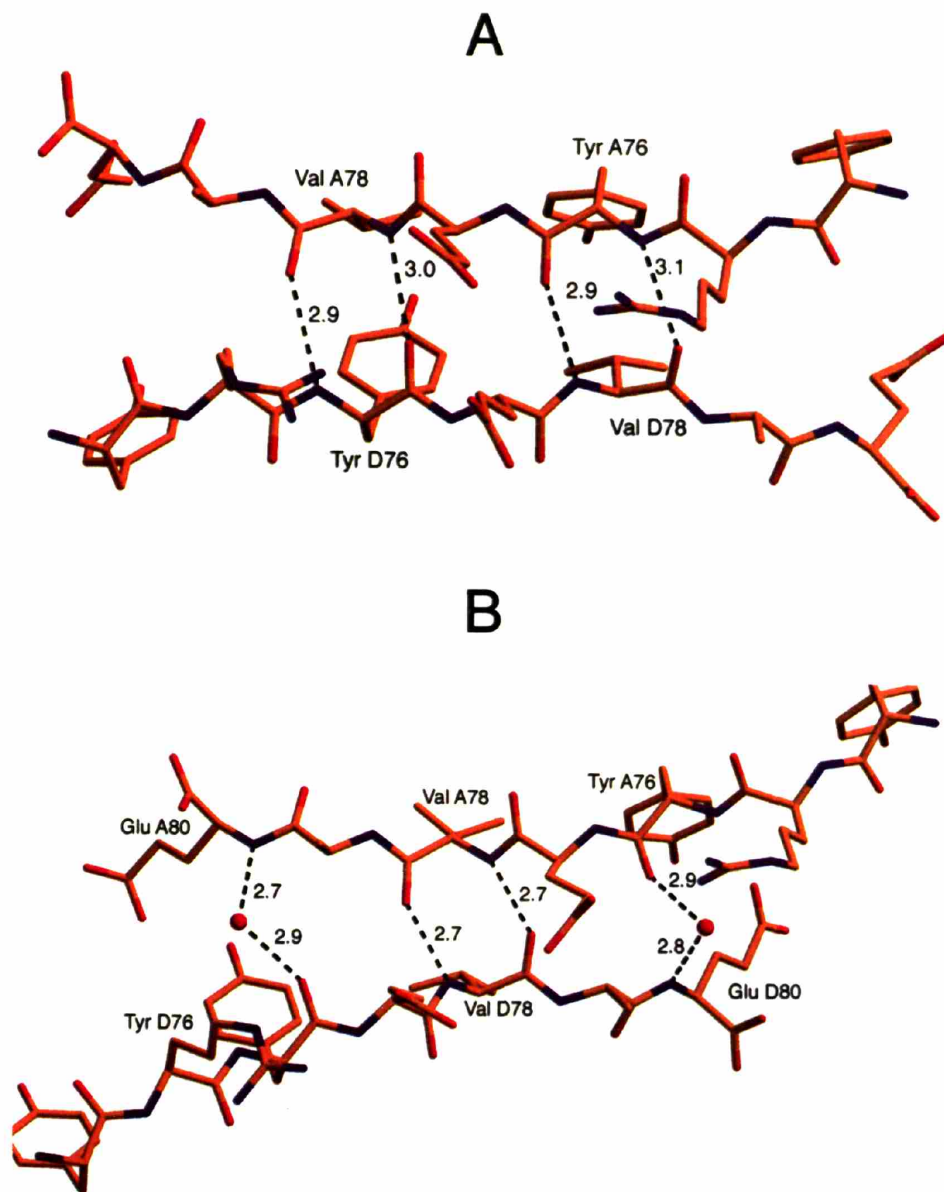
Figure 4.3—The dimer-dimer interface observed in the *B. subtilis* PurS tetramer *(1)*. (A) P2₁ crystal form. (B) C2 crystal form. Each interface is composed of just 4 hydrogen bonds. In the C2 crystal form, 2 of these bonds are mediated by water molecules.

Figure 4.4—(Top) In the homology model, a PurS dimer (green ribbon) is proposed to link PurQ (red) and smPurL (blue). (Bottom) A tetramer of PurS has also been modeled to form a 4 PurS: 2 smPurL: 2 PurQ complex. *(1)*

of lgPurL and links PurQ to smPurL. Homology models were also built using the PurS

tetramer with no unfavorable contacts (*1*). The exercise of homology building thus raised

the possibility that the FGAR-AT complex might be composed of 4 PurS: 2 smPurL: 2

PurQ. The differences in appearance of the PurS tetramers from different organisms

(Figure 4.2) and the small dimer:dimer interfaces (composed of just 4 hydrogen bonds in

the *B. subtilis* PurS) suggested that the quaternary structure of FGAR-AT is likely to be

composed of 2 PurS: 1 smPurL: 1 PurQ.

The goal of this chapter is to determine the quaternary structure in solution of

PurS itself and the FGAR-AT complex. This goal has proven to be challenging due to

PurS's unusual shape and the propensity of PurQ and smPurL to aggregate.

Consequently, multiple biophysical techniques were utilized. The quaternary structures

of PurS and the FGAR-AT complex have been investigated using size-exclusion

chromatography (SEC) and sedimentation velocity analytical ultracentrifugation (SV-

AUC). In addition, the small size of PurS facilitated amide backbone assignments by 2D

and 3D-NMR methods, which has led to a series of experiments supporting its dimeric

structure. Finally, quantitative Western blotting of PurS, PurQ, and smPurL grown under

different culture conditions suggest that the protein concentrations used in SEC and SV-

AUC experiments are similar to those observed *in vivo*. Together the data indicate that

PurS is a dimer in solution, and that the FGAR-AT complex is composed of 2 PurS: 1

smPurL: 1 PurQ.

4.2 Experimental

Materials and Methods

All proteins were isolated and quantified as described in Chapter 3. AUC

experiments were carried out in the Biophysical Instrumentation Facility for the Study of

Complex Macromolecular Systems (Department of Chemistry, MIT). NMR experiments

were carried out by Jens Wönhert at the Insitüt fur Organische Chemie, Johann Wolfgang

Goethe-Universität (Frankfurt, Germany).

Size-Exclusion Chromatography

SEC was performed using either a HiPrep 26/60 Sephacryl S-200 HR column (for

PurS and A128T PurQ, Amersham Biosciences) or a S-300 HR column (for smPurL and

the FGAR-AT complex, Amersham Biosciences) on a BioLogic LP system (Bio-Rad) at

4°C. The columns were equilibrated in either SEC buffer (50 mM KP_i, 75 mM NaCl pH

7.25) or SEC buffer with 0.1 mM ADP, 5 mM $MgCl_2$, and 25 mM L-glutamine.

Samples (500 μL) were loaded at 100 μM of each protein: PurS, smPurL, or A128T PurQ

or 100 μM of the 2PurS: 1smPurL: 1 A128T PurQ complex. Proteins were eluted at a

flow rate of 0.5 mL/min and 3 mL fractions were collected. Fractions were monitored at

280 nm and elution of the complex was monitored by the glutamine-dependent Bratton-

Marshall assay as described in Chapter 3. A standard curve was generated using

thyroglobulin (670 kD), bovine γ-globulin (158 kD), chicken ovalbumin (44 kD), equine

myoglobin (17 kD), and vitamin B_{12} (1.4 kD) (Bio-Rad), *E. coli* PurL (141 kDa), and *E.*

coli his-PurM (a 76 kDa dimer) and linear-regression analysis of the data with

KaleidaGraph software (Synergy). Standard deviations of observed elution times were

calculated from triplicate experiments using the elution standards.

Sedimentation Velocity Analytical Ultracentrifugation

SV-AUC experiments were performed with an An50Ti 8-hole rotor using an

Optima XL-1 analytical ultracentrifuge (Beckman Coulter, Fullerton, CA). Samples (400

μL) were placed in double-sector Epon centerpieces with either quartz or sapphire

windows depending on whether absorbance or interference optics were used to monitor

the sedimentation.

During the centrifugation, data was collected from each cell at ~ 4-5 min

intervals, and ~100 data sets equally-distributed during the length of the run were

included in the analysis. In all cases, SEDNTERP software from Dr. John Philo was used

to calculate buffer density, viscosity, and protein partial-specific volume from the amino

acid content (*3*). Data was analyzed by SEDFIT88 using a continuous sedimentation

coefficient distribution model derived from solutions to the Lamm equation (Equation

4.1) (*4*) wherein c is the concentration of the molecule of interest, t is time, r is the radial

position from the axis of rotaion, D is the diffusion coefficient of the molecule of interest,

s is the sedimentation coefficient, and ω is the angular velocity obtained by the sample

during centrifugation. This equation describes the concentration distribution of species

with respect to their sedimentation and diffusion coefficients in a centrifugal field. The

implementation of the Lamm equation by SEDFIT88 has been described (*5*). The

distribution of species obtained by SEDFIT was then integrated using Kaleidagraph

software (Synergy).

$$\frac{dc}{dt} = \frac{1}{r}\frac{d}{dr}\left[rD\frac{dc}{dr} - s\omega^2 r^2 c\right] \qquad (4.1)$$

PurS: PurS was dialyzed for 20 h at 4°C in a Slide-A-Lyzer cassette (Pierce) with

a 7 kDa molecular weight cutoff (MWCO) membrane against either PBS (pH 7.1) or 50

202

mM HEPES (pH 7.1), 20 mM MgCl$_2$, 80 mM KCl. In the former case, sedimentation of

PurS (100, 500, or 1000 μM monomer) was monitored by interference optics while

centrifuging at 50,000 rpm for 20 h at both 10 and 25°C. In the later case, sedimentation

of PurS (66 or 132 μM monomer) was monitored by absorbance optics with

centrifugation carried out at 50,000 rpm for 20 h at either 10 or 25°C.

A128T PurQ: Samples (57 μM) were dialyzed for 20 h at 4°C in a Slide-A-Lyzer

cassette (Pierce) with a 10 kDa MWCO membrane against PBS (pH 7.1). Sedimentation

was monitored by absorbance optics with centrifugation carried out at 45,000 rpm for 20

h at 10°C.

his-PurM, lgPurL, and smPurL: Samples of *E. coli* histag-PurM (25 μM), *E. coli*

lgPurL (7 μM), and smPurL (40 μM) were dialyzed for 20 h at 4°C in a Slide-A-Lyzer

cassettes (Pierce) with a 10 kDa MWCO membrane against PBS (pH 7.1).

Sedimentation was monitored by absorbance optics with centrifugation carried out at

40,000 rpm for 20 h at 10°C.

FGAR-AT Complex: A 2 PurS: 1 smPurL: 1 A128T PurQ complex (16 μM) was

dialyzed for 6 h at 4°C in a Slide-A-Lyzer cassette (Pierce) with a 7 kDa MWCO

membrane against 25 mM HEPES pH 7.2, 20 mM KCl, 20 mM MgCl$_2$, 0.1 mM ADP,

and 20 mM glutamine. Sedimentation was monitored by interference optics with

centrifugation carried out at 40,000 rpm for 24 h at 10°C.

^{15}N and ^{15}N/^{13}C Labeling of PurS for NMR Analysis

Expression of PurS was carried out as described in Chapter 3 except that a 50 mL

starter culture was used to inoculate 500 mL of minimal media, which contained [^{15}N]-

NH$_4$Cl (MARTEK BIO) and [U-^{13}C]-glucose (Cambridge Isotope Laboratories) as the

sole nitrogen and carbon sources. The media (493 mL) contained 42 mM Na_2HPO_4, 22 mM KH_2PO_4, 8.5 mM NaCl, and 0.5% (w/v) NH_4Cl (pH 7.4) and was autoclaved. To this solution, $CaCl_2$ (0.5 mL of a 100 mM solution, autoclaved), $MgSO_4$ (4 mL of a 1 M solution, autoclaved), glucose (0.5 mL of a 25% (w/v) solution, filter sterilized), and thiamine (0.5 mL of a 5 mg/mL solution, filter sterilized) were added. Metals (0.5 mL) were then added from a 1000x stock solution containing 2.5 g/L $CoCl_2 \cdot 6H_2O$, 1.5 g/L $MnCl_2 \cdot 4H_2O$, 2.25 g/L $CuSO_4 \cdot 5H_2O$, 3 g/L boric acid, 1.4 g/L MoO_3, 8.1 g/L $ZnCl_2$, and 62 mg/L $FeCl_3$. The isotopically-labeled PurS was isolated as described in Chapter 3 to give ~15 mg protein/g cells with >95% purity.

General NMR Methods

All NMR-experiments were carried out on Bruker DRX 600 MHz, AV 700, or AV 800 MHz spectrometers equipped with z-axis gradients and normal temperature or cryogenic triple-channel (^1H, ^{13}C, ^{15}N)-HCN probes. All spectra were processed and analyzed using the Bruker NMRSUITE (XWINNMR 3.5) and XEASY (6). All NMR-experiments were recorded in 90% H_2O/10% D_2O at 298 K. ^1H,^{15}N-HSQC-spectra were recorded using standard pulse sequences with d1=1.0-1.5s, 2-32 scans/increment, 1024 complex points and a spectral width of 16 ppm in the f2-dimension and 32-96 complex points and a spectral width of 22-24 ppm in the f1-dimension.

Assignment of PurS Backbone Resonances

Backbone assignments (H_N, N, $C\alpha$, $C\beta$, CO and $H\alpha$ chemical shifts) for PurS were obtained from analyzing a set of three-dimensional NMR-experiments carried out with a ^{13}C,^{15}N-labelled sample of 1.5 mM PurS in 20 mM KP_i (pH 6.2), 20 mM KCl, and 2 mM β-mercaptoethanol (NMR-buffer). The low pH of the buffer was used to increase

the intensity of the signal of the proton associated with the amide by decreasing the rate

of exchange with solvent. β-mercaptoethanol was used to prevent disulfide bond

formation during the days required for data acquisition.

Sequential assignments were obtained from analyzing 3D-HNCA (7) and 3D-

HNCACB (8) experiments. In the 3D-HNCA experiment each amide signal is correlated

with the Cα-chemical shifts of its own (HN$_{(i)}$ → Cα$_{(i)}$) and of the preceding amino acid

(HN$_{(i)}$ → Cα$_{(i-1)}$) (Figure 4.5). Amide signals that belong to sequential neighbors in the

protein sequence can therefore be identified by one shared Cα-chemical shift. However,

the Cα-chemical shift alone is often not sufficient to unambiguously link two amino

acids, since not all Cα-atoms in the protein have a unique Cα-chemical shift. The

resulting ambiguities can be resolved by the 3D-HNCACB-experiment. In this

experiment, each amide signal is correlated with the Cα- and the Cβ-chemical shifts of its

own (HN$_{(i)}$ → Cα$_{(i)}$/ Cβ$_{(i)}$) and of the preceding amino acid (HN$_{(i)}$ → Cα$_{(i-1)}$/ Cβ$_{(i-1)}$)

(Figure 4.5). Amide signals that belong to sequential neighbors in the protein sequence

can therefore be identified by one shared Cα-chemical shift and one shared Cβ-chemical

shift. HN$_{(i)}$ → Cα$_{(i)}$/ Cβ$_{(i)}$-correlations can be distinguished from HN$_{(i)}$ → Cα$_{(i-1)}$/Cβ$_{(i-1)}$

correlations in the HNCA- and HNCACB-experiments by comparing these with a 3D-

CBCA(CO)NH-experiment (9) (Figure 4.5). In the latter experiment only the HN$_{(i)}$ →

Cα$_{(i-1)}$/Cβ$_{(i-1)}$ correlations are observable.

For all 3D-triple resonance experiments 1024 complex points with a spectral

width of 16 ppm were used in the f3 (^{1}H-detected)-dimension. The ^{1}H-carrier frequency

was set at the water signal. A spectral width of 22 ppm was used in the ^{15}N-dimension

(f2) in all 3D-experiments with the ^{15}N-carrier frequency set to 119 ppm.
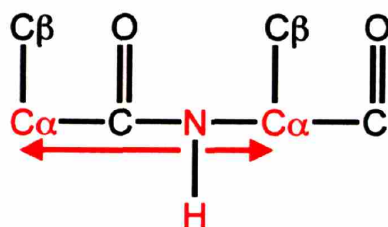
HNCA
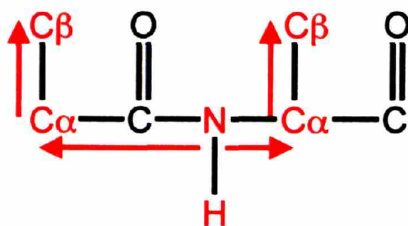
HNCACB
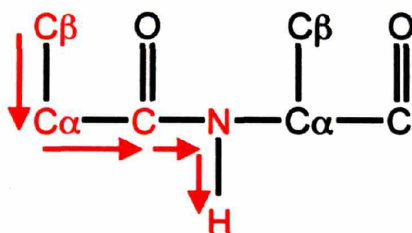
CBCA(CO)NH

Figure 4.5—Schematic representation of the NMR experiments used to assign PurS amide proton resonances. (Top) In the HNCA experiment, magnetization is transferred from the amide proton to the Cα carbons on either side of the amide, which allows assignment of each amide proton to two specific Cα carbons. (Middle) In the HNCACB experiment, magnetization is transferred from the amide protons to the Cβ carbons. This method provides some information about the protein side-chains that appear on either side of the amide (for example, if a peak appears in the HNCA spectra but not in the HNCACB spectra, then the amide must be next to a glycine, which lacks a Cβ). (Bottom) In the CBCA(CO)NH experiment, magnetization is transferred from the Cβ carbon to the amide of the next residue. This experiment gives information about the amino acid that immediately precedes the amide in the protein sequence.

The 3D-HNCA-experiment (7) was carried out over 1.5 days on a Bruker DRX 600 MHz spectrometer with 8 scans/increment, d1 = 1 s, 80 x 32 complex points in f1 and f2 and a spectral width of 32 ppm in the f1-dimension. The ^{13}C-carrier frequency was set to 54 ppm in the middle of the Cα-chemical shift region.

The 3D-HNCACB experiment (8) was recorded over 2.5 days on a Bruker AV 800 MHz spectrometer with a cryogenic probe using 16 scans/increment, d1 = 1.2s, 80 x 32 complex points in f1 and f2, and a spectral width of 65 ppm in the f1 (^{13}C)-dimension. The ^{13}C-carrier frequency was set to 40 ppm in the middle of the Cα/Cβ-chemical shift region.

A 3D-CBCA(CO)NH-experiment (9) was collected at 600 MHz over 2 days with 16 scans/increment, d1 = 1.1s, 64 x 32 points in f1 and f2 and a spectral width of 65 ppm in the f1-dimension. The ^{13}C-carrier frequency was set to 40 ppm.

CO-chemical shifts were obtained from a 3D-HNCO-experiment (7) collected at 600 MHz over 11 h with 4 scans/increment, d1=1.0s, 64x32 points in f1 and f2, spectral width =14 ppm in f1, and the ^{13}C-carrier frequency at 176 ppm.

Hα-chemical shifts were extracted from a 3D-HBHA(CO)NH-experiment (10) at 600 MHz with a cryogenic probe over 1.5 days with 8 scans/increment, d1 = 1.2s, 90 x 34 points in f1 and f2, spectral width = 8 ppm in f1, and the ^{13}C-carrier frequency at 36 ppm.

Identification of Secondary Structural Elements in PurS

In order to identify secondary structure elements of PurS in solution and compare them to the crystal structure (1), the deviations from random coil chemical shifts were calculated for Cα, Hα, N, and CO atoms and plotted against the residue number (11).

A 3D-^{15}N-edited NOESY-HSQC spectrum with a mixing time of 100 ms was recorded on Bruker AV 800 MHz spectrometer over 4 days on a 2 mM [^{15}N]-PurS sample in NMR-buffer to confirm the presence of inter-strand NOEs in the 3-strand β-sheet of PurS (8 scans/increment, d1=2s, 110 x 48 complex points in f1 and f2, spectral width=12 ppm in f1).

H/D Exchange Experiments to Monitor Solvent-Accessibility of Residues Proposed to be Involved in Tetramer Formation

A 0.5 mM ^{15}N-PurS sample in NMR-buffer was lyophilized and then reconstituted in D_2O. A series of [^{1}H,^{15}N]-HSQC-spectra were recorded to identify slowly exchanging amide groups. The first spectrum was recorded 1 min after dissolving the sample in D_2O with 2 scans/increment and only 64 complex points in the f1-dimension with d1=1s (experimental time = 4 min) on a Bruker 600 MHz spectrometer equipped with a cryogenic probe. Further spectra were recorded 30, 90 and 270 min after dissolving the sample in D_2O using standard conditions (8 scans/increment, 1024 complex points and 16 ppm spectral width in f2, 96 complex points in f1, 22 ppm spectral width in f1, ^{15}N-carrier frequency at 119 ppm, d1=1.5 s).

DOSY Spectroscopy to Measure the Rate of PurS Diffusion and the Hydrodynamic Radius of PurS

DOSY (diffusion ordered spectroscopy) experiments using the pulse sequence of Jones *et al.* (*12*) were carried out with 0.5 mM or 0.2 mM ^{15}N-labelled PurS-samples in D_2O with a 20-fold excess of dioxane (R_H = 0.212 nm) as an internal standard in 20 mM KP_i, 20 mM KCl, and 2 mM β-mercaptoethanol pH 6.2. Experiments were collected at 10 gradient strengths with 128 scans/experiment. Signal intensity was then plotted versus

the gradient strength for both the dioxane standard and PurS NMR signals, which allow

comparison of the diffusion properties for dioxane versus PurS. HYDROPRO software

(13) was used to predict the radius of hydration for the monomeric, dimeric, and

tetrameric species of PurS and compared to results obtained from the DOSY experiment.

Measurement of Longitudinal and Transverse Relaxation Rates for PurS Amide Protons

and Comparison to Predicted Values for the Monomeric, Dimeric, and Tetrameric Forms

of PurS

Longitudinal (T1) and transverse (T2) relaxation rates were measured using pulse

sequences as described by Wagner and coworkers (14) with a $[^{15}N]$-PurS sample (1.5

mM) in 20 mM KP_i (pH 6.2), 20 mM KCl, and 2 mM β-mercaptoethanol. Experiments

were performed with 8 scans/increment, d1= 4s and 96 increments in f1. For the T1-

measurements, seven different inversion recovery delays were used (10 ms, 50 ms, 100

ms, 250 ms, 500 ms, 750 ms, 1s). Experiments with delays of 100, 250, and 750 ms were

performed in duplicate. For T2-measurements, delays of 18 ms, 36 ms, 72 ms, 108 ms,

144 ms, 198 ms and 252 ms were used. Experiments with 36 ms, 108 ms and 198 ms

delays were performed in duplicate. Heteronuclear $^{15}N\{^1H\}$-NOE measurements were

made according to the pulse sequence of Kay *et al.* (15) with 16 scans/increment, d1=3s,

and 128 complex points in f1. During the NOE experiments, alternating proton-

presaturated and non-presaturated spectra were recorded. Peak intensities were analyzed

using the program Felix2000 (MSI). R1 and R2 relaxation rates were fitted from peak

heights to mono exponential two-parameter functions using macros provided by Palmer

and co-workers (16).

HYDRONMR (*17*) was used to predict the R1 and R2 values for the monomeric, dimeric and tetrameric forms of PurS based upon the crystal structure (*1*), and these predictions were compared to the experimental values.

Western Blotting to Determine Concentrations of FGAR-AT Proteins in vivo

B. subtilis strain AG174 (*pheA2 trpC2*, Grossman Laboratory, MIT) was grown in LB by inoculation of a culture (100 mL) with a single colony from a LB/agar plate. The cells were then grown at 37°C with shaking at 200 rpm with a doubling time of ~40 min. Cells were collected by centrifugation at OD_{600} = 0.7 during log phase and frozen at -80°C. The number of cells per OD was determined by dilution of the cells, 10^5 to 10^7-fold, into chilled LB media followed by plating of the resulting solutions onto LB/agar plates. For each dilution, 3 different volumes were plated with 2 replicates per volume. The cells/OD value was determined by counting colonies formed on each plate and averaging the results of 3 separate experiments (>40 different plates).

Cells were also grown under defined nutrient conditions in S750 minimal media (*18, 19*) according to procedures from the Grossman Laboratory. The medium (1 L) was composed of 100 mL 10x S750 salts (104.7 g/L MOPS, 13.2 g/L $(NH_4)_2SO_4$, 6.8 g/L KH_2PO_4, pH 7.0), 10 mL 100x trace metals (0.2 M $MgCl_2$, 70 mM $CaCl_2$, 5 mM $MnCl_2$, 0.1 mM $ZnCl_2$, 2 mM HCl, and 0.5 mM $FeCl_3$), 0.1% (w/v) glutamate, 40 μg/mL tryptophan, 40 μg/mL phenylalanine, 1% (w/v) glucose, and 1 μg/mL thiamin. A purine-rich medium was prepared by addition of 1 mM adenine and 1 mM guanosine to the minimal medium. All media components were filter sterilized rather than autoclaved. Cells were inoculated into 100 mL of minimal media using 2 mL of a saturated culture grown overnight in LB. Prior to inoculation, the cells were washed with 2 x 5 mL of

210

minimal medium. The cells (doubling time ~ 2 h) were grown and collected as described with LB medium.

To prepare cell lysate solutions for the Western blots, cells from a 100 mL growth (~0.4 g) were resuspended in 5 mL of 50 mM Tris pH 7.8 and 1% (w/v) SDS. The solution was then placed into a boiling water bath and stirred for 20 min to lyse the cells followed by brief sonication (30 s) at room temperature to shear cellular DNA (3/32" microprobe, VirTis). Protein concentration was determined using a Lowry assay with a BSA standard. Samples were prepared for electrophoresis by mixing the cell lysate 1:1 with either 2x Laemelli buffer (smPurL) or 2x tricine gel loading buffer (PurS and PurQ). Samples from the *B. subtilis* cell lysate were typically loaded at 1-10 μg lysate/well.

Standards were made by serial dilution of purified PurS, A128T PurQ, or smPurL into solutions containing 0.1 mg/mL *E. coli* K12 cell lysate supernatent in 0.1 M Tris pH 8.0 to prevent non-specific protein binding and to mimic transfer conditions of the proteins in the *B. subtilis* cell lysate. These solutions were then mixed 1:1 with 2x Laemelli buffer (smPurL) or 2x tricine gel loading buffer (PurS and A128T PurQ). In order to quantitate protein concentrations *in vivo*, 5-6 standards were run on each gel along with 3-4 unknown samples from the cell lysate. Typically, 0.5-6 ng for smPurL and PurQ and 0.1-0.8 ng for PurS were used to generate the standard curve.

Electrophoresis of PurS and PurQ was performed using 10-well 10% tricine SDS-PAGE gels (Gradipore), and electrophoresis of smPurL was performed using 10-well 10% tris-glycine SDS-PAGE gels (Gradipore). Blotting was performed at 20°C using an Invitrogen blotting apparatus for 2.5 h at 34 V onto PVDF membranes (Bio-Rad Immunoblot) in 192 mM gly, 25 mM Tris, 10% methanol (pH 8.8). After blotting,

membranes were typically blocked overnight at 4°C in 10% drymilk (w/v, Carnation) in PBS with 0.1% Tween 20. Complete transfer of the proteins from the gel was confirmed by staining with Coomassie dye, and two membranes were placed back-to-back to confirm that the proteins had not overtransferred during these conditions.

Antibodies (Abs) for PurS, A128T PurQ, and smPurL were produced by Covance in NWZ female rabbits. Due to its small size, PurS was derivitized with keyhole limpet hemocyanin (KLH) by Covance to improve its antigenicity. Abs used in these studies were all from the terminal bleed and were not purified before use. Blots were exposed to the 1°Ab for PurQ or PurS using a 1:10,000 dilution into blocking buffer or for smPurL using a 1:5,000 dilution. Blots were incubated for 1 h at 20°C followed by washing with PBS (4 x 20 min). Blots were exposed to the 2° Ab (1:3,000 dilution, Goat Anti-Rabbit IgG HRP conjugate, Pierce) for 1 h followed by washing with PBS as before. PurS blots were developed using Pierce FemtoMax substrate, while PurQ and smPurL blots were developed using Pierce Supersignal WestDura substrate. Each blot was then imaged and band density determined using a Bio-Rad ChemiDoc system. To determine the amount of protein in *B. subtilis* crude cell lysate, standard curves were generated based upon the observed band densities for the standards and fit by linear regression analysis. The concentration of each unknown sample from the same gel was determined for samples falling within the linear range of the standards. Six different samples from 2-3 different Western blots were averaged to determine the protein mass in the unknown samples (pg protein/μg cell lysate) and standard deviation. The number of molecules of each protein per cell (molecules/cell) was then calculated from the Western results by determining the number of cells per μg of cell lysate. Error in the calculation of the molecules/cell was

determined by propagating the relative (or percent) errors of the protein mass and cell

counting according to Equation 4.2.

$$\%error_{molecules/cell} = \sqrt{\%error_{mass}^{2} + \%error_{count}^{2}} \qquad (4.2)$$

4.3 Results

SEC Indicates a 2:1:1 FGAR-AT Complex is Present and that PurS and smPurL have

Unusual Migratory Properties

SEC is a common method used to determine protein quaternary structures. In this

method, the elution volume of a protein is monitored as it passes through a column whose

matrix contains channels into which a protein can diffuse. Smaller proteins can sample

more of the channel volume, leading to an increase in retention time and a later elution

volume. There are several limitations to this method. First, the elution volume of the

protein is dependent on the Stokes or hydrodynamic radius of the protein (R_S), rather than

directly upon the molecular weight. This leads to the common observation with many

proteins of aberrant SEC properties due to unusual molecular shapes *(20)*. Second, the

SEC column must be calibrated with MW standards, and the ability to accurately predict

molecular weight is dependent on how well these standards mimic the hydrodynamic

properties of the unknown protein. Finally, unlike the analytical SEC columns used in

Chapter 3, proteins elute from traditional, high-resolution SEC columns over the course

of hours.

Results from the SEC experiments are shown in Figure 4.6 and listed in Table 4.1.

In these experiments, MW standards from Bio-Rad were used; however, lgPurL and

PurM were also used to calibrate the column as these proteins may mimic the elution
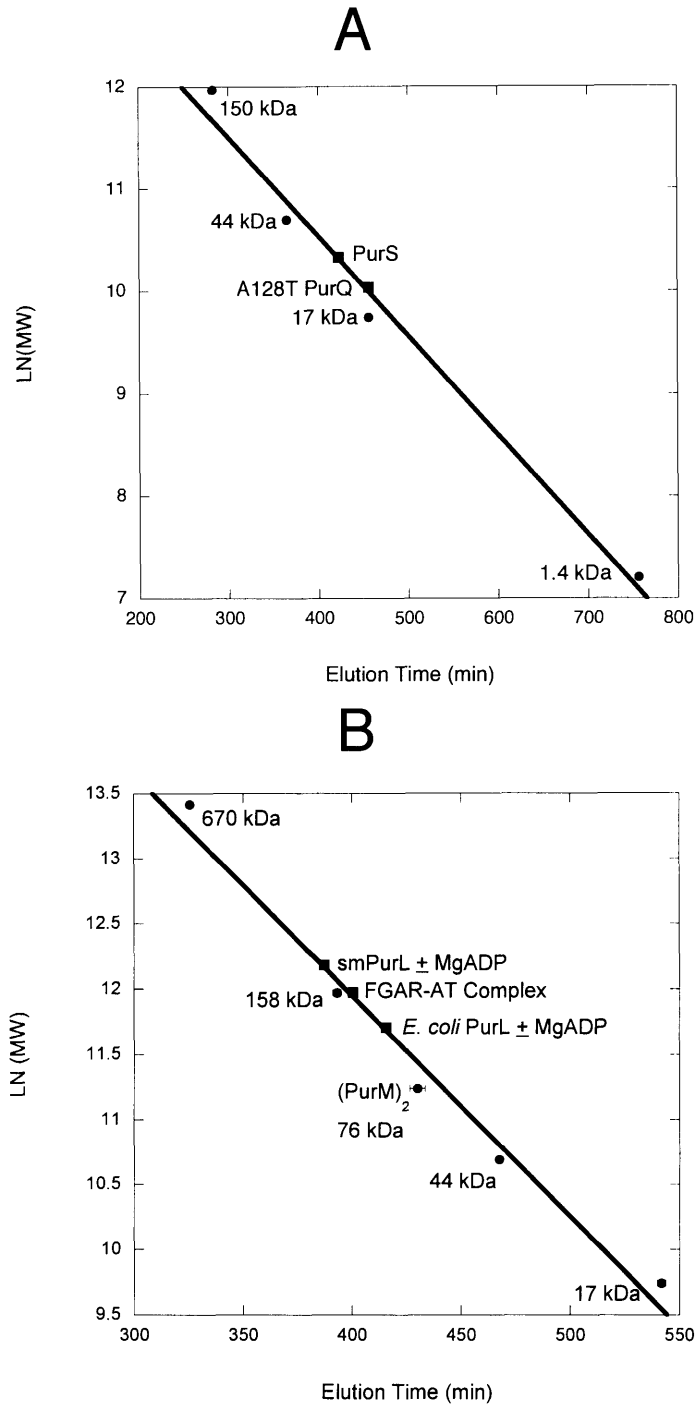
Figure 4-6—SEC results for the *B. subtils* FGAR-AT. (A) Elution of PurS and PurQ from a S200 column. PurS eluted as a 30 kDa species, and PurQ eluted as a 23 kDa species. (B) Elution of smPurL and the FGAR-AT complex from a S300 column. smPurL eluted as a 190 kDa species independent of the presence of MgADP. The FGAR-AT complex eluted as a 153 kDa species in the presence of MgADP and glutamine.

properties of the FGAR-AT complex and smPurL, respectively. Calibration of the

column with a PurS-like standard is not possible since PurS has a unique shape and no

other characterized proteins could be found with a similar fold in the Structural

Classification of Proteins (SCOP) Database (http://scop.mrc-lmb.cam.ac.uk/scop/).

Table 4.1: Determination of MW by SEC				
Sample	[Monomer] (μM)	Predicted MW (kDa)	Calculated MW (kDa)	Observed Quaternary Structure
His-PurM	100	38	76	Dimer
lgPurL	100	141	119	Monomer
PurS	100	10	30	Trimer
A128T PurQ	100	25	23	Monomer
SmPurL[a]	100	80	190	?
FGAR-AT Complex 2S: 1L: 1Q[b]	100	124	153	2S:1L:1Q

[a]Experiments carried out in the presence and absence of ADP in the elution buffer. [b]Experiments carried out in the presence of ADP and glutamine in the elution buffer.

SEC experiments on A128T PurQ revealed a monomeric species. Experiments on

smPurL and PurS were more problematic. smPurL migrated as a 190 kDa species and

not as the predicted 80 kDa monomer either in the presence of absence of Mg^{2+}-ADP in

the elution buffer. PurS, on the other hand, migrated as a 30 kDa trimer in contrast to

either the dimer or tetramer predicted by the crystal structures. Similar results for both

PurS and smPurL were obtained when the proteins were studied by analytical SEC

(Chapter 3). These results suggest that both PurS and smPurL have unusual migratory

properties.

Given these results, the method of Siegel and Monte (20) was used to correct the

SEC data for the unusual migratory properties of PurS and smPurL. This method utilizes

215

sedimentation coefficients obtained by analytical ultracentrifugation studies to determine

the MWs of proteins based upon SEC behavior according to Equation 4.3, in which S is

the sedimentation coefficient, N is Avogadro's number, η is the solvent viscosity, R_s is

the Stokes radius obtained by SEC, $\bar{v}$ is the protein partial specific volume, and ρ is the

solvent density. By combining R_s values from SEC with the sedimentation coefficient

obtained by AUC, factors related to molecular shape or unusual migratory properties

become minimized, and accurate MWs ($\sim$10% error) can be determined (20).

$$MW = \frac{SN(6\pi\eta R_s)}{(1 - \bar{v}\rho)} \qquad (4.3)$$

The standard curves used in the SEC experiments were regenerated using values

for the Stokes radius (R_S) for each of the standards vs. elution time (Figure 4.7) (20, 21).

The elution times of smPurL and PurS gave rise to R_S values of 2.60 and 3.97 nm,

respectively. The SV-AUC experiments described subsequently allowed the

sedimentation coefficients for both PurS and smPurL to be determined (2.08 and 5.50 S,

respectively). After solving Equation 4.3 using the experimental values for S and R_s, a

MW of 22.7 kDa was obtained for PurS, indicative of a dimeric species. For smPurL, a

corrected MW of 91.8 kDa was obtained, indicative of a monomeric protein.

SEC on the FGAR-AT complex was carried out in the presence of MgADP and

glutamine in the elution buffer, which has been shown previously to maximize protein

association (Chapter 3). These experiments revealed a 153 kDa species (predicted 124

kDa), closer to a 2:1:1 complex than the 4:2:2 complex (Table 4.1). However, the

elution time of the FGAR-AT complex differed from that observed with the lgPurL,

which migrated as a 119 kDa species (Table 4.1). This was unexpected since these

proteins are predicted to have similar shapes. Based upon this observation and the

216
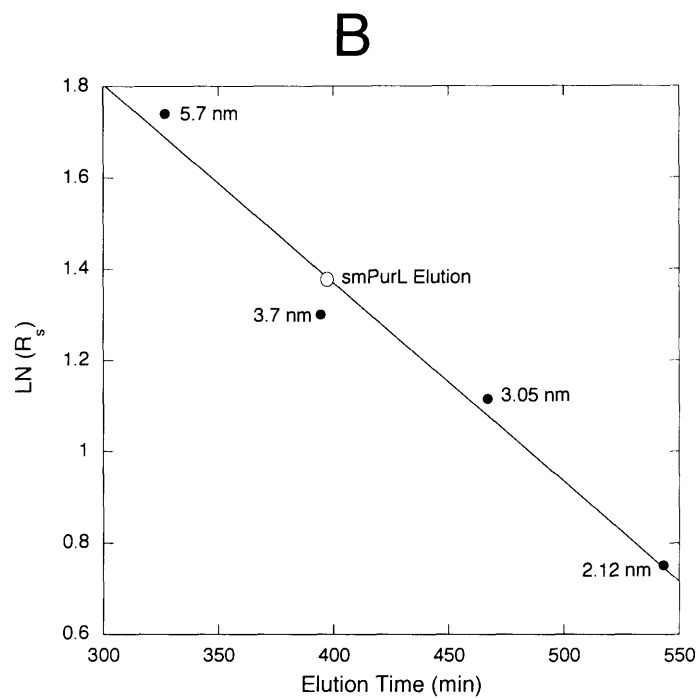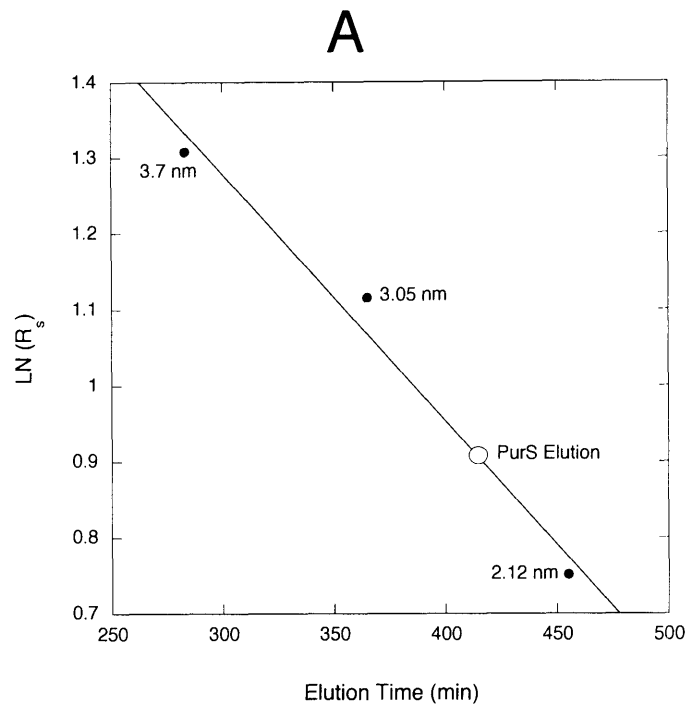
Figure 4-7—SEC results for the *B. subtils* FGAR-AT reploted to derive the Stokes radius (R_S) using literature values of R_S for the standards (A) S200 elution of PurS. (B) S300 elution of smPurL.

217

unusual migratory properties of PurS and smPurL, additional methods were sought to provide evidence for a PurS dimer and a 2:1:1 complex.

SV-AUC Experiments: Evidence for a 2:1:1 FGAR-AT Complex and a PurS Dimer

AUC is a very accurate method to determine the MW of a species in solution since the sedimentation of a particle in solution is directly dependent on the MW and three physical forces: the buoyant force, the frictional force, and the gravitational force. The relationship of these forces to the molecular weight is described by the Svedberg equation (Equation 4.4). In this equation, s is the sedimentation coefficient, which corresponds to the velocity of the particle per unit of gravitational acceleration and is proportional to the MW. $\bar{v}$ is the protein partial specific volume, ρ is the solvent density, N is Avogadro's number, and f is the frictional coefficient. The molecular shape is incorporated into the Svedberg equation by f, which is related to the protein radius (R) and the solvent viscosity (η) (Equation 4.5).

$$s \equiv \frac{MW(1-\bar{v}\rho)}{Nf} \qquad (4.4)$$

$$f = 6\pi\eta R \qquad (4.5)$$

Both sedimentation equilibrium (SE) and sedimentation velocity (SV) experiments are used to determine MW by AUC. However, given problems with PurQ and smPurL aggregation, SE-AUC experiments were not feasible due to the times typically needed to complete an experiment (days). Therefore, SV-AUC experiments which can be completed in hours were used to determine the MW of the components and the FGAR-AT complex using global data fitting to determine both the rate of sedimentation and the shape of the sedimenting boundary to take into account the diffusion properties of the protein (*5, 22*). The data analysis is carried out using SEDFIT

218

and the Lamm equation to model the sedimentation and diffusion parameters for a continuous distribution of species in solution. The advantage of this method of analysis is that it can accurately fit the MWs of multiple species in solution with high resolution, and baseline resolution has been demonstrated for equimolar mixtures of species with a 30% difference in molar mass (5). This proved to be particularly important for studies on the FGAR-AT complex as described below.

PurM and lgPurL were used as controls in the SV-AUC experiments. Determination of their MWs by the methods described above gave values of 74 and 140 kDa, close to those calculated based on the amino acid sequence (Table 4.2). SV-AUC was then carried out on PurS, A128T PurQ, and smPurL. In order to limit aggregation, SV-AUC experiments for smPurL and A128T PurQ were carried out at 10°C and at rotor speeds of 40,000 rpm to promote rapid sedimentation. Analysis of the data suggested that both species are monomeric in solution (Table 4.2).

Table 4.2: Determination of MW by SV-AUC

Sample	[Monomer] (μM)	Predicted MW (kDa)	Calculated MW (kDa)	Observed Quaternary Structure	% Abundance	RMSD of Fit to Observed Data
His-PurM[a]	25	38	74	Dimer	92	0.009
lgPurL[a]	7	141	140	Monomer	95	0.008
PurS[b]	1000	10	17	Dimer	94	0.005
PurQ[a]	57	25	22	Monomer	85	0.007
smPurL[a]	40	80	81	Monomer	95	0.007

[a]These samples were monitored with absorbance optics. [b]This sample was monitored by interference optics.

The stability of PurS allowed a number of SV-AUC experiments to be performed at 25° as well as 10°C, at different concentrations, and in different buffers to examine the

propensity of the protein to oligomerize. A typical result of is shown in Figure 4.8 in

which 1 mM PurS was sedimented in PBS at 25°C and monitored with interference

optics. The PurS concentration was chosen to maximize tetramer formation; however,

even under these conditions, only the presence of a dimer is observed (Figure 4.8). In

fact no tetramer was observed under any of the conditions (see Experimental), providing

strong evidence that PurS is a dimer.

Examination of the FGAR-AT complex was carried out in the presence of both

0.1 mM ADP and 20 mM glutamine to maximize chances of detection of the "active"

complex. The presence of ADP required the use of interference optics to monitor the

progress of the sedimentation. Efforts to minimize aggregation involved shortening the

dialysis time and carrying out the experiments at 10°C and 40,000 rpm. The results of the

experiment are shown in Figure 4.9. The data indicates that multiple species were

present in solution based upon the observation of multiple boundaries in the

sedimentation profile, and this was confirmed by fitting the data (rmsd = 0.006 fringes).

Table 4.3: SV-AUC Results for the FGAR-AT Complex

Assigned Peak	Predicted MW (kDa)	Calculated MW (kDa)	Observed Quaternary Structure	% Abundance
PurS Dimer/PurQ	20/25	19.1	N/A	16.6
Dimeric PurQ Aggregate[a]	50	42.9	Aggregate	7.2
SmPurL	80	75.6	Dimer	17.7
FGAR-AT Complex 2S: 1L: 1Q	124	127.8	2S: 1L: 1Q	51.2
?	?	200.0	Aggregate?	5.3
?	?	277.7	Aggregate?	1.6

[a]This aggregate was assigned based on appearance of this peak in many SV-AUC experiments on PurQ and PurQ mutant proteins (Chapter 5).
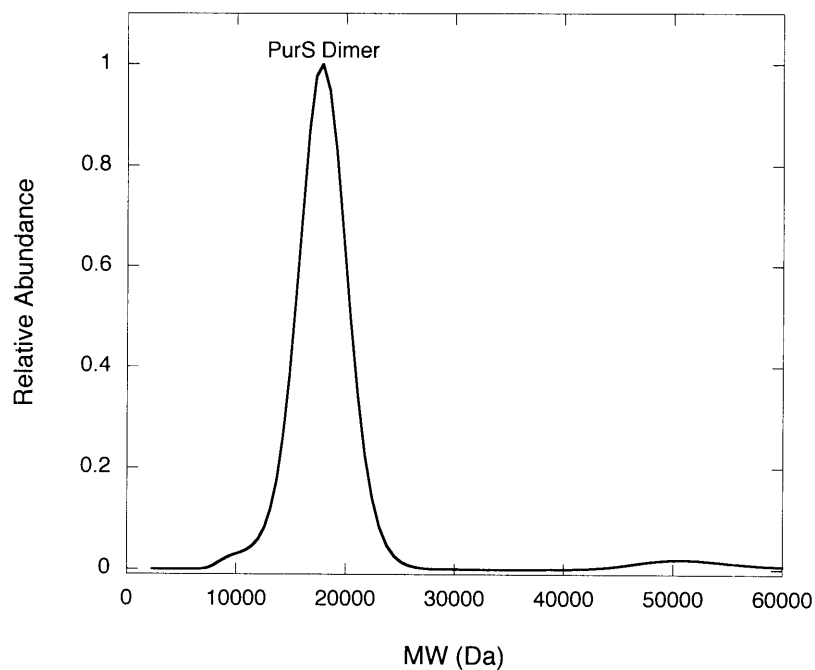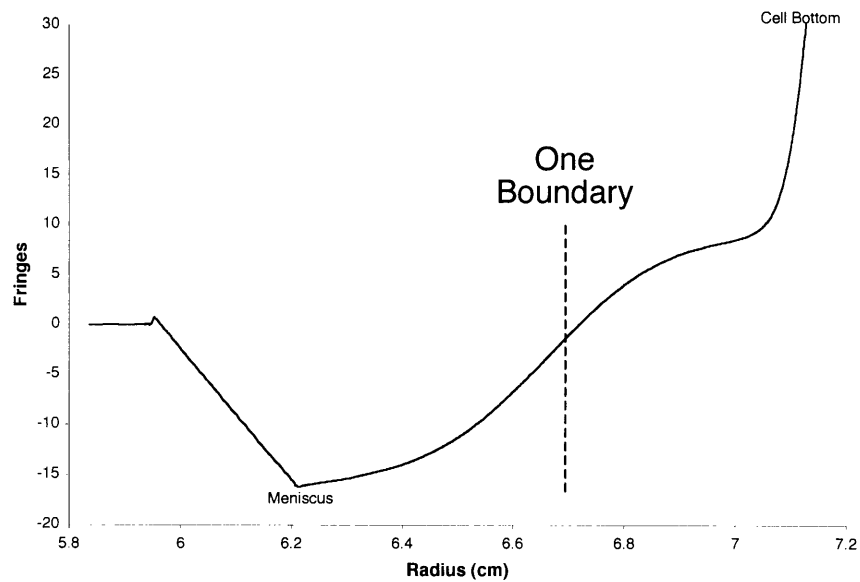
Figure 4-8—Results from SV-AUC experiments on PurS. (Top) Interference data obtained using a 1 mM solution of PurS at 50,000 rpm at 25°C in PBS. The data shows the presence of a single boundary, indicating that there is predominantly a single species in solution REF. (Bottom) Mass distribution of species in solution after SEDFIT analysis of the SV-AUC data.
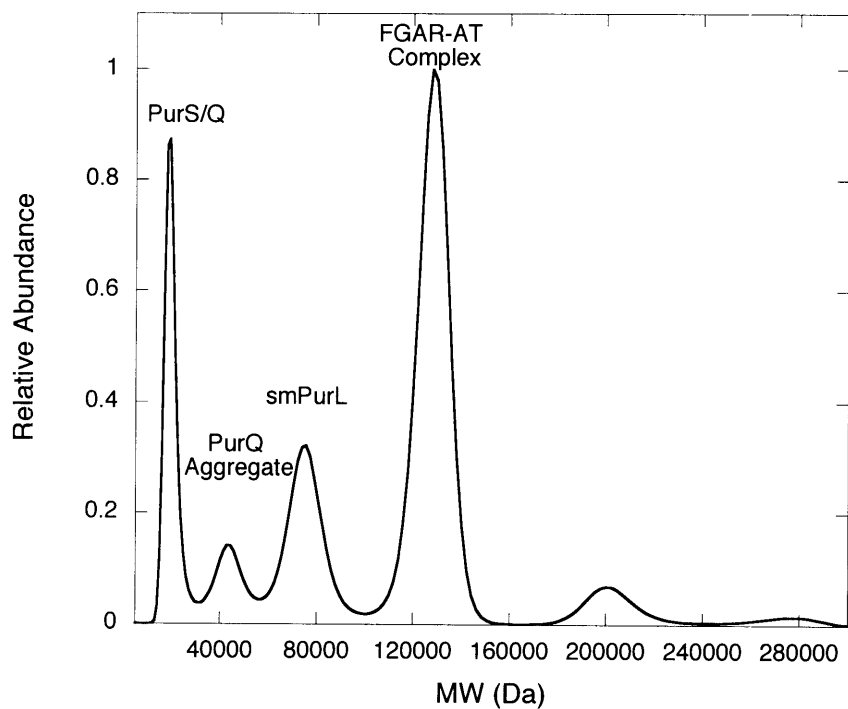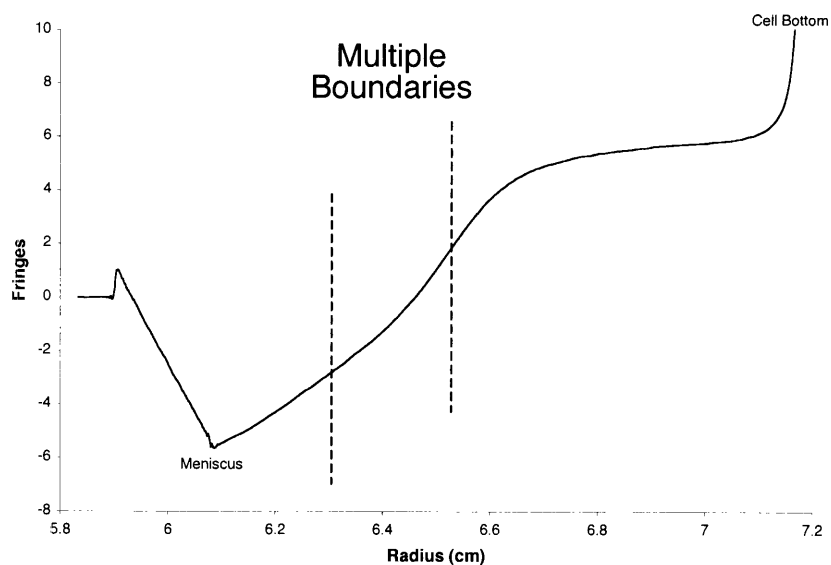
Figure 4-9— Results from SV-AUC experiments on the FGAR-AT complex. (A) Interference data obtained using a 16 μM FGAR-AT complex solution in HEPES buffer with 0.1 mM ADP and 20 mM glutamine. The data shows the presence of multiple boundaries indicating that more than one species is present in solution. (B) Fitting of the SV-AUC data (rmsd of the fit was 0.006 fringes) revealed that the predominant species in solution was the 2 PurS: 1 smPurL: 1 PurQ FGAR-AT complex (128 kDa calculated, 124 kDa predicted).

222

Analysis of the data by SEDFIT indicates that the predominant species in solution has a MW of 128 kDa, in comparison to the 124 kDa calculated for a 2: 1 :1 complex (Figure 4.9). Integration of the peaks obtained from the SEDFIT analysis indicates that the abundance of the 2: 1: 1 complex is low (51%), and multiple other species are present (Figure 4.9, Table 4.3). At lower MWs than the 2: 1: 1 complex, 3 species were observed that account for ~41% of the mass in the sample. It is likely that the 75.6 kDa, and 42.9 kDa peaks represent smPurL monomer (80 kDa) and an aggregate of A128T PurQ. The A128T PurQ aggregate has been seen in a number of SV-AUC experiments and typically appears between 40-50 kDa (see Chapter 5). A large peak was also observed at 19.1 kDa (16.6% abundance). It is possible that this represents the PurS dimer, although this peak could also contain A128T PurQ. These results indicated that the complex was partially dissociated during the SV-AUC experiment, and at least in the case of A128T PurQ, some aggregation was observed.

Two peaks were observed at MWs higher than that of the 2: 1: 1 complex. Both the 200 kDa and 278 kDa peaks had very low abundance (5.3 and 1.6%, respectively). These peaks were assigned as aggregates and not as the 4:2:2 complex (248 kDa) since the observed molecular weights were >10% removed from the predicted MW. However, it should be noted that fitting the MW of such low abundance species is difficult and the calculated molecular weight may have very large errors. Nevertheless, if a 4:2:2 complex is present under these conditions, then it must be <10% of the 2:1:1 complex in abundance, indicating that it is not the predominant species under these conditions.

Given the difficulties encountered in crystallizing of the FGAR-AT complex,

additional methods were investigated to provide confirmation of the quaternary structure

of PurS and the FGAR-AT complex and to provide additional insight into the validity of

the homology model. Multidimensional NMR spectroscopy potentially has the power to

address both of these issues. As a starting point to investigate the feasibility of this

method, the proton NMR spectra in 10% D_2O of PurS (1 mM) was examined in the

amide (8.1-8.8 ppm) and methyl (0-1.5 ppm) regions (data not shown). The data

indicated that PurS is stable and non-aggregated and the chemical shifts were sufficiently

sharp and dispersed to allow assignment with appropriate labeling techniques.

Isotopically-labeled PurS protein was produced in which the protein was either

fully-labeled with ^{15}N or both ^{15}N and ^{13}C. These samples were prepared by expressing

PurS in *E. coli* BL21(DE3) grown in minimal media containing $^{15}NH_4Cl$ and [^{13}C]-

glucose as the sole nitrogen and carbon sources. Expression and purification of the

labeled PurS proteins was carried out as described in Chapter 3 for unlabeled PurS with

similar yields (~15-20 mg /g cells).

Amide Backbone Assignments

In the NMR experiments described subsequently to study the PurS quaternary

structure, only the amide backbone proton resonances must be assigned. The amide-

backbone assignments were achieved with the use of a [^{13}C, ^{15}N]-PurS sample and a

battery of multi-dimensional NMR experiments including HNCA, HNCACB,

CBCA(CO)NH, and HBHA(CO)NH (*7-10*). These experiments define in different ways

the connectivity of the amide proton to either the preceding or following amino acid side
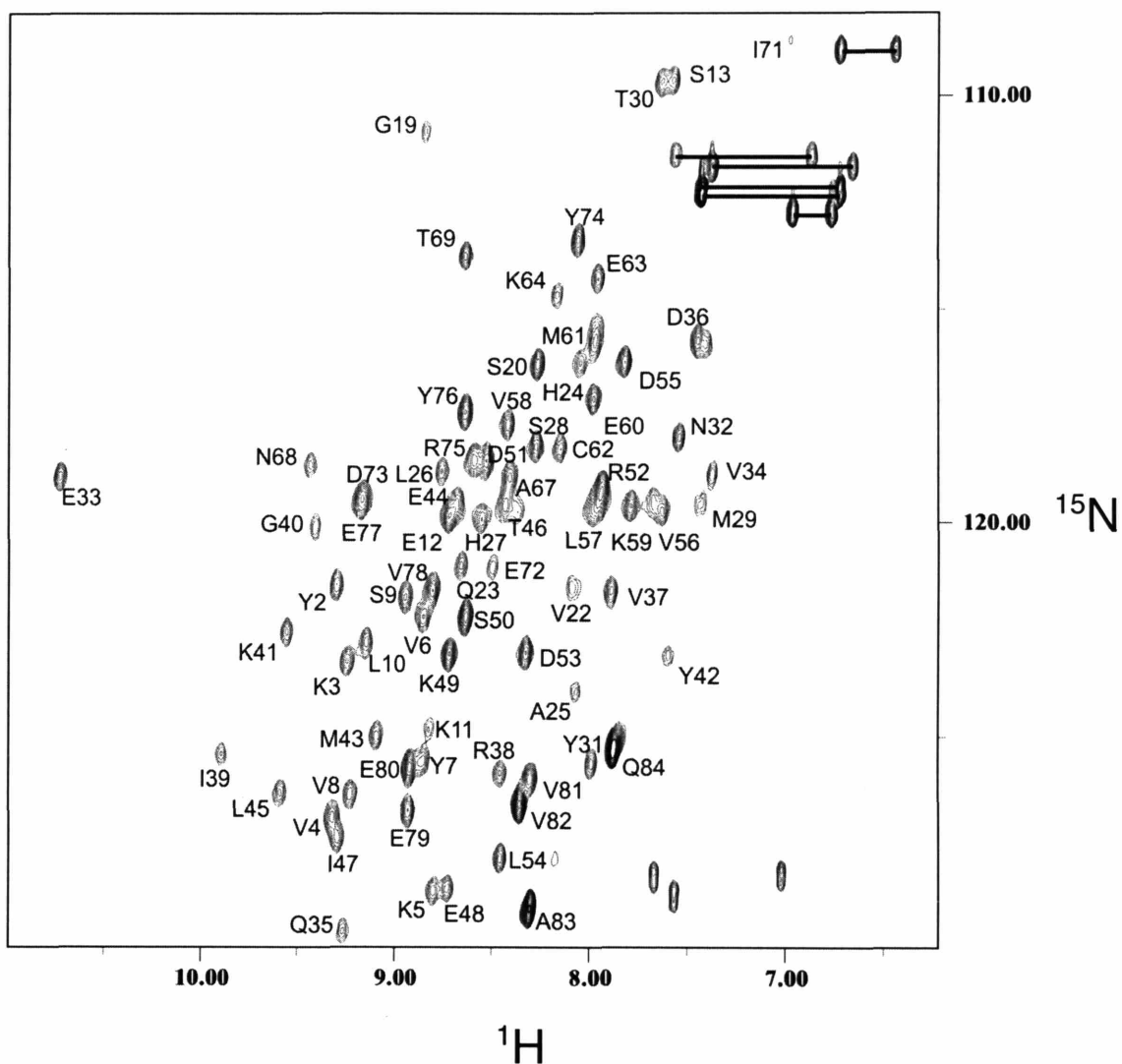
Figure 4.10—HSQC of amide protons in ^{15}N-labeled PurS (1.5 mM, recorded at 600 MHz). Peaks are labeled according to the appropriate PurS residue number. The unlabeled peaks in the upper right are from glutamine and asparagine side chains. The number of amides assigned was 75 out of a total of 84.

225

chain (Figure 4.5). Together, the experiments allowed the complete assignment of amide backbone resonances except for residues 14-18, 21, 65-66, and 70 (Figure 4.10).

Confirmation of PurS Secondary Structure in Solution

While a solution structure of PurS has not been determined, data obtained from the amide assignment process has been used to determine PurS secondary structure in solution based on observed deviations of the $^{13}C\alpha$ and ^{13}CO chemical shifts from those observed in a random coil (*11*). Both the $^{13}C\alpha$ and ^{13}CO nuclei are sensitive to the peptide backbone torsion angles, and consequently, these nuclei typically exhibit downfield shifts of ~2.5 ppm when incorporated into helices and upfield shifts of ~2.0 ppm in sheets compared to their random coil values (*11*). By plotting each residue's deviation from a random coil chemical shift, secondary structure elements in proteins can be readily identified by looking for patterns of positive (helices) and negative (strands) deviations. Results from this experiment are shown in Figure 4.11 for the $C\alpha$ carbons. Comparison of the shift patterns to the secondary structural elements of PurS derived from the crystallographic data indicate that PurS in solution adopts a similar secondary structure as observed in the crystal structures (*1*). Further evidence in support of these secondary structure assignments was obtained by observation of interstrand NOEs in the 3-strand β-sheet found in the PurS monomer (data not shown).

H/D Exchange Experiments Indicate that Residues at the Crystallographic Dimer:Dimer Interface are Solvent Accessible

The dimer:dimer interface proposed in the PurS tetramer can be directly probed by NMR spectroscopy by measurement of the rate of amide hydrogen exchange in D_2O. The rate of exchange can be measured by collecting ^{15}N-HSQC spectra at known
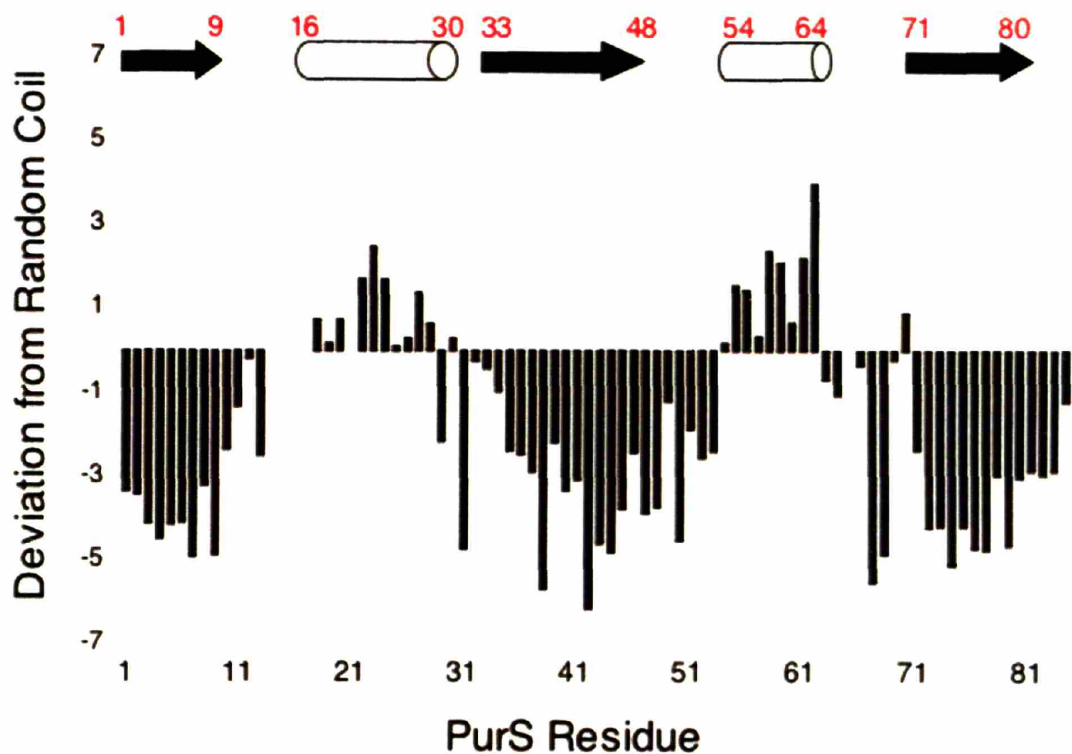
Figure 4.11—Deviation from random coil chemical shifts of Cα carbons in PurS. Negative deviations are indicative of β-strands, while positive deviations are indicative of α-helices. For reference, the secondary structure assignment of PurS from the crystal structure is indicated at the top of the figure. These results indicate that PurS in solution has the same secondary structure as observed in the crystal structures.

timepoints after reconstituting a lyophilized protein sample in D_2O. If an amide proton is exchanged for deuterium, its signal disappears from the HSQC spectrum. It is predicted that if an amide is involved in hydrogen-bonding interactions that comprise the dimer:dimer interface, then it should be shielded from solvent exchange and exchange more slowly than solvent-accessible protons. While accessible protons exchange very rapidly with solvent ($\sim$50 s^{-1} at pH 7.0) (23), protons protected within a protein environment may exchange over min to h time-scales (24).

The temporal-resolution in this experiment is limited by the amount of time required to prepare the sample, tune and shim the NMR spectrometer, and collect sufficient data for analysis using the HSQC method. The shortest time interval in these experiments was 5 min and was achieved using a 600 MHz spectrometer and a cryoprobe to increase the NMR signal and allow collection of HSQC spectra of PurS that were complete with only 2 scans.

Comparison of the HSQC spectrum in Figure 4.10 with that taken after 5 min exposure to D_2O (Figure 4.12) indicates that the majority of the amide protons of PurS have not exchanged. Those that have exchanged (Table 4.4) are predominantly surface-exposed residues on PurS. One of the exceptions is V78, which resides at the crystallographic dimer:dimer interface in both crystal forms (Figures 4.3 and 12). The amide of V78 is thus behaving like a surface-accessible residue and is likely not involved in a protein interface. After 30 min, the amide of Y76 (also predicted to be part of the dimer:dimer interface, Figure 4.3) has also exchanged, indicating that it also is much less shielded from solvent relative to the majority of amide protons (Figure 4.13). As a control, amides at the monomer:monomer interface were examined. These residues
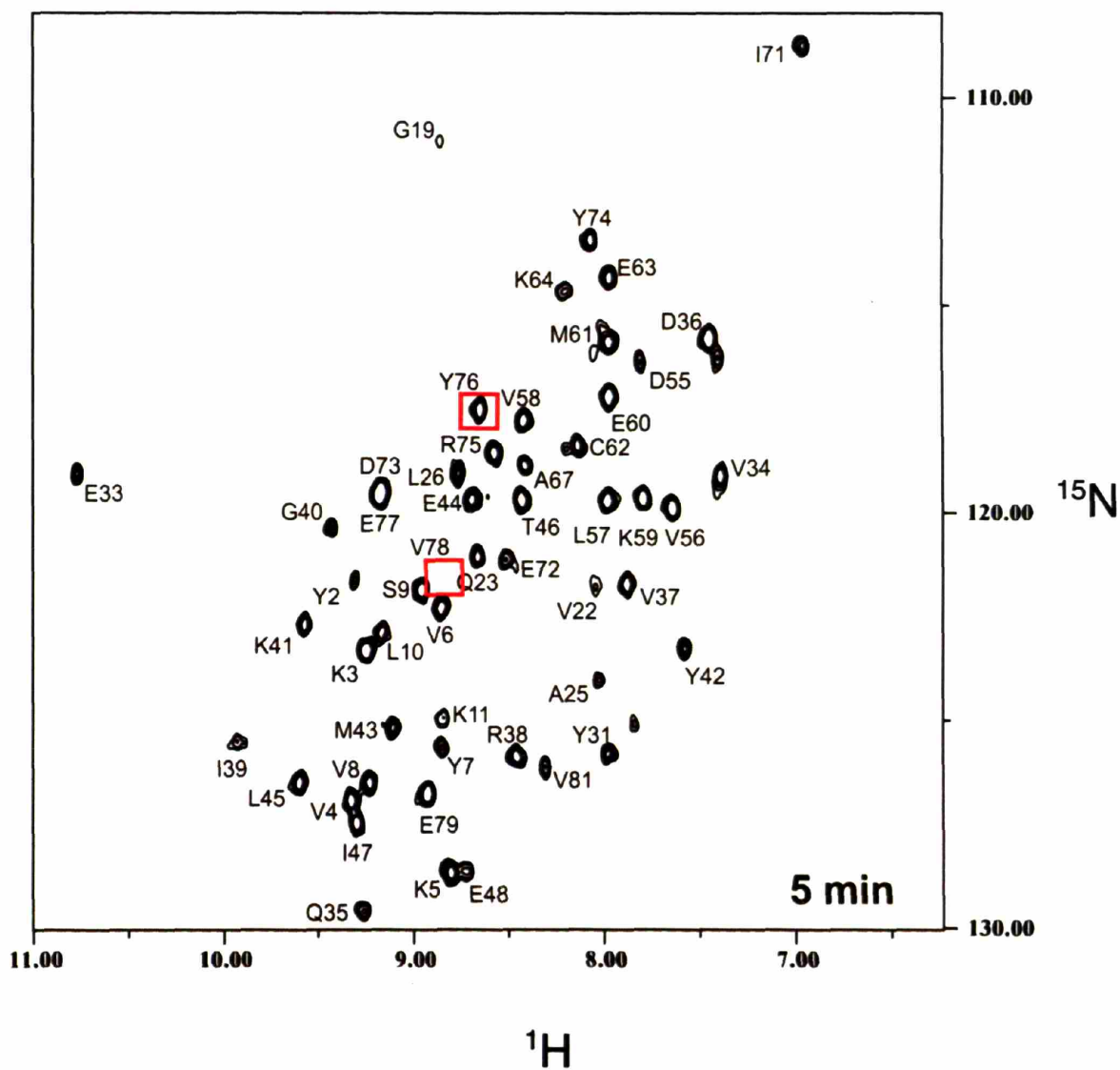
Figure 4.12—Results from H/D exchange experiments on PurS after 5 min of exposure to D$_2$O. The positions of peaks resulting from the Y76 and V78 amides at the dimer:dimer interface are boxed in red. After only 5 min, the V78 proton has already completely exchanged with solvent deuterium.
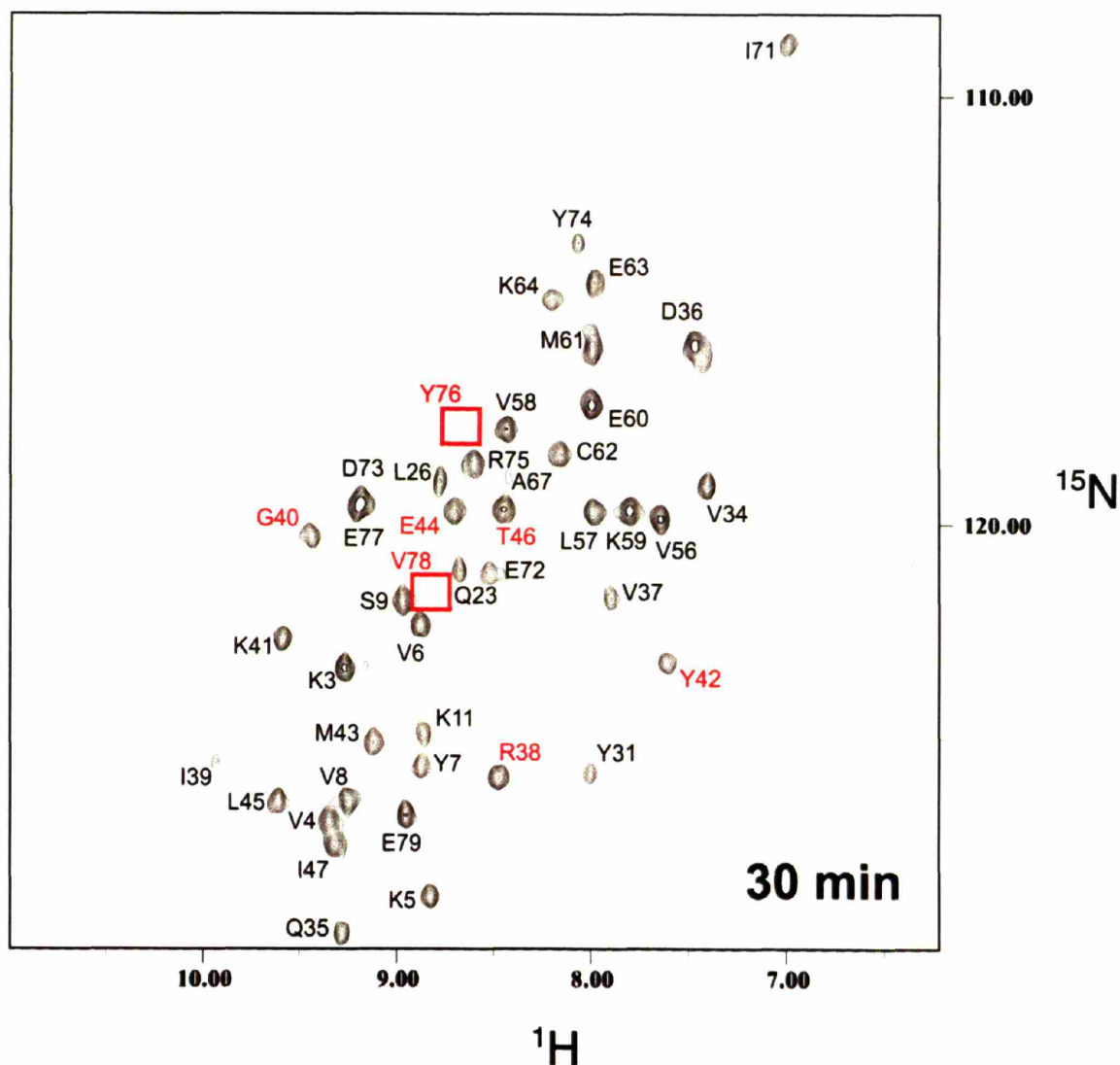
Figure 4.13—Results from H/D exchange experiments on PurS after 30 min of exposure to D₂O. The position of peaks resulting from the Y76 and V78 amides at the dimer:dimer interface are boxed in red. After 30 min, both the Y76 and V78 protons have fully exchanged, indicating that a stable tetramer is not present. Protons located at the monomer:monomer interface (R38, G40, Y42, E44, and T46) are still present and are labeled in red. This indicates that the PurS dimer is very stable and protons involved in dimer formation are shielded from solvent.

(R38, G40, Y42, E44, and T46) are all present at 30 min (Figure 4.13) and even after 270 min in D_2O, they have not exchanged (data not shown). These results indicate that the PurS dimer is a very stable structure and that amides at the monomer:monomer interface are shielded from solvent. In contrast, if a PurS tetramer is present, then amides at the tetramer interface are readily solvent-accessible, suggesting a "weak" interaction.

Table 4.4: PurS Amides that Have Exchanged with D_2O after 5 min

Residue	Location
E12	Surface
S13	Surface
S20	Helix 1
H24	Helix 1
S28	Surface
M29	Surface
T30	Surface
N32	Surface
D51	Surface
D53	Surface
N68	Surface
T69	Surface
V78	Dimer:Dimer Interface
V82	Surface
A83	Surface
Q84	Surface

NMR Experiments to Measure PurS Size in Solution Provide Evidence for a PurS Dimer

Several additional types of NMR methods can provide information about the molecular size and shape of a protein in solution. For PurS, experiments were carried out to determine its rotational correlation time (T1/T2 measurements) and the rate of molecular diffusion along the long axis of the NMR tube (DOSY experiments). Each of these methods independently provides evidence for a PurS dimer in solution.

Both the longitudinal (T1 or R1) and transverse (T2 or R2) relaxation times are dependent on the correlation time for a molecule in a magnetic field (τ_c, the time in which
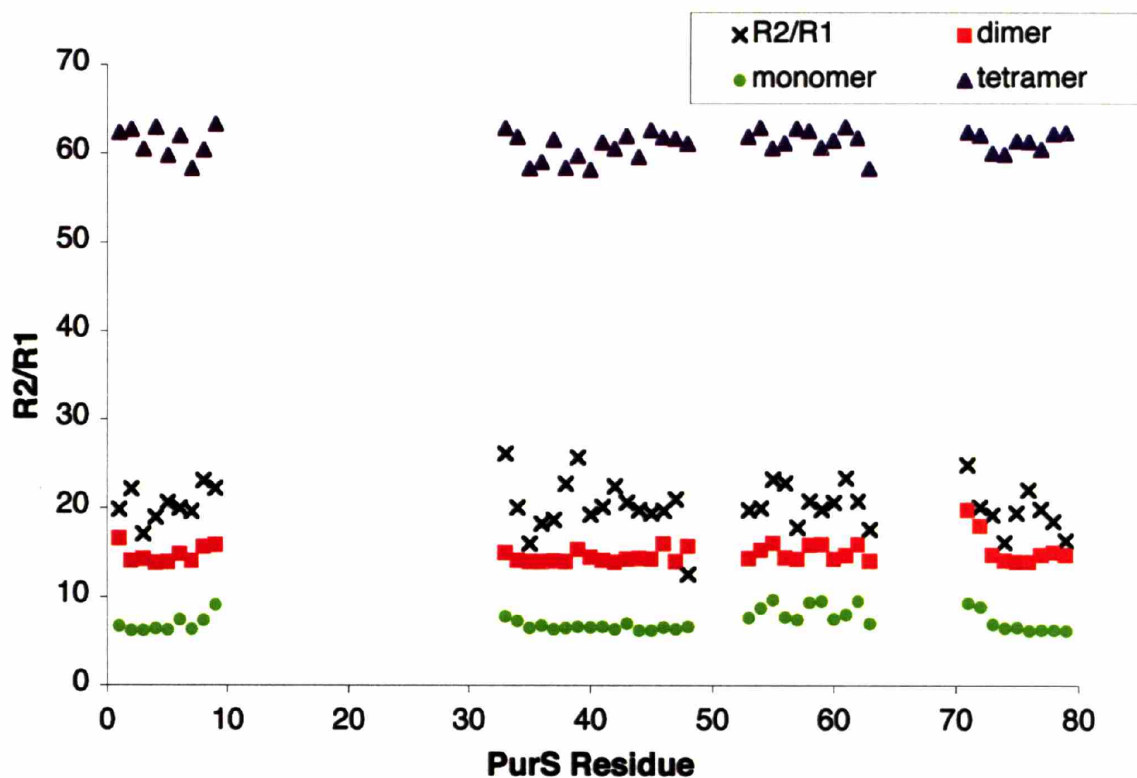
Figure 4.14—Measurement of magnetic relaxation properties of amide protons in PurS. The ratio of transverse (R2) to longitudinal (R1) relaxation was determined for the indicated PurS residues (✗). Missing data points represent residues for which relaxation data could not be determined. Predicted R2/R1 ratios obtained by HYDRONMR are shown for the PurS monomer (●), dimer (■), and tetramer (▲). The data are closest to that predicted from a PurS dimer.

a molecule undergoes 1 radian of rotation). The correlation time is, in turn, dependent on the molecular mass. Consequently, the ratio of R2/R1 can be informative about molecular size (*25, 26*). As shown in Figure 4.14, different R2/R1 ratios are predicted for the PurS monomer, dimer, and tetramer. These ratios were predicted by HYDRONMR using the crystal structure of PurS, and results from this program typically contain errors of 4.3% between the calculated and experimental values (*27*).

R1 and R2 values were determined for the PurS amide protons corresponding to the non-loop regions of PurS (residues 1-12, 19, 22-48, 50-63, 66-68, and 70-81). The R1/R2 ratios for each amide proton are shown in Figure 4.14. The experimental values obtained for PurS are closest to those predicted for the dimer and are all far removed from those predicted for the tetramer. These results indicate that in solution, the rotational correlation time for PurS corresponds to a dimeric species.

Molecular size can also be determined by NMR by measuring the rate at which molecules diffuse along the long axis of the NMR tube (*12, 28, 29*). These experiments are carried out using DOSY spectroscopy in which a magnetic gradient is applied along the length of the NMR tube. By applying an identical gradient after a time delay, proton signals are only detected if the molecule experiences the same magnetic field strength from both gradients, which only occurs if the molecule has not diffused significantly in the NMR tube during the time delay. The changes in protein ^1H peak intensities versus magnetic field strength have thus been compared to an internal dioxane standard with a known hydrodynamic radius ($R_H^{dioxane}$). The hydrodynamic radius of the protein ($R_H^{protein}$) can be calculated using the relationship shown in Equation 4.6 where $d_{dioxane}$ and $d_{protein}$ are diffusion parameters for dioxane and the protein, respectively,
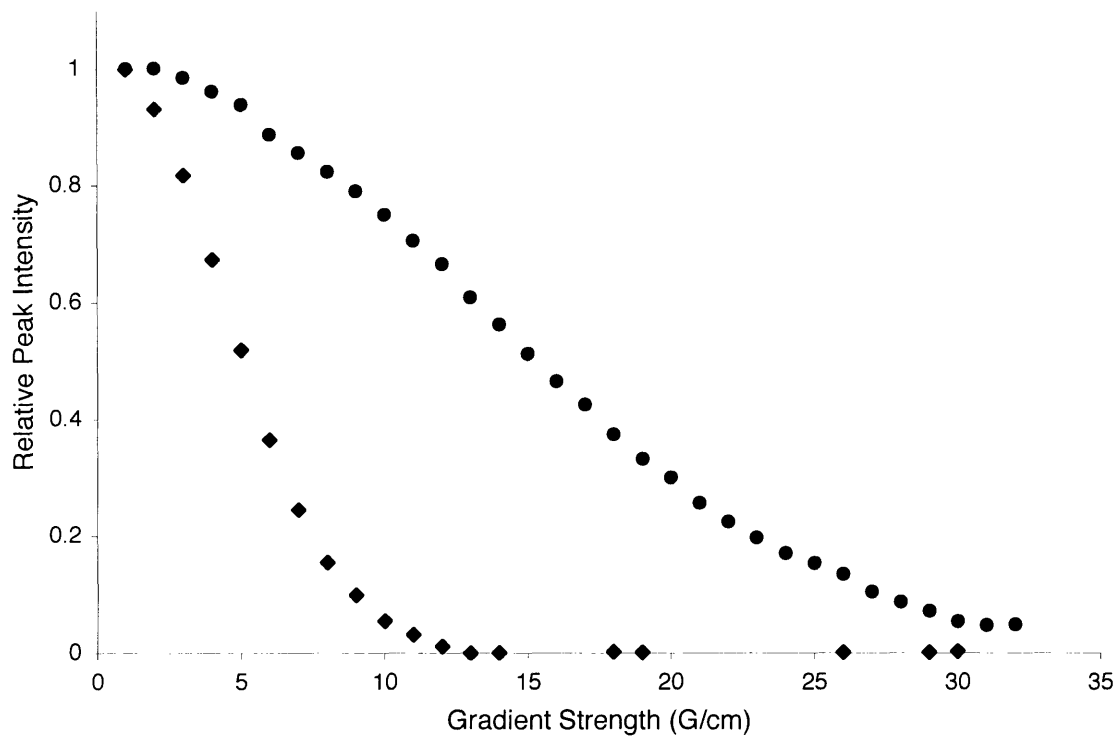
Figure 4.15—Measurement of diffusion properties of PurS by DOSY. The intensities of PurS ^{1}H methyl peaks were measured as a function of magnetic gradient strength (●). The sample contained an internal dioxane standard (◆). Comparison of the diffusion properties of PurS relative to dioxane indicate that PurS is a dimer in solution.

obtained by monitoring the change in NMR signal intensity vs. the magnetic gradient strength.

$$R_H^{protein} = \frac{d_{dioxane}}{d_{protein}} R_H^{dioxane} \qquad (4.6)$$

Five experiments were carried out at two different PurS concentrations to determine R_H for PurS in comparison to dioxane. The results of a typical experiment are shown in Figure 4.15. All of the experiments are in close agreement, giving a value of 2.4 $\pm$ 0.2 nm for PurS. This value is closest to that predicted for a PurS dimer using HYDROPRO hydrodynamic bead-modeling software, which gives R_H values of 2.3 nm and 2.7 nm for the PurS dimer and tetramer. HYDROPRO uses a series of beads of defined hydrodynamic properties to mimic the 3-dimensional structure of a protein. Determination of R_H values with HYDROPRO is very accurate and typical errors in this calculation are 2% (13), indicating that dimer and tetramer can be distinguished based on R_H . Measurements of both the rotational correlation time (R2/R1) and translational diffusion (DOSY) for PurS by NMR provide evidence that PurS is a dimer in solution.

Quantitative Western Analysis of the FGAR-AT Complex Reveals an FGAR-AT Complex is Present in High Concentrations in B. subtilis

One drawback of the biophysical methods described in this chapter, particularly the NMR experiments, is that they are all carried out at high protein concentrations 10-1000 μM. Given the influence protein concentration may play on protein quaternary structure and the problems associated with smPurL and PurQ aggregation, quantitative Western blotting was used to determine the concentrations of the individual components *in vivo*. As shown in Figures 4.16-18, antibodies produced against PurS, A128T PurQ, or smPurL could easily be used to detect the proteins in *B. subtilis* cell lysates. The number
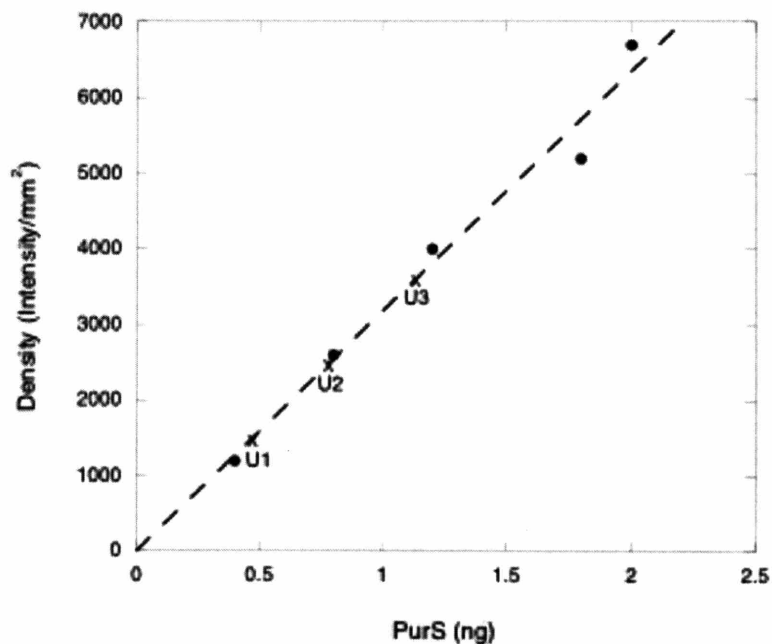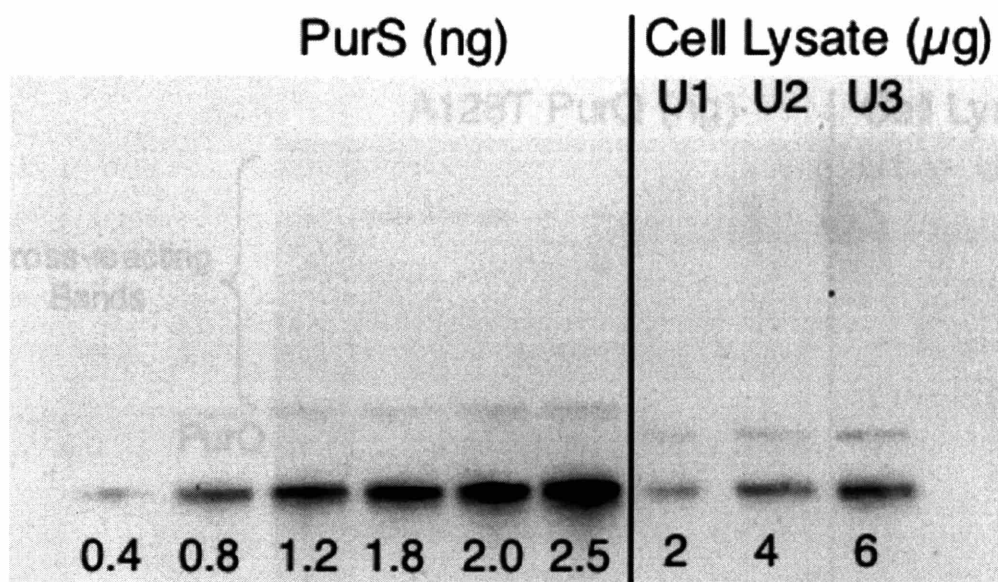
Figure 4.16—Western blot analysis of PurS in *B. subtilis* cell extracts. Standards from 0.4—2.0 ng of PurS were used to create a standard curve. This standard curve was then used to calculate the amount of PurS present per μg of *B. subtilis* cell lysate. The positions of the samples from the cell lysate on the standard curve are noted (U1, U2, and U3).
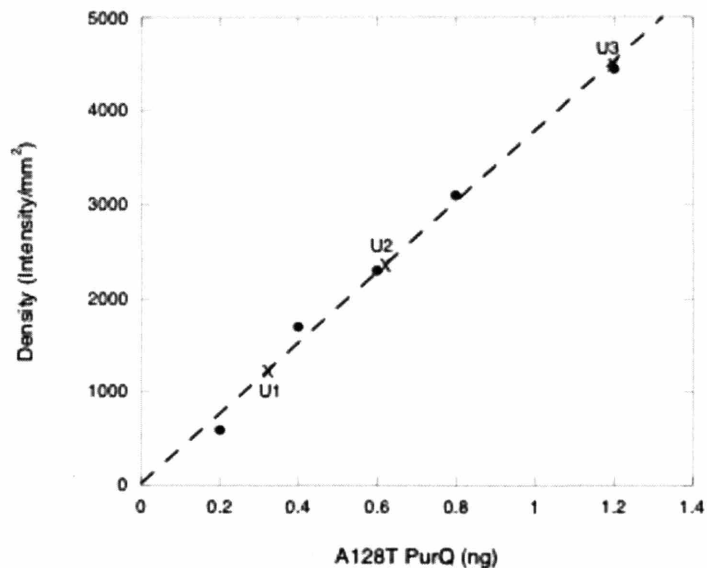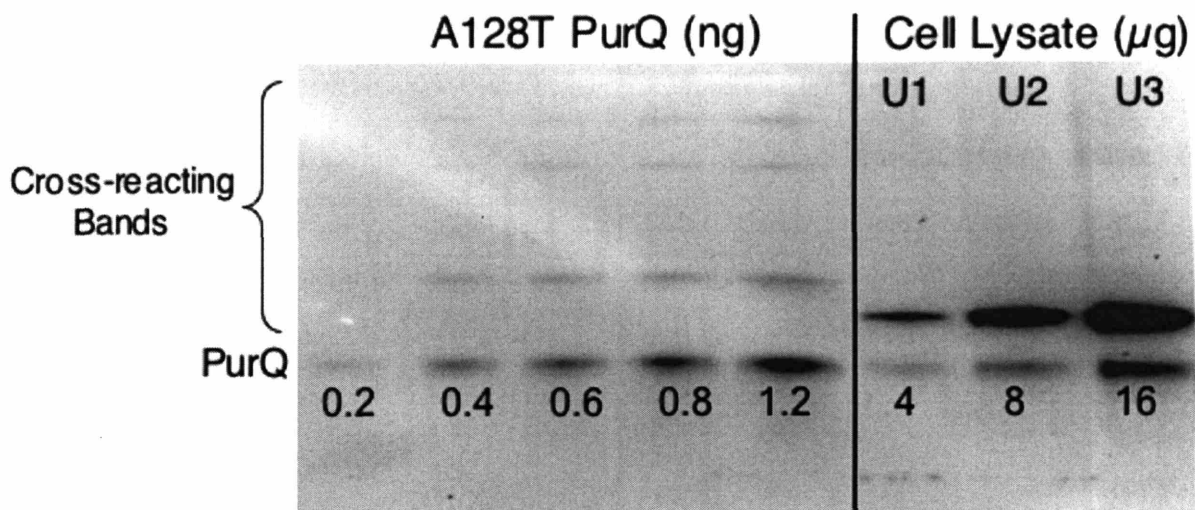
Figure 4.17—Western blot analysis of PurQ in *B. subtilis* cell extracts. Several strongly cross-reacting bands were detected with the PurQ Ab. Standards from 0.2—1.2 ng of A128T PurQ were used to create a standard curve. This standard curve was then used to calculate the amount of PurQ present per µg of *B. subtilis* cell lysate. The positions of the samples from the cell lysate on the standard curve are noted (U1, U2, and U3).
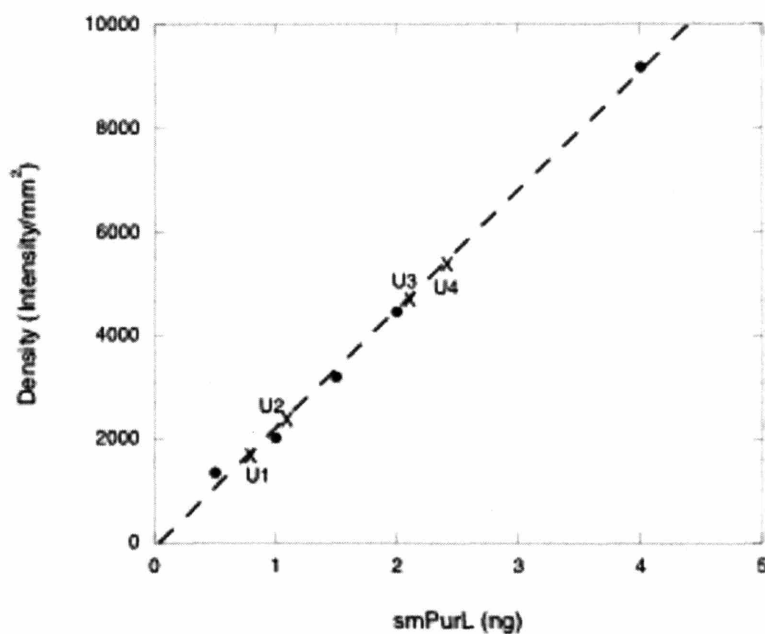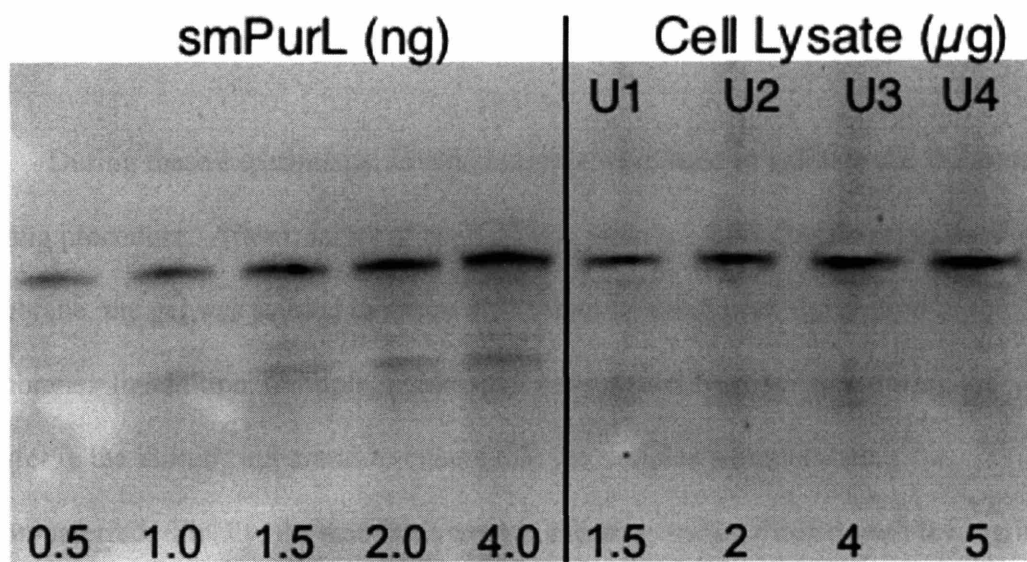
Figure 4.18—Western blot analysis of smPurL in *B. subtilis* cell extracts. Standards from 0.5—4.0 ng of smPurL were used to create a standard curve. This standard curve was then used to calculate the amount of smPurL present per μg of *B. subtilis* cell lysate. The positions of the samples from the cell lysate on the standard curve are noted (U1, U2, U3, and U4).

of molecules per cell was then determined by comparison of samples of *B. subtilis* cell

lysate to results of a standard curve generated from homogenous proteins purified from *E.*

coli.

During these experiments, several controls were used to validate the Western

blotting procedure. After transfer of each protein from the SDS-PAGE gel to the PVDF

membrane, the gel was stained to ensure that all protein had been transferred to the

membrane. In addition, multiple membranes were placed back-to-back during the

transfer in the blotting apparatus to ensure that the samples were not being

overtransferred. Finally, the standards used in the assays were diluted with 0.1 mg/mL *E.*

coli cell lysate in order to buffer the proteins, prevent non-specific binding to microfuge

tubes or pipette tips, and to mimic transfer conditions out of cell lysate.

Table 4.5: Quantitative Western Results for the FGAR-AT Proteins

	pg protein/μg cell lysate		
Protein	LB	Minimal	Minimal + Purines
PurS	50 ± 15	800 ± 144	51 ± 12
PurQ	190 ± 40	735 ± 124	108 ± 20
smPurL	480 ± 70	2806 ± 360	362 ± 105

The results obtained directly from the Western blotting analysis (pg protein/ μg

cell lysate) are summarized in Table 4.5 for *B. subtilis* grown in minimal media, purine-

rich minimal media with 1 mM adenine and guanosine, and LB media. The standard

deviation for each sample is derived from an average of 6 samples from 2 or 3 different Western blots. Typical errors in the mass were ~20% (Table 4.5). These results indicate that there is a large upregulation in the FGAR-AT complex proteins in minimal media.

In order to calculate the number of molecules of each protein per cell, the number of cells loaded per μg of cell lysate was first determined by counting the number of colony forming units per OD_{600} by replica plating and colony counting. This proved to be a very error prone process giving a value of $3.2 \pm 1.4 \times 10^8$ cells per 1 OD_{600} (a 44% error). The numbers of molecules per cell under the different growths are reported in Table 4.6. Propagation of the errors from the Western Blotting (Table 4.5) and the cell counting using Equation 4.2 result in errors of ~50% in values reported in Table 4.6. However, these results indicate that under purine-rich conditions the FGAR-AT complex is present at ~17,000 copies per cell and that the complex is increased ~5-fold in minimal medium to ~90,000 copies per cell. These values can be used to determine approximate concentrations for the complex in the cell using average *B. subtilis* cell dimensions of 1.38 x 0.6 μm for cells grown in minimal media (*30*). Based upon these dimensions, values of ~8 μM FGAR-AT complex in the cell are obtained under purine-rich conditions and ~40 μM in minimal media.

Table 4.6: Molecules per Cell of the FGAR-AT Proteins		PurS	PurQ	smPurL
LB	Molecules per cell (x10⁻⁴)[a]	1.1 ± 0.6	1.6 ± 0.8	1.3 ± 0.6
	Ratio[b]	0.86 ± 0.28	1.3 ± 0.3	1
Minimal + Purines	Molecules per cell (x10⁻⁴)[a]	2.0 ± 1.3	1.7 ± 1.0	1.7 ± 1.2
	Ratio[b]	1.16 ± 0.44	0.97 ± 0.33	1
Minimal	Molecules per cell (x10⁻⁴)[a]	26.3 ± 16.4	9.4 ± 5.9	11.0 ± 6.8
	Ratio[b]	2.4 ± 0.6	0.85 ± 0.18	1
[a]Molecules of PurS monomer. [b]Ratio of PurS Monomer.				

One interesting observation from these studies is that PurS is upregulated more than smPurL and PurQ in minimal media. The ratio of each protein relative to smPurL demonstrates that these changes result in a higher ratio of PurS under different growth conditions (Table 4.6). In rich media, the ratio is ~1 PurS: 1 smPurL: 1 PurQ; however, in minimal media the ratio changes to ~2 PurS: 1 smPurL: 1 PurQ. In the latter case, the ratio observed is the same as that determined by biochemical studies for maximal activity of the FGAR-AT (Chapter 3). How and why specific upregulation of PurS occurs remains unknown.

4.4 Discussion

Results from this chapter provide strong evidence for the presence of a PurS dimer in solution and a 2:1:1 FGAR-AT complex. SV-AUC experiments under multiple conditions were only able to detect a PurS dimer in solution. These findings are supported by several solution NMR experiments. DOSY experiments indicate that the translational diffusion properties of PurS in solution most closely matched those predicted for a PurS dimer. T1 and T2 relaxation measurements of amide protons also support a dimeric structure for PurS. Finally, H/D exchange experiments indicate that protons at the predicted dimer:dimer interface readily exchanged with solvent D_2O, implying that this interface is readily solvent accessible. Together the data suggest that PurS is a dimer in solution and that the crystallographic tetramers are crystallization artifacts.

Data from SEC and SV-AUC were obtained that support the conclusion that the FGAR-AT has a 2 PurS:1 smPurL: 1 A128T PurQ stoichiometry. Experiments carried out on the FGAR-AT complex were particularly difficult due to the susceptibility of the

241

proteins to aggregate. While SEC allowed ready detection of the complex by measurement of glutamine-dependent FGAM synthesis, many SV-AUC experiments were carried out before conditions could be found that gave interpretable data with minimum aggregation. Critical to the success of the SV-AUC experiments was shortening the dialysis time prior to the experiment and centrifuging the samples at high speed and low temperatures (40,000 rpm at 10°C) to promote rapid sedimentation. The SEDFIT program was able to deconvolute the multiple species in solution, and indicated that the predominant species was the 2:1:1 complex (51%); however, even under these conditions some aggregation and dissociation of the complex was apparent. Several low-abundance, high molecular weight species were also observed at 200 and 278 kDa; however, these species could not be readily assigned.

Two interesting observations from the SEC studies are the unusual migratory properties of PurS and smPurL. Using typical SEC procedures to determine MW, PurS migrates as a trimer while smPurL migrates as a dimer. These results have been observed in both phosphate and HEPES buffers with both standard SEC columns as well as the analytical SEC columns utilized in Chapter 3. Since SV-AUC experiments allowed determination of sedimentation coefficients for both PurS and smPurL to be determined, the method of Monte and Siegel was applied to correct the SEC results (20). The reanalysis of the SEC data gave MWs closer to a PurS dimer and smPurL monomer. The unusual migratory properties for smPurL are surprising since it should be structurally homologous to the PurM homodimer, which migrates close to its predicted molecular weight.

One drawback of many of the techniques used in this chapter is that they all require high protein concentrations. SEC experiments were carried out at 100 μM, SV-AUC experiments were carried out at 10—1,000 μM, and NMR experiments were conducted at 200-1000 μM PurS. Because of aggregation problems and the insensitivity of the biophysical methods, quantitative Western blotting was used to determine the concentrations of PurS, PurQ, and smPurL in *B. subtilis*. The results summarized in Table 4.6 indicate that the proteins are present at high concentrations inside the cell. In purine rich media conditions, the proteins are present at ~8 μM (~17,000 copies/cell). Furthermore, they are upregulated in the absence of purines to ~40 μM (~90,000 copies/cell). These concentrations are similar to values obtained by Johannes Rudolph during studies of the *E. coli* purine biosynthetic proteins. In Rudolph's studies, lgPurL concentrations ranged from 3.6—13 μM under repressed and depressed conditions, respectively (*31*). Analysis of other enzymes in the pathway showed concentrations ranging from 1—50 μM (*31*).

Since the SV-AUC experiments on the FGAR-AT complex were carried out at 16 μM, this method was probing physiologically relevant FGAR-AT concentrations. This highest PurS concentration observed by Western blotting was ~100 μM in minimal medium. While several SV-AUC experiments were carried out near 100 μM (see Experimental), the insensitivity of NMR required much higher PurS concentrations to be used than are observed physiologically; however, no evidence for tetramerization was obtained using several methods.

The high concentrations of the proteins found *in vivo* also clarifies results from Chapter 3 which showed a strong concentration dependence on the specific activity of the

FGAR-AT. In those studies, activity dropped sharply below 0.1 μM. This result may be explained by the observation that the FGAR-AT normally exists at μM concentrations inside the cell, and at lower concentrations the complex may never form.

The data from this chapter provide no evidence for the 4: 2: 2 model that has previously been proposed (Figure 4.4B) (*1*). This simplifies future studies aimed at understanding the role of PurS in FGAM synthesis. Based upon analogy with the N-terminal domain of lgPurL (Figure 4.1), PurS may play a role in linking PurQ and smPurL, possibly during NH_3 channeling. A simplified 2 PurS; 1 smPurL: 1 PurQ model for the FGAR-AT complex will make testing this model more straightforward since it eliminates the possibility of a PurS tetramer coordinating activities between two sets of PurQ:smPurL complexes in a 4: 2: 2 model.

The amenability of PurS for NMR studies has important implications for future analysis of the FGAR-AT. So far, crystallographic studies of the assembled *B. subtilis* have not been successful. In addition, efforts to study complex assembly by isothermal titration calorimetry (to determine dissociation constants) resulted in extensive aggregation and precipitation of PurQ and smPurL. It may be possible to use NMR to provide evidence for the docking model (Figure 4.4A) by titrating PurS with PurQ and smPurL. Sites in PurS that interact with PurQ and smPurL could be identified by looking for changes in the chemical shifts of PurS residues, and this type of titration may even be able to determine K_ds for PurS in the FGAR-AT complex under different conditions (+/- glutamine, for example). Data from future NMR experiments may provide the evidence needed to clarify the role of PurS in NH_3 channeling between PurQ and smPurL.

4.5 References

(1)   Anand, R., Hoskins, A. A., Bennett, E. M., Sintchak, M. D., Stubbe, J., and Ealick, S. E. (2004) A model for the *Bacillus subtilis* formylglycinamide ribonucleotide amidotransferase multiprotein complex. *Biochemistry 43*, 10343-52.

(2)   Batra, R., Christendat, D., Edwards, A., Arrowsmith, C., and Tong, L. (2002) Crystal structure of MTH169, a crucial component of phosphoribosylformylglycinamidine synthetase. *Proteins 49*, 285-8.

(3)   Laue, T. (2001) Biophysical studies by ultracentrifugation. *Curr. Opin. Struct. Biol. 11*, 579-83.

(4)   Behlke, J. and Ristau, O. (1997) Molecular mass determination by sedimentation velocity experiments and direct fitting of the concentration profiles. *Biophysical J. 72*, 428-34.

(5)   Schuck, P. (2000) Size-distribution analysis of macromolecules by sedimentation velocity ultracentrifugation and lamm equation modeling. *Biophys J 78*, 1606-19.

(6)   Bartels, C., Xia, T., Billeter, M., Güntert, P., and Wüthrich, K. (1995) The program XEASY for computer-supported NMR spectral analysis of biological macromolecules. *J. Biol. NMR 6*, 1-10.

(7)   Ikura, M., Kay, L. E., and Bax, A. (1990) A novel approach for sequential assignment of 1H, 13C, and 15N spectra of proteins: heteronuclear triple-resonance three-dimensional NMR spectroscopy. Application to calmodulin. *Biochemistry 29*, 4659-67.

(8)   Wittekind, M. and Mueller, L. (1993) HNCACB, a high-sensitivity 3D NMR experiment to correlate amide-proton and nitrogen resonances with the α- and β-carbon resonances in proteins. *J. Magn. Reson. 101*, 201-205.

(9)   Grzesiek, S. and Bax, A. (1992) Correlating backbone amide and side chain resonances in larger proteins by multiple relayed triple resonance NMR. *J. Am. Chem. Soc. 114*, 6291-6293.

(10)   Grzesiek, S. and Bax, A. (1993) Amino acid type determination in the sequential assignment procedure of uniformly 13C/15N-enriched proteins. *J. Biomol. NMR 3*, 185-204.

(11)   Wishart, D. S. and Sykes, B. D. (1994) The 13C chemical-shift index: a simple method for the identification of protein secondary structure using 13C chemical-shift data. *J. Biomol. NMR 4*, 171-80.

(12)   Jones, J. A., Wilkins, D. K., Smith, L. A., and Dobson, C. M. (1997) Characterization of protein unfolding by NMR diffusion measurements. *J. Biol. NMR 10*, 199-203.

(13)   Garcia De La Torre, J., Huertas, M. L., and Carrasco, B. (2000) Calculation of hydrodynamic properties of globular proteins from their atomic-level structure. *Biophysical J. 78*, 719-30.

(14)   Dayie, K. T. and Wagner, G. (1994) Relaxation-rate measurements for ^{15}N-^{1}H groups with pulsed-field gradients an preservation of coherence pathways. *J. Magn. Reson. (A) 111*, 121-126.

(15) Kay, L. E., Torchia, D. A., and Bax, A. (1989) Backbone dynamics of proteins as studied by ^{15}N inverse detected heteronuclear NMR spectroscopy: application to staphylococcal nuclease. *Biochemistry 28*, 8972-9.

(16) Stone, M. J., Fairbrother, W. J., Palmer, A. G., 3rd, Reizer, J., Saier, M. H., Jr., and Wright, P. E. (1992) Backbone dynamics of the *Bacillus subtilis* glucose permease IIA domain determined from ^{15}N NMR relaxation measurements. *Biochemistry 31*, 4394-406.

(17) Garcia de la Torre, J., Huertas, M. L., and Carrasco, B. (2000) HYDRONMR: prediction of NMR relaxation of globular proteins from atomic-level structures and hydrodynamic calculations. *J. Magn. Reson. 147*, 138-46.

(18) Vasantha, N. and Freese, E. (1980) Enzyme Changes During *Bacillus subtilis* Sporulation Caused by Deprivation of Guanine Nucleotides. *J. Bact. 144*, 1119-1125.

(19) Freese, E. B., Vasantha, N., and Freese, E. (1979) Induction of Sporulation in Developmental Mutants of *Bacillus subtilis. MGG 170*, 67-74.

(20) Siegel, L. M. and Monty, K. J. (1966) Determination of molecular weights and frictional ratios of proteins in impure systems by use of gel filtration and density gradient centrifugation. Application to crude preparations of sulfite and hydroxylamine reductases. *Biochim Biophys Acta 112*, 346-362.

(21) *CRC Handbook of Biochemistry and Molecular Biology* (1975-1976), CRC Press, Cleveland, OH.

(22) Ralston, G. (1993) *Introduction to Analytical Ultracentrifugation*, Beckman Instruments, Inc., Fullerton, CA.

(23) Englander, S. W., Sosnick, T. R., Englander, J. J., and Mayne, L. (1996) Mechanisms and uses of hydrogen exchange. *Curr. Opin. Struct. Biol. 6*, 18-23.

(24) Zhang, Y. Z., Paterson, Y., and Roder, H. (1995) Rapid amide proton exchange rates in peptides and proteins measured by solvent quenching and two-dimensional NMR. *Protein Sci. 4*, 804-14.

(25) Bernado, P., Akerud, T., Garcia de la Torre, J., Akke, M., and Pons, M. (2003) Combined use of NMR relaxation measurements and hydrodynamic calculations to study protein association. Evidence for tetramers of low molecular weight protein tyrosine phosphatase in solution. *J. Am. Chem. Soc. 125*, 916-23.

(26) Japelj, B., Waltho, J. P., and Jerala, R. (2004) Comparison of backbone dynamics of monomeric and domain-swapped stefin A. *Proteins 54*, 500-12.

(27) Bernado, P., Garcia de la Torre, J., and Pons, M. (2002) Interpretation of ^{15}N NMR relaxation data of globular proteins using hydrodynamic calculations with HYDRONMR. *J Biomol. NMR 23*, 139-150.

(28) Wilkins, D. K., Grimshaw, S. B., Receveur, V., Dobson, C. M., Jones, J. A., and Smith, L. J. (1999) Hydrodynamic radii of native and denatured proteins measured by pulse field gradient NMR techniques. *Biochemistry 38*, 16424-31.

(29) Wirmer, J., Schlorb, C., Klein-Seetharaman, J., Hirano, R., Ueda, T., Imoto, T., and Schwalbe, H. (2004) Modulation of compactness and long-range interactions of unfolded lysozyme by single point mutations. *Angew. Chem. Int. Ed. Engl. 43*, 5780-5.

(30)   Burdett, I., Kirkwood, T., and Whalley, J. (1986) Growth-kinetics of individual *Bacillus subtilis* cells and correlation with nucleoid extension. *J. Bact. 167*, 219-230.

(31)   Rudolph, J. (1993) PhD thesis, Department of Chemistry, Massachusetts Institute of Technology, Cambridge.

Chapter 5:

Mutagenesis of PurQ and Studies on FGAR-AT Complex Formation

5.1 Introduction

Amidotransferases (ATs) contain one of two types of glutaminase domains (*1*).

The NTN domain contains a catalytic cysteine at its N-terminus (hence the designation

N-terminal nucleophile or NTN). These domains are always found on the same

polypeptide chain as the AT, and PurF is the prototype for this class of ATs. The second

glutaminase domain is the triad domain and always contains a conserved $CX_{80\text{-}100}HPE$

motif, in which the cysteine is the catalytic nucleophile. Anthranilate synthase (TrpEG,

Figure 5.1), imidazole glycerol phosphate synthase (HisHF, Figure 5.1), *p*-aminobenzoate

synthase (PabAB, Figure 5.1), and the FGAR-AT (lgPurL or the PurS, smPurL, PurQ

complex) all contain triad class glutaminase domains, and these domains may be found

either fused to the AT or as a separate protein, usually in tight complex with the AT.

PurQ is an atypical member of the triad AT family since it does not form a tight complex

with smPurL and PurS, and the FGAR-AT complex can only be isolated in the presence

of Mg^{2+}-ADP (a structural cofactor for smPurL) and glutamine (Chapter 3).

Recently interest in triad glutaminases has resurfaced due to several remarkable

features of these enzymes. First, biochemical studies on the CPS and PabAB have

indicated that the glutamate residue in the triad motif is not necessary for catalysis,

indicating that these enzymes do not require a catalytic triad (*2, 3*). This result is

intriguing since the acidic residue is universally conserved in all triad domains, implying

that it may have another essential, non-catalytic function. Both the Raushel and Walsh

groups have speculated that the conserved glutamate may be involved in coordinating

interactions between the AT and glutaminase (*2, 3*).

PRFAR, R = ribose 5'-phosphate

Chorismate, R = -O-C(CH₂)COO⁻

Chorismate, R = -O-C(CH₂)COO⁻
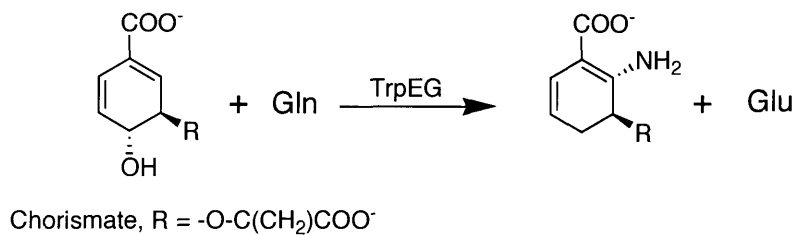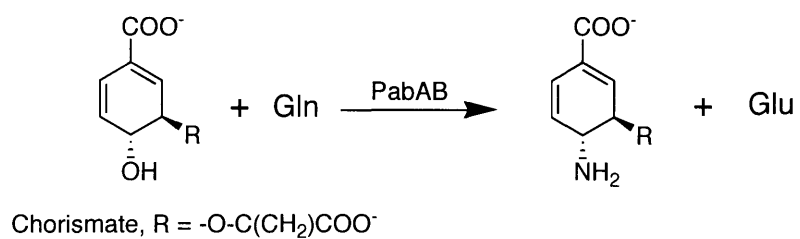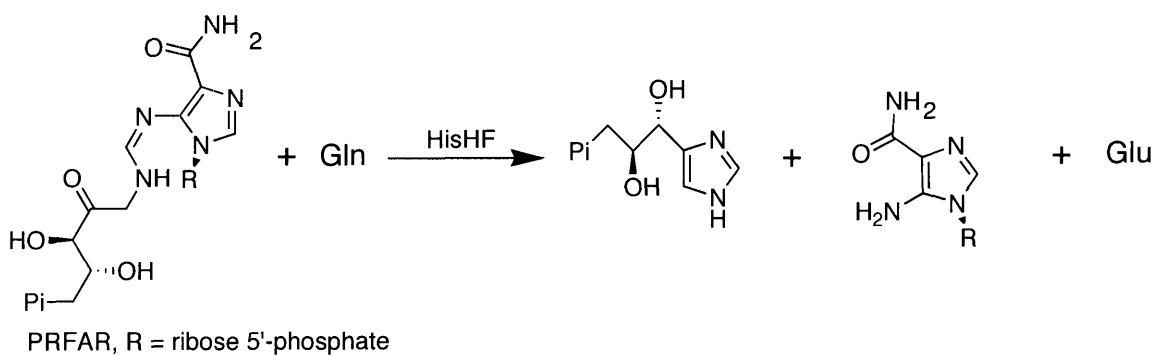
Figure 5.1—AT reactions catalyzed by HisHF, PabAB, and TrpEG.

Second, in the absence of the AT subunit and/or the AT•substrate complex, triad glutaminase domains posess very low levels of glutaminase activity. For example, results from Chapter 3 indicated that in the absence of smPurL and PurS, A128T PurQ possesses a glutaminase activity of only 0.002 s^{-1}. In the presence of the other subunits and ATP, the glutaminase activity is stimulated to 0.044 s^{-1}, and the activity is further stimulated by the presence of FGAR to a rate of 2.5 s^{-1}. These findings are typical of many triad AT enzymes, and this phenomenon has best been studied in the case of HisHF in which the glutaminase activity is stimulated 4900-fold in the presence of the AT substrate N^1-[(5'-phosphoribulosyl)formimino]-5-aminoimidazole-4-carboxamide ribonucleotide (PRFAR) (4). How binding of an AT substrate stimulates glutaminase activity is still not well understood.

The present chapter utilizes a variety of site-directed mutants of PurQ in order to address enzyme activity of PurQ and features that are important for formation of the FGAR-AT complex. Mutations were made in an A128T PurQ background to either the conserved triad residues (C86, H194, or E196) or residues involved in glutamine-binding (D55 and Q90). The latter residues were identified in PurQ by homology to the glutaminase domain of *Salmonella* lgPurL (28% identity), which has been crystallized with a glutamylthioester in the glutaminase active site (Figure 5.2) (5). Each mutant's impact on complex formation was assessed by the use of competition assays against the active enzyme. Interpretation of these results was complicated due to difficulties in measuring glutamine binding to the proteins; however, results from D55 and Q90 mutants provide additional support for the model reported in Chapter 3 that glutamine-binding is important for FGAR-AT complex formation. The C86A and C86S mutants
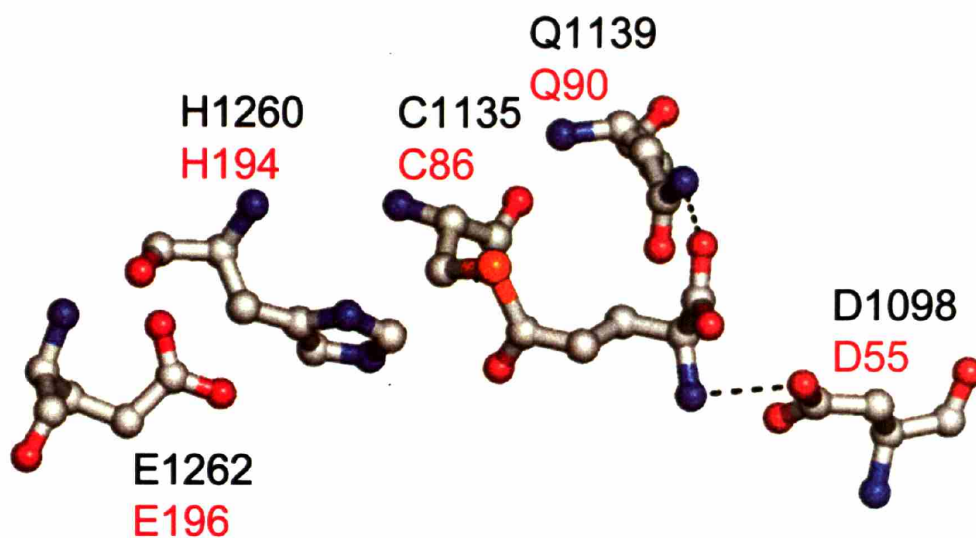
Figure 5.2—Structure of the glutamylthioester present in the glutaminase active site of the *Salmonella* lgPurL crystal structure (1t3t.pdb). *Salmonella* residues are numbered in black, and the homologous residues in *B. subtilis* PurQ are numbered in red. The conserved triad glutaminase residues are C1135, H1260, and E1262. Dashed lines represent hydrogen-bonding interactions observed in the crystal structure.

indicate that a PurQ-glutamylthioester is not necessary for complex formation during

turnover. Interestingly, neither the E196A nor E196D mutants were competitive against

wt PurQ, despite the observation that E196A was an active glutaminase and can support

FGAM synthesis. This result is discussed in light of similar findings in CPS, HisHF, and

PabAB. A role for E196 in complex formation is presented based upon observations

from the *Salmonella* lgPurL crystal structure.

5.2 Experimental

Materials and Methods

A128T PurQ, PurS, and smPurL were purified as described in Chapter 3. The

Bratton-Marshall assay to monitor FGAM formation was carried out as described in

Chapter 3. Circular dichroism and analytical ultracentrifuge data were collected at the

Bioinstrumentation Facility for the Study of Complex Macromolecules (Department of

Chemistry, MIT).

Mutagenesis of PurQ

PurQ mutants were generated using the pET-A128T-PurQ plasmid and the

Quikchange Mutagenesis kit (Stratagene). Due to the inability to purify and characterize

the WT enzyme (see Chapter 3), all mutants were generated in the A128T PurQ

background. Mutations were made to the catalytic triad residues (C86S, C86A, H194Q,

E196D, E196Q, and E196A) and the residues proposed to be involved in glutamine-

binding (D55A, D55N, Q90A, and Q90E). The primers (Invitrogen) used are listed Table

5.1. In all cases the reverse primer is the exact complement of the forward primer.

Sequences of the mutants were confirmed by DNA sequencing at the MIT Biopolymers

Facility.

Table 5.1: Primers Used in PurQ Mutagenesis[a]	
Mutant	Forward Primer
C86A	GAAAACCTGTTCTTGGCGTC**GC**AAACGGATTCCAGATTTTACAGG
C86S	CCTGTTCTTGGCGTC**AGT**AACGGATTCCAGATTT
D55A	AGGATTTTCTTACGGCG**CT**TACTTAAGATGCGGCG
D55N	GAGGATTTTCTTACGGCA**AT**TACTTAAGATGCGGCGC
Q90A	TGGCGTCTGTAACGGATTC**GC**AATTTTACAGGAGCTTGGGC
Q90E	GTCTGTAACGGATTC**GAG**ATTTTACAGGAGCTTGG
E196A	GCCTCACCCT**GCG**CGCGCGGTCG
E196D	GCCTCACCCT**GAC**CGCGCGGTCG
E196Q	GCCTCACCCT**CAG**CGCGCGGTCG
H194Q	GGCATGATGCCT**CAG**CCTGAGCGCG
T128A	GACGAAACCTTATTCACAG**CA**TGGTACGAAAAGGGAG

[a]In all cases the reverse primer is the exact compliment of the forward primer. The site of the mutation is in bold.

Expression and Purification of Mutant PurQ Enzymes

Expression and purification of the C86A, C86S, D55N, D55A, Q90A, and Q90E A128T PurQs were carried out as previously described for A128T PurQ (Chapter 3). For the remaining mutants, a slightly altered expression and purification protocol was employed. To obtain soluble protein with the E196D and E196Q PurQs, bacterial growth was carried out at 25°C, and protein expression was induced at OD_{600} of 0.7 with 1 mM IPTG and grown for an additional 6 h. For H194 or E196 PurQs, the purification was essentially as described in Chapter 3 except that 0.05 volumes of 10% (w/v) streptomycin sulfate was used to precipitate the DNA and 200 U of DNase I (Roche) was included in the lysis buffer. Subsequent to purification, the identity of each mutant was confirmed by ESI-MS (MIT Biopolymers Facility).

254

PurQ Activity Assays

The modified Bratton-Marshall assay was used to determine activity of the PurQ

mutants by monitoring glutamine-dependent FGAM formation from the assembled

FGAR-AT complex (*6*). In this assay, the FGAR-AT complex (10 μM) was made by

mixing 10 μM smPurL, 10 μM PurQ double mutant, and 20 μM PurS in 50 mM HEPES

pH 7.2, 20 mM MgCl$_2$, 80 mM KCl, 20 mM L-glutamine, 10 mM ATP, and 0.1 mM

ADP. The mixture was incubated on ice for 5 min before each assay.

Assays were performed in standard *B. subtilis* FGAR-AT assay buffer: 50 mM

HEPES pH 7.2, 20 mM MgCl$_2$, 80 mM KCl, 10 mM ATP, 0.2 U PurM, 1 mM FGAR,

and 20 mM L-glutamine. Enzyme was diluted between 1:100 and 1:20 into the assay

buffer, and the reaction was allowed to proceed at 37°C for 2-30 min before being

quenched as previously described (Chapter 3). K_m and k_{cat} determinations for glutamine

were made by varying the glutamine concentration from 0-200 mM in the presence of 1

mM FGAR and 10 mM ATP. Data were fit with Kaleidagraph software (Synergy) to

Equation 5.1.

$$v = \frac{V_{max}[S]}{K_m + [S]} \qquad (5.1)$$

Competition Assays between A128T and Mutant PurQs

A stock solution of PurS (40 μM) and smPurL (20 μM) was first made in 50 mM

HEPES pH 7.2, 20 mM MgCl$_2$, 80 mM KCl, 10 mM ATP, 0.1 mM ADP, and either 20 or

200 mM glutamine. A separate solution containing A128T PurQ (20 μM) and variable

amounts of the double mutant PurQs (0 to 10 equivalents) was then made in the same

buffer. The PurQ solution (50 μL) was then combined with the PurS:smPurL solution

(50μL) and allowed to incubate on ice for 5 min before each assay. After incubation, the

255

solution was diluted 1:100 into assay buffer and glutamine-dependent FGAM synthesis was monitored using the Bratton-Marshall assay.

Circular Dichroism Spectroscopy

Circular dichroism (CD) spectra of each PurQ mutant were collected on an AVIV Model 202 CD spectrophotometer (AVIV Biomedical, Inc., Lakewood, NJ). Proteins were dialyzed before the experiment against 2 x 500 mL of 10 mM KP_i pH 7.2 buffer for 16 h using a Slide-A-Lyzer cassette with a 10 kDa molecular weight cutoff (MWCO) membrane (Pierce). Samples were then diluted to 10 μM in argon degassed dialysis buffer. Spectra were collected with five replicates at 25°C in a 0.1 cm path length quartz cuvette by scanning from 300-190 nm in 1.0 nm increments with a 0.5 s integration time and 1 nm bandwidth.

Sedimentation Velocity Analytical Ultracentrifugation (SV-AUC)

Before each SV-AUC experiment, protein samples were dialyzed against PBS pH 7.2 (2 x 1L) for 24 h in a Slide-A-Lyzer cassette with a 10 kDa MWCO membrane (Pierce). Centrifugation was performed using an Optima XL-1 analytical ultracentrifuge (Beckman Coulter, Fullerton, CA) with a 400 μL sample volume in double-sector Epon centerpieces with quartz windows in an An50Ti 8-hole rotor at 45,000 rpm. Sedimentation of each sample (57 μM) was monitored at 10°C for 20 h with continuous scanning at 280 nm. Experiments with the C86S and C86A A128T double-mutants were also performed in PBS buffer containing 50 mM glutamine.

SEDNTERP software from Dr. John Philo was used to calculate buffer density (g/mL), viscosity (Poise), and protein partial-specific volume from the amino acid content (mL/g) (7). Data (~200 traces for each experiment) were fit using Sedfit88 from

0.5 to 10 S using a continuous distribution of sedimentation coefficients derived from solutions to the Lamm equation (*8*). The resulting distributions were then integrated using Kaleidagraph software (Synergy).

Analytical Size-Exclusion Chromatography (SEC)

Analytical SEC to determine the extent of PurQ aggregation under the enzyme assay conditions was performed at 4°C using a BioCAD Sprint perfusion chromatography system (Applied Biosystems) with an analytical Bio-Silect SEC250 column (300 mm x 7.8 mm, Bio-Rad). The column was equilibrated and eluted in filtered and degassed SEC buffer (50 mM KP$_i$, 75 mM NaCl, pH 7.25). Prior to injection, each mutant PurQ was incubated in FGAR-AT assay buffer at 100 μM for 5 min at 37°C in the absence of PurS and smPurL. The sample was then applied to the column using a 100-μL injection loop and eluted with a flow rate of 1 mL/min. Peak volumes were determined by integration with Kaleidagraph software (Synergy).

Expression of histag-A128T and histag-WT PurQ in B. subtilis

Histag-A128T-PurQ in plasmid pET-28a contained the A128T PurQ gene and a N-terminal hexahistidine tag (MGSSHHHHHHSSGLVRGSH-) and was a gift of the Ealick Laboratory, Cornell University. The tagged construct was amplified using PCR, the Kod HiFi Polymerase (Novagen), and the primers Q-HindIII (5'-GC**AAGCTT**T<u>AAGGAGG</u>AAGCAGGTATGGGCAGCAGCCATCAT-3') and Q-SphI (5'- GC**GCATGC**TCAAGCAGTAGTGACATGAGTTTCCC-3'). The forward primer incorporates both a 5' HindIII restriction site (bold) and an optimized *B. subtilis* ribosomal binding site (underlined) (*9*). The reverse primer incorporates a 3' SphI cleavage site (bold).

257

In order to express histag-PurQ in *B. subtilis*, the PCR product was digested with HindIII and SphI and ligated into the pDG148 vector (*9*) digested with the same enzymes. This vector is commonly used for expression of proteins in *B. subtilis*. The ligation product was transformed into DH5α *E. coli* grown on 50 μg/mL ampicillin, and plasmids containing the insert (pDG148-his-A128T-PurQ) were isolated and sequenced. The plasmid containing the wt PurQ sequence (pDG148-his-wt-PurQ) was made by Quikchange mutagenesis (Stratagene) of the pDG148-his-A128T-PurQ plasmid using the T128A primers (Table 5.1).

In order to obtain plasmid DNA suitable for transformation of *B. subtilis*, plasmids were transformed into the *recA* mutant *E. coli* strain AG1111 (*araD139 (ara-leu)7697 lacX74 galU galK rpsL hsdR F' proAB+ lacIq lacZM15 Tn10*, Grossman Laboratory, MIT) grown on 50 μg/mL ampicillin and plasmids were isolated using standard miniprep and maxiprep procedures (Qiagen).

B. subtilis strain AG174 (*trpC2 pheA1*, Grossman Laboratory) was transformed using a procedure developed by the Grossman Laboratory (MIT). A single colony was used to inoculate 5 mL of LB media and allowed to grow overnight at 37°C to saturation. This culture (100 μL) was then used to inoculate 3 mL of LB media and the bacteria allowed to grow at 37°C for ~ 2 h until OD_{600} = 1.0. A portion of this culture (0.5 mL) was then used to inoculate 9.5 mL of MD media in a 125 mL flask (MD media contains 9.3 mL 1.1x PC media (10x PC media contains 107 g/L K_2HPO_4, 60 g/L KH_2PO_4, 10g/L trisodium citrate dihydrate, adjusted to pH 7.5 with KOH), 0.4 mL 50% glucose, 0.188 mL 100 mg/mL potassium aspartate, 37.5 μL 10 mg/mL L-tryptophan, 37.5 μL 10 mg/mL L-phenylalanine, 37.5 μL 2.2 mg/mL ferric ammonium citrate, and 22.5 μL 1 M

MgSO$_4$). The flask was shaken at 37°C for 4 h, after which time the bacteria were competent for DNA transformation.

Cells were transformed by mixing 0.3 mL of the competent cells with 5-50 μg of plasmid DNA and incubating at 37°C for 30 min before plating on LB/agar plates with 2.5 μg/mL neomycin. After overnight incubation at 37°C, single colonies were used to inoculate 5 mL of LB with 20 μg/mL kanamycin and allowed to grow overnight at 37°C. Cells from the liquid culture were streaked onto LB/agar plates containing 20 μg/mL kanamycin and incubated as before. The resulting colonies were used to inoculate cultures for expression of histag PurQs.

Expression of histag-A128T or histag-wt PurQ was performed by addition of IPTG to *B. subtilis* cells transformed with the appropriate plasmid during growth at 37°C in minimal media (see Chapter 4) containing 20 μg/mL kanamycin. IPTG was added to a final concentration of 0.1 mM when the cells reached an OD$_{600}$ of 0.1, and growth was allowed to proceed until an OD$_{600}$ of 0.7-0.9 was reached at which time the cells were harvested and frozen. Expression levels of the histag-PurQs was monitored by Western blotting as described in Chapter 4, and the expression conditions described above resulted in expression levels that closely match that of the wt protein.

Use of a Ni^{2+}-Affinity Column to Isolate the FGAR-AT Complex

Cells (~0.5 g) were resuspended in 4 mL of PD buffer (50 mM HEPES pH 7.2, 1 mM imidazole, 80 mM KCl, 20 mM MgCl$_2$). Experiments were also conducted with PD buffer containing 0.1 mM ADP and/or 20 mM glutamine. When added, these compounds were present at all stages of the experiment. Control experiments were performed using identical procedures with *B. subtilis* cells not transformed with pDG148-his-wt-PurQ or

pDG148-his-A128T-PurQ. Lysozyme (Sigma) was added to the cell suspension to a final concentration of 10 mg/mL, and the solution was stirred at 37°C for 15 min followed by brief sonication of the reaction mixture on ice for 30 s at 50% power (3/32" microprobe, VirSonic100, Virtis). The lysate was then cleared by centrifugation at 14,000 rpm at 4°C for 10 min.

The resulting supernatant (3.8mL) was combined with 1 mL of Ni-NTA resin (Qiagen) equilibrated in the appropriate PD buffer. The supernatant was slurried with the resin for 1 h at 20°C with gentle rocking. The resin was then placed into a 1 x 5 cm disposable column (Bio-Rad) and the supernatant removed by gravity flow. The resin was washed with 25 mL of PD buffer, followed by 25 mL of PD buffer with 15 mM imidazole until no protein could be detected in the eluate by Bradford assay. Proteins were eluted with 5 mL of 300 mM imidazole in PD Buffer and analyzed by Western blotting using procedures described in Chapter 4.

A slightly altered procedure was used to study the effects of DON-inactivation on the isolation. Cells were resuspended in PD buffer (without ADP or glutamine) and lysed as described above. Following centrifugation, the supernatant was brought to 0.1 mM ADP, 10 mM ATP, 10 mM DON, and 1 mM FGAR. The lysate was then incubated for 15 min at 37°C. A small amount of precipitate formed during this time and was removed by brief centrifugation. The resulting solution was then mixed with Ni-NTA resin, and the procedure was followed as described above using PD buffer in all the subsequent steps.

5.3 Results

PurQ Mutagenesis and Mutant Protein Expression

Mutagenesis using the Quikchange protocol was used to prepare PurQs containing mutations in either the conserved triad residues (C86A, C86S, H194Q, E196D, E196Q, and E196A) or to glutamine binding residues (D55N, D55A, Q90E, and Q90A) based upon homology to the *Salmonella* lgPurL crystal structure (Figure 5.2). Given the problems encountered in attempting to purify the wt PurQ enzyme (Chapter 3), all of the mutant PurQs were in the A128T PurQ background.

The PurQ double mutants were grown, expressed, and purified using the protocols for A128T PurQ with some minor modifications (see Experimental). Typical yields for each mutant were 10 mg/g cells. The PurQ mutants were judged to be >90% pure based upon SDS-PAGE analysis (Figure 5.3) and the identity of each mutant was confirmed by ESI-MS (Table 5.2).

Table 5.2: ESI-MS Results for PurQ Mutants

Protein	Calculated MW	Observed MW
A128T	24814.1	24816.0
C86S/A128T	24798.1	24801.4
C86A/A128T	24782.1	24785.4
D55N/A128T	24813.2	24816.6
D55A/A128T	24770.1	24773.2
Q90A/A128T	24757.1	24760.4
Q90E/A128T	24815.1	24818.3
H194Q/A128T	24805.1	24801.5
E196D/A128T	24800.1	24807.5
E196A/A128T	24756.1	24751.5
E196Q/A128T	24813.2	24807.0

Kinetic Characterization of PurQ Mutants

The activity of the PurQ mutants were determined using using the Bratton-Marshall assay in the presence of smPurL and PurS to monitor glutamine-dependent

261
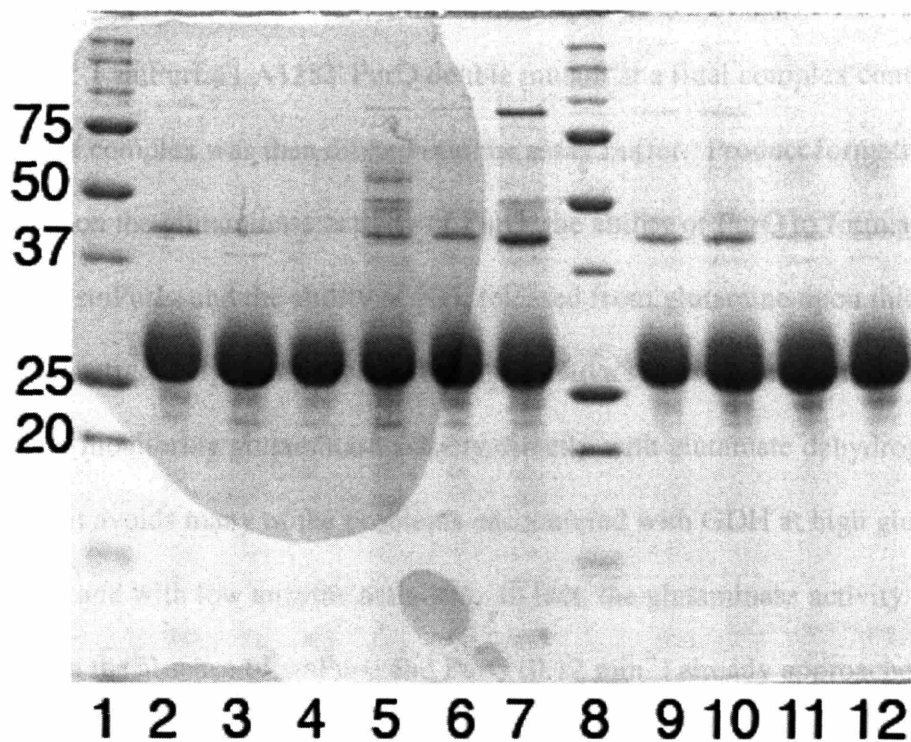
Figure 5.3—15% SDS-PAGE of the purified A128T double mutant PurQs. (Lanes 1 and 8) Bio-Rad MW markers, (Lane 2) C86A, (Lane 3) C86S, (Lane 4) H194Q, (Lane 5) E196A, (Lane 6) E196D, (Lane 7) E196Q, (Lane 9) D55A, (Lane 10) D55N, (Lane 11) Q90A, (Lane 12) Q90E. Approximately 2 μg of protein was loaded into each well. A128T PurQ typically runs slightly heavier than its true molecular weight (24.8 kDa).

FGAM formation. With each mutant, the FGAR-AT complex was reconstituted by mixing 2 PurS: 1 smPurL; 1 A128T PurQ double mutant at a final complex concentration of 10 μM. The complex was then diluted into the assay buffer. Product formation in this assay depends on the glutaminase activity of PurQ, the ability of PurQ to form a complex with PurS and smPurL, and the ability of NH_3 released from glutamine upon thioester formation to be effectively transferred between the active sites. The advantage of using this assay over monitoring glutaminase activity directly with glutamate dehydrogenase (GDH) is that it avoids many of the problems encountered with GDH at high glutamine concentrations and with low enzyme activities. In fact, the glutaminase activity of A128T PurQ in the absence of smPurL and PurQ (0.12 min^{-1}) already approaches the lower limit of detection ~0.05 min^{-1} for the assay. In addition, the low glutaminase activities observed with the PurQ mutants were difficult to distinguish from an *E. coli* glutaminase that often co-purifies with PurQ (see Chapter 3). By monitoring FGAM formation, specificity for glutaminase activities related only to the PurQ mutants was obtained.

The effects of the mutations on PurQ enzymatic activity matched predictions based on studies of other triad ATs including carbamoyl phosphate synthase (CPS), PABA Synthase (PabAB), and anthranilate synthase (*2, 3, 10-14*). Mutation of Cys86, involved in covalent-catalysis, to either a serine or an alanine inactivated the enzyme (lower limit of detection <0.001 s^{-1}). H194, thought to be required for deprotonation of the catalytic cysteine was mutated to glutamine, was also found to be inactive (Table 5.3). This phenotype of the analogous histidine to glutamine mutation has been previously observed in CPS and PabAB (*3, 15*). It is interesting to note that while

mutation of the triad residue E196 to either an aspartate or a glutamine inactivated the

protein, the alanine mutant retained considerable activity ($k_{cat} = 0.38$ s^{-1}), 10% of the

A128T PurQ (Table 5.3). These results indicate that E196 is not essential for activity,

consistent with results from the corresponding mutants in PabAB and CPS (*2, 3*).

Subsequent experiments designed to monitor PurQ aggregation (SV-AUC and SEC)

revealed that the E196Q mutant was extensively aggregated during these experiments;

consequently, work on this particular mutant was not pursued further.

Table 5.3: Kinetic Parameters for the PurQ Mutants
determined during FGAM Synthesis^a

Mutant	K_m Gln (mM)	k_{cat} (s^{-1})
A128T	1.3	2.5
C86S/A128T	ND^b	ND
C86A/A128T	ND	ND
D55A/A128T	ND	ND
D55N/A128T	5.7	0.0307
Q90A/A128T	~72	~0.054
Q90E/A128T	~282	~0.5322
H194Q/A128T	ND	ND
E196A/A128T	34	0.38
E196Q/A128T	ND	ND
E196D/A128T	ND	ND

^{a}Kinetic parameters were determined using the
Bratton-Marshall assay to monitor FGAM formation
from a 2 PurS: 1 smPurL: 1 PurQ mutant complex.
^{b}ND = no detectable activity

Predictably, mutation of residues thought to interact with the carboxylate (Q90)

and amino (D55) moieties of glutamine resulted in enzymes with elevated $K_{m(gln)}$ values

and reduced k_{cat}s. Only in the case of the D55N mutation could an actual rather than an

apparent K_m and k_{cat} be determined (Table 5.3) due to problems saturating the mutants

with glutamine (as shown in Figure 5.4 for the Q90A mutant).
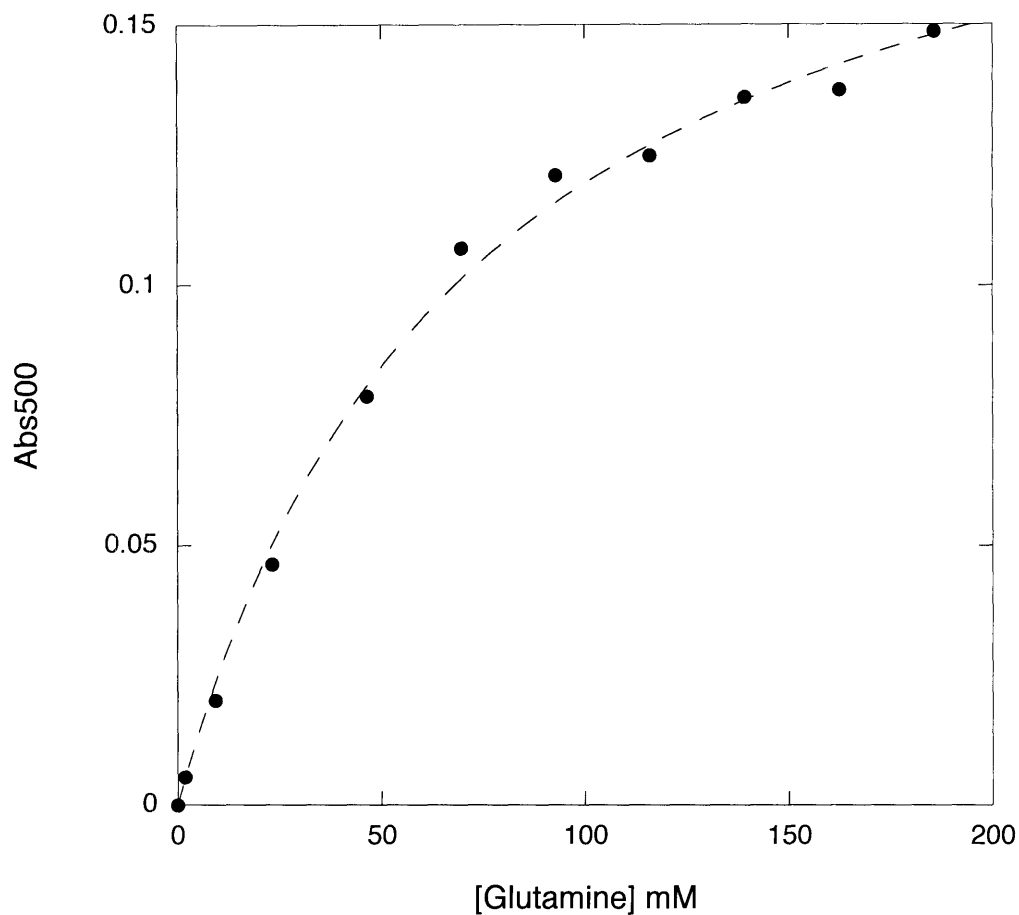
Figure 5.4—Determination of the K_m for glutamine for the Q90A mutant PurQ. As was typical of many of the PurQ mutants, the enzyme could not be saturated with glutamine due to the solubility limit of the substrate (200 mM). Therefore, an approximate K_m was determined (~72 mM).

Competition Experiments between A128T PurQ and Glutamine-Binding Mutants

The ability of each mutant PurQ (D55A, D55N, Q90A, and Q90E) to form a

FGAR-AT complex during turnover was assessed using competition assays against wt

PurQ. Based on observations from Chapter 3 in which glutamine is necessary for

complex assembly, it was predicted that the mutant's ability to compete with the wt

protein should be dependent on its ability to bind glutamine, as reflected by its K_m. In

addition, if the mutant becomes saturated with glutamine, then it should be able to

interact with smPurL/PurS with the same affinity as the wt enzyme, resulting in a 50%

inhibition of activity with the addition of 1 equivalent of mutant.

This hypothesis was first tested with the D55N PurQ mutant ($K_m = 5.7$ mM). At

20 mM glutamine, the mutant showed competitive behavior with A128T PurQ (Figure

5.5A). A reciprocal plot shows that the data can be fit to a straight line (Figure 5.5B),

and predicts that 1 equivalent of D55N results in 28% inhibition of activity. Increasing

the glutamine concentration to saturate the D55N mutant results in an increase in the

competitive behavior (Figure 5.5A). A fit to this data (Figure 5.5B) indicates that at

saturating glutamine concentrations, 1 equivalent of D55N can now inhibit activity by

45%. Thus, under saturating glutamine concentrations the D55N mutant is acting as a

competitive inhibitor of A128T PurQ. This result confirms previous findings for the

importance of glutamine-binding to formation of the FGAR-AT complex.

Unfortunately, analysis of the other glutamine-binding mutants (D55A, Q90E,

and Q90A) is not as straightforward. Accurate K_ms for glutamine could not be

determined for either Q90A or Q90E, and the K_d for glutamine could not be determined
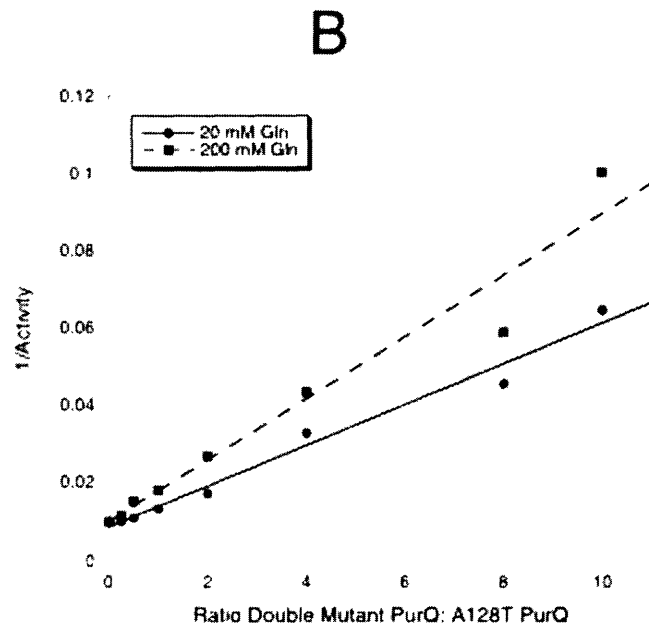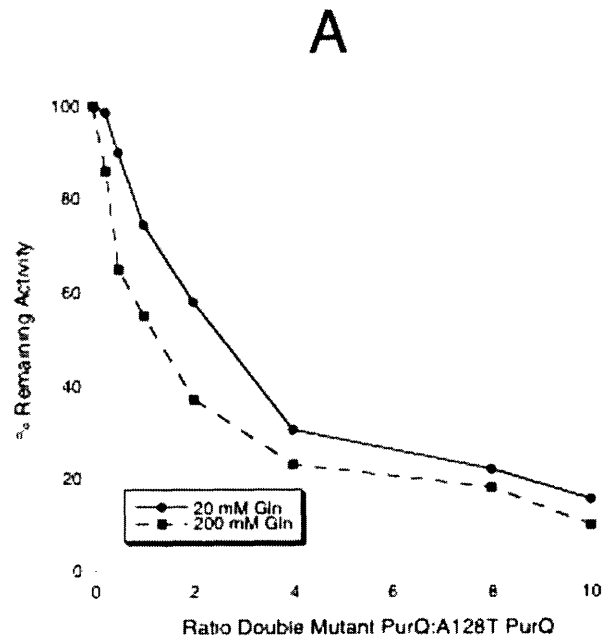
Figure 5.5—Competition assays with the D55N PurQ mutant at 20 and 200 mM glutamine. (A) The D55N mutant (K_m 5.7 mM) was competitive with A128T PurQ at 20 mM glutamine. The mutant became more competitive at a saturating level of glutamine (200 mM). (B) A reciprocal plot shows that the inhibitory effects of the D55N mutant can be fit to a straight line (y = 0.0053x + 0.00087, R^2 = 0.98 at 20 mM glutamine and y = 0.0079x + 0.0101, R^2 = 0.95 at 200 mM glutamine).
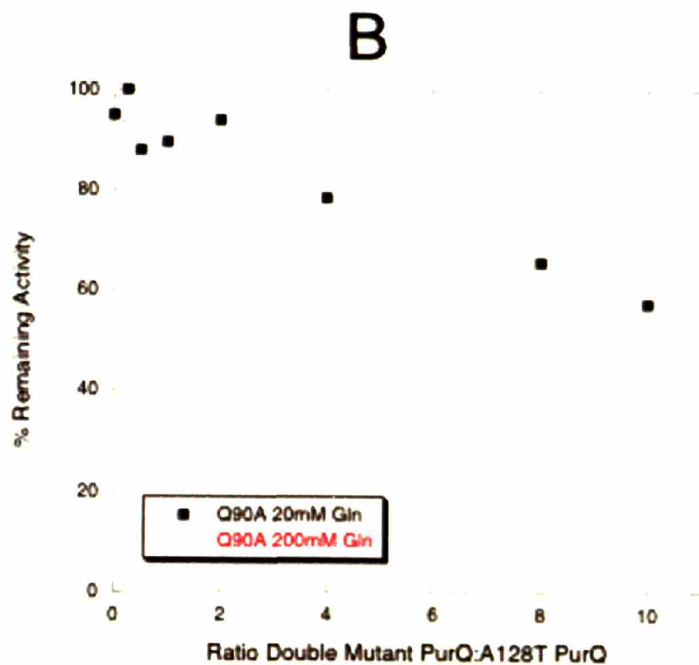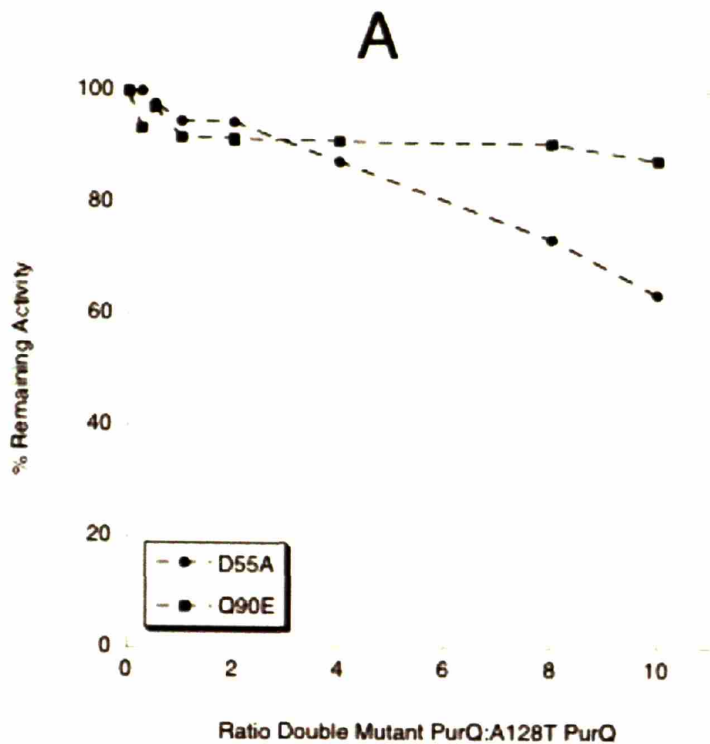
Figure 5.6—(A) Competition results for the inactive D55A mutant and the Q90E mutant (K_m ~282 mM). (B) The Q90A mutant (K_m ~ 72 mM) showed an increase in competitive behavior at 200 mM glutamine compared to 20 mM.

for the inactive D55A mutant. The Q90E mutant (K_m ~282 mM) was not competitive with A128T PurQ (Figure 5.6A); however, a large enough amount of glutamine could not be added to the solution to determine if it is a competitive protein under saturating conditions. Results obtained for Q90A (K_m ~72 mM, Figure 5.6B) indicated that it does possess some glutamine-dependent increase in competitive behavior; however, this enzyme could also not be saturated with substrate under the assay conditions.

Competition Assays between A128T PurQ and Conserved Triad Mutants

Competition assays were also carried using PurQs containing mutations to the conserved triad residues C86, H194, and E196. Unfortunately, since all of these mutants except E196A are inactive, glutamine K_ms could not be determined. Efforts to measure glutamine binding by other methods such as isothermal titration calorimetry (ITC) and fluorescence titration were unsuccessful. Thus, all of the experiments reported below contain the caveat that the amount of glutamine bound to PurQ is unknown; however, it is assumed that the mutants exhibit similar glutamine-binding properties as A128T PurQ and are saturated under the experimental conditions.

As shown in Figure 5.7A, the C86A and C86S double mutants were both competitive with A128T PurQ. Reciprocal plot analysis of the data (Figure 5.7B) indicates that the inhibition of activity observed with the C86 mutants is linear and that 1 equivalent of C86A or C86S is enough to decrease the observed activity by 54% and 45%, respectively. The simplest interpretation of the data is that the mutants are acting as competitive inhibitors of A128T PurQ and can interact with smPurL and PurS with comparable affinity as A128T PurQ. The ability of the C86A mutant to form a FGAR-
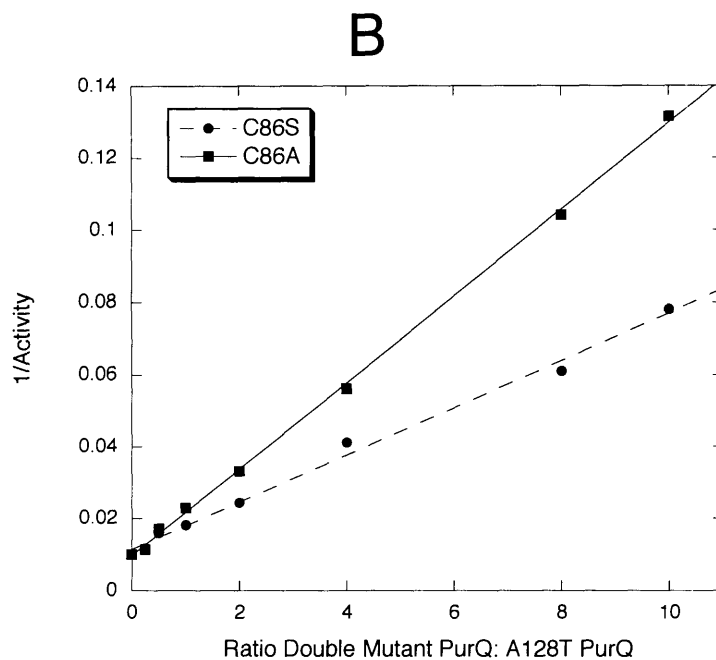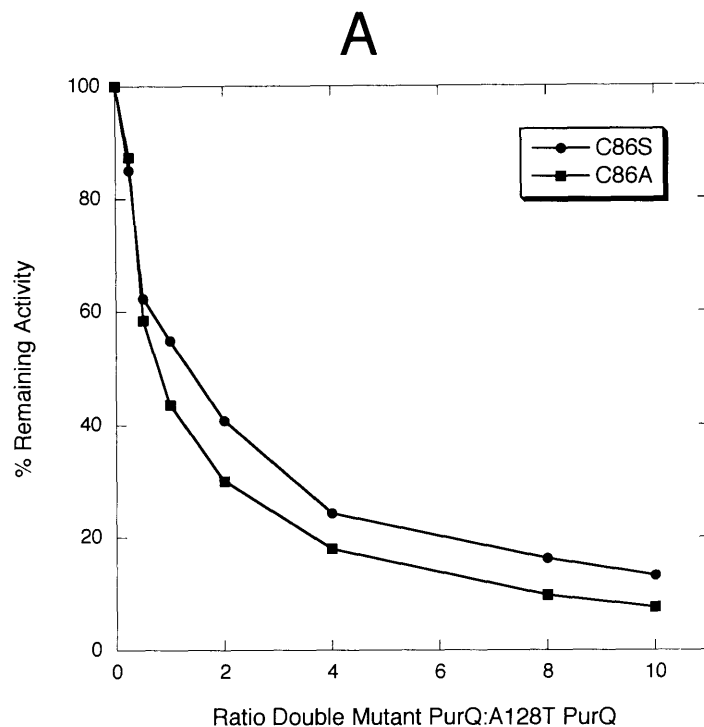
Figure 5.7—Inhibition of wt A128T PurQ FGAR-AT complex formation by C86X A128T Pur mutants in the presence of 20 mM glutamine. (A) Both C86A and C86S double mutants competed effectively with A128T PurQ. (B) A reciprocal plot showed that the inhibitory effects of each mutant can be fit to a straight line (y = 0.01201x + 0.00097, R^2 = 0.99 for the C86A mutant and y = 0.00657x + 0.011436, R^2 = 0.99 for the C86S mutant).

AT complex is particularly informative since it indicates that a covalent PurQ-glutamine complex is not essential for FGAR-AT complex formation during turnover conditions. Similar results have been obtained by Walsh and coworkers on PabAB using a C79S mutation (*3*).

Competition assays with the inactive H194Q PurQ showed that it is also able to compete with A128T PurQ, and ~8 equivalents are necessary to decrease the observed activity by 50% (Figure 5.8A). Surprisingly, none of the E196 mutants are competitive with wt PurQ at either 20 or 200 mM glutamine (Figure 5.8B). E196A, in particular, warrants further investigation since this is an active enzyme, capable of supporting FGAM synthesis with only a 10-fold decrease in k_{cat}. The K_m for glutamine for this enzyme is 34 mM, and at 200 mM glutamine, the glutamine binding site is saturated. If E196A formed an FGAR-AT complex under these conditions, one would have expected only ~10% remaining activity at a ratio of 10:1 mutant:A128T PurQ. However, no significant loss of activity is observed (Figure 5.8B). These results indicate that the E196A mutation substantially alters interactions between PurQ and smPurL/PurS and suggests that E196 may play an important role in complex formation.

Biophysical Characterization of PurQ Mutants

The necessity for altered expression and purification protocols for several PurQ mutants due to aggregation and solubility problems prompted an investigation of the PurQ mutant proteins by CD spectroscopy, SV-AUC, and analytical SEC. CD spectra of the A128T PurQ displayed features at 208 and 220 nm (Figure 5.9A). These features

271

A

B
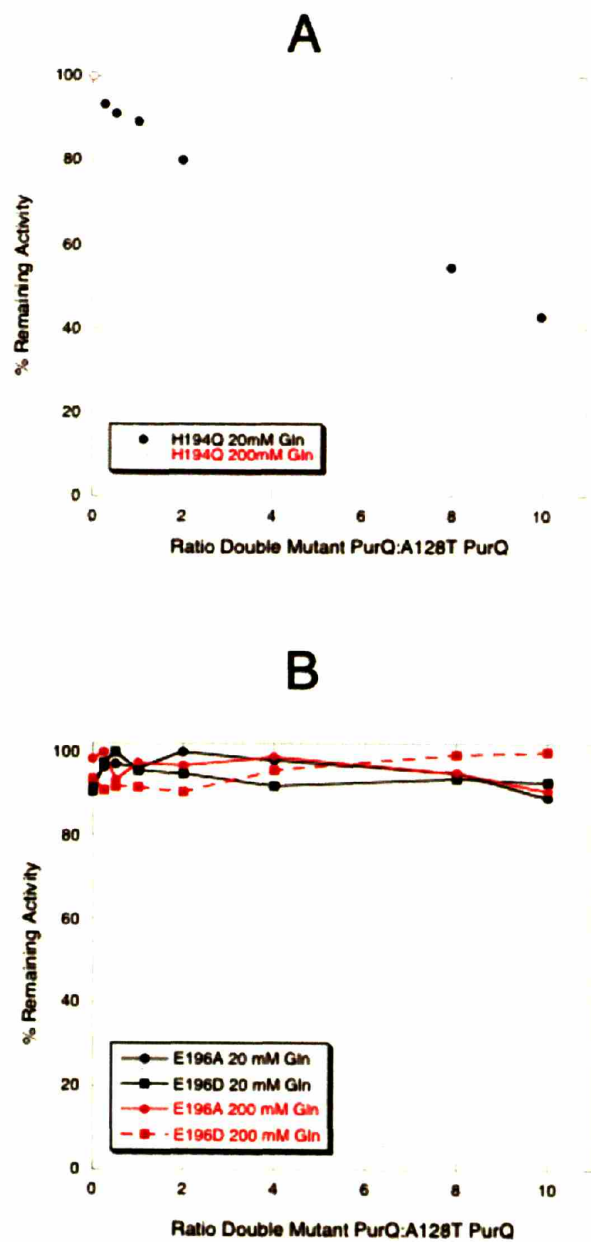
Figure 5.8—Competition assays between conserved triad residue PurQ double mutants (H194Q, E196A, E196D) and A128T PurQ. (A) H194Q, which is inactive, was partially competitive with A128T PurQ at 20 mM glutamine (black), and a slight increase in competitive behavior was observed at 200 mM glutamine (red). (B) The E196 mutants were not competitive with A128T PurQ at either 20 or 200 mM glutamine.

were similar in all mutants studied (C86A, C86S, H194Q, D55A, D55N, Q90A, and

Q90E) except for E196. E196A, D, and Q PurQs all show a sharpening at 208 nm,

indicating an increase in either the α-helical or random coil content of the protein relative

to A128T PurQ (Figure 5.9B).

SV-AUC experiments were then used to determine whether PurQ mutants have

aggregated and if so, to what extent. As listed in Table 5.4, the amount of aggregate

present in each sample varied greatly. In particular, the C86 and E196 mutants contained

large amounts of aggregate by SV-AUC (Figure 5.10A and B). Furthermore, the

inclusion of glutamine in the SV-AUC experiment did not substantially alter the amount

of aggregate present in the C86 mutants (Figure 5.11). The results with the C86 mutants

are inconsistent with results from the competition experiments described above. Based

on the level of aggregation observed by SV-AUC, substantial increases in the amount of

PurQ mutant needed to achieve 50% inhibition would have been expected. An alternate

method was used to determine the amount of aggregate in PurQ samples under conditions

used for the competition experiments.
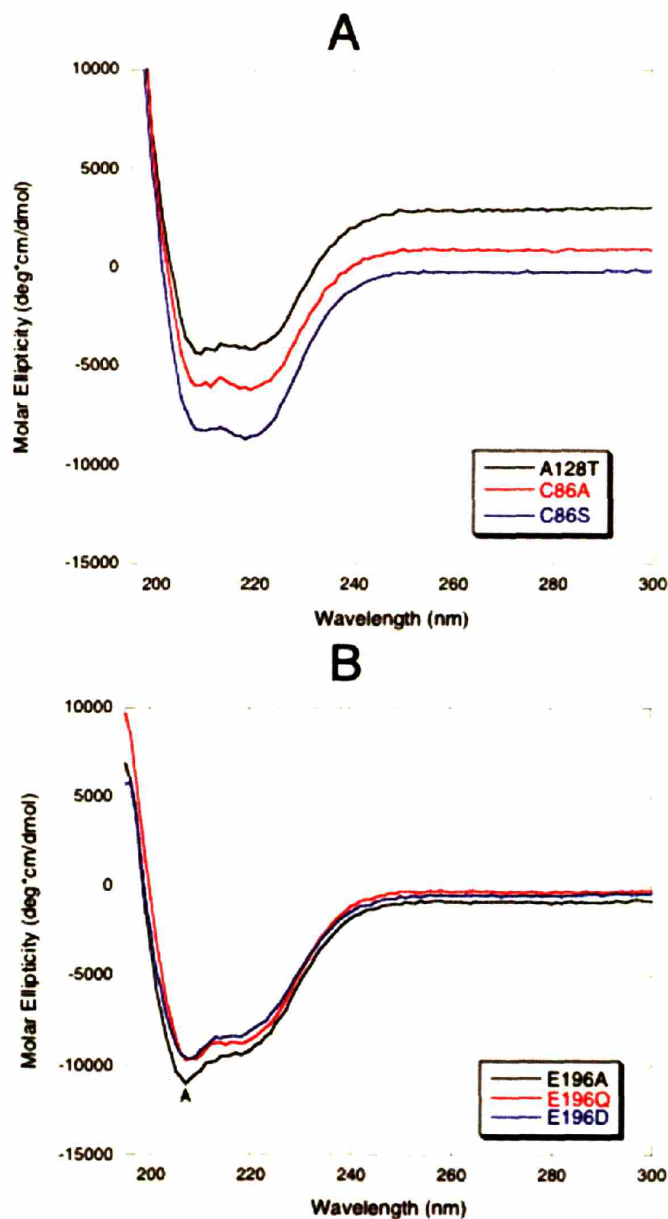
Figure 5.9—CD spectra of A128T and double mutant PurQs. (A) Most of the PurQ mutants show CD spectra similar to A128T PurQ. The spectra of A128T PurQ is characteristic of a mixed α/β-protein with features at 208 and 220 nm. The CD spectra of all the double mutants except for those to E196 are similar to that of A128T, and data for the C86A and C86S mutants are shown (data is offset for easier comparison). (B) CD spectra of the E196 mutant proteins show a sharpening and increase in the 208 nm feature relative to the 220 nm peak (arrow). This indicates an increase in either the α-helical or random coil content of the mutant proteins.

274
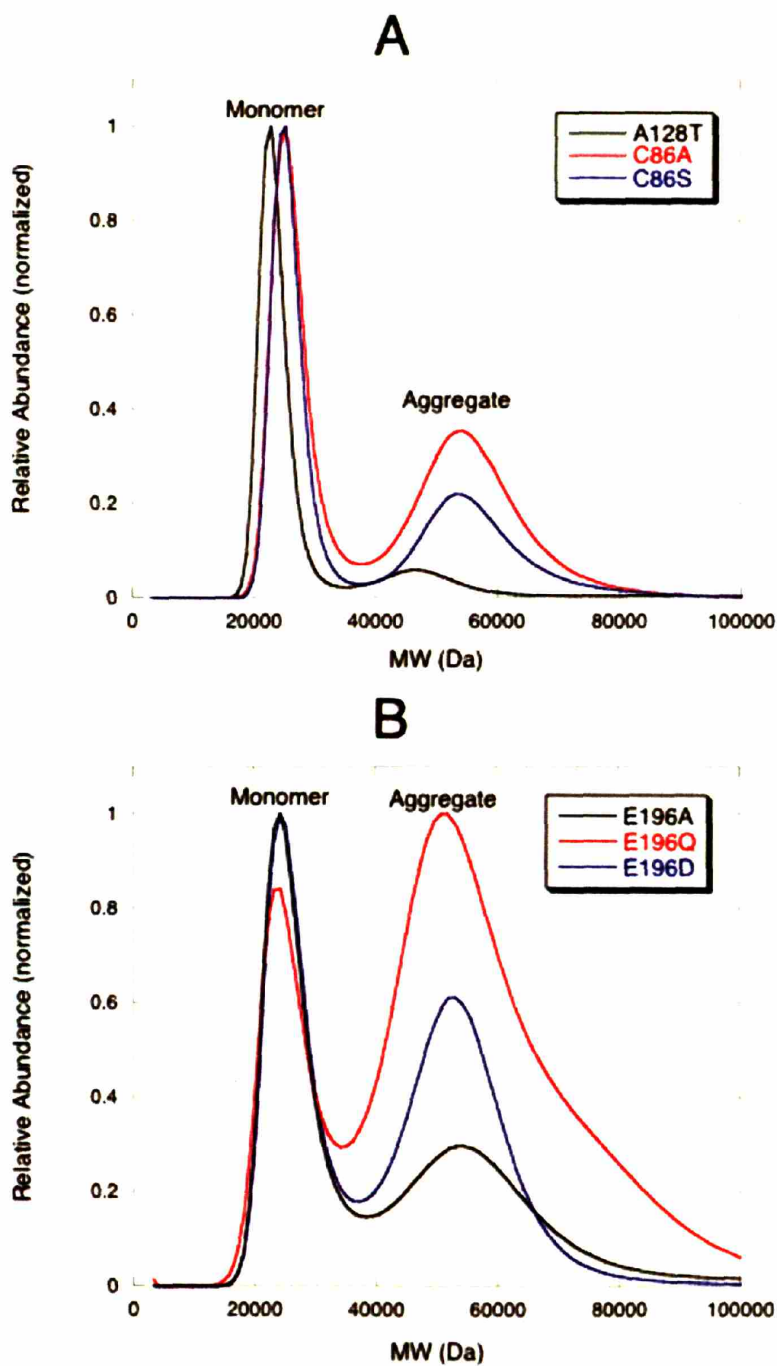
Figure 5.10—Quantitation of the amount of aggregate present in PurQ mutants by SV-AUC. (A) The distribution of species present in solution for the A128T (black), C86A/A128T (red), and C86S/A128T proteins (blue). (B) The E196 double mutants contained substantially more aggregate than other mutations.
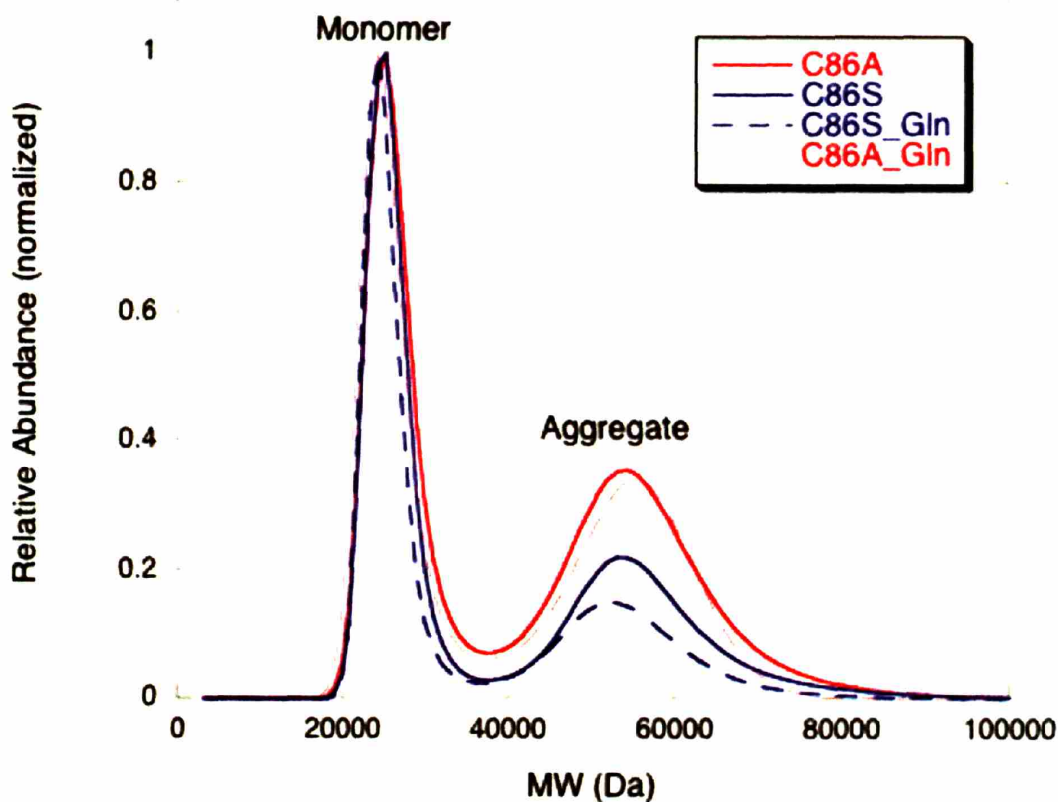
Figure 5.11—Efforts to try to reverse or prevent aggregate formation by inclusion of glutamine in the SV-AUC experiment. SV-AUC was carried out in the presence of 50 mM glutamine with the inactive C86A and C86S double mutant PurQs. Comparison of experiments in the presence (dashed lines) and absence (solid lines) of glutamine shows that it had little effect on the aggregate content.

Table 5.4: Quantitation of Aggregated Species Present in Mutant PurQs by SV-AUC and SEC

Mutant	Active	% Aggregate by SV-AUC	% Aggregate by SEC
A128T	Yes	15	8[a]
C86S/A128T	No	41	8
C86A/A128T	No	50	15
D55A/A128T	No	24	ND[b]
D55N/A128T	Yes	31	ND
Q90A/A128T	Yes	7	ND
Q90E/A128T	Yes	8	ND
H194Q/A128T	No	13	ND
E196A/A128T	Yes	47	18
E196Q/A128T	No	78	53
E196D/A128T	No	57	16

[a]Determined from analytical SEC results presented in Chapter 3 [b]ND = not determined

The C86 and E196 PurQ mutants were incubated in FGAR-AT assay buffer for 5 min at 37°C, after which time the solution was applied to an analytical SEC column to determine the extent of protein aggregation. As shown in Figure 5.12A and B, the amount of aggregation observed using this method was significantly less for the C86A, C86S, E196A, and E196D mutants relative to what was observed by SV-AUC (Table 5.4). In addition, the extent of aggregation was comparable to that seen with A128T PurQ. These studies indicate that the mutants likely aggregated during the dialysis step prior to performing the SV-AUC experiment. The E196Q mutant showed substantial amounts of aggregate using both methods, indicating that this mutant is highly prone to aggregation (Table 5.4).

Histag Affinity Purification of the FGAR-AT Complex from B. subtilis

The studies presented above and in Chapter 3 on heterologously-expressed and purified PurS, PurQ, and smPurL suggest that glutamine is essential in formation of the
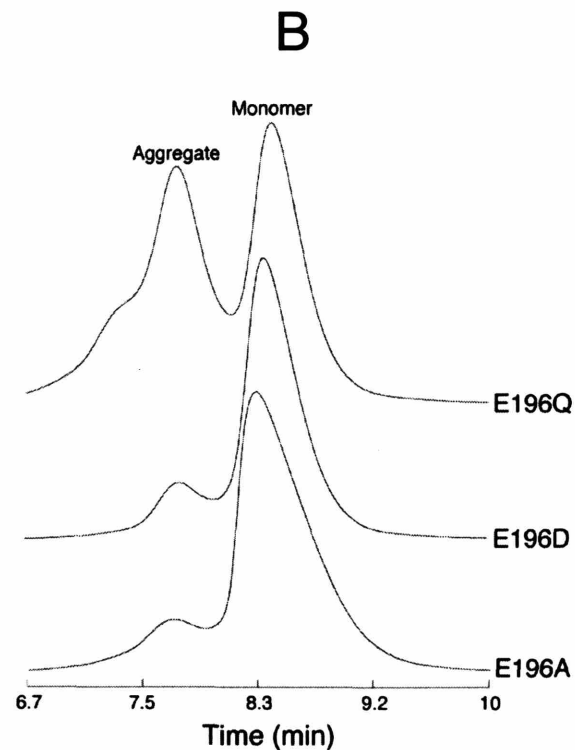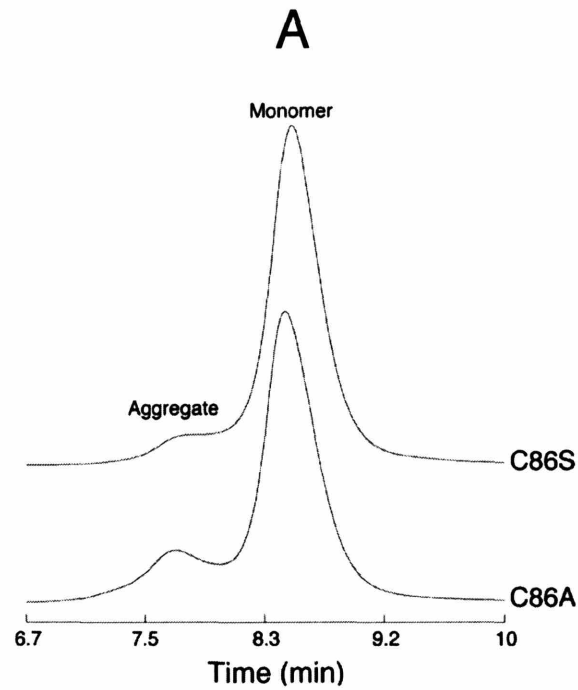
Figure 5.12—Analytical SEC analysis of the amount of aggregate present in C86 and E196 PurQ mutants during assay conditions. For the C86A, C86S, E196A, and E196D mutants, the amount of aggregate present is less than what was observed by SV-AUC, indicating that these mutants aggregated during dialysis or centrifugation. Large amounts of aggregate were observed by both SV-AUC and SEC for the E196Q mutant.

FGAR-AT complex. The complex formation occurs at relatively high concentrations of glutamine due to the high K_m exhibited by PurQ (1.3 mM). Given that the intracellular glutamine concentration in *B. subtilis* is also very high (1-7 mM) (*16*), this suggested that glutamine might also be important for formation of the FGAR-AT complex *in vivo*. In order to test this hypothesis, a method was developed to affinity purify the *B. subtilis* FGAR-AT from the native organism either in the presence or absence of glutamine with the use of a histidine-tagged PurQ. By comparing the amounts of PurS and smPurL isolated under the varying conditions, the impact of glutamine on isolation of the endogenous FGAR-AT can be addressed. Previous studies

have indicated that histag-A128T PurQ has the same activity as A128T PurQ and can reconstitute the FGAR-AT complex *in vitro* (data not shown).

In order to express histag-PurQ in *B. subtilis*, the gene was first placed into the pDG148 vector (*9*). This vector encodes low-copy origins of replication for both *E. coli* and *B. subtilis* allowing the vector to be propagated in *E. coli* before transformation into *B. subtilis*, which requires 5-50 μg of plasmid per transformation. Once inside *B. subtilis*, protein expression from pDG148 is under control of the *lac* promoter and can be induced with IPTG.

The histag-wt-PurQ and histag-A128T-PurQ genes were readily subcloned into pDG148. After transformation into *B. subtilis* strain AG174, it was determined that induction with 0.1 mM IPTG during log phase growth in minimal media gave expression levels of his-PurQ that closely matched that of the endogenous PurQ (~40μM, Chapter 4). Under these conditions, his-wt PurQ was expressed at a ratio of 0.8 $\pm$ 0.1 his-wt PurQ:1 endogenous PurQ, while histag-A128T-PurQ was expressed at a level of 0.9 $\pm$
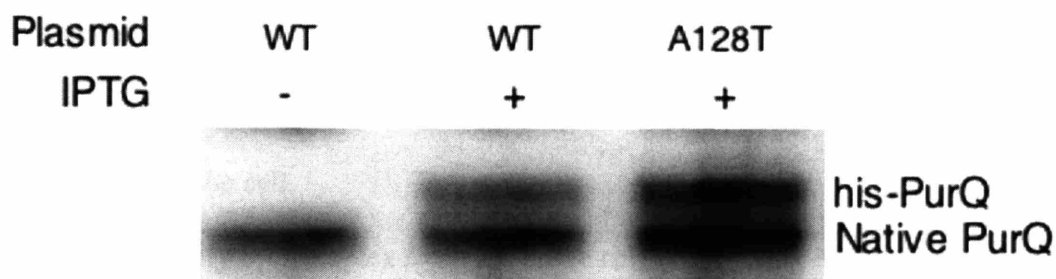
Figure 5.13—Induction of either his-wt-PurQ or his-A128T-PurQ in *B. subtilis* with IPTG. *B. subtilis* was transformed with plasmids containing either the his-wt-PurQ (WT) or his-A128T-PurQ (A128T) genes under control of an IPTG-inducible *lac* promoter. Expression levels compared to the endogenous proteins were determined by Western blotting to be 0.8 ± 0.1 his-wt PurQ:1 native PurQ and 0.9 ± 0.1 his-A128T-PurQ:1 native PurQ.

0.1 his-A128T PurQ:1 endogenous PurQ (Figure 5.13). Additional experiments showed that the expression of his-PurQ does not alter the expression levels of PurS or smPurL (data not shown). This means that his-PurQ and the endogenous PurQ are competing for PurS and smPurL in the cell.

Efforts to purify the complex from the crude cell lysate using Ni^{2+}-affinity chromatography were carried out under a variety conditions with either PD buffer, PD enriched with 0.1 mM ADP, enriched with 20 mM glutamine, or enriched with both ADP and glutamine. In addition, a similar experiment was carried out in the presence of the glutaminase-inhibitor DON. The results of these experiments are shown in Figure 5.14 and summarized in Tables 5.5-7. PurS is only isolated with histag PurQ in the presence of either glutamine or DON. Glutamine or DON-inactivation had little effect on the amount of smPurL isolated with the histag-A128T PurQ, but dramatically increased the amount isolated using histag-wt PurQ (Table 5.7). Based on these results, glutamine also plays a role in complex assembly for wt PurQ and between endogenous *B. subtilis* proteins.

It is also interesting to note that the presence of ADP in the buffer did not affect the amount of complex isolated (Figure 5.14, Lanes 1 and 2). Based on results from Chapter 3, it is likely that the endogenous smPurL already contains the ADP cofactor. Unlike smPurL over-expressed in *E. coli*, ADP appears to be tightly bound to the endogenous *B. subtilis* smPurL and did not dissociate during the purification.
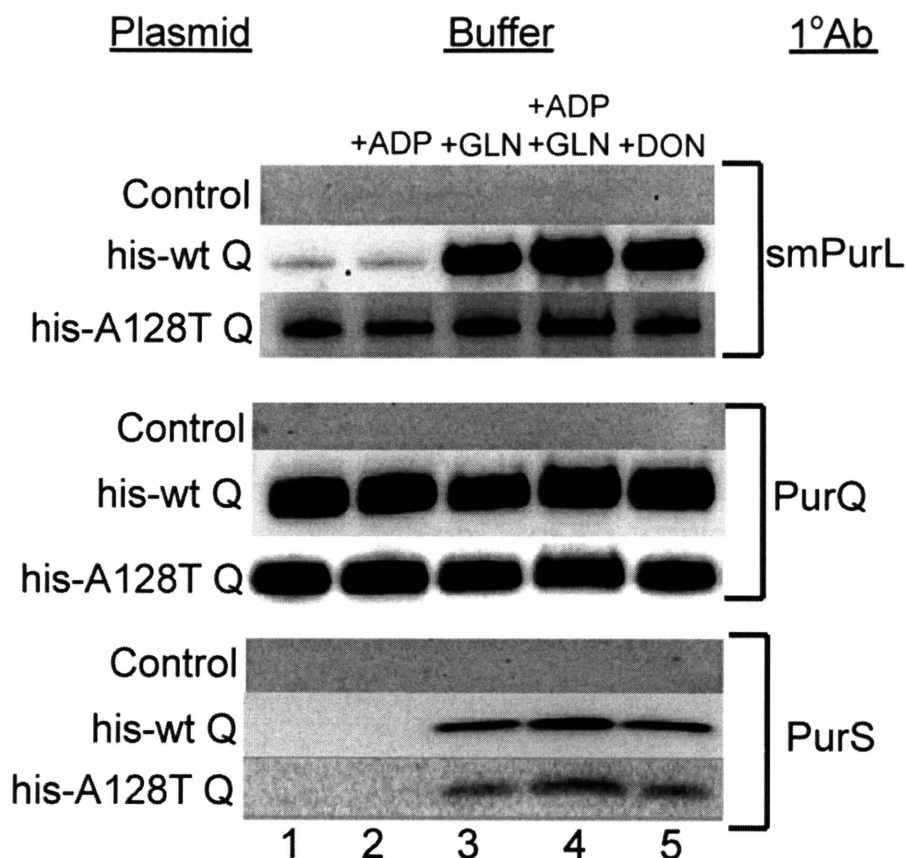
Figure 5.14—Results from the affinity purification experiments using histag PurQs. Affinity purifications were performed using *B. subtilis* transformed with either histag-wt-PurQ or histag-A128T-PurQ and a control containing no plasmid (left column). Purifications were performed with the same crude lysate under different conditions using either PD buffer (Lane 1), PD buffer with ADP and/or glutamine (Lanes 2-4), or by DON-inactivating the cell lysate (Lane 5). Proteins were then detected by Western blotting using the 1° Abs listed in the right column. The band intensities in each horizontal row are directly comparable. PurS could only be detected in experiments containing glutamine (Lanes 3 and 4) or when the cell lysate was DON-inactivated (Lane 5).

Table 5.5: Normalized Amounts of his-PurQ Isolated after Affinity Purification

Plasmid	Protein	--	+ADP	+Gln	+ADP/GLN	+DON
			PD Buffer Components			
His-wtQ	PurQ	1.03	0.89	0.71	1	0.99
His-A128T Q	PurQ	1.05	1.21	0.98	1	0.97

Table 5.6: Normalized Amounts of PurS Isolated after Affinity Purification

Plasmid	Protein	--	+ADP	+Gln	+ADP/GLN	+DON
			PD Buffer Components			
His-wtQ	PurS	ND	ND	0.84	1	0.66
His-A128T Q	PurS	ND	ND	0.55	1	0.68

Table 5.7: Normalized Amounts of smPurL Isolated after Affinity Purification

Plasmid	Protein	--	+ADP	+Gln	+ADP/GLN	+DON
			PD Buffer Components			
His-wtQ	smPurL	0.04	0.09	0.94	1	0.70
His-A128T Q	smPurL	0.73	0.54	0.91	1	0.83
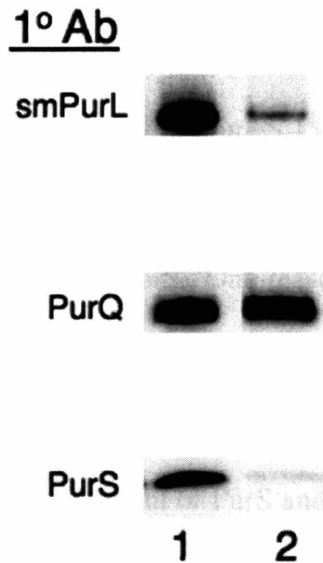
Figure 5.15—Analysis of the ratio of PurS:PurQ:smPurL obtained in the affinity purification experiments by Western blotting. Lane 1 contains a standard with a ratio of 2 PurS: 1 smPurL: 1 A128T PurQ. Lane 2 is the complex isolated with his-wt-PurQ in the presence of ADP and glutamine. Band intensities in lanes 1 and 2 are directly comparable and each lane contains approximately the same amount of PurQ.

While the results from the affinity purification experiments are intriguing, these experiments had several faults. First, FGAM synthesis could not be detected in any of the isolated complexes. Second, as shown in Figure 5.15, a 2 PurS: 1 smPurL: 1 PurQ complex was not isolated. With both the histag-wt and histag-A128T PurQs, the histag PurQ was in large excess of smPurL and PurS. One reason for the inability to isolate a 2:1:1 complex is due to the presence of both histag and endogenous PurQ in the cell. Based upon quantitative Western blotting results from cells grown in minimimal media (Chapter 3), this limits the maximum amount of PurS and smPurL that can be isolated with histag PurQ to ~1 PurS: 0.5 smPurL: 1 PurQ. Still, analysis of the results presented in Figure 5.15 indicate that the amount of PurS and smPurL isolated falls well-below these values, with an estimated yield of ~10%. The lack of a 2:1:1 complex likely explains the inability to detect activity in the isolated complexes and indicates that the FGAR-AT complex may be dissociating during the affinity purification. Future attempts to isolate the *in vivo* FGAR-AT complex may benefit from the construction of a gene knockout strain of *B. subtilis* to remove the endogenous PurQ and the use of a higher-affinity FLAG or myc-tag to facilitate active complex purification.

5.4 Discussion

The *B. subtilis* FGAR-AT is unique among triad glutaminases for several reasons including the fact that it is the only triad AT that requires an auxiliary protein with no enzymatic activity (PurS) for function. In addition, while high levels of activity can be obtained from the reconstituted FGAR-AT with a protein ratio of 2 PurS: 1 smPurL: 1 A128T PurQ, the protein complex can only be isolated in the presence of Mg^{2+}-ADP and glutamine (Chapter 3). Structural analysis of the *Salmonella* lgPurL and homology

modeling of the *B. subtilis* smPurL indicate that ADP is acting as a structural cofactor (*5,*

17). The necessity for glutamine for complex assembly is less clear since most ATs do

not require glutamine for interaction between the glutaminase and AT domains (or

proteins). The results of this reconstitution are strikingly similar to those required to

isolate a PabAB complex. PabAB catalyzes formation of 4-amino-4-deoxychorismate

from chorismate and glutamine during the first step of *p*-aminobenzoate synthesis (Figure

5.1), with PabA catalyzing the glutaminase activity and PabB the AT activity. PabAB is

the only other AT system exhibiting weak protein interactions between the AT and

glutaminase. In this case, pre-incubation of the proteins with glutamine is also required

to isolate a complex by SEC (*18*), and it has recently been discovered that PabB contains

a tightly bound tryptophan that may be acting as a structural co-factor analogous to ADP

in smPurL (*19*).

Glutamine Binding but Not an Active PurQ is Important for FGAR-AT Complex

Formation during Turnover Conditions

Initial studies using SEC analysis indicated that glutamine is required to detect

complex formation in the FGAR-AT. To provide additional evidence for the necessity of

glutamine binding to PurQ for complex assembly, competition assays between mutant

PurQs with altered glutamine-binding properties and A128T PurQ were used. The model

predicts that mutant PurQs that cannot bind glutamine would be unable to compete with

A128T PurQ and consequently decrease FGAM synthesis activity. However, upon

saturation of the mutant with glutamine, the ability to compete should be restored. This

hypothesis was tested with the D55N PurQ mutant (Figure 5.5). When the mutant was

not saturated with glutamine, 1 equivalent of D55N only decreased the activity by 28%.

Under saturating conditions, the mutant became a stronger inhibitor of FGAM synthesis and 1 equivalent could decrease the observed activity by 45%. Similar experiments were attempted with the D55A, Q90A, and Q90E mutants. While some of these mutants were competitive (Figure 5.6), interpretation of the data in these cases was complicated by the inability to saturate the mutants with glutamine and measure accurate K_ms.

The C86A and C86S mutants were able to compete most effectively with A128T PurQ (Figure 5.7) with 1 equivalent of mutant inhibiting activity by ~50%. Physical characterization of these mutants relative to A128T PurQ by SEC suggest that they are monomers with ~10% of protein in an aggregated state; although, the mutants do have an increased tendency to aggregate during SV-AUC. The efficient competition suggests binding of glutamine equivalent to A128T PurQ, as was assumed. Thus, during turnover conditions, an active PurQ is not necessary for complex formation with smPurL and PurS.

The Conserved Triad Glutamate is Important for FGAR-AT Complex Formation

The results mentioned in the previous section support studies from Chapter 3 that suggested glutamine is essential for FGAR-AT complex formation. Competition experiments can also serve as a probe for identifying residues in PurQ important for FGAR-AT complex formation. As was mentioned in the introduction, mutation of the conserved triad glutamate in CPS and PabAB has resulted in speculation that this residue may be playing a role in linking the glutaminase and AT domains (*2, 3*). In the case of CPS, mutation of E355 to either an alanine or an aspartate resulted in an enzyme with wt levels of glutamine hydrolysis and carbamoyl phosphate synthesis; however, in an E355Q mutant, coupling between the glutaminase and ATPase activities was lost and no

carbamoyl phosphate was synthesized (2). This result led Raushel and co-workers to speculate that this residue was involved in communication between the AT and glutaminase.

In the case of PabAB, mutation of the conserved residue E170 to either an alanine or aspartate resulted in an active enzyme, while the glutamine and lysine mutants were inactive (3). In addition, the E170Q mutant was competitive with active PabA for complex formation with PabB, while E170K was not. Walsh and coworkers suggested that in lieu of an essential chemical role, E170 may be playing a role in PabA and PabB interactions (3).

Results from the E196 PurQ mutants corroborate findings made by Raushel and Walsh that the glutamate is not part of a catalytic triad. The E196A PurQ has 10% activity of A128T PurQ (Table 5.3). This supports the idea that E196 does not play a direct chemical role in glutamine hydrolysis; however, this residue may still be important for correctly positioning H194 in the PurQ active site. Surprisingly, despite this activity, E196A is not competitive with A128T PurQ even in 200 mM glutamine where the mutant should be saturated with glutamine (K_m = 34 mM). In fact, none of the E196 mutants were competitive under the conditions examined. One hypothesis for these observations is that E196 is essential for complex formation between smPurL and PurQ. Mutation of this residue may result in a small structural change that effects the PurQ:smPurL interface. CD spectra of the E196 mutants (Figure 5.9) supports the possibility of an altered structure for the protein.

Structural Insight into the Role E196 May Play in Complex Formation

The crystal structure of the *Salmonella* lgPurL provides insight as to why

mutations to E196 may affect PurQ's interface with smPurL (Figure 5.16) (*5*). The

residue immediately adjacent to the triad glutamate (E1262) is an arginine (R1263) that is

involved in an interdomain contact with the AT (via D657). These residues are

conserved in the *B. subtilis* FGAR-AT (Figure 5.16). The connection of E1262 is

through a H_2O molecule to the δ-nitrogen of R1263. Mutation of the glutamate could

alter interactions between R1263 and D657. Whether a similar connectivity occurs in *B.*

subtilis FGAR-AT is not known; however, this model could be tested via further

mutagenesis studies.

E196 Could Also Play a Role in Coupling Glutaminase and AT Activities

Recent studies from the Davisson lab on HisHF (Figure 5.1) have implicated the

importance of R1263 in communication between the AT and glutaminase domains of the

FGAR-AT (*20*). Davisson's group has identified a pair of interdomain contacts in HisHF

that appear to be important for coupling glutaminase and AT activities. As shown in

Figure 5.17, an interdomain contact between glutaminase residue K196 and AT residue

D357 was observed in the HisHF crystal structure. Importantly, K196 is on the same

loop and is immediately adjacent to the conserved triad glutamate residue, E195.

Mutation of K196 and D357 resulted in uncoupling of glutaminase and AT activities in

HisHF (up to 110 glutamines were hydrolyzed per AT product formed), and MD

simulations suggest that interactions between D357, K196, E195, and H193 are

responsible for triggering the glutaminase activity of HisHF in the presence of the AT

substrate (*20*). Davisson has suggested that many triad ATs utilize a similar mechanism
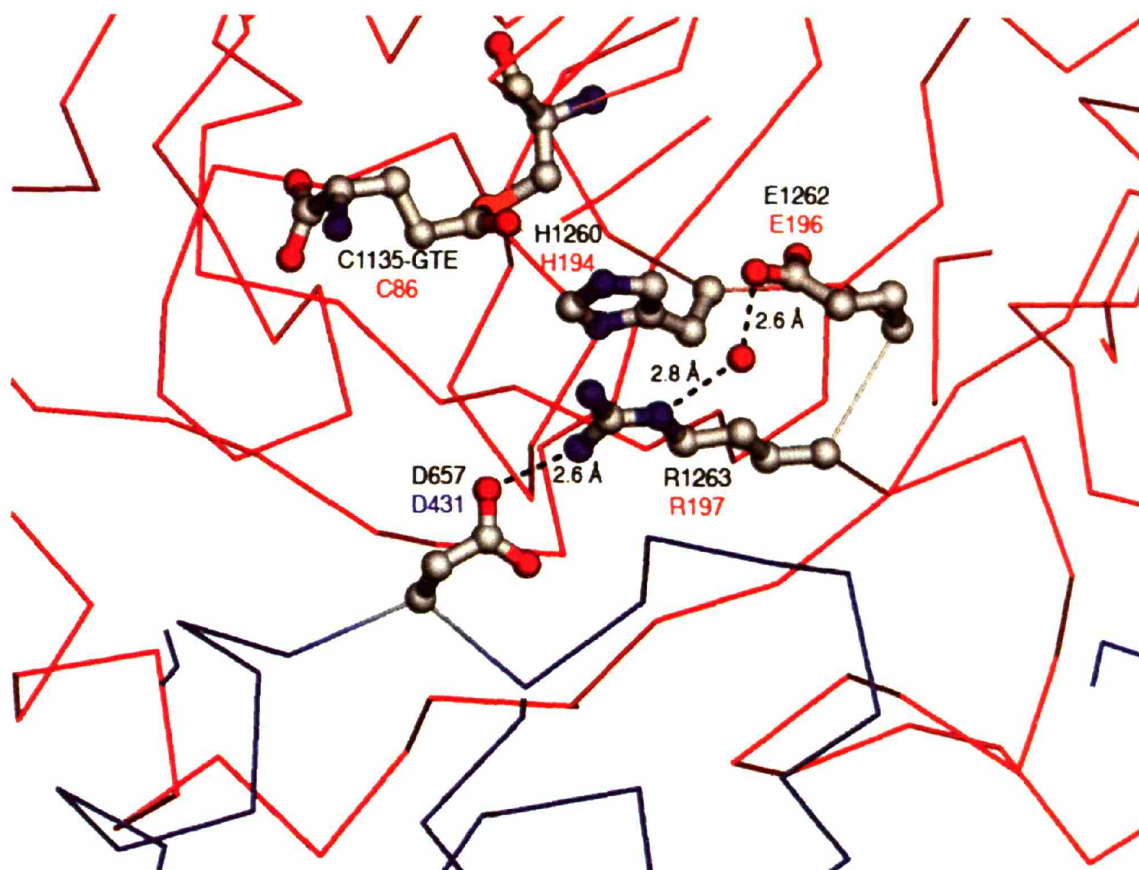
Figure 5.16—Possible role for the conserved triad glutaminase residue E1262 in linking the glutaminase (red) and AT domains (blue). Residues from the *Salmonella* lgPurL structure are labeled in black, and the glutamylthioester (GTE) is shown at C1135. Homologous residues in *B. subtilis* PurQ and smPurL are labeled in red and blue, respectively. A salt-bridge between D657 and R1263 has been proposed to play a key role in linking the glutaminase to the AT domain. E1262 is adjacent in sequence to R1263 and is hydrogen-bonded to that residue via a bridging water molecule. In experiments with the *B. subtilis* FGAR-AT complex, mutation of E196 in PurQ may disrupt this connection and alter the R197-D431 interaction proposed between PurQ and smPurL.

Anthranilate Synthase
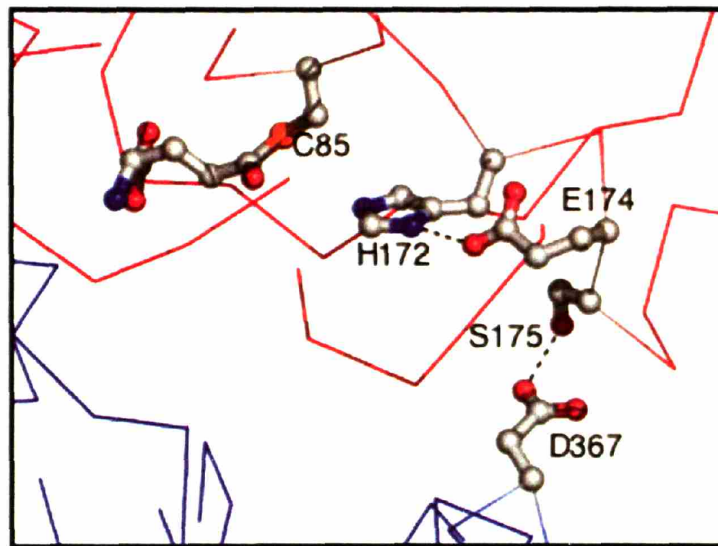
HisHF
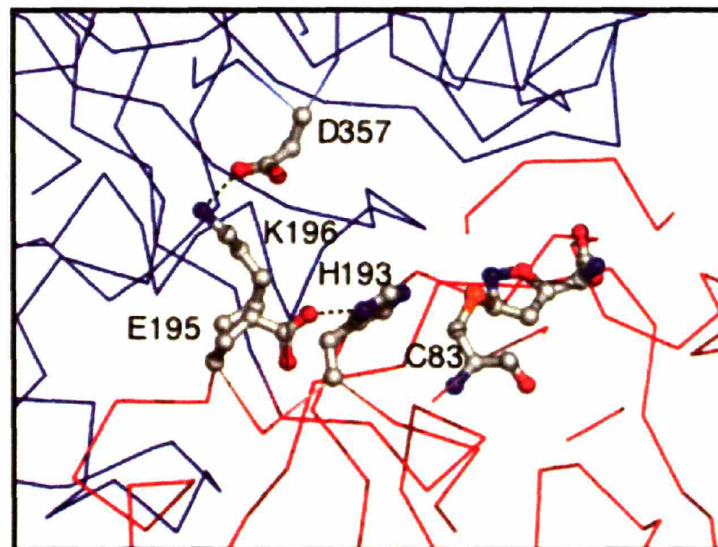
Figure 5.17—Interdomain contacts implicated by Davisson and coworkers that may be essential for linking the AT (blue) and glutaminase domains (red). (Top) In the structure of anthranilate synthase containing a glutamylthioester at C85, E174 is hydrogen bonded to triad residue H172 and is adjacent to S175 which interacts with the AT domain residue D367. (Bottom) In the structure of HisHF inactivated with acivicin at C83, E195 interacts with triad residue H193 and is adjacent to K196 which interacts with AT domain residue D357.

of activating the glutaminase domain for catalysis, and in most cases, the residue immediately adjacent to the triad glutamate is involved in a key interdomain contact. For example, in the case of anthranilate synthase (which is highly homologous to PabAB), S175 was observed to be in an interdomain contact with D367 (Figure 5.17). S175 is immediately adjacent to the conserved triad glutamate E174. Given the interaction between D657, R1263, and E1262 observed in the lgPurL crystal structure (Figure 5.16), these residues may also be important for coupling AT and glutaminase activities in FGAR-AT. Further mutagenesis studies are needed on PurQ to address the importance of interactions between E196, R197, and smPurL residue D431 on FGAM synthetic activity.

Glutamine is Also Important for Assembly of the Endogenous B. subtilis FGAR-AT

Given the difficulties that have been encountered in assembling the *B. subtilis* FGAR-AT, questions were raised concerning FGAR-AT assembly inside the cell. To address this issue, a histag-PurQ was expressed at physiologically relevant levels in *B. subtilis* and used to affinity purify the FGAR-AT complex either in the presence of absence of glutamine. The results from these experiments (Figure 5.14) indicate that glutamine also plays an important role for holding the FGAR-AT complex together in *B. subtilis*, and PurS could only be co-purified in the presence of glutamine or by DON-inactivating the cell lysate. Thus, it seems unlikely that observations made *in vitro* are artifacts of using heterologously expressed and purified enzymes.

Future Studies

Future studies on the role of glutamine binding to PurQ should focus on several areas. First, a structure of PurQ is needed to address conformational changes that may

292

occur upon glutamine binding, complex formation with smPurL/PurS, and conversion to an active glutaminase. So far, neither of the PurQs from *B. subtilis* or *T. maritima* have been crystallized. Given that PurQ is a relatively small enzyme (24 kDa), structural information may be obtained by NMR methods if conditions are found to limit protein aggregation. Work on ^{15}N-labeled PurQ by Professor Jens Wöhnert (U. Texas Medical Center—San Antonio) has already indicated that PurQ is folded and stable under NMR conditions for short time periods (personal communication). NMR may be particularly useful in addressing dynamic motions of PurQ that may occur upon substrate binding or during activation of the glutaminase activity.

Second, kinetic work should be done to further investigate the role glutamine plays in FGAR-AT complex formation. The work presented here and in Chapter 3 strongly indicates that glutamine is required for complex formation, and results from the C86A mutant indicates that complex formation is not contigent on formation of a PurQ-glutamylthioester. The implication of this finding is that the FGAR-AT has evolved to specifically recognize the PurQ-substrate complex. Evidence to support this model could come from kinetic studies that compare the rate of FGAR-AT complex formation to the rate of glutamylthioester formation in the PurQ-glutamine complex. If complex formation proceeds faster than glutamylthioester formation, then the FGAR-AT complex may have evolved to specifically interact with the non-covalent PurQ-substrate complex.

Finally, the recent results by Davisson and coworkers on HisHF provide a new avenue to examine reaction coupling in the FGAR-AT (*20*). Mutations to R197 in PurQ and D431 in smPurL should be made and thoroughly investigated with respect to both kinetics and product stoichiometry. Based on results presented in this chapter and the

crystal structure of the *Salmonella* lgPurL, E196 may also be involved in this interaction and should be included in these studies. These experiments may illuminate how PurQ becomes activated for glutamine hydrolysis during FGAM synthesis; however, how ATP and FGAR binding information directly impacts the D657(smPurL):R197 (PurQ) interaction over a distance of ~25 Å will require more thorough investigations.

5.5 References

(1)   Zalkin, H. and Smith, J. L. (1998) Enzymes utilizing glutamine as an amide donor. *Adv. Enzymol. Relat. Areas Mol. Biol. 72*, 87-144.

(2)   Huang, X. and Raushel, F. M. (1999) Deconstruction of the catalytic array within the amidotransferase subunit of carbamoyl phosphate synthetase. *Biochemistry 38*, 15909-14.

(3)   Roux, B., and Walsh, C. T. (1993) p-Aminobenzoate synthesis in *Escherichia coli*: mutational analysis of three conserved amino acid residues of the amidotransferase PabA. *Biochemistry 32*, 3763-8.

(4)   Myers, R. S., Jensen, J. R., Deras, I. L., Smith, J. L., and Davisson, V. J. (2003) Substrate-induced changes in the ammonia channel for imidazole glycerol phosphate synthase. *Biochemistry 42*, 7013-22.

(5)   Anand, R., Hoskins, A. A., Stubbe, J., and Ealick, S. E. (2004) Domain organization of *Salmonella typhimurium* formylglycinamide ribonucleotide amidotransferase revealed by X-ray crystallography. *Biochemistry 43*, 10328-42.

(6)   Hoskins, A. A., Anand, R., Ealick, S. E., and Stubbe, J. (2004) The formylglycinamide ribonucleotide amidotransferase complex from *Bacillus subtilis*: metabolite-mediated complex formation. *Biochemistry 43*, 10314-27.

(7)   Laue, T. M., Shah, B. D., Ridgeway, T. M., and Pelletier, S. L. (1992) in *Analytical ultracentrifugation in biochemistry and polymer science* (Harding, S., Ed.) pp 90-125, The Royal Society of Chemistry, Cambridge, UK.

(8)   Schuck, P. (2000) Size distribution analysis of macromolecules by sedimentation velocity ultracentrifugation and Lamm equation modeling. *Biophysical J. 78*, 1606-1619.

(9)   Joseph, P., Fantino, J. R., Herbaud, M. L., and Denizot, F. (2001) Rapid orientated cloning in a shuttle vector allowing modulated gene expression in *Bacillus subtilis*. *FEMS Microbiol Lett 205*, 91-7.

(10)   Miles, B. W., Mareya, S. M., Post, L. E., Post, D. J., Chang, S. H., and Raushel, F. M. (1993) Differential roles for three conserved histidine residues within the large subunit of carbamoyl phosphate synthetase. *Biochemistry 32*, 232-40.

(11)   Thoden, J. B., Miran, S. G., Phillips, J. C., Howard, A. J., Raushel, F. M., and Holden, H. M. (1998) Carbamoyl phosphate synthetase: caught in the act of glutamine hydrolysis. *Biochemistry 37*, 8825-31.

(12)   Thoden, J. B., Huang, X., Raushel, F. M., and Holden, H. M. (1999) The small subunit of carbamoyl phosphate synthetase: snapshots along the reaction pathway. *Biochemistry 38*, 16158-66.

(13)   Amuro, N., Paluh, J. L., and Zalkin, H. (1985) Replacement by site-directed mutagenesis indicates a role for histidine 170 in the glutamine amide transfer function of anthranilate synthase. *J. Biol. Chem. 260*, 14844-9.

(14)   Paluh, J. L., Zalkin, H., Betsch, D., and Weith, H. L. (1985) Study of anthranilate synthase function by replacement of cysteine 84 using site-directed mutagenesis. *J. Biol. Chem. 260*, 1889-94.

(15)   Miran, S. G., Chang, S. H., and Raushel, F. M. (1991) Role of the four conserved histidine residues in the amidotransferase domain of carbamoyl phosphate synthetase. *Biochemistry 30*, 7901-7.

(16)   Deshpande, K. L., Katze, J. R., and Kane, J. F. (1981) Effect of glutamine on enzymes of nitrogen metabolism in *Bacillus subtilis*. *J. Bacteriol. 145*, 768-74.

(17)   Anand, R., Hoskins, A. A., Bennett, E. M., Sintchak, M. D., Stubbe, J., and Ealick, S. E. (2004) A model for the *Bacillus subtilis* formylglycinamide ribonucleotide amidotransferase multiprotein complex. *Biochemistry 43*, 10343-52.

(18)   Rayl, E. A., Green, J. M., and Nichols, B. P. (1996) *Escherichia coli* aminodeoxychorismate synthase: analysis of pabB mutations affecting catalysis and subunit association. *Biochim. Biophys. Acta. 1295*, 81-8.

(19)   Parsons, J. F., Jensen, P. Y., Pachikara, A. S., Howard, A. J., Eisenstein, E., and Ladner, J. E. (2002) Structure of *Escherichia coli* aminodeoxychorismate synthase: architectural conservation and diversity in chorismate-utilizing enzymes. *Biochemistry 41*, 2198-208.

(20)   Myers, R. S., Amaro, R. E., Luthey-Schulten, Z. A., and Davisson, V. J. (2005) Reaction coupling through interdomain contacts in imidazole glycerol phosphate synthase. *Biochemistry 44*, 11974-85.

Chapter 6:

Identification of Residues Essential for PurL Catalysis and Relationship of these

Residues to Other PurM-Superfamily Members

6.1 Introduction

When the crystal structure of PurM was determined in 1999 by the Ealick and Stubbe Laboratories, it was discovered that the enzyme possessed a unique fold and served as the prototype of a new superfamily of ATP-binding enzymes defined by a conserved DX_4GAXP motif in which the aspartate was believed to be essential for ATP binding (*1*). Only 5 members of this superfamily have thus far been identified: PurM, PurL, thiamine monophosphate kinase (ThiL), selenophosphate synthetase (SelD), and an ATP-dependent hydrogenase maturase protein (HypE) (*1*). Each of these superfamily members is thought to transfer the γ-phosphate of ATP to substrate in either a kinase reaction (ThiL and SelD) or during formation of a proposed phosphorylated-substrate intermediate (PurM, PurL, HypE) (Figure 6.1). The common chemistry of the superfamily members was proposed to be an iminophosphate. In the cases of ThiL and SelD, the phosphorylation was proposed to involve a phosphoryl-enzyme intermediate in which phosphate is transferred to the amide backbone of a conserved amino acid in the active site (*2*).

Structures of the *Salmonella* lgPurL, *T. maritima* smPurL, and *A. aeolicus* ThiL have recently been determined and the identity of the superfamily has been confirmed by observation of common fold (Figure 6.2) (*2*). The central feature of the PurM-superfamily is a dimeric protein in which an 8-stranded β-barrel forms the monomer:monomer interface. In the case of smPurL and lgPurL, the monomers have been fused to create a single chain that exhibits pseudosymmetry about the central barrel. Based upon the location of conserved residues and ATP site-labeling studies on PurM with *p*-fluorosulfonylbenzoyl adenosine (FSBA), the active sites of the enzymes are believed to exist in a cleft between the N-terminal and C-terminal halves of each monomer, with 2 active sites per dimer (*1-3*).
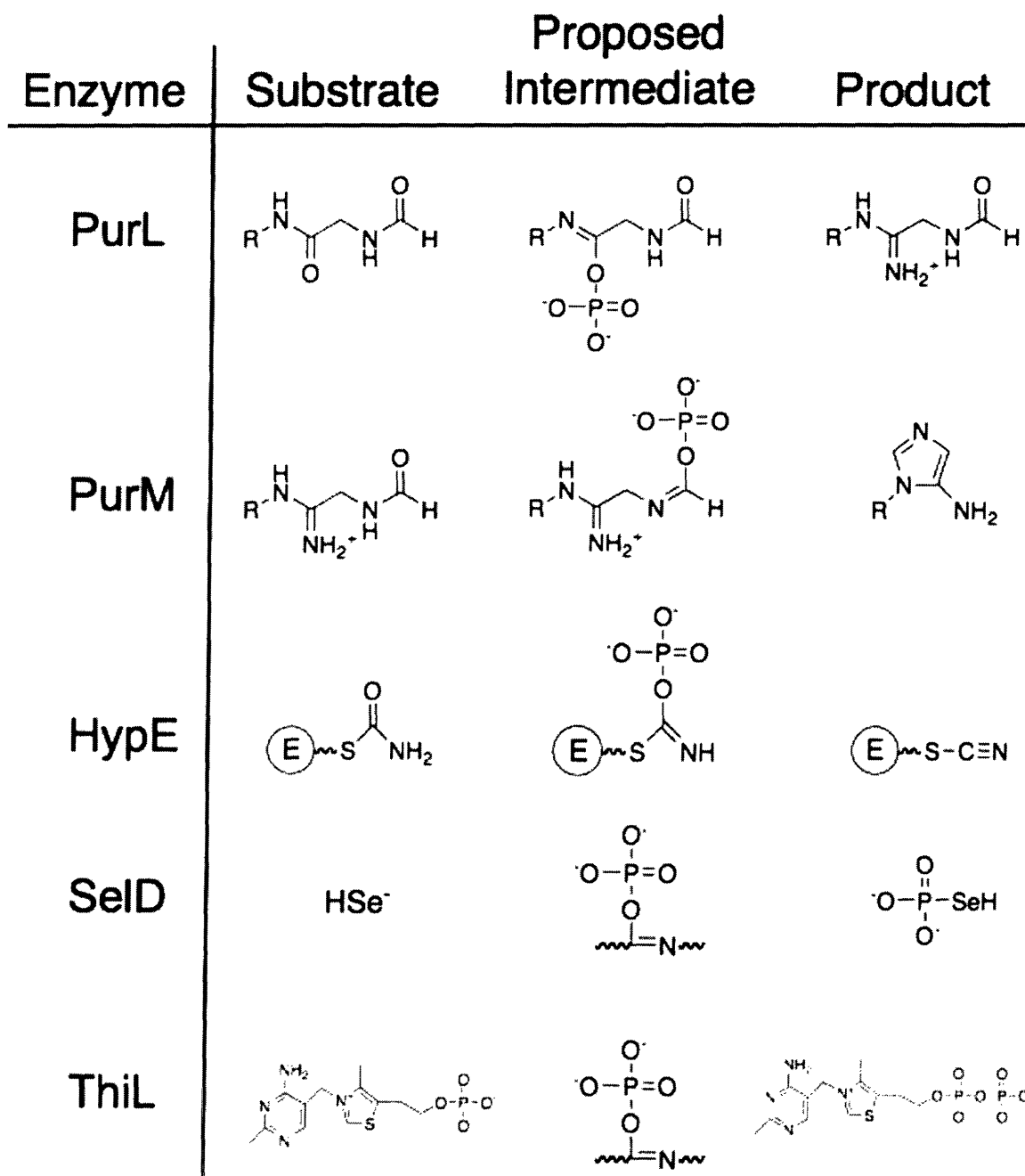
Figure 6.1—Members of the PurM-superfamily of enzymes. PurL, PurM, and HypE are proposed to use the γ-phosphate of ATP to generate an iminophosphate intermediate. In HypE, this is proposed to occur on an enzyme-liked thiocarbamate. SelD and ThiL are kinases that phosphorylate selenide and thiamin monophosphate, respectively, and have been proposed to also utilize iminophosphate intermediates, possible derived from an amide of the protein backbone.
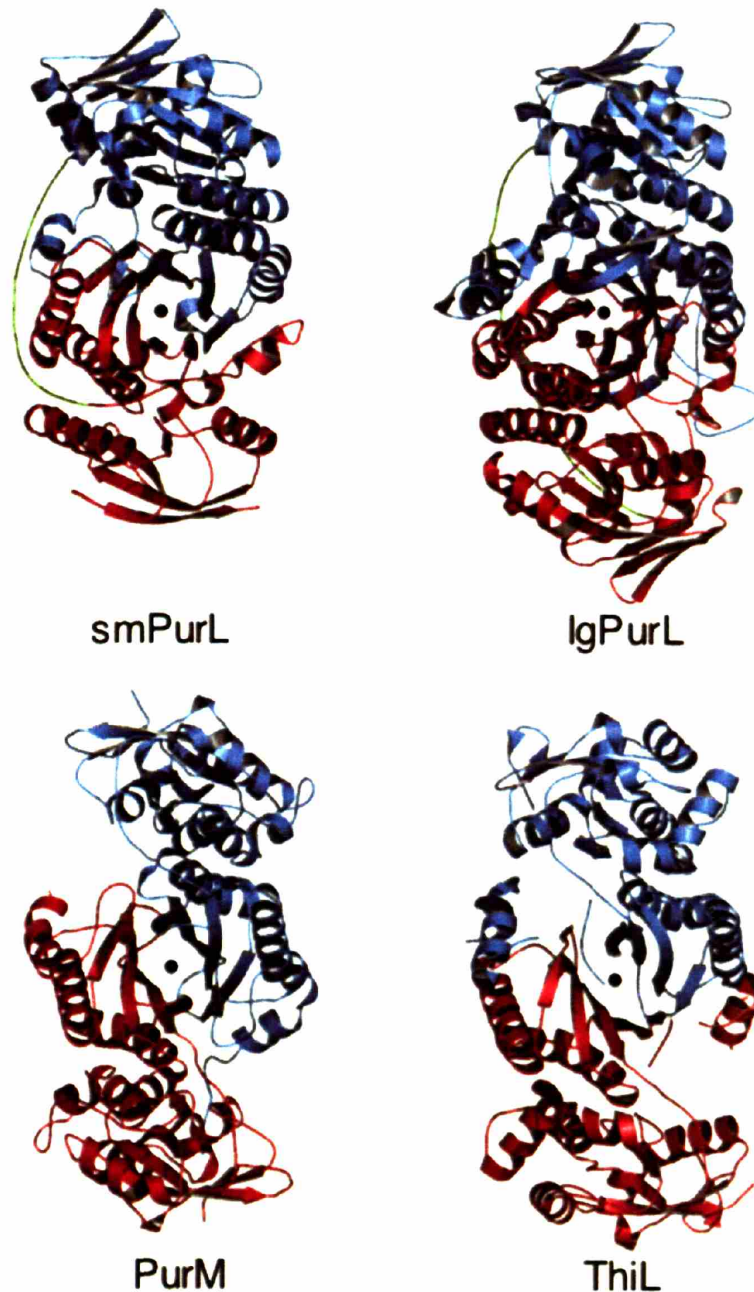
Figure 6.2—Comparison of the crystal structures of *T. maritima* smPurL (1vk3.pdb), the AT domain of *Salmonella* lgPurL (1t3t.pdb), *E. coli* PurM (1cli.pdb), and ThiL (1vqv.pdb). In smPurL and lgPurL, the N- and C-terminal halves of the pseudodimer are colored in blue and red, respectively. The linker domains connecting the N- and C-terminal halves are shown in green. In PurM and ThiL, subunits of the homodimer are colored in blue and red. Each structure shows a conserved β-barrel core, the center of which is noted with the black dot.

Despite structures of several members of this superfamily, analysis of the active site has been complicated because neither lgPurL nor PurM has yet been crystallized with substrates or products. Given that these enzymes possess a novel ATP-binding motif, difficulties have been encountered in efforts to model ATP or purine substrates into the active sites, making identification of residues important for catalysis difficult. Experiments in the past few years sought to crystallize the *B. subtilis* smPurL with ATP and FGAR in hopes that it would be able to provide new information about the active site architecture in this superfamily; however, as noted in the preceeding chapters, aggregation problems encountered throughout studies on smPurL have thus far inhibited these efforts.

In order to provide new information about the active sites of PurM-superfamily members, the *T. maritima* smPurL was cloned, expressed, and purified in collaboration with the Ealick Laboratory. Structures of *T. maritima* smPurL in complex with FGAR, ATP, ADP, and a ternary complex with FGAR and β,γ-methyleneadenosine 5'-triphosphate (a non-hydrolyzable ATP-analog, AMP-PCP) have very recently been determined by Maria Morar and Ruchi Anand in the Ealick Laboratory. The solutions of the *T. maritima* structures were facilitated by the structure of *T. maritima* smPurL in the apo form which has recently appeared from the Joint Center for Structural Genomics (1vk3.pdb). These structures identified for the first time the mechanism of ATP-binding by members of the PurM-superfamily and identified two histidine residues in the active site that may be important for catalysis. Mutagenesis studies of these residues to alanines confirm their importance for activity. A mechanism is proposed for fomation of a putative iminophosphate intermediate by smPurL using the active site architecture. Model structures have also been created for HypE and SelD and features of the active sites of these enzymes are compared to structures of PurM, PurL, and ThiL. These results indicate that while ATP-binding

is highly conserved in the PurM-superfamily, conserved histidines identified in PurL are not conserved in all superfamily members.

6.2 Experimental

Materials and Methods

β-FGAR was prepared from chemically synthesized α/β-GAR using the PurT glycinamide ribotide transformylase as previously described (*4*). The PurT plasmid was a gift from H. Holden, University of Wisconsin-Madison (*5*). *E. coli* PurM containing a N-terminal histidine tag was purified as described (his-PurM, specific activity 1-2 U/mg) (*1*). ATP, ADP, PEP, NADH, and pyruvate kinase/lactate dehydrogenase (a pre-mixed glycerol solution 660 U/mL PK/ 1350 U/mL LDH) were purchased from Sigma. NH$_4$Cl was from Mallinckrodt. All spectrophotometric assays were carried out on a Cary 3 UV-Vis spectrophotometer with temperature regulation using a Lauda water bath. Circular dichroism and analytical ultracentrifugation experiments were carried out in the Biophysical Instrumentation Facility for the Study of Complex Macromolecular Systems (Department of Chemistry, MIT).

Cloning of the T. maritima purL Gene

The *T. maritima purL* gene was cloned from genomic DNA (ATCC) by standard PCR procedures using the KOD HiFi DNA polymerase (Novagen) and the primers TML-NdeI: 5'-GC**CATATG**AAGTTGAGATATCTGAACATTCTCAAGG-3' and TML-NotI: 5'-AAATATG**CGGCCG**CTCACCTCGAGAGCGTTCCGATCTCCTTC-3'. Taq DNA polymerase (Invitrogen) was then used to create 3'-A overhangs on the PCR product, which was then ligated into the pCRII-TOPO vector (Invitrogen) in a topoisomerase-dependent reaction to make pCRII-TOPO-TML. Colonies containing the insert were then selected by blue-white screening on X-Gal containing media. The insert was isolated from the pCRII-TOPO-TML

302

plasmid by digestion with NdeI and NotI (New England BioLabs) and ligated into pET-24a

(Novagen) at the same restriction sites to create pET-TML. Sequencing of the gene by the MIT

Biopolymers Facility revealed a silent mutation at nucleotide position 891 corresponding to a

ATC→ATT change in the ile codon.

Mutagenesis of T. maritima smPurL

H32A and H72A mutants of *T. maritima* smPurL were created from the pET-TML

plasmid by Ruchi Anand (Ealick Laboratory, Cornell University) using Quikchange mutagenesis

and the details will be described elsewhere (Morar, M. *et al.,* manuscript in preparation).

Protein Expression and Purification

Both the wt and mutant *T. maritima* smPurLs were expressed and purified by Ruchi

Anand and Maria Morar (Ealick Laboratory, Cornell University) using identical procedures. The

pET-TML plasmid containing either the wt or the mutant smPurL gene was transformed into

Rosetta(DE3) *E. coli* (Novagen). Single colonies were used to inoculate 5 mL of LB with 35

μg/mL kanamycin and 30 μg/mL chloramphenicol and allowed to grow overnight at 37°C. The

saturated culture was then used to inoculate 1 L of LB media containing the same antibiotics.

The culture was grown at 37°C with shaking at 200 rpm, and after an OD_{600} of 0.7 was reached,

the temperature was lowered to 25°C, and cells were induced with 200 μM IPTG for 6 h. The

cell pellet was collected by centrifugation and stored at -80°C (yield ~ 4 g/L).

Cells (~4 g) were resuspended in 40 mL of TM buffer (50 mM HEPES pH 7.8, 100 mM

NaCl) with the addition of COMPLETE Protease Inhibitors (Roche) and lysed by sonication

while cooling in an ice water bath. Cell debris was removed by centrifugation at 17,000 rpm for

20 min. The lysate was then loaded onto a HiTrap MonoQ FF column (10/10, Pharmacia)

equilibrated in TM buffer and washed until the A_{280} < 0.1. The protein was eluted with a 0.1 to

1 M NaCl gradient (150 x 150 mL) at a flow rate of 2 mL/min while collecting 5 mL fractions. Fractions containing smPurL eluted at ~200 mM NaCl and were concentrated to 10 mL using a YM30 Centricon (Millipore).

The concentrated protein was desalted with a Hi-Load Superdex 75 column (26/60, Pharamacia) equilibrated in TM buffer. Protein was eluted with TM buffer at a flow rate of 2 mL/min, and 2 mL fractions were collected. Protein containing fractions were concentrated to 10 mg/mL and frozen in liquid N_2. Typical protein yields were ~10 mg protein/g cells.

Crystallization and Structure Determination of the T. maritima smPurL

The crystal structures of the *T. maritima* smPurL in complex with FGAR, ADP, ATP, and a ternary complex with FGAR and β,γ-methyleneadenosine 5'-triphosphate (AMP-PCP) were determined by Maria Morar and Ruchi Anand by molecular replacement using the structure of apo-smPurL (1vk3.pdb, unpublished) solved by the Joint Center for Structural Genomics (JCSG). The details will be described elsewhere (Morar, M. *et al.,* manuscript in preparation).

Sedimentation Velocity Analytical Ultracentrifugation (SV-AUC)

SV-AUC experiments were performed using an Optima XL-1 analytical ultracentrifuge (Beckman Coulter, Fullerton, CA). Before each experiment, protein samples were dialyzed against 50 mM Tris, 20 mM KCl, 20 mM $MgCl_2$ pH 8.0 for 24 h in a Slide-A-Lyzer cassette with a 10 kDa molecular weight cut-off (MWCO) membrane (Pierce). Samples (400 µL) were then diluted to 9.7 µM and placed in double-sector Epon centerpieces with quartz windows in an An60Ti 4-hole rotor. Sedimentation was monitored by continuous scanning at 280nm along the length of the cell at 30,000 rpm for 24 h at 25°C.

SEDNTERP software from Dr. J. Philo was used to calculate buffer density (1.00197 g/mL), viscosity (0.01002 Poise), and protein partial-specific volume from the amino acid

content (0.7444 mL/g) (*6*). Data (~100 traces for each experiment) were fit using SEDFIT88

from 0.5 to 20 S using a continuous distribution of sedimentation coefficients derived from

solutions to the Lamm equation (*7*).

Circular Dichroism Spectroscopy

Circular dichroism (CD) Spectra were collected on an AVIV Model 202 CD

spectrophotometer (AVIV Biomedical, Inc., Lakewood, NJ). Proteins were dialyzed before the

experiment against 10 mM KP_i pH 7.0 buffer for 16 h using a Slide-A-Lyzer cassette (Pierce)

with a 10 kDa MWCO membrane. Spectra were collected for each sample (5 µM) at 25°C in a

0.1 cm path length quartz cuvette in argon-degassed dialysis buffer by scanning from 300-190

nm at 0.5 nm increments with a 0.2 s integration time.

Enzyme Assays

T. maritima smPurL was assayed in the absence of PurS and PurQ by monitoring NH_4Cl-

dependent FGAM formation. FGAM synthesis was monitored directly using a coupled,

discontinuous assay with his-PurM and the modified Bratton-Marshall assay (*8*). Each assay

contained in a final volume of 400 µL: 100 mM Tris pH 8.0, 20 mM KCl, 20 mM $MgCl_2$, 1.5

mM PEP, 10 U/mL PK, 20 U/mL his-PurM, 750 mM NH_4Cl, 10 mM ATP, and 2 mM β-FGAR.

The reaction was initiated by the addition of enzyme (~1-10 µg) and incubated at 37°C before

being quenched with 100 µL of 1.33 M KP_i pH 1.4/20% tricholoracetic acid followed by

derivitization and quantitation of AIR (*8*).

ADP synthesis was monitored using a coupled assay at 37°C with PK and LDH,

monitored continuously with NADH oxidation at 340 nm (ε = 6200 $M^{-1}cm^{-1}$). The assay buffer

was the same as described above except that it also contained 0.2 mM NADH, 20 U/mL PK, and

42 U/mL LDH.

Determination of Kinetic Constants

Kinetic parameters for ATP were determined using the PK/LDH coupled assay with 0-10 mM ATP in the presence of sub-saturating amounts of FGAR (2 mM) and saturating amounts of NH_4Cl (750 mM). Kinetic parameters for FGAR were determined using the Bratton-Marshall assay with 0 to 5 mM FGAR in the presence of saturating amounts of ATP (10 mM) and NH_4Cl (750 mM). For the H72A *T. maritima* smPurL, the concentration of FGAR was varied from 0 to 32 mM. Parameters for NH_4Cl were determined using the Bratton-Marshall assay with 0 to 750 mM NH_4Cl in the presence of saturating amounts of ATP (10 mM) and sub-saturating amounts of FGAR (2 mM). Data was analyzed using a nonlinear regression analysis with KaleidaGraph (Synergy) computer software and Equation 6.1.

$$v = V_{max}[S]/(K_m + [S]) \qquad (6.1)$$

Structure-Based Sequence Alignments and Modeling of SelD and HypE

CLUSTALW (http://www.ebi.ac.uk/clustalw/) was initially used to perform a sequence-based alignment with *E. coli* PurM (1cli.pdb), *T. maritima* smPurL (1vk3.pdb), and *A. aeolicus* ThiL (1vqv.pdb) (*9*). The text file for the alignment was then manually edited based upon the secondary structure information from the crystal structures. Using the edited sequence alignment, ESPript 2.2 (http://espript.ibcp.fr/ESPript/ESPript/) was used to create the structure-based alignment (*10*).

Model structures for *E. coli* SelD and HypE were generated using the programs HHpred and Modeller ver.7 (http://protevo.eb.tuebingen.mpg.de/toolkit/) based upon the crystal structures for *E. coli* PurM (1cli.pdb), *A. aeolicus* ThiL (1vqv.pdb), the N-terminal half of the

AT domain of *Salmonella* lgPurL (1t3t.pdb), and the N-terminal half of *T. maritima* smPurL

(1vk3.pdb) (*11, 12*).

6.3 Results

Expression and Purification of T. maritima smPurL

Expression and purification of smPurL was carried out by Maria Morar and Ruchi Anand

in the Ealick Laboratory. In order to express *T. maritima* smPurL in high yield, the Rosetta

(DE3) cell line was used which contains additional copies of the "rare" tRNAs for the AUA,

AGG, AGA, CUA, CCC, and GGA codons. Protein was then purified from the cell lysate in a

single step by MonoQ Sepharose chromatography followed by desalting with a Sephadex G75

gel filtration column.

Structure of the Ternary Complex with AMP-PCP and FGAR

While several crystal structures of *T. maritima* smPurL were obtained by the Ealick

Laboratory, the results presented in this chapter will focus on the structure obtained from co-

crystallization of smPurL with FGAR and a non-hydrolyzable ATP analog (AMP-PCP) at 2.7 Å

(Figure 6.3). The structure of the AMP-PCP binding site reveals a function for the conserved

DX_4GAXP motif. The corresponding asparate (D94) serves as a ligand to a magnesium ion

bridging the β and γ phosphates of AMP-PCP (Figure 6.3). The role for the remaining 3 residues

in the consensus motif is less clear since they do not come into contact with either substrate.

These residues are located on a turn that follows D94 and may be involved in stabilizing the β-

barrel structure at the core of the enzyme and forming the hydrophobic pocket (I42, L45, V474)

for binding of the adenine ring.

A close examination of the FGAR-binding site reveals that the amide that is converted to

an amidine during the reaction is located between two histidines (His32 and His 72, Figure 6.4).

307
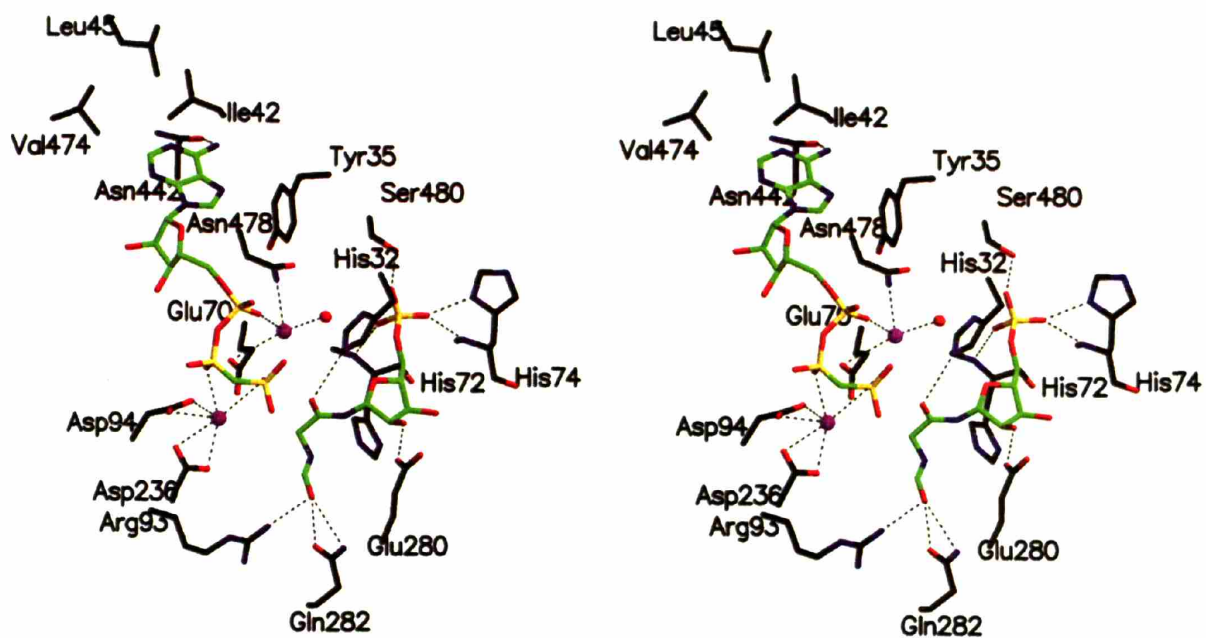
Figure 6.3—Stereoview of FGAR and AMP-PCP bound to the active site of *T. maritima* smPurL. D94 is part of the conserved DX_4GAXP motif and is responsible for coordinating a magnesium ion located between the β- and γ-phosphates of AMP-PCP. Figure courtesy of Maria Morar (Cornell University).
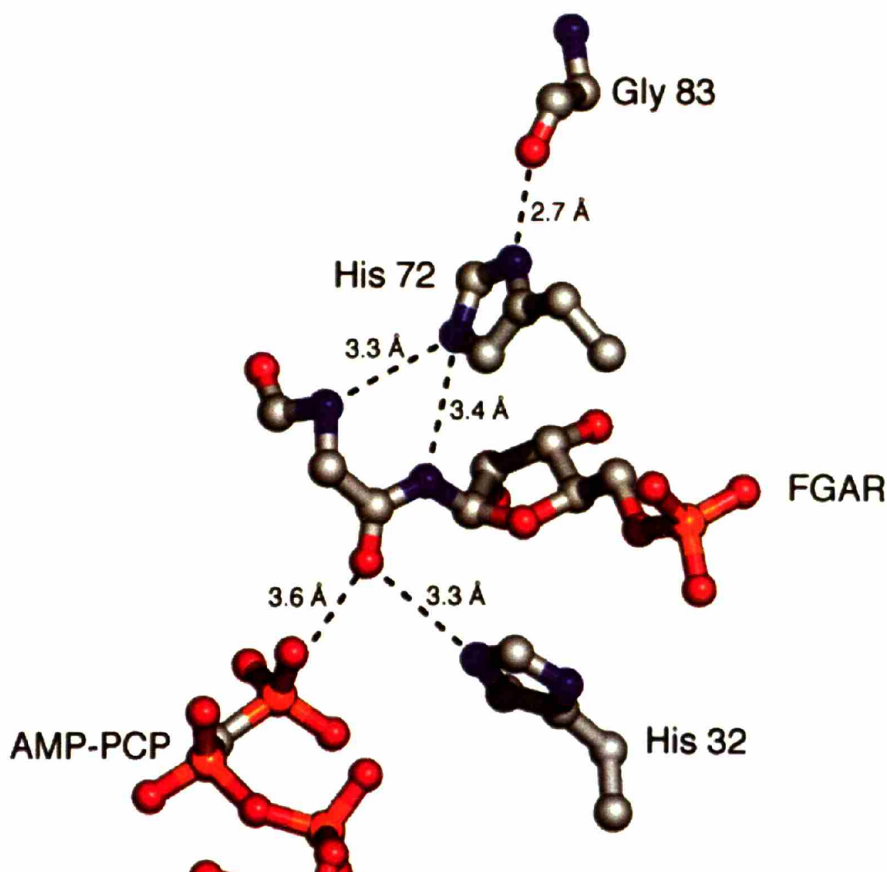
Figure 6.4—Close up of conserved FGAR-binding residues and distances observed in the ternary complex crystal structure. In the structure, the carbonyl oxygen of the FGAR amide is not in line for direct attack on AMP-PCP. Small conformational changes during turnover may bring the γ-phosphate and oxygen into alignment. Conformational changes may also occur in H32 so that this residue may be directly hydrogen-bonded to the carbonyl, γ -phosphate of ATP, or a proposed phosphorylated intermediate. The δN of H32 has no hydrogen-bonding interactions.

The amide oxygen of FGAR is positioned 3.6 Å from the γ-phosphate of AMP-PCP; too far for effective interaction and the oxygen is not oriented correctly for in-line attack. The proximity of the histidines to the amide of FGAR and the observation that these histidines, along with a glycine hydrogen-bonded to H72, are absolutely conserved across both large and smPurL sequences implicated a role for these residues in catalysis or FGAR-binding. Neither of the ring nitrogens of the H32 are involved in hydrogen-bonding interactions in the crystal structure, and a similar relationship between histidine and ATP could only be found in nucleoside diphosphate kinases (which utilize a phospho-histidine intermediate) (*13*) and in phosphoenolpyruvate carboxykinase (in which the histidine also acts as a ligand to an essential Mn^{2+}) (*14*). The importance of H32 and H72 in catalysis was examined by preparation of the corresponding alanine mutants.

Activity of wt smPurL

In order to study the mutant enzymes, an assay was developed to detect FGAM formation with the wt enzyme. Given that a *T. maritima* FGAR-AT complex has not yet been reconstituted from smPurL, PurQ, and PurS, smPurL, activity must be monitored by NH_4Cl-dependent FGAM synthesis. This assay has previously been shown to be effective in measuring the activity of *B. subtilis* smPurL (Chapter 3). Both ADP and FGAM formation can be monitored using either PK/LDH or PurM as the coupling enzymes.

At 37°C and pH 8.0, *T. maritima* smPurL FGAM synthetase activity was readily observable and the enzyme had a specific activity of 0.34 U/ mg. Assays were attempted at higher temperatures in order to replicate physiological conditions for the thermophilic enzyme; however, protein precipitation was observed at ≥ 50°C. Therefore, efforts to study the reaction under physiological conditions were not pursued further. It is possible that the enzyme is only

heat-stable as the assembled FGAR-AT complex. As with the *B. subtilis* enzyme, the NH₄Cl-

dependent activity is not ADP-dependent since inclusion of PEP and PK in the assay buffer

(which rapidly removes any ADP generated during turnover) had no effect on the observed

activity.

Table 6.1: Kinetic Parameters for the *T. maritima* smPurL		
	K_m (mM)	k_{cat} (s^{-1})
WT Enzyme		
FGAR	1.05 ± 0.06	0.40 ± 0.01
ATP[a]	0.35 ± 0.04	0.34 ± 0.01
NH₄Cl[a]	153 ± 7	0.39 ± 0.01
H32A Mutant	ND[b]	< 0.001 s^{-1}
H72A Mutant		
FGAR[c]	~ 38 mM	~ 0.02

[a]These are apparent K_ms due to subsaturating FGAR. [b]No activity could be detected above the lower limit of detection for the Bratton-Marshall assay. [c]The enzyme could not be saturated with FGAR; therefore, these values are approximations.

A kinetic analysis of the enzyme revealed several interesting features (Table 6.1).

First, the k_{cat} for both the ATPase and FGAM synthetase activities are similar (0.34 vs. 0.4 s^{-1},

respectively), indicating that ATP hydrolysis is coupled to FGAM formation. The lower ATPase

k_{cat} is the result of using a subsaturating amount of FGAR (2 mM). The k_{cat} values are nearly

10-fold higher than those obtained for the *B. subtilis* smPurL under similar conditions (k_{cat} =

0.044 s^{-1}). The high activity is surprising since the enzyme is being assayed at nearly 50°C less

than its temperature optimum under physiological conditions. Second, it is interesting to note

that the enzyme can be readily saturated with NH₄Cl (K_m = 153 mM at 2 mM FGAR, Figure

6.5). Assuming that the enzyme uses NH₃ as its actual substrate, this corresponds a K_m of 5.7

mM at pH 8.0 indicating that the enzyme displays a similar K_m for NH₃ as the *B. subtilis* smPurL

(K_m = 3.5 mM) .
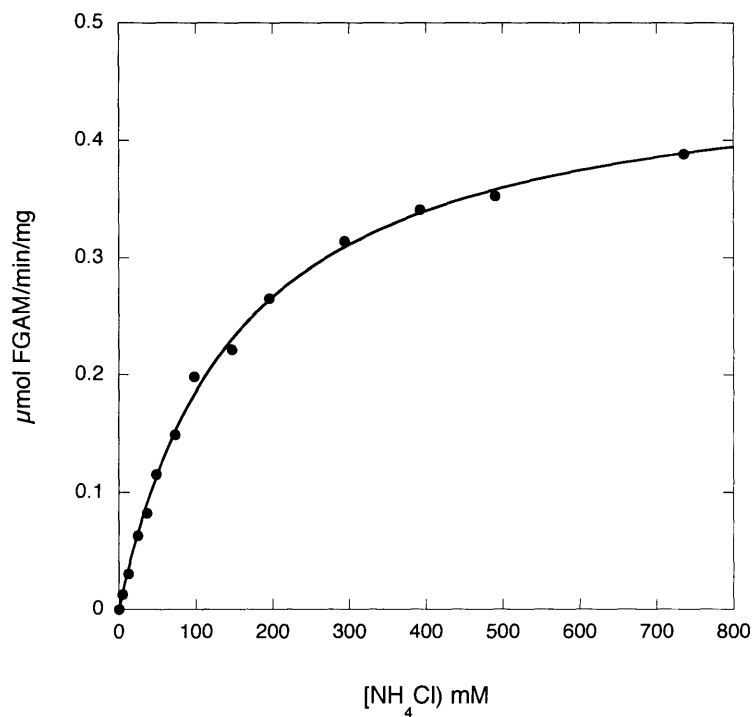
Figure 6.5—K$_m$ determination for NH$_4$Cl for wt *T. maritima* smPurL. At 750 mM NH$_4$Cl, the enzyme can be saturated with substrate (K$_m$ = 153 mM).
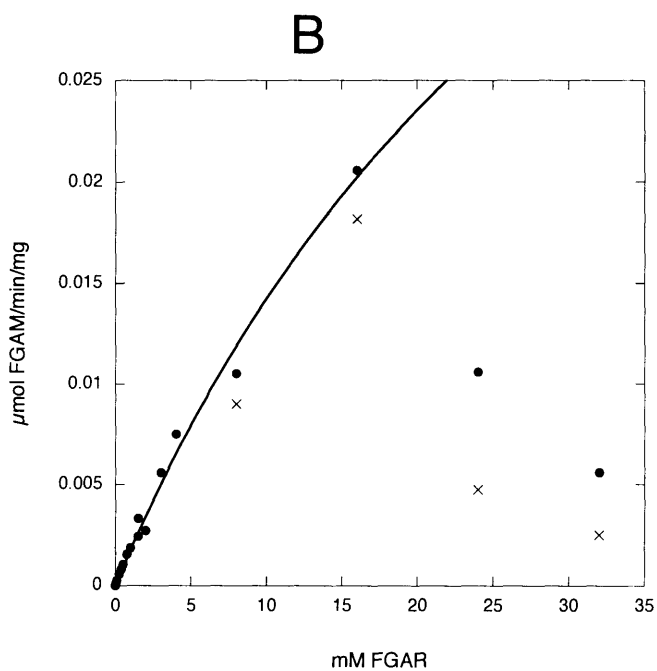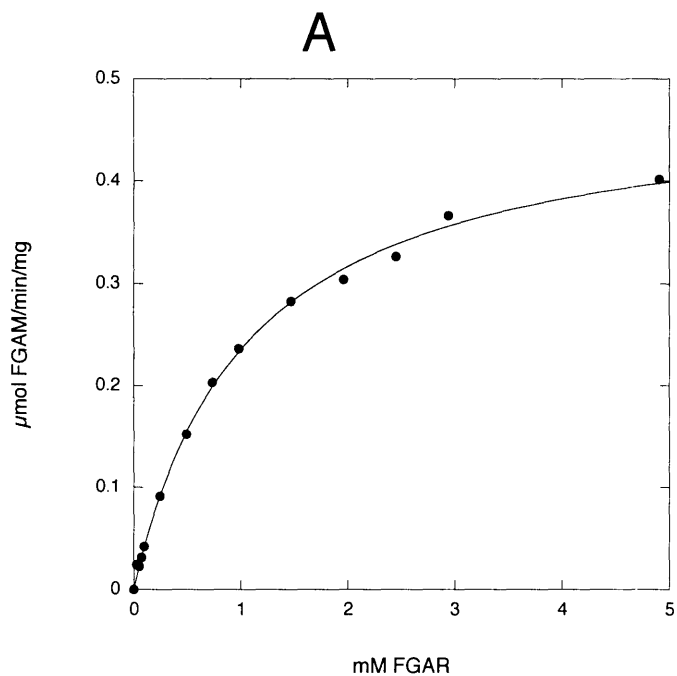
Figure 6.6—Comparison of the Michaelis-Menten plots for FGAR for the wt (A) and (B) H72A mutant *T. maritima* smPurL enzymes. (A) The wt enzyme could easily be saturated with FGAR and a K_m of 1 mM was determined. (B) The H72A mutant could not be saturated with up to 16 mM FGAR, and severe substrate inhibition was observed at 24 and 32 mM FGAR (●). The inhibition was observed in multiple experiments (×).

313

Activity of H32A and H72A smPurL

Assays of the H32A and H72A smPurL mutants revealed that both residues are important for the function of the enzyme (Table 6.1). No FGAM formation was detected with the H32A mutant at enzyme concentrations up to 11.6 mg/mL after 1 h of incubation in the presence of 10 mM ATP, 4 mM FGAR, and 750 mM NH$_4$Cl. Given the sensitive nature of the Bratton-Marshall assay for aminoimidazole formation, a lower limit of detection on activity for this mutant could be set at $\leq$ 0.1 nmol/min/mg, 1/4000 the activity of the wt enzyme. Thus, His32 is essential either for binding or catalysis.

The H72A mutant displayed very low levels of FGAM production and exhibited a dramatically increased K$_m$ for FGAR (k$_{cat}$ ~ 0.02 s^{-1}, K$_m$ ~ 37.9 mM, Table 6.1). Interpretation of the kinetic data for this mutant was complicated since unlike the wt enzyme, the H72A mutant could not be saturated with FGAR and severe substrate inhibition that could not be modeled with standard equations was observed above 16 mM FGAR (Figure 6.6). While the source of this inhibition has not yet been identified, one possibility is that residual triethylamine from the purification of FGAR is interfering with the assay at high FGAR concentrations. These data indicate that mutation of H72 to an alanine results in decreased affinity for FGAR and retains ~5% of wt activity. While H72 is not essential for catalysis, it is important for FGAR binding due to its possible interactions with both amides of FGAR (Figure 6.4).

Biophysical Characterization of wt and mutant smPurL

Given the problems encountered with *B. subtilis* smPurL aggregation, it was important to determine that the effects on activity observed with the wt *T. maritima* smPurL and the H32A and H72A mutants are not the result of protein aggregation or misfolding. Folding of the mutants relative to the wt protein can be analyzed by CD spectroscopy and aggregation by SV-AUC

experiments. In addition, the H72A mutant has been crystallized by Maria Morar in the presence of AMP-PCP.

As shown in Figure 6.7, CD spectra of the wt and mutant enzymes are very similar, providing evidence that the mutant smPurLs are folded. To interrogate protein aggregation, SV-AUC was carried out, and the data (Figure 6.8) indicate that the predominant species in solution for both the wt and mutant enzymes is the smPurL monomer. The observed molecular weights were very close to the calculated value (wt calculated = 65,969 Da, wt observed = 66,030 Da (rmsd = 0.0045), H32A observed = 64,554 Da (rmsd = 0.0044), H72A observed = 71,081 Da (rmsd = 0.0044)). The H72A mutant enzyme, however, contained a high molecular weight species (likely an aggregated dimer of smPurL, 26% abundance). Despite the presence of aggregate, the H72A mutant has been crystallized in the presence of AMP-PCP and its structure determined. Superposition of the wt ternary complex structure and the H72A structure revealed that the mutant has little effect on the overall structure or to the active site architecture (Figure 6.9); however, it is possible that a correctly folded, non-aggregated species was selectively crystallized out of an heterogeneous solution of the H72A mutant.
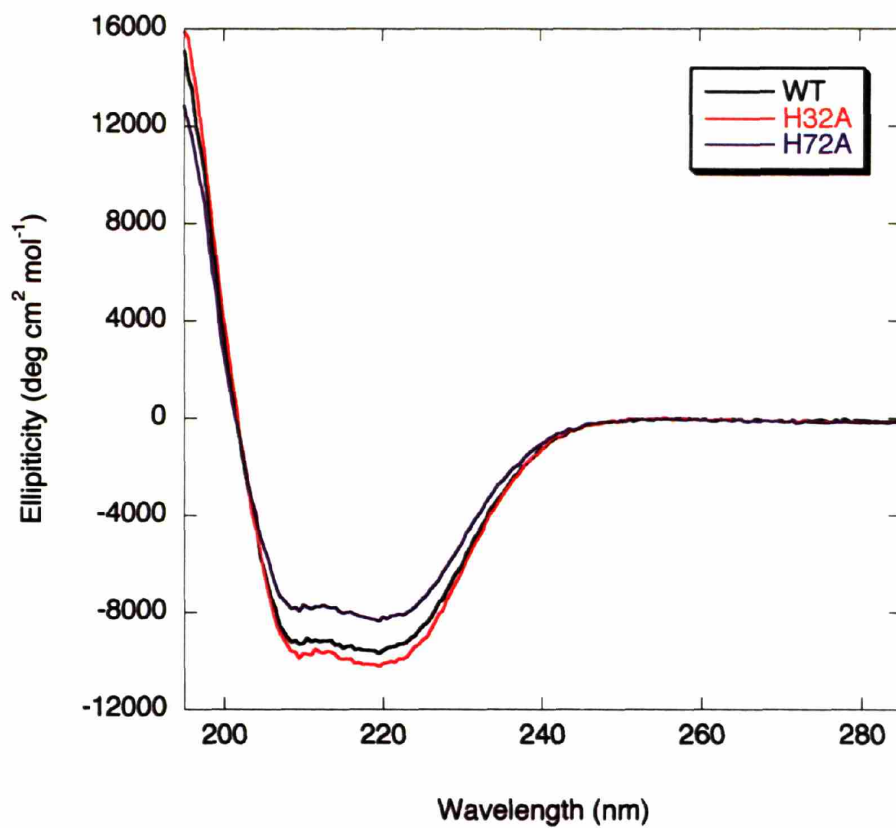
Figure 6.7—CD spectra for the *T. maritima* wt (black), H32A (red), and H72A (blue) smPurLs.
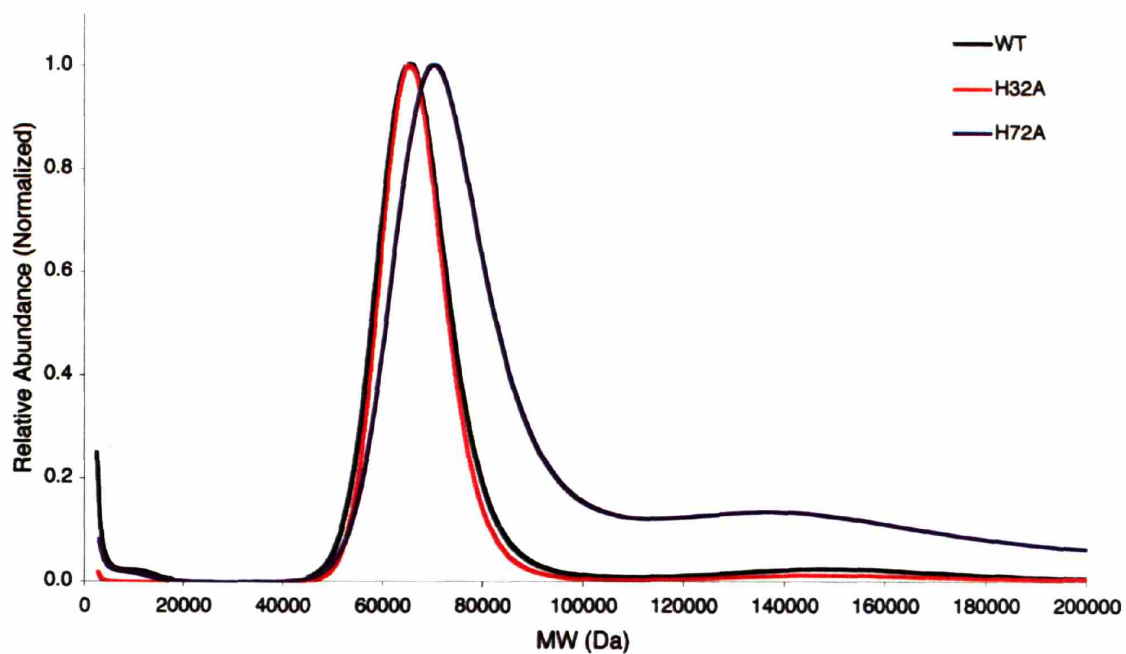
Figure 6.8—Results from SV-AUC experiments on wt (black), H32A (red), and H72A (blue) *T. maritima* smPurLs. Both the wt and H32A are monomers in solution. The H72A mutant contains a small amount of aggregate.

Figure 6.9—Backbone overlay of the ternary complex of wt smPurL with FGAR and AMP-PCP (blue) and the binary complex crystal structure of the H72A mutant with AMP-PCP (black). AMP-PCP and His32 are shown in stick representation and labeled in the structures. The active sites of the mutant and wt enzymes are superimposable indicating that the mutation did not cause a large conformational change in the enzyme.

6.4 Discussion

The structures of smPurL in complex with substrate and substrate analogs have provided the first insight into the mechanisms of ATP-binding by the PurM-superfamily. The ATP-binding site is characterized by a hydrophobic pocket for the adenine ring at the monomer:monomer interface and coordination of phosphates by bridging magnesium ions. The aspartate of the DX_4GAXP motif provides a ligand to the magnesium ion coordinating the β,γ-phosphates of AMP-PCP. The remainder of the motif (GAXP) lies in a turn between an α-helix containing the aspartate and a β-strand that composes part of the central β-barrel in the pseudo-dimeric structure. The location of the DX_4GAXP motif is conserved in all structures of PurM-superfamily members available to date.

Co-crystallization of the enzyme with FGAR has provided insight into the ribonucleotide binding site. The most striking feature of this site is the presence of two conserved histidine residues located near the proposed site of chemistry. H72 is positioned between the two amides of FGAR, while H32 lies between the nucleophilic oxygen of the FGAR amide and the γ-phosphate of ATP (Figure 6.4). No other residues are observed in the proximity of the phosphorylation site. Since these histidines are absolutely conserved among all smPurL and lgPurL sequences, they must be involved in binding and/or catalysis.

Proposed Mechanisms for Amidine Formation

Research by Westheimer and coworkers demonstrated that methyl metaphosphate can facilitate the addition of aniline to ethylbenzoate to produce *O*-ethyl-*N*-phenylbenzimidate and methylphosphate (*15*). A mechanism to account for this observation is shown in Figure 6.10 in which methyl metaphosphate generated from fragmentation of methyl hydrogen *erythro*-1,2-dibromo-1-phenylpropylphosphonate activates the ester for nucleophilic attack. This reaction

319

A

B

C
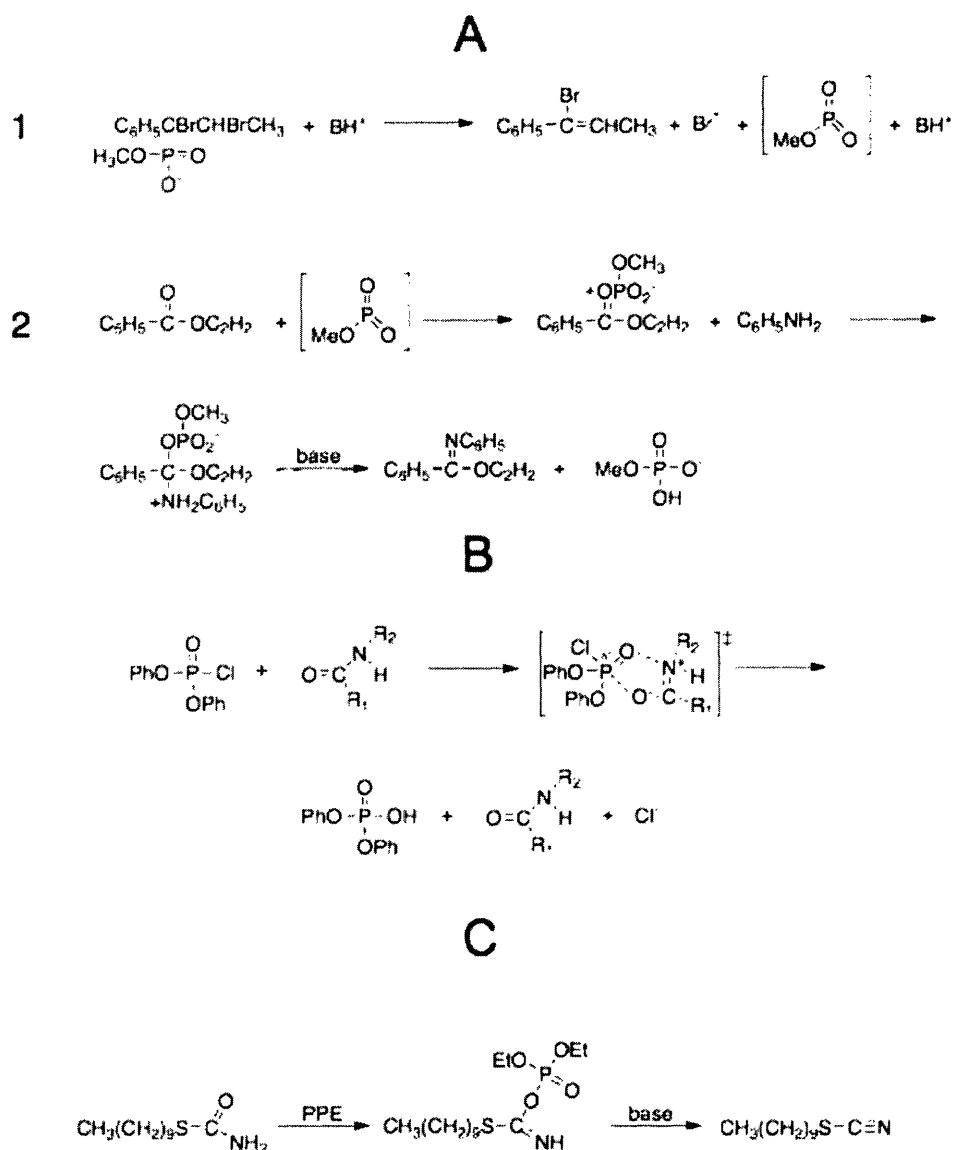
Figure 6.10—Examples of carbonyl reactivity towards phosphorous compounds. (A) A reaction scheme proposed by Westheimer for reaction of ethylbenzoate with methyl metaphosphate *(15)*. Methyl metaphosphate is proposed to be generated by fragmentation of the phosphonate in (1). The methyl metaphosphate then is proposed to activate the ester carbonyl in (2) for nucleophilic attack by aniline. This scheme has been proposed to be an excellent model for the PurL-catalyzed reaction. (B) Popov *et al.* have studied amide catalyzed hydrolysis of diphenyl chlorophosphate *(18-20)*. For *N*-monosubstituted amides, an associative mechanism has been proposed involving a five-membered ring transition state and a pentacoordinate phosphorous species. (C) In a model for the HypE reaction, Bock and co-workers were able to dehydrate *S*-(-*n*-decyl) thiocarbamate with ethyl polyphosphate followed by base treatment *(25)*. An iminophosphate intermediate was proposed, but not isolated.

320

with an ester carbonyl is similar to that of ATP, using a dissociative transition state, activating

the amide oxygen of FGAR for attack by NH_3. This work allowed Westheimer to propose two

possible mechanisms for amidine formation (Figure 6.11) (15). In the first case, the reaction

proceeds by a tetrahedral intermediate generated by NH_3 attack on the amide followed by ATP-

mediated phosphorylation. While in the second case, an iminophosphate is initially formed by

ATP, which is followed by NH_3 attack. Westheimer's demonstration of carbonyl reactivity

towards metaphosphate favors the iminophosphate mechanism, although a phosphorylated

FGAR intermediate has yet to be identified during FGAM synthesis despite extensive efforts by

the Stubbe Laboratory.

Recently, dehydration of amides without the direct use of ATP has been demonstrated in

several non-ribosomal peptide synthetase systems during the synthesis of thiazole or oxazole

rings (16, 17). However, the ^{18}O-transfer experiments carried out by Schendel in the Stubbe

Laboratory provide strong evidence that ATP is directly involved in the transfer mechanism in

the case of lgPurL, and presumably smPurL, since the ^{18}O-label was transferred from the FGAR

amide to phosphate during the reaction (8).

Insight into the mechanism of nucleophilic activation of an amide oxygen has more

recently come from studies of Popov et al. This group has demonstrated that amides can

catalyze hydrolysis of benzoylchloride and diphenyl chlorophosphate in an aprotic medium (18-

20). Two mechanisms were proposed for these reactions: nucleophilic attack by the amide

oxygen or general base catalysis. Structure-function studies using a variety of amides favored

the former mechanism (18-20). While no intermediates were trapped in their experiments, for N-

monosubstituted amides, it was been postulated that the reaction proceeds via an associative
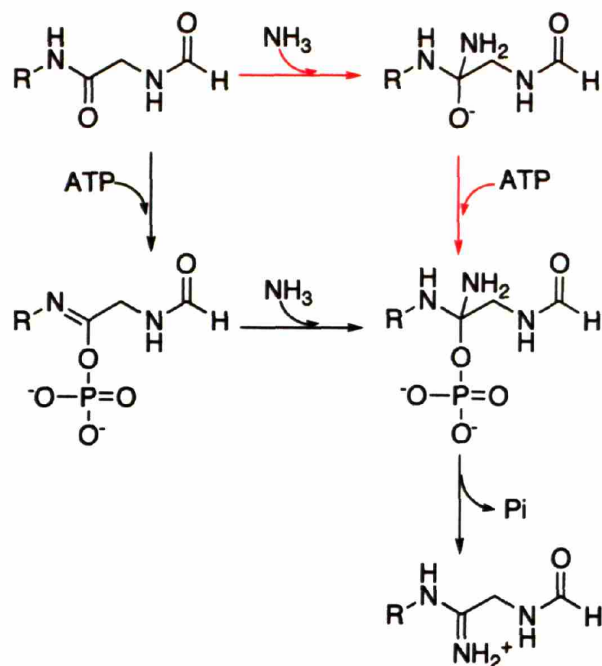
Figure 6.11—Proposed reaction mechanisms for PurL by Westheimer *(15)*. The reaction is believed to proceed either through an iminophosphate intermediate (black arrows) or by initial tetrahedral intermediate formation (red arrows).

mechanism by formation of a pentacoordinate phosphorous species in a five-membered ring

transition state (Figure 6.10B) (*20*).

In addition, it has been known since the 1930s that amides react with $POCl_3$ (*21*), which

in the presence of amines can lead to amidine formation (*22*). However, there have been no

mechanistic studies on these reactions, and only two reports of isolation of a putative

phosphorous adduct to the amide oxygen (*23, 24*). In both cases, the adduct was isolated in

anhydrous solvent (ether or THF) and characterized by optical and IR spectroscopy. Further

evidence for amide reactivity comes from a model system for the HypE catalyzed reaction

(Figure 6.10C). HypE catalyzes formation of an enzyme-linked thiocyanate from a

thiocarbamate (Figure 6.1). In a model system for this reaction, *S*-(*n*-decyl) thiocarbamate was

readily dehydrated in the presence of ethyl polyphosphate (PPE) in $CHCl_3$ followed by the

addition of triethylamine (*25*). While no intermediates were isolated, the reaction gave the

corresponding thiocyanate in 55% yield, and an iminophophate intermediate was proposed.

The active site structure of the smPurL•FGAR•AMP-PCP ternary complex offers a new

opportunity to think about the mechanism of amidine formation. An early hypothesis, despite

mismatched pK_as,was that H72 deprotonated the amide of FGAR to activate the oxygen for

nucleophilic attack on ATP with a neutralized charge on the γ-phosphate. However, based on

literature precedent, deprotonation of FGAR is not required for the amide to function in this

capacity. This may explain why the H72A mutant retains some activity and avoids the

requirement for perturbation of the pK_a's for H72 or FGAR so that deprotonation of an amide by

an imidazole to occur. In addition, given the current structural information, it is unclear how the

charge on the γ-phosphate would be neutralized to allow nucleophilic attack to proceed. A

bridging Mg^{2+} is observed between the β- and γ-phosphates; however, no positively charged

protein sidechains interact with the γ-phosphate in the structure with AMP-PCP. One possibility is that H32 is protonated and can interact with ATP during turnover conditions, and this possibility is discussed in greater detail below. Given the observations detailed above, an alternate role for H72 may be to fix the position of the amide nucleophile of FGAR with respect to the γ-phosphate of ATP and lower the entropic barrier of the reaction. A similar effect of constraining the position of the nucleophiles has been observed in model phosphoryl transfer reactions (26) and has been implicated in nucleoside diphosphate kinases (27). In the former case, hydrolysis of phosphorylated pyridines by $Mg(OH)^+$ was proposed to be accelerated by correct positioning of the hydroxide ion and the phosphate group due to interactions between the phosphate and Mg^{2+} (26). In the latter case, nucleoside diphosphate kinases utilize a phosphoryl-histidine intermediate to transfer phosphate from ATP to a NDP. Herschlag and coworkers have mutated this catalytic histidine to glycine and have studied the ability of imidazole or other small nucleophiles to rescue ATP hydrolysis activity (27). These results suggested that free imidazole cannot fully substitute for the histidine side-chain and positioning of the histidine nucleophile by the enzyme is an important component of catalysis (27).

In the model studies of Popov et al., amide reactivity was studied using electrophiles containing a very good leaving group (Cl⁻) (18-20). In order for ADP to act as a good leaving group, charges on the phosphates must be neutralized. Unlike many ATP-binding sites, the active site of smPurL does not contain positively charged residues that interact with the phosphates of ATP, nor is the nucleotide located in a position for charges to be stabilized by a helix dipole (Figure 6.3). Neutralization of the negative charges on the phosphates appear to stem entirely from interaction with the two Mg^{2+} ions, while interactions from the hydroxyl group of Y35 and the backbone amide proton of A239 may help orient the phosphate chain. The

only other residue in the active site capable of stabilizing negative charge is H32. This residue is located in between the FGAR amide and the γ-phosphate of AMP-PCP, but in the ternary complex structure, it is not in hydrogen-bonding orientation to either group. The lack of hydrogen bonds to H32 leave its protonation state undetermined; however, the orientation of the residue may change during catalysis or in the presence of ATP in order to provide hydrogen-bonding interactions with the γ-phosphate. In this case, a protonated H32 may help to stabilize negative charge on either ATP or a phosphorylated FGAR intermediate. Mutagenesis results from the H32A mutant indicate that this residue is important for catalysis; however, further studies using H32Q mutants may provide additional clues concerning the role of this residue in FGAM synthesis.

The lack of residues capable of neturalizing phosphate charge within the smPurL active site also indicate that the reaction might proceed via a dissociative mechanism of phosphate transfer. This mechanism would require less charge neutralization in the transition state than an associative mechanism (Figure 6.12) (*28, 29*). Hydrolysis of ATP in solution has been well studied and is known to proceed via a dissociative mechanism (*28*). Phosphoryl-transfer reactions in enzymes are less well-understood; however, there have been several examples in which dissociative mechanisms have been proposed (*29*). If the reaction proceeds with a dissociative, metaphosphate intermediate, than the reaction of ATP and FGAR will be analogous to model reactions carried out by Westheimer (Figure 6.10A).

Dissociative
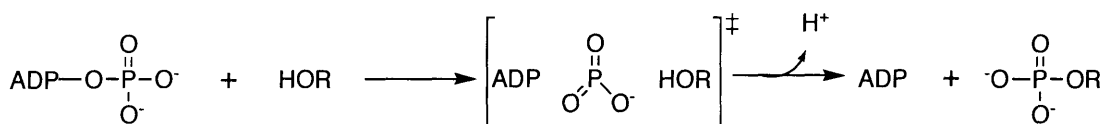
Associative
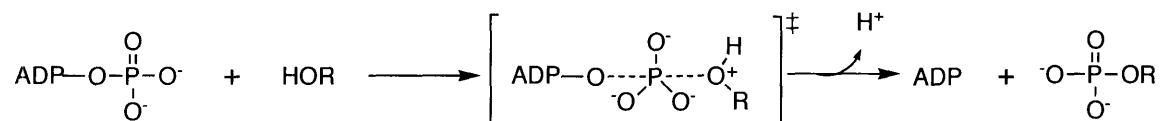
Figure 6.12—Dissociative and associative models for phosphoryl transfer from ATP to an alcohol (ROH). In the dissociative mechanism, a metaphosphate transitation state is proposed with a single negative charge on a phosphoryl oxygen. In the associative mechanism, a pentacovalent phosphorane is proposed in the transition state with three negative charges on the phosphorous oxygens. This figure was adapted from *(28)*.

Histidines are Not Part of a Conserved Mechanism of Catalysis in the PurM-Superfamily

While the function of conserved histidines H32 and H72 is still not understood, their location in the smPurL structure and their importance for enzyme activity suggest that similar histidines may be involved in catalysis in other PurM-superfamily members. All superfamilies, by definition, have a common mechanism (*30*), and in this case, the use of histidines to stabilize negative charge on the phosphate-leaving group may be the common mechanism that unites members of the PurM-superfamily. However, previous sequence alignments alone failed to identify any conserved histidines.

Given the recent structures of a number of PurM-superfamily members, one can now perform structure-based sequence alignments previously not possible. Structure-based sequence alignments generated for smPurL and PurM (Figure 6.13) indicate that H32 and H72 are not conserved in PurM. However, when the structures of PurM and smPurL are superimposed using Swiss PDB-Viewer, two conserved histidines in PurM (His190 and His247) become readily apparent (Figure 6.14). These residues are in the same approximate locations as the residues in smPurL, but they have been flipped 180° to the other side of the active site. The reason for the change in location may be due to movement of the site of phosphorylation to the terminal amide of FGAM from the internal amide of FGAR. Thus, their presence may imply conservation of mechanism (Figure 6.1). However, this proposal contains the caveat that FGAM may bind differently to PurM than FGAR does to smPurL. Simple rotations of the FGAR side chain about the C1'-N1, C2-C3, or C3-N4 bonds are not enough to bring the terminal amide near H190 and H247 in PurM. In addition, neither smPurL residue H74, which ligates the 5'-phosphate of FGAR, nor E280, which ligates the 2'-OH of FGAR, are conserved in PurM and homologous residues are not easily identified. This has complicated identification of the FGAM-binding site
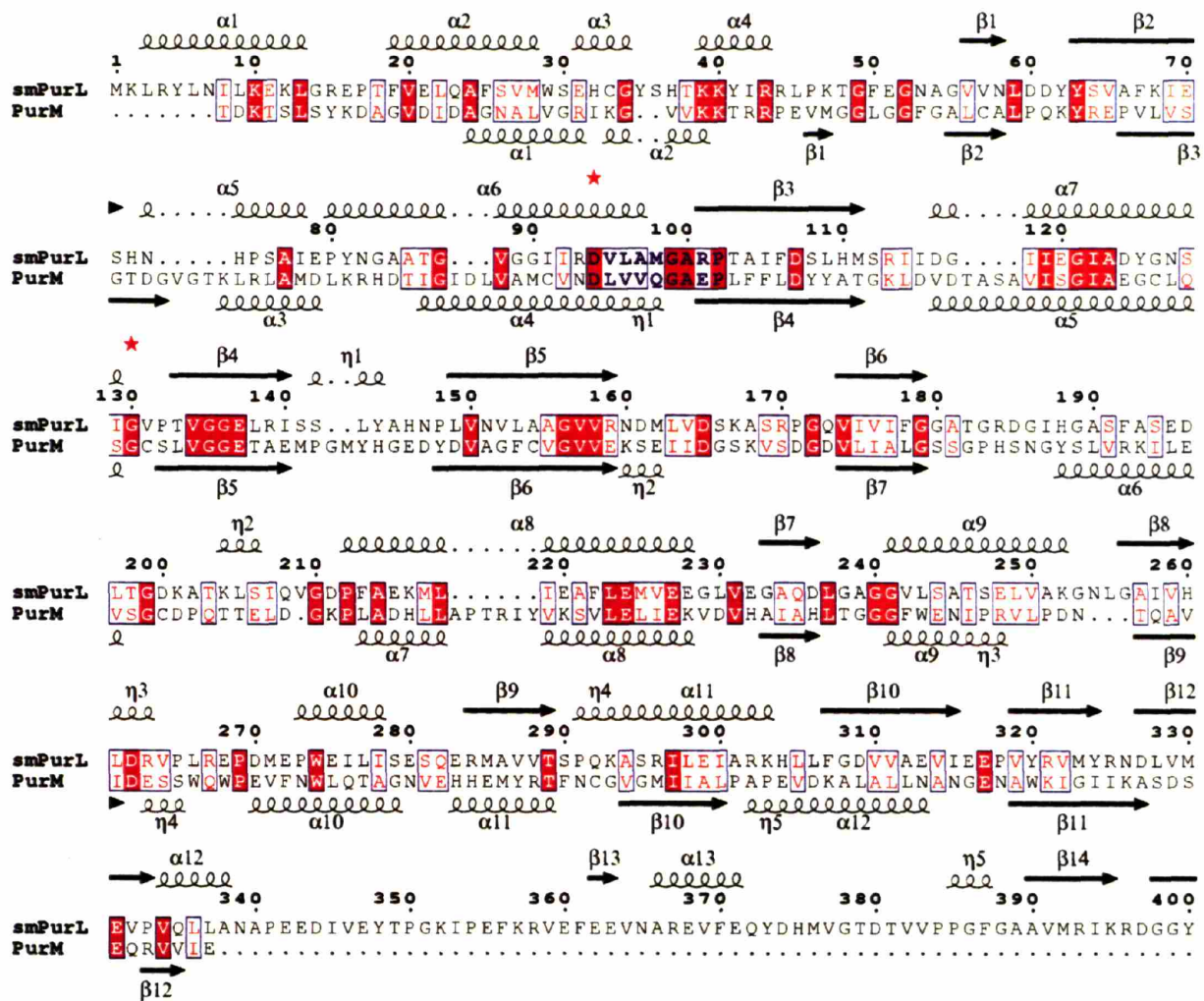
Figure 6.13—Structure-based sequence alignment of *E. coli* PurM with the N-terminal domain of *T. maritima* smPurL. The Dx₄GAxP motif is shown in blue and in each structure the aspartate is found in an α-helix, while GAxP occurs in a turn between the helix and a β-strand. H32 and H72 from smPurL are denoted with red stars. Neither of these histidines are conserved by structure or sequence with PurM.
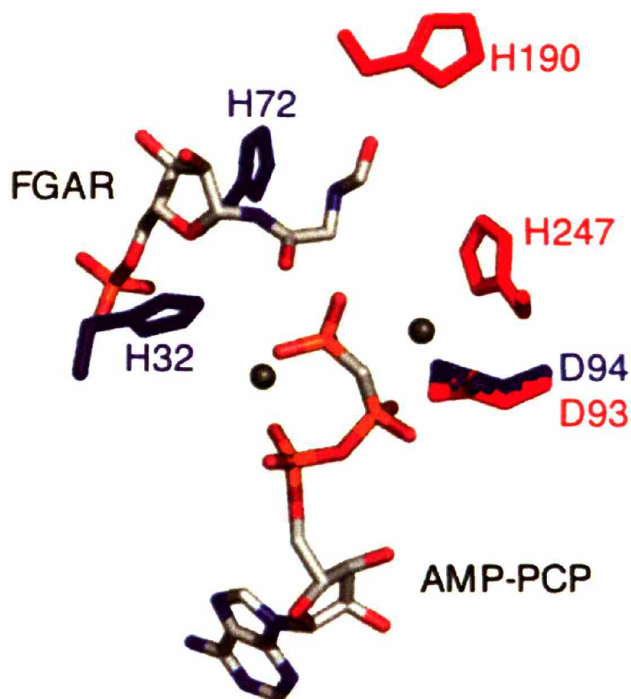
Figure 6.14—Identification of conserved histidines in PurM (red) by superimposition of the smPurL structure (blue). Structures were superimposed using the Cα backbone with Swiss PDB-Viewer (http://www.expasy.org/spdbv/). FGAR and AMP-PCP are shown in stick-figure representation, and the Mg^{2+} ions are shown as grey spheres. The ATP-binding sites of smPurL and PurM aligned and the conserved aspartates of the DX$_4$GAXP motifs are superimposable (D93 and 94). H190 and 247 in PurM may be analogous to H72 and H32 in smPurL, respectively. Histidines in PurM are not located on the same secondary structural elements as in smPurL and appear to occupy a different orientation in the active site.

in PurM, and leads to uncertainty concerning the role of H190 and H247 in the absence of

crystallographic or biochemical data. Efforts to extend these observations to other members of

the PurM superfamily indicate that histidines are not conserved active site residues. Conserved

histidines were identified by CLUSTALW sequence alignments of >20 diverse ThiL, SelD, and

HypE genes. These results are summarized in Table 6.2. With the use of Modeller and sequence

Table 6.2: Conserved Histidine Residues among PurM-Superfamily Members

Protein	Residue	In the Active Site?	Location
smPurL (*T. maritima*)	H32	Yes	Adjacent to γ-phosphate of ATP and FGAR amide
	H72	Yes	Ligand to FGAR amides
PurM (*E. coli*)	H190	Yes	FGAM Binding site (predicted)
	H247	Yes	Adjacent to γ-phosphate of ATP (predicted)
ThiL (*Aquifex aeolicus*)	H50	No	Part of Monomer:Monomer Interface
	H185	Yes	In the same region as H190 of PurM
	H305	Unknown	At the disordered C-terminus
HypE (*E. coli*, modeled)	H165	Yes	In the same region as H190 of PurM
	H280	No	Surface
SelD (*E. coli*,modeled)	H13	No	Surface
	H198	No	Surface
	H236	No	Buried

alignments between family members (Figure 6.15), model structures of *E. coli* SelD and HypE

were made based upon all available crystal structures for PurM-superfamily members (Figure

6.16). Both the β-sheet regions that comprise the monomer:monomer interface, the active site

cleft, and residues involved in ATP binding could be identified in the modeled structures. These

landmarks allowed the position of each conserved histidine within a family member to be

determined relative to the enzyme active site. These results indicate that a histidine located near

```
              1         10        20        30        40        50        60
HypE     ....MQQLINSLFMEAFANPWLAEQEDQARLDLAQLVAEGDR...LAFSTDSYVIDPLFFPGGN......
PurM     TDKTSLSYKDAGVDIDAGNALVGRIKGVVKKTRRPEVMGGLGGFGALCALPQKYREPVLVSGTDGVGTKL
ThiL     ....MRLKELGEFG.......LIDLIKKTLESKVIGDDTAPVEYCSKKLLLTTDVLNEGVHFLRSYI
SelD     MSENSIRLTQYSHGAGCGCKISPKVLETILHSEQAKFVDPNLLVGNETRDDAAVYD..LGNGTSVISTTD
smPurL   ...MKLRYLNILKEKLGREPTFVELQAFSVMWSEHCGYSHTKKYIRRLPKTGFEGNAGVVNLDDYYSVAF
                                            *

              70        80        90        100       110       120       130
HypE     ...............IGKLAICGTANDVAVSGAIPRYLSCGFILEE.GLPMETLKAVVTSMAETARAAGI
PurM     RLAMD....LKRHDTIGIDLVAMCVNDLVVQGAEPLFFLD.YYATG.KLDVDTASAVISGIAEGCLQSGC
ThiL     P..........EAVGWKAISVNVSDVIANGGLPKWALISLNLPE.DLEVSYVERFYIGVKRACEFYKC
SelD     FFMPI....VDNPFDFGRIAATNAISDIFAMGGKPIMAIAILGWPINKLSPEIAREVTEGGRYACRQAGI
smPurL   KIESHNHPSAIEPYNGAATGVGGIIRDVLAMGARPTAIFDSLHMSR......IIDGIIEGIADYGNSIGV
             *

              140       150       160       170       180       190
HypE     AIVTGDTKVVQRGAVDKLFINTAG..MGAIPANIHWGAQTLTAGDVLLVSGTLGDHGATILNLRECLGLD
PurM     SLVGGETAEMP.GMYHGEDYDVAGFCVGVVEKSEIIDGSKVSDGDVLIALGSSGPHSNGYSLVRKILEVS
ThiL     EVVGGNISKSE.......KIGISVFLVGETER..FVGRDGARLGDSVFVSGTLGDSRAGLELLLMEKEEY
SelD     ALAGGHSIDAP.......EPIFGLAVTGIVPTERVKKNSTAQAGCKLFLTKPLG...IGVLTTAEKKSLL
smPurL   PTVGGELRISS...LYAHNPLVNVLAAGVVRNDMLVDSKASRPGQVIVIFGGATGRDGIHGASFASEDLT
                                                       *

              200       210       220       230       240       250       260
HypE     G..ELVSDCAVLTPLIQTLRDIPGVKALRD.....ATRGG.VNAVVHEFAAACGCG..IELSEAALPVKP
PurM     G..CDPQTTELDGKPLADHLLAPTRIYVKS.....VLELI.EKVDVHAIAHLTGGGFWENIPRVLPDNTQ
ThiL     EPFELALIQRHLRPTARIDYVKHIQKYANA.....SMDIS.DGLVADANHLAQRSGVKIEILSEKLPLSN
SelD     KPEHQGLATEVMCRMNIAGASFANIEGVKA.....MTDVTGFGLLGHLSEMCQGAGVQARVDYEAIPKLP
smPurL   GDKATKLSIQVGDPFAEKMLIEAFLEMVEEGLVEGAQDLGAGGVLSATSELVAKGNLGAIVHLDRVPLRE
                                                                *

              270       280       290       300       310       320       330
HypE     AVRGVCELLGLD...ALNFANEGKLVIAVER.....NAAEQVLAALHSHPLGKDAALIGEVVERKGVRLA
PurM     AVIDESSWQWPE...VFNWLQTAGNVEHHEMYR.TFNCGVGMIIALPAPEVDKALALLNANGEN.....A
ThiL     ELKMYCEKYGKN...PIEYALFGGEDYQLLFT...HPKERWNPFLDMTEIGRVEEGEGVFVDG.....
SelD     GVEEYIKLGAVPGGTERNFASYGHLMGEMPREVRDLLCDPQTSGGLLLAVMPEAENEVKATAAEFGIELT
smPurL   PDMEPWEILISESQERMAVVTSPQKASRILEIARKHLLFGDVVAEVIEEPVYRVMYRNDIVMEVPVQLLA

              340       350       360
HypE     GLYGVKRTLDLPHAEPLPRIC.
PurM     WKIGIIKASDSEQRVVIE....
ThiL     ......KKVEPKGWKHF.....
SelD     AIGELVPARGGRAMVEIR....
smPurL   NAPEEDIVEYTPGKIPEFKRVE
```
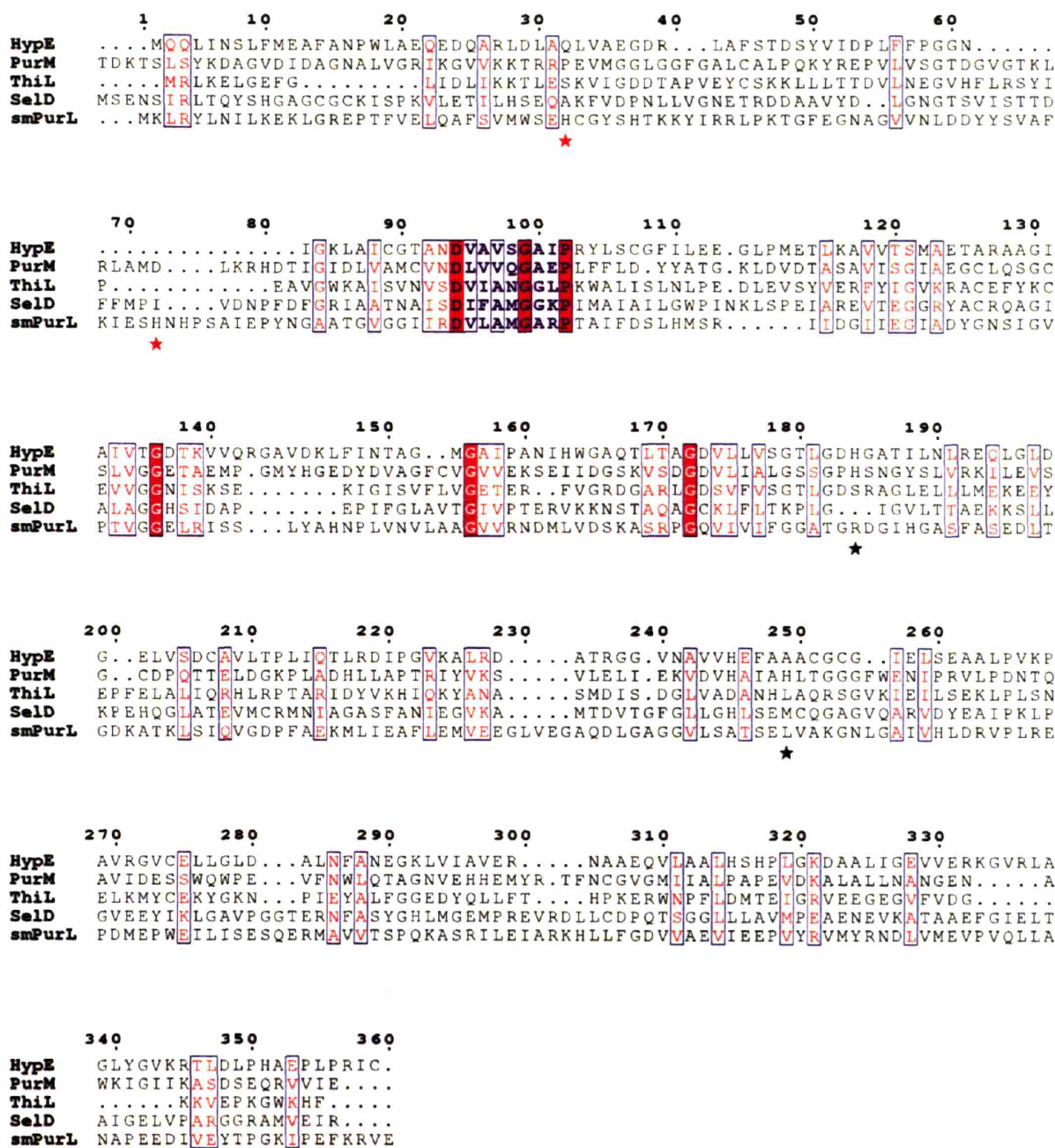
Figure 6.15—Sequence alignment of *E. coli* HypE, *E. coli* PurM, *A. aeolicus* ThiL, *E. coli* SelD, and *T. maritima* smPurL. Residues are numbered according to smPurL. The conserved DX₄GAXP motif is shown in blue. Conserved histidines in smPurL (H32 and H72) are shown with red stars. Conserved histidines in PurM (H190 and H247) are shown with black stars. The conserved glycines highlighted in this alignment are not part of the active site. They are instead part of the central β-barrel.
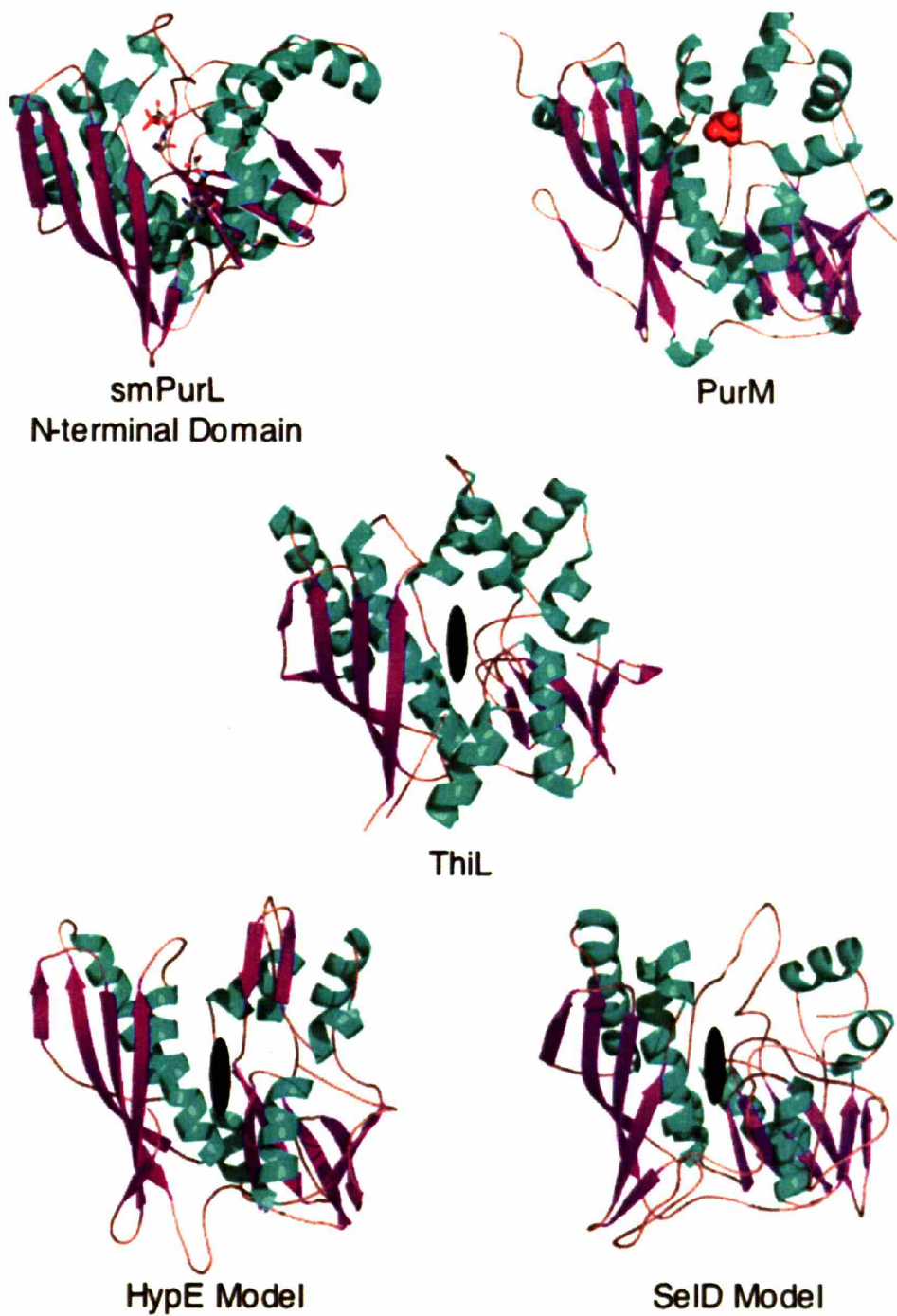
Figure 6.16—Comparison of HypE and SelD model structures to those observed for smPurL, PurM, and ThiL. In all cases, the active site is a cleft located in the center of the structure. In the smPurL structure, AMP-PCP and FGAR are bound in the cleft. In the PurM, structure SO_4^{2-} is observed in the cleft. The clefts in ThiL, HypE, and SelD have been marked with a black oval.

the γ-phosphate of ATP is not conserved across PurM-superfamily members (Table 6.2) and

rules out a common phosphorylated-histidine intermediate or the use of a conserved histidine in

electrostatic stabilization. However, it is possible that like members of the crotonase superfamily

(*30*), members of the PurM-superfamily share a common mechanism without conservation of

active site residues. A common dissociative mechanism of phosphoryl-transfer may be the

unifying feature of the PurM-superfamily; however, testing this hypothesis will require extensive

investigation into several superfamily members.

Future experiments on PurL mechanism should be aimed at providing direct evidence for

an iminophosphate intermediate, assuming the reaction does not proceed through initial

tetrahedral intermediate formation (Figure 6.11). smPurL may provide a new direction for

efforts to trap an iminophosphate. Previous efforts by Ernest Mueller in the Stubbe Laboratory

to detect a phosphorylated intermediate either directly or by ATP/ADP exchange and positional-

isotope-exchange (PIX) experiments were unsuccessful in the case of lgPurL (*31*). In the case of

PurM, efforts to detect an iminophosphate could be difficult since after phosphorylation,

intramolecular attack by FGAM creates the aminoimidazole. With smPurL, it is possible that the

iminophosphate could be generated by withholding the NH_3 nucleophile necessary for FGAM

formation. These experiments may be particularly successful on the *T. maritima* smPurL, which

shows a 10-fold higher rate of NH_3-dependent FGAM formation than other PurLs and may give

rise to successful PIX experiments. A second strategy that could be employed is to reduce the

iminophosphate in the active site of smPurL. Due to the absence of the N-terminal (PurS) and

glutaminase (PurQ) domains, the active site of smPurL may be more open than in lgPurLs.

Reducing agents may be able to diffuse into the active site without denaturing the protein and

trap a phosphorylated-FGAR intermediate in order to finally provide evidence for

iminophosphate formation.

6.5 References

(1)   Li, C., Kappock, T. J., Stubbe, J., Weaver, T. M., and Ealick, S. E. (1999) X-ray crystal structure of aminoimidazole ribonucleotide synthetase (PurM), from the *Escherichia coli* purine biosynthetic pathway at 2.5 Å resolution. *Structure 7*, 1155-66.

(2)   Anand, R., Hoskins, A. A., Stubbe, J., and Ealick, S. E. (2004) Domain organization of *Salmonella typhimurium* formylglycinamide ribonucleotide amidotransferase revealed by X-ray crystallography. *Biochemistry 43*, 10328-42.

(3)   Mueller, E. J., Oh, S., Kavalerchik, E., Kappock, T. J., Meyer, E., Li, C., Ealick, S. E., and Stubbe, J. (1999) Investigation of the ATP binding site of *Escherichia coli* aminoimidazole ribonucleotide synthetase using affinity labeling and site-directed mutagenesis. *Biochemistry 38*, 9831-9.

(4)   Marolewski, A., Smith, J. M., and Benkovic, S. J. (1994) Cloning and characterization of a new purine biosynthetic enzyme: a non-folate glycinamide ribonucleotide transformylase from E. coli. *Biochemistry 33*, 2531-7.

(5)   Thoden, J. B., Firestine, S. M., Benkovic, S. J., and Holden, H. M. (2002) PurT-encoded Glycinamide Ribonucleotide Transformylase. *J. Biol. Chem. 277*, 23898-23908.

(6)   Laue, T. M., Shah, B. D., Ridgeway, T. M., and Pelletier, S. L. (1992) in *Analytical ultracentrifugation in biochemistry and polymer science* (Harding, S.E., Ed.) pp 90-125, The Royal Society of Chemistry, Cambridge, UK.

(7)   Schuck, P. (2000) Size distribution analysis of macromolecules by sedimentation velocity ultracentrifugation and Lamm equation modeling. *Biophysical J. 78*, 1606-1619.

(8)   Schendel, F. J., Mueller, E., Stubbe, J., Shiau, A., and Smith, J. M. (1989) Formylglycinamide ribonucleotide synthetase from *Escherichia coli*: cloning, sequencing, overproduction, isolation, and characterization. *Biochemistry 28*, 2459-71.

(9)   Higgins, D., Thompson, J., and Gibson, T. J. (1994) CLUSTAL W: improving the sensitivity of progressive multiple sequence alignment through sequence weighting, position-specific gap penalties and weight matrix choice. *Nucleic Acids Research 22*, 4673-4680.

(10)   Gouet, P., Courcelle, E., Stuart, D. I., and Metoz, F. (1999) ESPript: multiple sequence alignments in postscript. *Bioinformatics 15*, 305-308.

(11)   Söding, J., Biegert, A., and Lupas, A. N. (2005) The HHpred interactive server for protein homology detection and structure prediction. *Nucleic Acids Research 33*, W244-W248.

(12)   Sali, A. and Blundell, T. L. (1993) Comparitive protein modelling by satisfaction of spatial restraints. *J. Mol. Biol. 234*, 779-815.

(13)   Morera, S., Chiadmi, M., LeBras, G., Lascu, I., and Janin, J. (1995) Mechanism of phosphate transfer by nucleoside diphosphate kinase: X-ray structures of the phosphohistidine intermediate of the enzymes from Drosophila and Dictyostelium. *Biochemistry 34*, 11062-70.

(14)   Tari, L. W., Matte, A., Goldie, H., and Delbaere, T. J. (1997) Mg^{2+}-Mn^{2+} clusters in enzyme-catalyzed phosphoryl-transfer reactions. *Nat. Struct. Biol. 4*, 990-994.

(15)   Satterthwait, A. C. and Westheimer, F. H. (1980) Monomeric Methyl Metaphosphate: Reactions with Carbonyl Groups. *J. Am. Chem. Soc. 102*, 4464-4472.

(16) Kelly, W. L., Hillson, N. J., and Walsh, C. T. (2005) Excision of the epothilone synthetase B cyclization domain and demonstration of in trans condensation/cyclodehydration activity. *Biochemistry 44*, 13385-93.

(17) Marshall, C. G., Burkart, M. D., Keating, T. A., and Walsh, C. T. (2001) Heterocycle formation in vibriobactin biosynthesis: alternative substrate utilization and identification of a condensed intermediate. *Biochemistry 40*, 10655-63.

(18) Popov, A. F., Savelova, V. A., Sadovskii, Y. S., Solomoichenko, T. N., Piskunova, Z. P., and Lobanova, O. V. (2001) Reactivity of Carboxamides toward Benzoyl Chloride in Acetonitrile. *Russian J. Organic Chem. 37*, 1117-1123.

(19) Popov, A. F., Sadovskii, Y. S., Solomoichenko, T. N., Savelova, V. A., Lobanova, O. V., and Piskunova, Z. P. (2000) Nucleophilic Substitution at a Four-Coordinate Phosphorous Atom. Reactivity of Carboxylic Acid Amides toward Diphenyl Chlorophosphate in Acetonitrile. *Russian J. Organic Chem. 36*, 715-724.

(20) Popov, A. F., Lobanova, O. V., Savelova, V. A., Sadovskii, Y. S., Solomoichenko, T. N., and Piskunova, Z. P. (2002) Comparison of Carboxamides Reactivity with Respect to Benzoyl Chloride and Diphenyl Chlorophosphate in Acetonitrile. *Russian J. Organic Chem. 38*, 1624-1628.

(21) Shah, R. C., Deshpande, R. K., and Chaubal, J. S. (1932) Condensation of Benzanilides and p-Dialkylanilines with Phosphorous Oxychloride as Condensing Agent, and the Mechanism of the Reaction. *J. Chem. Soc.*, 642-650.

(22) Kantlehner, W. (1991) *Synthesis of Iminium Salts, Orthoesters and Related Compounds*, Comprehensive Organic Synthesis, Vol. 6, Pergamon Press, Oxford, England.

(23) Bredereck, H., Gompper, R., Klemm, K., and Rempfer, H. (1959) Reaktionen von Saureamide-Acylhalogenid-Addukten: Darstellung substituierter Amidine und Amidrazone. *Chem. Ber.*, 837-849.

(24) Yale, H. L., Bergeim, F. H., Sowinski, F. A., Bernstein, J., and Fried, J. (1962) New Boron Heterocycles. 5-, 6-, and 7-Membered Systems Containing Nitrogen Oxygen and Sulfur. *J. Amer. Chem. Soc. 84*, 688-690.

(25) Reissmann, S., Hochleitner, E., Wang, H., Paschos, A., Lottspeich, F., Glass, R. S., and Böck, A. (2003) Taming of a Poison: Biosynthesis of the NiFe-Hydrogenase Cyanide Ligands. *Science 299*, 1067-1070.

(26) Herschlag, D. and Jencks, W. P. (1990) Catalysis of the hydrolysis of phosphorylated pyridines by Mg(OH)+: a possible model for enzymatic phosphoryl transfer. *Biochemistry 29*, 5172-9.

(27) Admiraal, S. J., Schneider, B., Meyer, P., Janin, J., Veron, M., Deville-Bonne, D., and Herschlag, D. (1999) Nucleophilic Activation by Positioning in Phosphoryl Transfer Catalyzed by Nucleoside Diphosphate Kinase. *Biochemistry 38*, 4701-4711.

(28) Admiraal, S. J. and Herschlag, D. (1995) Mapping the transition state for ATP hydrolysis: implications for enzymatic catalysis. *Chem. Biol. 2*, 729-39.

(29) Allen, K. N. and Dunaway-Mariano, D. (2004) Phosphoryl group transfer: evolution of a catalytic scaffold. *TIBS 29*, 495-503.

(30) Gerlt, J. A. and Babbitt, P. C. (2001) Divergent evolution of enzymatic function: mechanistically diverse superfamilies and functionally distinct suprafamilies. *Annu. Rev. Biochem. 70*, 209-46.

(31) Mueller, E. J. (1993), PhD Thesis, Department of Chemistry, Massachusetts Institute of Technology, Cambridge.

Appendix

Additional NMR Experiments to Determine PurS Quaternary Structure

Background:

In addition to the NMR experiments carried out by Jens Wönhert in Chapter 4, several

other NMR methods were utilized to determine PurS quaternary structure. NOESY data were

obtained for PurS in an effort to detect NOEs across the putative dimer:dimer interface. In

addition, residual dipolar couplings (RDCs) were measured for PurS to determine the orientation

of PurS in an aligning media and compare these results with predictions made from the crystal

structure. However, these experiments were not conclusive, and current NMR investigations are

focused on providing additional RDC and NOESY data.

Experimental:

NOESY Experiments

A 3D-^{15}N-edited NOESY-HSQC spectrum with a mixing time of 100 ms (Bruker AV

800 MHz, 8 scans/increment, d1=2s, 110 x 48 complex points in f1 and f2, spectral width=12

ppm in f1, ~ 4 days) was recorded on a 2 mM ^{15}N-only-labelled PurS sample in NMR-buffer.

Using the backbone assignments obtained in the 3D-triple resonance experiments, the 3D-^{15}N-

edited NOESY-HSQC spectrum was analyzed for presence of long-range NH-NH-NOEs across

the β-strands comprising the monomer:monomer and dimer:dimer interfaces.

RDC Measurements to Determine the Orientation of PurS in an Aligning Media

Residual dipolar couplings were measured by collecting ^{1}H,^{15}N-HSQC-spectra without

proton-decoupling in the f1-dimension or using ^{1}H,^{15}N-HSQC-experiments, where the **Inphase**-

and the **Antiphase**-component of the NH-doublet are recorded in separate spectra in an

interleaved fashion (Ottiger, M. , Delaglio, F., Bax, A. (1998) *J. Magn. Reson.*, 131, 373-378) of

0.5 mM ^{15}N-labelled PurS in NMR-buffer in the presence or absence of 10mg/ml of the filamentous phage Pf1 (Hansen, M. R., Mueller, L., Pardi, A. (1998) *Nat. Struct. Biol.*, 5, 1065-1074). The residual dipolar couplings (D_{NH}) were calculated by measuring the difference in the splitting of the signals for each NH-group in the presence of phage ($J_{NH}+D_{NH}$) and subtracting the splitting in the absence of phage (J_{NH}). The measured residual dipolar couplings together with the structures of the hypothetical dimeric and tetrameric forms of PurS (as extracted from the x-ray structure of the tetramer) were used to calculate the orientation of the alignment tensor of the protein using the program ORDERTEN_SVD (Losonczi, J. A., Andrec, M., Fischer, M. W., Prestegard, J. H. (1999) *J. Magn. Reson.*, 138, 334-342). The experimentally determined alignment tensor was then compared with the alignment tensor predicted for the dimeric and tetrameric PurS by the program PALES (Zweckstetter, M., Bax, A. (2000) *J. Am. Chem. Soc.* 122:3791–3792).

Results and Discussion:

NOESY Experiments

Despite the observation of NOEs across the monomer:monomer interface, no NOEs were detected across residues predicted to be involved in the dimer:dimer interface of PurS. While this would suggest that the tetramer is not present, the data was inconclusive for several reasons. First, based on the PurS tetramer crystal structures, the distances predicted to be measured in the NOESY experiment are very long: 4.6 Å between the amide protons of Y76 and V78 in the $P2_1$ crystal form and 5.9 Å between the amide protons of E77 and A79 in the C2 crystal form. This means that any observed NOEs would by very weak. In addition, due to amide proton exchange, NOEs observed from amides are inherently weak. Finally, the NOEs predicted between Y76 and V78 would appear very close to the diagonal, which increases noise and artifacts in the NOESY

338

spectrum. Consequently, the lack of NOEs in the spectrum from residues at the proposed tetramer interface could be explained by reasons other than lack of tetramer formation. In order to provide more conclusive NOE evidence, additional NOESY data are being collected on a [^{2}H, ^{13}C, ^{15}N]-PurS sample. This should allow direct observation of NOEs between amide protons and the carbonyl carbons believed to be part of the tetramer interface.

RDC Experiments

In the presence of an aligning media such as filamentous phage, proteins will preferentially orient themselves with respect to the applied magnetic field. This orientation is dependent on molecular shape. For PurS, the dimer and tetramer were predicted to have different alignments (Figure A.1, Top). Comparison of PurS HSQCs in the presence and absence of phage allowed the residual dipolar couplings (RDCs) for the protein to be determined as previously described, and this in turn was used to calculate an alignment tensor and orientation for the protein in the magnetic field. As shown in Figure A.1, the measured RDCs match those predicted for a molecular alignment corresponding to a PurS dimer ($R^2 = 0.91$). This result indicates that the orientation of PurS in the magnetic field is indicative of the molecular shape of the PurS dimer. While the above result is compelling, additional RDC experiments are needed in different aligning medias to confirm that these results are not an artifact of PurS interacting with the phage.
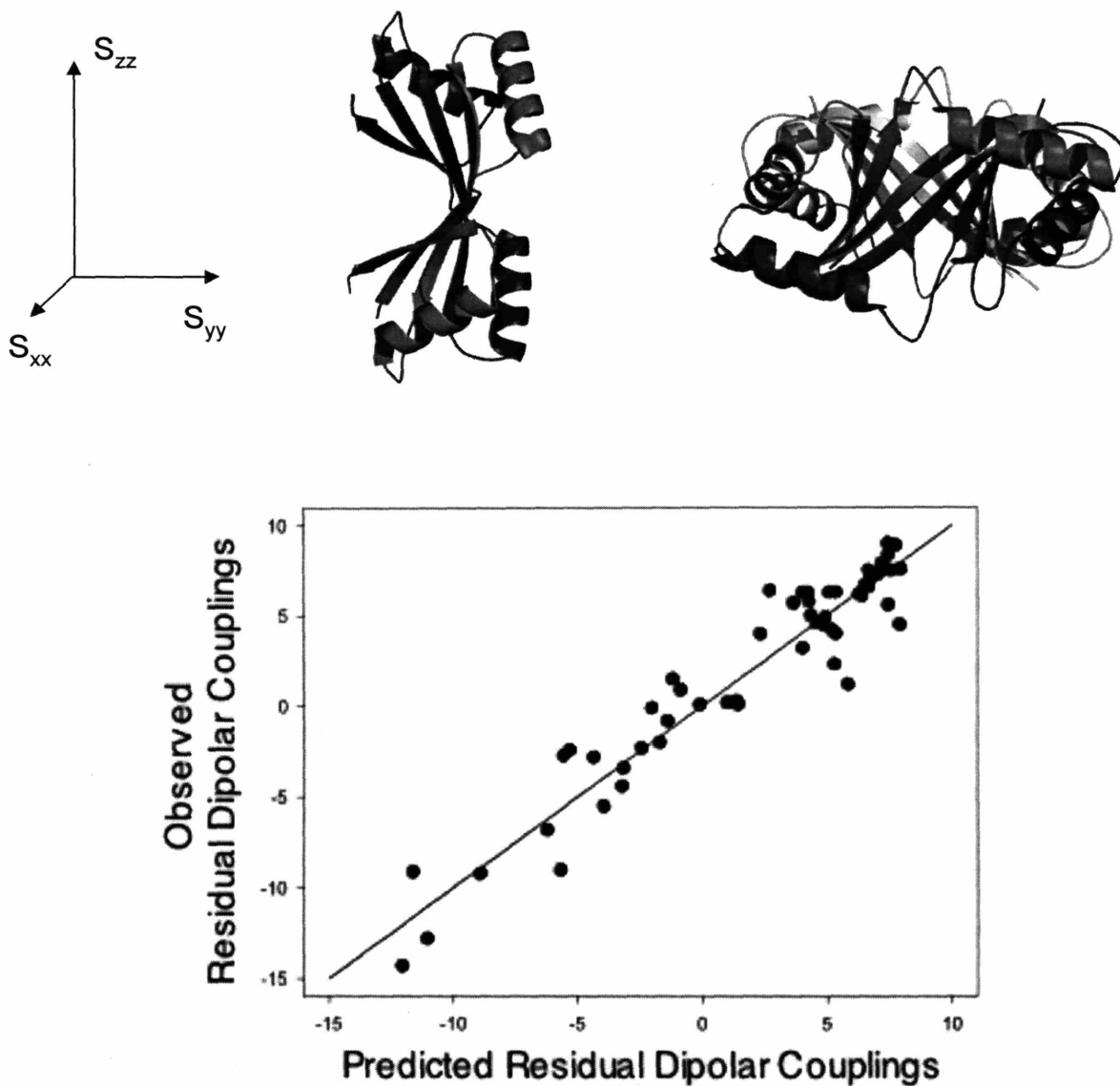
Figure A.1—Alignment of PurS in a magnetic field based upon RDCs. (Top) The PurS dimer and tetramer are predicted to orient themselves differently in magnetic field along S_{zz}. (Bottom) Correlation between observed RDCs and those predicted from the PurS dimer structure. The agreement between the predicted and observed values indicates that a PurS dimer is present in solution.

Education

Ph. D.	Massachusetts Institute of Technology Biological Chemistry, Thesis Advisor: Prof. JoAnne Stubbe	2006
B. S.	Purdue University Chemistry	2000

Research Experience

Massachusetts Institute of Technology Graduate Research Assistant	Cambridge, MA	2000-2006
Purdue University Undergraduate Research Assistant	West Lafayette, IN	1997-2000

Publications and Conferences

Ilin, S., Hoskins, A., Ohlenschlager, O., Jonker, H.R., Schwalbe, H., and Wohnert, J., *Chembiochem*, **2005**, 6(9): 1611-18.

Hoskins, A. and Stubbe, J., 19th Annual Symposium of the Protein Society, August, 2005, Boston, MA.

Hoskins, A.A., Anand, R., Ealick, S.E., and Stubbe, J., *Biochemistry*, **2004**, 43(32): 10314-27.

Anand, R., Hoskins, A.A., Stubbe, J., and Ealick, S.E., *Biochemistry*, **2004**, 43(32): 10328-42.

Anand, R., Hoskins, A.A., Bennett, E.M., Sintchak, M.D., Stubbe, J., and Ealick, S.E., *Biochemistry*, **2004**, 43(32): 10343-52.

Hoskins, A., Anand, R., Ealick, S.E., and Stubbe, J., Enzymes Gordon Conference, July, 2004, Meriden, NH.

Hoskins, A. and Stubbe, J., 18th Enzyme Mechanisms Conference, January 2003, Galveston, TX.

Ilin, S., Hoskins, A., Schwalbe, H., and Wohnert, J., *J. Biol. NMR*, **2003**, 25(2): 163-4.

Klewer, D.A, Hoskins, A., Zhang, P., Davisson, V.J., Bergstrom, D.E., LiWang, A.C., *Nucleic Acids Res.*, **2000**, 28(22): 4514-22.

Honors and Awards

National Science Foundation Fellowship	2000-2003
Outstanding Teaching Assistant	2000
Carroll County Cancer Society Fellowship	2000
Hypercube Scholar	2000
Phi Beta Kappa	1999-2000
Mortar Board	1999-2000
Ben Freiser Award in Analytical Chemistry	1999
Eli Lilly-Purdue Alumni Scholarship	1996-2000